Group 6 Metal Complexes in Olefination Reactions

Gruppe-6-Metallkomplexe in Olefinierungen

DISSERTATION

der Mathematisch-Naturwissenschaftlichen Fakultät
der Eberhard Karls Universität Tübingen
zur Erlangung des Grades eines
Doktors der Naturwissenschaften
(Dr. rer. nat.)

vorgelegt von
M. Sc. Simon Trzmiel
aus Nürtingen

Tübingen
2022

Gedruckt mit Genehmigung der Mathematisch-Naturwissenschaftlichen Fakultät der Eberhard Karls Universität Tübingen.

Tag der mündlichen Qualifikation:	06.05.2022
Dekan:	Prof. Dr. Thilo Stehle
1. Berichterstatter:	Prof. Dr. Reiner Anwander
2. Berichterstatterin:	Prof. Dr. Doris Kunz

Group 6 Metal Complexes in Olefination Reactions

Simon Trzmiel

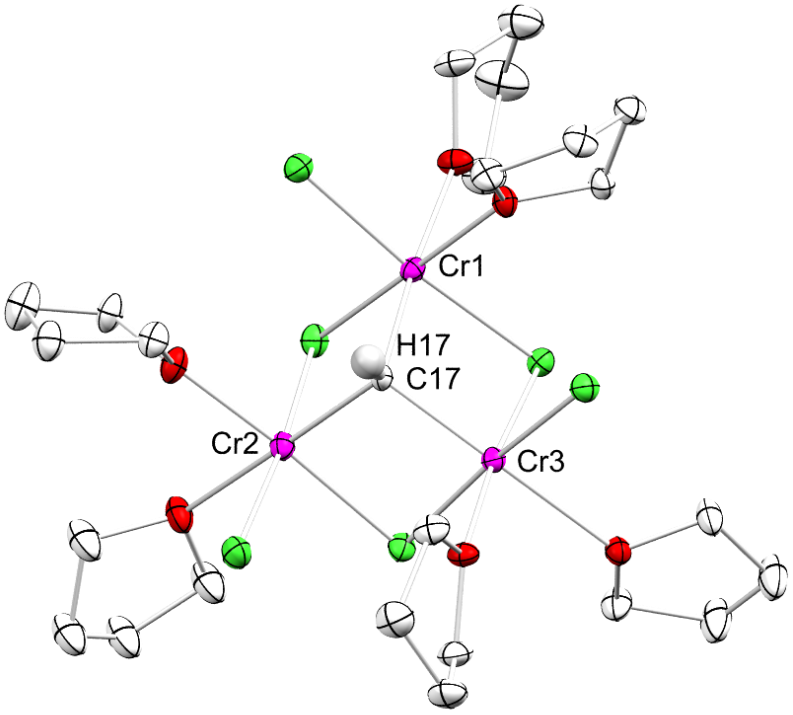

Preface

The following PhD thesis consists of a study on the reactivity and structure of chromium(II/III), molybdenum(V) and tungsten(V/VI) complexes toward carbonylic compounds, namely aldehydes and ketones, a summary of the main results, and original scientific papers. The work has been carried out at the Institut für Anorganische Chemie of the Eberhard Karls Universität Tübingen, Germany, over the period from April 2018 to April 2022 under the supervision of Prof. Dr. Reiner Anwander. Funding has been gratefully received from the Deutsche Forschungsgemeinschaft (DFG).

“See first, think later, then test. But always see first. Otherwise, you will only see what you were expecting. Most scientists forget that.”

— Douglas Adams

Acknowledgements

First, I would like to thank my supervisor Prof. Dr. Reiner Anwander. Thank you for giving me the opportunity to work in your group and laboratory. Thank you for providing this exceptionally interesting research topic, high standard equipment, and laboratory as well as advice whenever needed. Your guidance and mentoring have significantly increased the quality of this work.

I would like to especially thank Dr. Cäcilia Maichle-Mössmer for introducing me to single crystal X-ray structure analysis, her help with difficult samples and for solving even the most complicated of structures. You were always helpful when I had problems with picking or measuring sensitive crystals. Your lessons and help are an indispensable part of this thesis. Further thanks to Dr. Daniel Werner for his kind introduction and the provided help and information regarding the Takai Reagent and the world of chromium chemistry.

Special thanks also to Prof. Dr. Wolfgang Scherer and Jan Langmann from the University of Augsburg for their help, advice, and measurements regarding magnetic properties of chromium complexes.

My thanks also to Dr. Klaus Eichele, Priska Kolb and Dominik Brzecki for maintaining the high standard equipment, as well as their help in all aspects regarding NMR spectroscopy. I wish to thank Wolfgang Bock and Mohammed Ghani for performing the elemental analyses and Dr. Jochen Glaser for the ICP measurements.

I further thank Tobias Wolf and especially Elke Niquet for maintaining the laboratory equipment and their friendly and always helpful nature.

Many thanks to Sabine Ehrlich for all her administrative work and the help with anything related to forms. Additionally, I want to thank the staff of the metal, electronics and glass workshops for manufacturing and repairing lab equipment.

I further like to thank my current and former coworkers of the Anwander group for the time spent together working on our research as well as the time we spent outside the laboratory, for all the discussions, chemistry related or not, and for your friendship. Further thanks go to Damir Barisic, Dr. Uwe Bayer, Tassilo Berger, Dr. Verena Birkelbach, Martin Bonath, Denis Burghardt, Dennis Buschmann, Dr. Dominic Diether, Dr. Jochen Friedrich, Dr. Christoph Hollfelder, Markus Katzenmayer, Felix Kracht, Lars Hirneise, Jakob Lebon, Dr. Yucang Liang, Dr. Leilei Luo, Eric Moinet, Alexandros Mortis, Jonas Riedmaier, Theresa Rieser, Dr. Dorothea Schädle, Dr. David Schneider, Andrea Sonström, Georgios Spiridopoulos, Dr. Christoph Stuhl, Dr. Renita Thim Dr. Benjamin Wolf and Gernot Zug for the very supportive and friendly atmosphere in the lab. I would also like to thank my students for their contributions to my research and the time spent working on their projects.

Besonderer Dank gilt auch Jan Wahl und Dr. Florian Fetzer sowie all meinen Freunden. Ohne euch und eure Unterstützung wäre diese Arbeit nie zu Ende gebracht worden.

Zu guter Letzt möchte ich mich bei meiner Familie bedanken. Meinen Eltern Petra und Alfred sowie meinem Bruder Dennis, gilt mein Dank für ihre uneingeschränkte Unterstützung jeglicher Art, vor und während meines Studiums und während der Doktorarbeit.

Contents

Abbreviations

Ar	Aryl	EA	Elemental Analysis
Bn	Benzyl	*e.g.*	*exempli gratia*
*n*Bu	*n*-Butyl	Et	Ethyl
*t*Bu	*tert*-Butyl	*et al.*	*et alii* or *et aliae*
COSY	Correlated Spectroscopy	HMBC	Heteronuclear Multiple Bond Correlation
Cp	Cyclopentadienyl	HMDSO	Hexamethyldisiloxan
Cp*	C_5Me_5	HMPA	Hexamethylphosphoramide
Cp’	$C_5H_4SiMe_3$	HSQC	Heteronuclear Single Quantum Coherence
DCM	Dichloromethane	IR	Infrared
DEPT	Distortionless Enhancement Polarization Transfer	M	Metal
DME	Dimethoxyethane	Me	Methyl
DMF	Dimethylformamide	NMR	Nuclear Magnetic Resonance
Dipp	2,6-Di*iso*propylphenyl	Oe	Oersted
do	Donor	OMes	2,4,6-Trimethylphenyl
DRIFT	Diffuse Reflectance Infrared Fourier Transform	Ph	Phenyl

*i*Pr	*iso*-Propyl
Py	Pyridine
r.t.	Ambient temperature
SQUID	Superconducting Quantum Interference Device
TMEDA	Tetramethylethylenediamine
THF	Tetrahydrofuran
TEEDA	Tetraethylethylenediamine
UV-Vis	Ultraviolet–Visible
μ_B	Bohr Magneton
μ_{eff}	Effective Magnetic Moment

Summary

Group 6 metal olefinaton reagents are some of the lesser-known examples of complexes used in modern chemistry. Although olefinations are essential in organic synthesis, some of these reactions are still not fully investigated regarding their active species and the involved mechanisms.

Studies on the Takai reaction by Dr. Daniel Werner raised further questions regarding the reactivity and mechanism of the used $CrCl_2/CHI_3$ system. The findings with respect to the stoichiometry of this redox reaction sparked interest in the reactivity and applicability of the found product $[Cr_3(\mu_2\text{-}Cl)_3(\mu_3\text{-}CH)(thf)_6]$. Optimization of the synthesis of $[Cr_3(\mu_2\text{-}Cl)_3(\mu_3\text{-}CH)(thf)_6]$ and its derivatization to $[Cp^R{}_3Cr_3(\mu_2\text{-}Cl)_3(\mu_3\text{-}CH)]$ (R = C_5H_5, $C_5H_4SiMe_3$, C_5Me_5) gave the opportunity to study the elusive $[Cr^{III}\text{-}\mu_3\text{-}CH]$ compound class for the first time. Magnetic measurements of these compounds revealed strong paramagnetic properties and complicated electronic/magnetic coupling interactions depending on the substituents. Enhanced stability as well as observable ^1H NMR signals of these paramagnetic compounds could assist in elucidating the intricate reactivity of chromium alkylidyne compounds in extended studies.

The search for precursors with properties similar to $CrCl_2$ while simultaneously engaging in the redox transformation of Cr–X to Cr–CHX gave access to a multitude of new Cr^{II} siloxide compounds. These complexes show properties and coordination geometries based on the sterics of the incorporated ligands as well as the used solvent and donor molecules. Starting with $Cr[N(SiMe_3)_2]_2(thf)_2$, its protonolysis with various silanols gave access to the complexes $Cr_3(OSiEt_3)_2(\mu\text{-}OSiEt_3)_4(thf)_2$ and $Cr_2(OSi\textit{i}Pr_3)_2(\mu\text{-}OSi\textit{i}Pr_3)_2(thf)_2$. Exposure of these compounds to vacuum in aliphatic solvents generated the homoleptic compounds $[Cr(\mu\text{-}OSiEt_3)_2]_4$ and $[Cr_3(OSi\textit{i}Pr_3)_2(\mu\text{-}OSi\textit{i}Pr_3)_4]$. Readily available starting materials and rapid, high yield reactions make these compounds interesting precursors for further studies in the field of Cr^{II} and its coordination chemistry.

Finally, investigations into the elusive Kauffmann compounds revealed several new molybdenum(V), tungsten(V) and tungsten(VI) species. The heteroleptic siloxide complexes $[MoOCl\{OSi(O\textit{t}Bu)_3\}_2(thf)_{1\text{-}2}]$ and $[WOCl_2\{OSi(O\textit{t}Bu)_3\}_2(thf)]$ were synthesized and fully characterized. Metathesis reactions with pertinent organolithium and potassium reactants generated $[LiMoO(\mu_2\text{-}CH_2SiMe_3)_2\{OSi(O\textit{t}Bu)_3\}_2]$, $[WO(CH_3)_2\{OSi(O\textit{t}Bu)_3\}_2(thf)]$ and $[WO(\mu_2\text{-}CH_2\text{-}R)_2\{OSi(O\textit{t}Bu)_3\}_2]$ (R = $SiMe_3$, Ph). The obtained alkyl complexes did not show

any significant olefination reactivity in reactions with aldehydes and ketones probably due to steric hindrance but might help to better understand the Kauffmann reagents and reactions.

Zusammenfassung

Gruppe-6-Metall-Olefinierungsreagenzien gehören zu den weniger bekannten Komplexverbindungen, die in der modernen Chemie Anwendung finden. Trotz der Wichtigkeit von Olefinierungen in der organischen Synthese sind einige dieser Reaktionen bis heute nicht vollständig aufgeklärt, sowohl in Bezug auf die aktive Spezies als auch den Reaktionsmechanismus.

Untersuchungen der Takai-Reaktion durch Dr. Daniel Werner warfen neue Fragen bezüglich der Reaktivität und des Mechanismus des eingesetzten $CrCl_2/CHI_3$-Systems auf. Durch seine Erforschung der Stöchiometrie dieser Reaktion war schnell das Interesse an der Reaktivität und Anwendbarkeit des gefundenen Produktes $[Cr_3(\mu_2\text{-}Cl)_3(\mu_3\text{-}CH)(thf)_6]$ geweckt. Optimierung der Synthese von $[Cr_3(\mu_2\text{-}Cl)_3(\mu_3\text{-}CH)(thf)_6]$ und die Derivatisierung zu $[Cp^R{}_3Cr_3(\mu_2\text{-}Cl)_3(\mu_3\text{-}CH)]$ (R = C_5H_5, $C_5H_4SiMe_3$, C_5Me_5) eröffnete zum ersten Mal die Möglichkeit der Untersuchung dieser schwer fassbaren $[Cr^{III}\text{-}\mu_3\text{-}CH]$ Verbindungsklasse. Magnetische Messungen dieser Verbindungen zeigten starke paramagnetische Eigenschaften und komplizierte elektronische/magnetische Kopplungen in Abhängigkeit der Liganden. Die erhöhte Stabilität als auch die Beobachtbarkeit von ^{1}H-NMR-Signalen dieser paramagnetischen Verbindungen könnten dabei helfen, die komplexe Reaktivität von Cr-Alkylidinen in weiterführenden Studien zu verstehen.

Die Suche nach Vorstufen mit ähnlichen Eigenschaften zu $CrCl_2$, welche gleichzeitig aktiv in der Redox-Transformation von Cr–X zu Cr–CHX sind, führte zur Entdeckung einiger neuer Cr^{II}-Siloxidverbindungen. Die gefundenen Verbindungen zeigen interessante Eigenschaften und Koordinationsgeometrien in Abhängigkeit des sterischen Anspruchs der Silyoxy-Liganden, sowie den Einfluss von Lösemittel und Donormolekülen. Die Protonolyse von $Cr[N(SiMe_3)_2]_2(thf)_2$ mit verschiedenen Silanolen resultierte in den Komplexen $Cr_3(OSiEt_3)_2(\mu\text{-}OSiEt_3)_4(thf)_2$ und $Cr_2(OSi\textit{i}Pr_3)_2(\mu\text{-}OSi\textit{i}Pr_3)_2(thf)_2$. Die gefundenen THF-Addukte bilden in aliphatischen Lösemitteln im Vakuum die homoleptischen Verbindungen $[Cr(\mu\text{-}OSiEt_3)_2]_4$ und $[Cr_3(OSi\textit{i}Pr_3)_2(\mu\text{-}OSi\textit{i}Pr_3)_4]$. Einfach zugängliche Edukte und kurze Reaktionszeiten mit hohen Ausbeuten machen diese Verbindungen als Vorstufen für die weitere Forschung an Cr^{II} und seiner komplexen Reaktivität attraktiv.

Zu guter Letzt führte die Untersuchung der Kauffmann-Reagenzien zur Entdeckung mehrerer neuer Molybdän(V)-, Wolfram(V)- und Wolfram(VI)- Verbindungen. Die heteroleptischen

Siloxid-Komplexe [MoOCl{OSi(O*t*Bu)$_3$}$_2$(thf)$_{1\text{-}2}$] und [WOCl$_2$\{OSi(O*t*Bu)$_3$}$_2$(thf)] wurden vollständig charakterisiert. Metathesereaktionen mit geeigneten Organolithium- und Organokaliumreagenzien ermöglichten den Zugang zu den Alkyl-Komplexen [LiMoO(μ_2-CH$_2$-SiMe$_3$)$_2$\{OSi(O*t*Bu)$_3$}$_2$], [WO(CH$_3$)$_2$\{OSi(O*t*Bu)$_3$}$_2$(thf)] und [WO(μ_2-CH$_2$-R)$_2$\{OSi(O*t*Bu)$_3$}$_2$] (R = SiMe$_3$, Ph). Diese zeigten zwar keine signifikante Aktivität in Olefinierungen mit Aldehyden und Ketonen, vermutlich bedingt durch den hohen sterischen Anspruch, doch die gefundenen Komplexe könnten dabei helfen die Kauffmann-Reagenzien näher zu beleuchten.

Publications

Publications incorporated into this thesis

Paper I Beyond Takai's Olefination Reagent: Persistend Dehalogenation Emerges in a Chromium(III)-μ_3-Methylidyne Complex
S. Trzmiel, J. Langmann, D. Werner, C. Maichle-Mössmer, W. Scherer, R. Anwander
Angew. Chem.: **2021**, *133*, 20202-20208, doi:10.1002/ange.202106608.
Angew. Chem. Int. Ed. **2021**, *60*, 20049-20054, doi: 10.1002/anie.202106608.

Paper II Chromous siloxides of variable nuclearity and magnetism
S. Trzmiel, J. Langmann, D. Werner, C. Maichle-Mössmer R. Anwander
Dalton Trans., **2022**, *51*, 5072-5081, doi: 10.1039/D2DT00354F.

Personal Contribution

Paper I:

Synthesis for $[Cr_3(\mu_2\text{-}Cl)_3(\mu_3\text{-}CH)(thf)_6]$ was planned by Dr. Daniel Werner, later optimized and conducted by me. SQUID magnetometer measurements were conducted by J. Langmann from the University of Augsburg. Other reactions and analyses described were planned and conducted by me. Analyses include one-dimensional (^1H, $^7Li\{^1H\}$,), two-dimensional (^1H-^{13}C HSQC, ^1H-^{13}C HMBC) NMR spectroscopic methods, Evans' Method (magnetic moment), DRIFT spectroscopy, UV/Vis spectroscopy and elemental analyses preparation. Manuscript writing was also done by me.

Some reactions and analyses were conducted during my master thesis.

Elemental analyses were performed by Wolfgang Bock. The structural analyses by single crystal X-ray diffraction were performed by Dr. Cäcilia Maichle-Mössmer and me. GC/MS measurements were conducted by the Abteilung Massenspektrometrie of the University of Tübingen. ICP measurements were conducted by Dr. Jochen Glaser.

Paper II:

All reactions described were planned and conducted by me. SQUID magnetometer measurements were conducted by J. Langmann from the University of Augsburg. All other analyses were planned and conducted by me. Analyses include one-dimensional (^1H, $^7Li\{^1H\}$) NMR spectroscopic methods, Evans' Method (magnetic moment), DRIFT and UV/Vis spectroscopy. Manuscript writing was also done by me.

Elemental analyses were performed by Wolfgang Bock. The structural analyses by single crystal X-ray diffraction were performed by Dr. Cäcilia Maichle-Mössmer and me. Structural refinements and solutions were done by Dr. Cäcilia Maichle-Mössmer.

Objective of the Thesis

The main emphasis of this thesis is to identify and study the structure and reactivity of group 6 metal complexes derived from active species in known olefination reactions with aldehydes and ketones.

Chapter A gives an overview of the known aspects of the Takai and Kauffmann olefination reagents and reactions and chromium(II) siloxide compounds. Focus will be on the generation of original compounds and the findings related to their development since their discovery and or characterization.

Chapter B contains a summary of the main results of this thesis and is divided in three parts:

- Synthesis, Derivatization and Characterization of $[Cr_3(\mu_2\text{-}Cl)_3(\mu_3\text{-}CH)(thf)_6]$
- Reactivity of $[Cr^{III}\text{-}\mu_3\text{-}CH]$ Compounds with Aldehydes and Ketones
- Synthesis and Characterization of Cr^{II} Siloxides

In **Chapter C** unpublished results, which are not part of a publication or manuscript, are presented. This contains the synthesis and characterization of Mo(V), W(V) and W(VI) compounds of relevance for the Kauffmann Reaction.

Chapter E is a compilation of publications.

A

Group 6 Metal Complexes in Olefination Reactions

1 Introduction

Over the past century, many olefinations have been developed and intensively researched.[1] Today, olefination reactions are some of the most fundamental tools in modern organic synthesis.[2] Regarding olefination reactions, group 6 metals are of interest with chromium as part of the TAKAI reaction while molybdenum and tungsten are utilized in the KAUFFMANN reaction.[3–5]

The TAKAI reaction is well established in the synthesis of natural substances and precursor compounds for further synthesis since many years. Numerous examples in research have used this protocol due to high tolerance for functional groups, excellent selectivity and functionalized products, predestined for further synthesis.[6,7] Some examples include Debilisone C[8],+-Superstolide A[9] or (+)-Ambruticin.[10] Following the discovery in 1986, the original reaction was continuously refined, and the scope increased vastly. Today, the $CrCl_2/CH_xX_y$ (X = Cl, Br, I) system can be adapted to produce unsubstituted alkenes in the TAKAI-UTIMOTO reaction[11], perform cyclopronanations on terminal alkenes to iodo[12] or trimethylsilyl[13] substituted cyclopropanes or even include boron[14] and tin[15] substituents.

The KAUFFMANN reaction on the other hand had no application for a long time, but found its use in, e.g., the total synthesis of (+)-Axenol and (-)-Gleenol by SPRITZNER *et al* in 2002.[16,17] Since then, many other syntheses have incorporated or investigated the KAUFFMANN reagents.[18–22] The reagents are easily accessible, and show interesting properties such as high and controllable selectivity, low basicity and therefore high proton tolerance.[23–25]

Interestingly, the structures of the active species of the TAKAI reaction have remained elusive only until recently.[26] The composition and hence solid-state structure of the KAUFFMANN reagent is unconfirmed to this day and is still in need for definite proof. The structural elucidation is impeded by complicated formation, instability, and generation of side products of similar composition.[27]

This work gives an overview of the synthesis and characterization of various organo-chromium molybdenum and tungsten compounds with the goal of identifying structures and structural motifs comparable to the active species of the TAKAI and the KAUFFMANN transformations. In order to elucidate the reactivity of these mostly unstudied compounds, different synthesis approaches were applied. Variation of solvents, ligands, and reaction conditions led to the discovery and characterization of compounds encouraging future research and illuminating the

reactivity involved in these reactions. The first part focuses on the TAKAI reaction and compounds generated by variation of the $CrCl_2/CHI_3$ system. The second part covers Cr^{II}-siloxide complexes generated as alternative precursors for TAKAI-like compounds. The last part will focus on molybdenum and tungsten compounds characterized as part of the research on the KAUFFMANN reagent.

In this thesis, various oxidation states of chromium, molybdenum, and tungsten are mentioned and therefore shown in distinct colors. (Cr^{II}: blue, Cr^{III}: red, Mo^{V}: turquoise, W^{V}: orange, W^{VI}: purple).

2 Organochromium Compounds in the TAKAI Olefination

2.1 The TAKAI Reaction

The TAKAI olefination is one of the name reactions involving organochromium compounds, which is to this day applied in contemporary organic chemistry. The name reaction has been incorporated in many total syntheses of natural substances as well as the synthesis of many precursor compounds.[6] Discovered in 1986 by Kazuhiko TAKAI, this reaction is based on organochromium(III) compounds generated in a $CrCl_2/CHX_3$ system.[3] Over the years, many additions to this original reaction were made, and the scope of possible applications was vastly increased. The original TAKAI reaction consisted of six equivalents of $CrCl_2$ reacted with two equivalents CHI_3 and one equivalent of benzaldehyde in THF at 0 °C. This specific reaction enabled the (E)-selective olefination of benzaldehyde to (E)-iodostyrene in 87% yield with an E/Z ratio of 94/6 (Scheme A1).

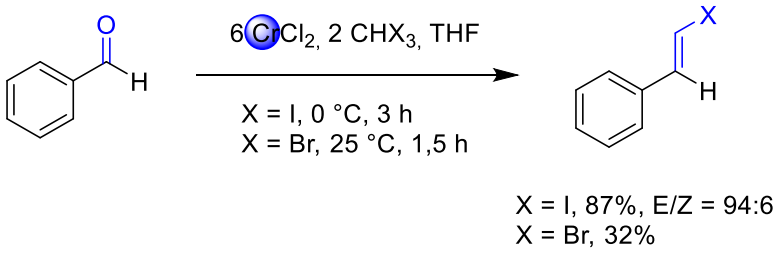

Scheme A1 Original TAKAI reaction with benzaldehyde as published 1986.[3]

As stated in the original publication, the E/Z ratio increased in the order of I < Br < Cl but the rates of reaction decreased I > Br > Cl. Substrate reactivity was found to decrease from aldehydes to ketones, enabling the selective olefination of aldehyde functions in the presence of ketones and other functional groups. The high (E)-selectivity as well as the tolerance for other functional groups made this reaction a viable tool for organic synthesis, giving halogenide substituted products directly applicable in further reactions. Although the $CrCl_2/CHX_3$ system was intensively studied and used over the following decades, the main active species has remained elusive until 2018.[26]

2.2 Formation and Reactivity

The formation of the active reagent was proposed in the original publication by TAKAI in 1986 based on observations in the studied reactions. Two possible active species and their reactivity toward aldehyde substrates was suggested, as shown in Scheme A2.[3]

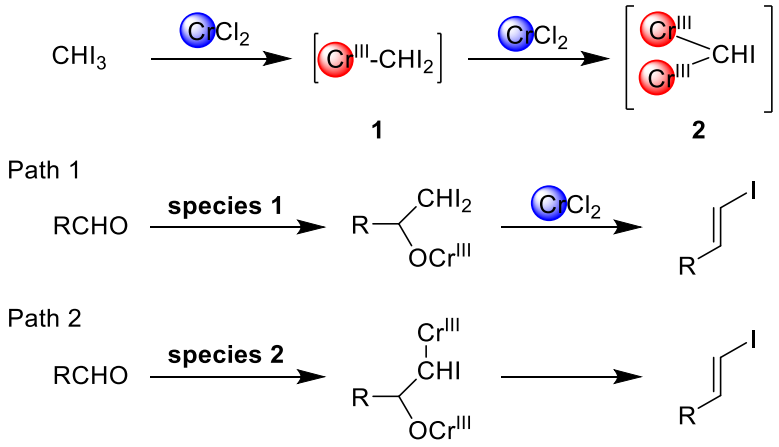

Scheme A2. Proposed formation and reaction of the original TAKAI reagent.[3]

The reaction of the haloform with one equivalent of $CrCl_2$ leads to a chromium dihalido-methanide **1** followed by further reaction with a second equivalent of $CrCl_2$ to a dichromium monohalido-methylidene **2**. In the original publication, compound **2** was proposed as the more likely candidate responsible for the observed reaction outcomes following path 2. Over the next years, further contributions to the original TAKAI reaction shed light on the structure of involved compounds.[3,13,26,28,29]

In 1987 the reaction was closer examined for R_2CHX_2 (X = Cl, Br, I) compounds. The reaction showed a similar decreasing order of reactivity for I>Br>Cl with 1,1-dibromo and 1,1-dichloroethane giving yields of 14% and no ethylidenation, underlining the importance of the use of diiodo substituted substrates in the reaction.[11] Addition of pertinent donor ligands has been known to increase the reductive properties of chromium(II), accelerating the reaction, thus leading to the use of $CrCl_2$ activated with DMF (Dimethylformamide).[30,31] This $CrCl_2$-DMF complex yielded the best results and was prepared by stirring $CrCl_2$ with equimolar amounts of DMF in tetrahydrofuran (THF) at 25 °C before the addition of further substrates.[11,32]

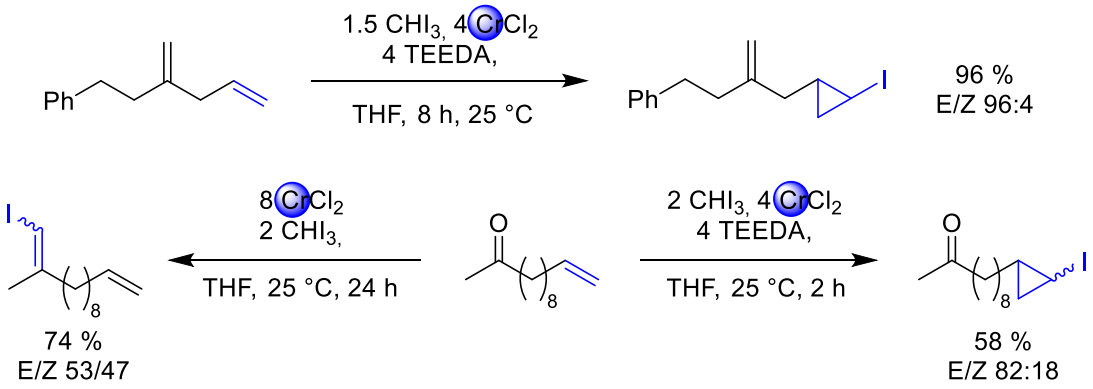

Scheme A3. Modified TAKAI reaction by addition of TEEDA from 2003.[12]

By changing the original stoichiometry of the reaction and through the addition of TMEDA (N,N,N',N'-tetramethylethylenediamin) or TEEDA ((N,N,N',N'-tetraethylethylenediamine), it was possible to generate *trans*-iodocyclopronanated products from compounds with terminal alkene functions.[12] It was observed that cyclopropanation was the preferred outcome only after addition of TMEDA or TEEDA (Scheme A3). The alteration of the reaction outcome led to the assumption of the formation of different reactive species by addition of Lewis basic diamine compounds. Such modified reaction conditions were also investigated regarding steric hindrance of the substrates. It was found that the reactivity strongly decreased with increasing steric hindrance, when an (*E*)-disubstituted alkene [(*E*)-2-dodecene], a 1,1-disubstituted alkene (2-methyl-1-undecene), and a trisubstituted alkene (2-methyl-2-dodecene) were recovered in high yields (99%, 95%, 97%) after 24h. The reaction also showed high tolerance for other functional groups including benzyl ethers, silyl ethers as well as tertiary amine, ester, and amide groups.[12,29,33]

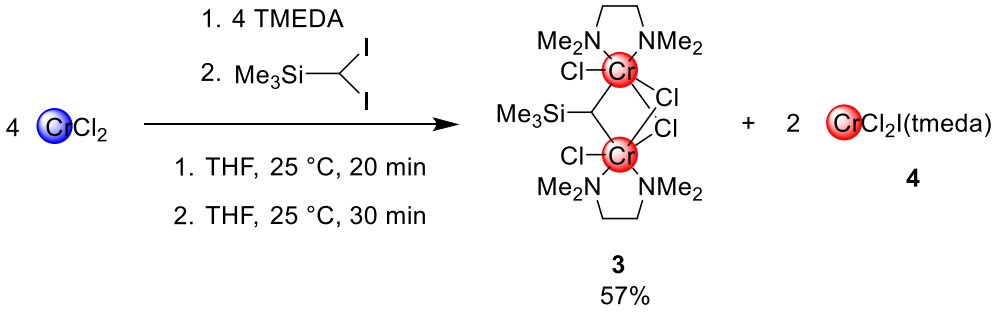

Scheme A4. Reaction of $CrCl_2$ with TMEDA and $SiMe_3CHI_2$ to **3** as published by TAKAI in 2003.[12]

Several years later, TAKAI *et al.* were able to identify and characterize the reactive compound $[Cr_2Cl_4(\mu_2\text{-}CHSiMe_3)(tmeda)_2]$ (**3**) generated by the reaction of four equivalents of $CrCl_2$, four equivalents of TMEDA and one equivalent of $SiMe_3CHI_2$ in THF at 25 °C in 57% yield

(Scheme A4).[13] This discovery marked the first fully characterized active species derived from a reaction corresponding to the original TAKAI reagent. Isolation of **3** was achieved due to the stabilizing properties of the diamine ligand and reduced reactivity induced by a bulky -$SiMe_3$ ligand on the reactive center. Compound **3** shows controllable reactivity through addition of TMEDA to silyl-cyclopropanated compounds or the exclusion thereof to silyl-substituted alkene products. The reaction also revealed the generation of $CrCl_2I$(tmeda) (**4**) as a side product, indicating a stepwise reaction through two single-electron transfers. This reactivity has been described and studied for Cr^{2+} reductions in the past and further explains the need for high amounts of $CrCl_2$ in similar reactions (Scheme A5).[34]

The first step in this mechanism is the attack of chromium(II) chloride on one iodine ligand with the subsequent transfer to the chromium atom, generating an alkyl-diiodido radical and one equivalent of $Cr^{III}Cl_2I(thf)_3$. The second step involves a second equivalent of chromium(II) chloride reacting with the alkyl radical to form the Cr–C bond. The first step of this sequence is the rate-determining step.[28]

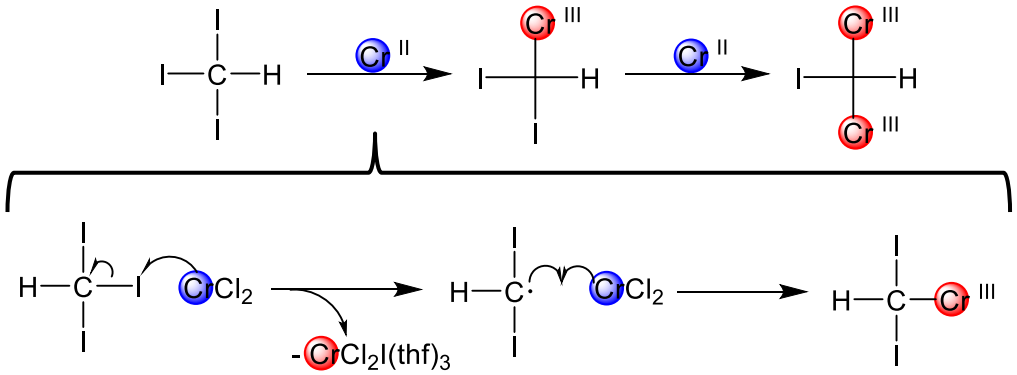

Scheme A5. Top: Schematic reaction of CHI_3 with Cr^{II} salts. Bottom: First step of the single electron transfer mechanism of the reduction of iodoform with $CrCl_2$ as described by TAKAI in 2004.[28]

Until 2018, the structure of the active species of the original reaction was never structurally characterized. WERNER *et al.* published the X-ray crystal structure along with evidence for the reactive pathway of the original compound by showing similar reactivity in siloxide stabilized Cr^{III}-(μ_2-CHI) compounds.[26] It was shown, that in fact the dichromium monohalido-methylidene **2**, as suggested by TAKAI in 1986, was the active species. Further evidence for the reductive formation mechanism over a two-step single-electron transfer was the characterization of $CrCl_2I(thf)_3$ as side product of the original reaction by X-ray crystallography. By addition of four equivalents of $KOSi(O\mathit{t}Bu)_3$ during the formation of **2** it was possible to confirm the formation of $[Cr_2Cl_2\{OSi(O\mathit{t}Bu)_3\}_2(\mu_2\text{-CHI})(thf)_4]$ (**5**) in small

amounts. It was not possible to generate compound **5** by direct reaction of $[Cr\{OSi(OtBu)_3\}_2]_2$ with 1/3 equivalents of CHI_3 in THF, which gave only oxidation to trivalent $[Cr\{OSi(OtBu)_3\}_2I(thf)_3]$. It was shown, that reaction of $[Cr\{OSi(OtBu)_3\}_2]_2$ with either 1 or ½ equivalents of CHI_3 in C_6D_6 resulted in the generation of the di-iodo-methanide species $[Cr^{II/III}_2I_2\{OSi(OtBu)_3\}_2(CHI_2)]$ (**6**) and the iodide species $[Cr^{II/III}_2\{OSi(OtBu)_3\}_4I]$ (**7**), both showing mixed valency of the involved chromium (Scheme A6). Compound **6** is further supporting evidence for the possibility to alter the structure of Cr^{III}-(μ_2-CHX) type compounds through use of different solvents and additives in TAKAI-like reactions. Furthermore, investigation of the reactivity of **6** with PhCHO in THF gave (Z)-iodostyrene in approximately 60% yield, exhibiting opposite selectivity to the original compound **2**. Until then, (Z)-selectivity of this reaction has only been discovered in the reaction of 6-chlorosalicylaldehyde under standard TAKAI conditions as published by GEDDIS *et al*. in 2017.[35]

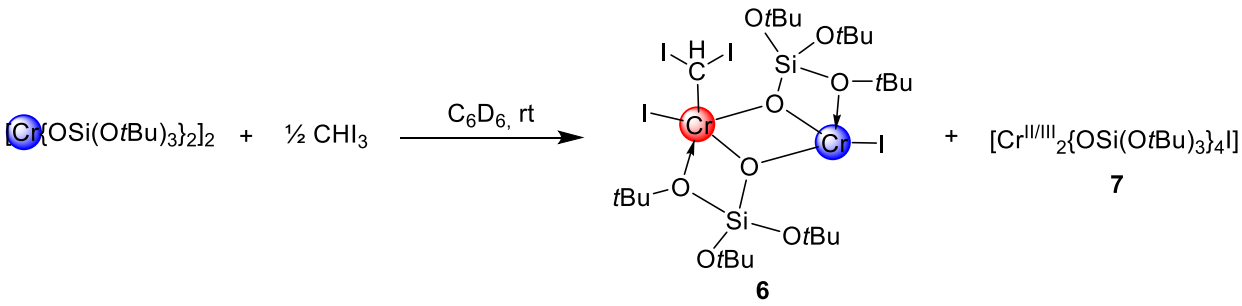

Scheme A6. Reaction of $[Cr\{OSi(OtBu)_3\}_2]_2$ and CHI_3 to **6** and **7** as published by WERNER *et al.* in 2018.[26]

WERNER *et al*. were also able to show that the addition of ½ equivalents of CHI_3 to $[Cr\{OSi(OtBu)_3\}_2(tmeda)]$ in C_6D_6 resulted in the formation of zwitterionic $[Cr\{OSi(OtBu)_3\}_2(tmeda\text{-}CHI)][I]$ (**8**) and $[Cr\{OSi(OtBu)_3\}_2I(tmeda)]$. This result suggests a nucleophilic attack of TMEDA on the CHI_2 moiety and subsequent loss of one iodido ligand followed by insertion of TMEDA into the Cr-CHI bond (Scheme A7). This research regarding diversified TAKAI-like reactions helps not only to understand the role of TMEDA itself in similar systems, but further illuminates the versatile reactivity of chromium-methanide and methylidene compounds.

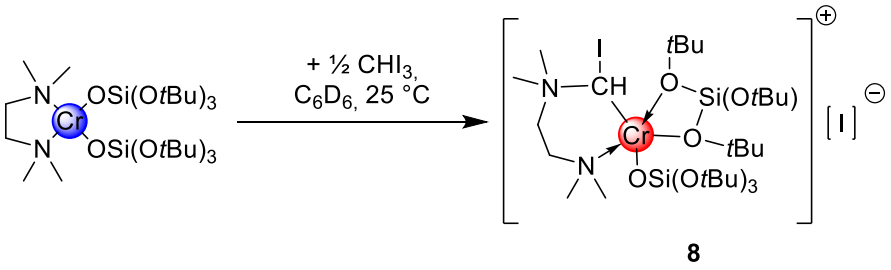

8

Scheme A7. Generation of **8** from CHI_3 and [Cr{OSi(O*t*Bu)$_3$}$_2$(tmeda)] in C_6D_6.[26]

In 2020 and simultaneously to this work, KUROGI *et al.* were able to generate $[CrCl(thf)_2]_3(\mu_3\text{-}CCl)(\mu_2\text{-}Cl)_3$ (**9**) through reaction of CCl_4 with six equivalents of $CrCl_2$ in THF at 0 °C in 86% yield. In the process of isolation of **9**, it was also possible to isolate $[CrCl(thf)_2)]_3(\mu_3\text{-}CH)(\mu\text{-}Cl)_3$ (**10**) in small amounts. **9** was characterized and investigated regarding reactivity while, **10** was not completely characterized and only commented on in the Supporting information.[36]

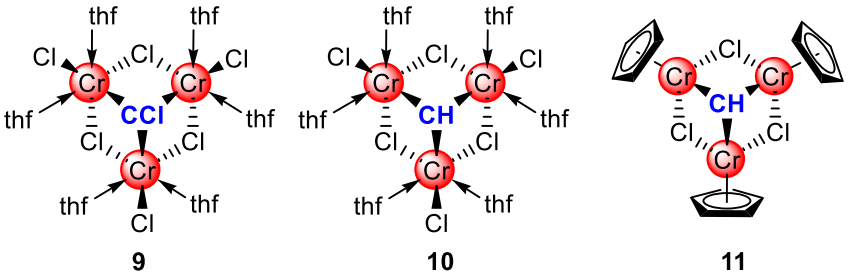

9 **10** **11**

Figure A1 Structure of **9** KUROGI 2021; **10** KUROGI 2021 discovered simultaneous to this work, **11** RICHESON 1986.[36,37]

The generation of **9** signifies the third step in the $CrCl_2/CX_4$ system, with **10** being the ultimate step in the original TAKAI $CrCl_2/CHX_3$ procedure. Isolation and characterization of these compounds enables research of their reactivity for the first time. The overall structure is comparable with the trinuclear chromium(III) methylidyne compound $[Cp_3Cr_3(\mu_2\text{-}Cl)(\mu_3\text{-}CH)]$ (**11**) isolated by RICHESON et. al. in 1986. For a long time, **11** was the only known Cr^{III} methylidyne compound and was never researched regarding reactivity or properties. Compound **11** was generated by heating $[CpCrMe(\mu_2\text{-}Cl)]_2$ (**12a**) in toluene to 60 °C for several hours with a yield of 23%. Throughout the heating, the evolution of methane, ethane and ethylene was observed. When compound **12a** and $[CpCrEt(\mu_2\text{-}Cl)]_2$ (**12b**) were reacted with nucleophiles (PPh_3, py, Cl^-) the dimers were readily cleaved to compounds [CpCrRCl(L)] (R = Me, Et, L = PPh_3, py, Cl) (**13**) (Scheme A8).[37]

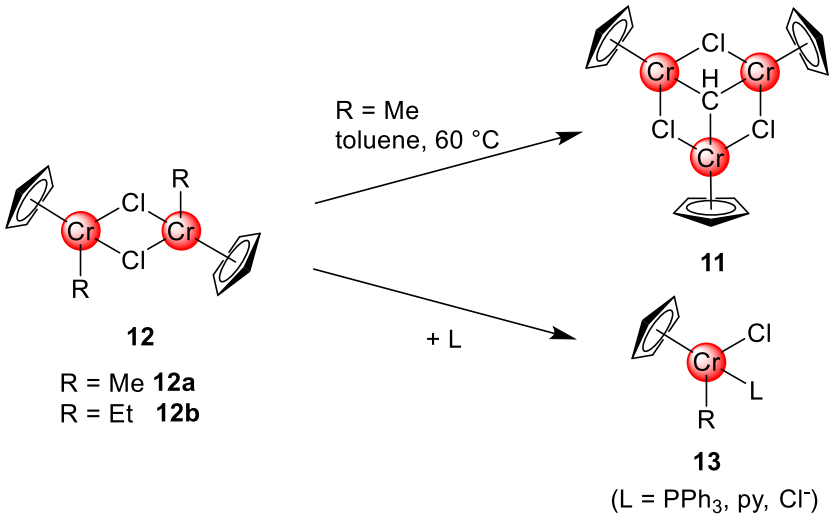

Scheme A8. Generation of **11** from **12a**. Reaction of **12a** and **12b** with nucleophiles to monomeric **13**.[37]

3 Chromium(II) Siloxides as Precursors for TAKAI-like Reactions

In order to shed light on the structure, formation and reactivity of the TAKAI reagent, siloxy ligands in the form of [OSi(O*t*Bu)$_3$] proved to be a key strategy for the isolation of highly reactive chromium iodo-methanide (Cr-CHI$_2$) and bridging iodo-methylidene (Cr^{III}-μ$_2$-CHI-Cr^{III}) species.[26] Siloxy ligands have been extensively studied in transition metal chemistry and also to support lanthanide complexes.[38,39] By introducing siloxy ligands, solubility issues of highly polar inorganic compounds (such as CrCl$_2$) can be circumvented, enabling reactions in solvents of lower polarity (e.g. *n*-hexane, *n*-pentane and toluene).[40,41] Solvent polarity as well as donating properties of solvents and ligands have been studied regarding their influence on reaction acceleration and increasing the reductive capabilities of Cr^{II} compounds.[6] The findings clearly indicate that a higher solubility of Cr^{II} salts also increases the reactivity in reductions. Donating ligands such as ethylenediamine, TMEDA, TEEDA, DMF and THF have been investigated and shown to increase and in some cases immensely alter the reactivity of Cr^{II} compounds.[6,28,30,42] Even though siloxy ligands in the form of -OSiR$_3$ (R = Ph, *t*Bu, (O*t*Bu)$_3$) have also been shown to stabilize Cr^{II} complexes, only a small number of compounds have been structurally characterized and studied. The heteroleptic tetrameric complex [Cr(μ$_2$-Cl)$_4$(μ$_2$-OSi*t*Bu$_3$)]$_4$ (**14**, Figure A2) was synthesized and characterized in 2005 by SYDORA *et al.* The reaction of CrCl$_2$ with 0.73 equivalents of Na(silox) (silox = OSi*t*Bu$_3$) in THF produced the putative *trans*-(*t*Bu$_3$SiO)CrCl(THF)$_2$ which, after subsequent thermolysis gave **14** in good yield. When reacted with Na(silox), **14** gave the ate complex [(*t*Bu$_3$SiO)Cr(μ$_2$-OSi*t*Bu$_3$)$_2$]Na·C$_6$H$_6$ (**15**).[43] SYDORA *et al*. also published the structure of the dimeric [(*t*Bu$_3$SiO)Cr]$_2$(μ-OSi*t*Bu$_3$)$_2$] (**16**, Figure A2) in 2006.[44] Compound **16** was generated by the reaction of CrCl$_2$ with 1.5 equivalents of Na(silox) in THF and showed an interesting geometry described as “butterfly dimer containing pseudo-trigonal chromous centers”.[44] In 2011, QIU *et al*. were able to isolate and characterize Cr$_2$(OSiPh$_3$)$_2$(μ-OSiPh$_3$)$_2$(thf)$_2$ (**17**, Figure A2) in a reaction of CrCl$_2$, HOSiPh$_3$ and NaH in THF at 60 °C in good yield.[45]

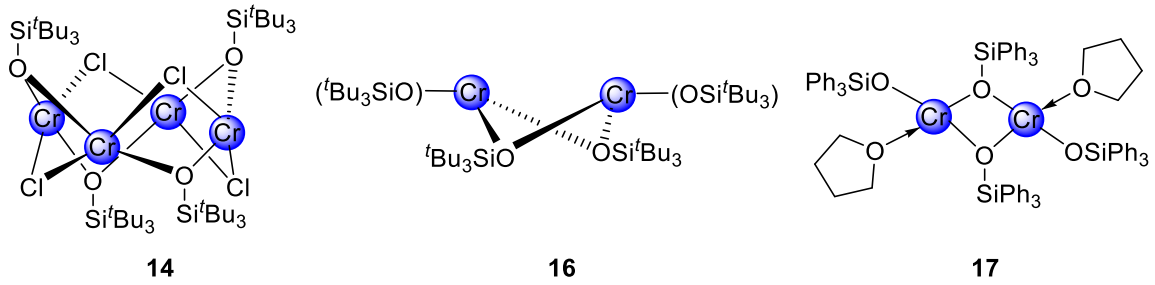

14 **16** **17**

Figure A2 Examples of known Cr^{II} siloxide complexes **13**, **16** and **17**.

Siloxy ligands are known and studied in a wide variety of steric bulk ($OSiMe_3$, $OSi\textit{i}Pr_3$, $OSiEt_3$, $OSi\textit{t}Bu_3$, $OSiPh_3$, $OSi(O\textit{t}Bu)_3$). Through selection of the right size of ligand, it is possible to guide the geometry of complexes from multimetallic molecules to monomers.[39,41,46]

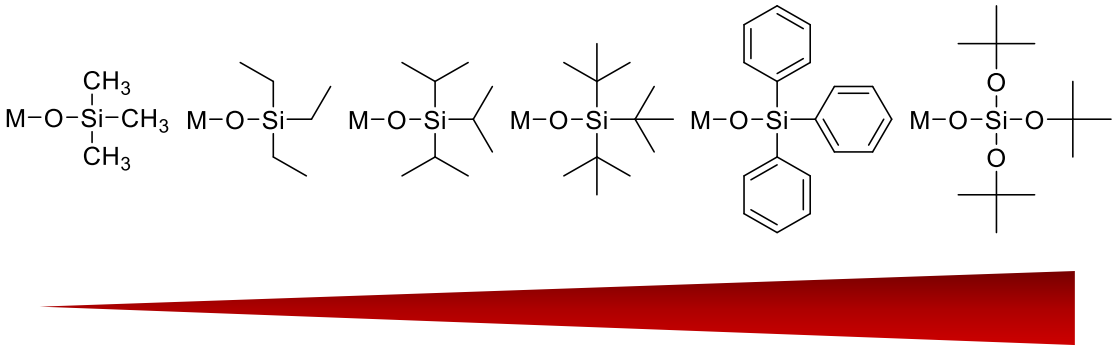

Figure A3. Sterical hindrance of selected siloxy ligands in increasing order from left to right.

Three different bonding modes can be described for siloxy ligands in transition metal siloxide complexes of the type $M[OSi(OR)_3]_x$, enabling multidentate bonding modes, capable of further stabilizing compounds. First, monodentate bonding *via* the oxygen atom as terminal ligands (Type 1), as a bridging μ_2-$OSi(OR)_3$ ligand with dative donation to a second metal center (Type 2) and multidentate coordination involving the *tert*-butoxy groups of the ligand (Type 3).[47] Examples for the different bonding types 1 and 2 are abundant (e.g, compounds **14**, **16** and **17**), but scarce for type 3. In 1990 MCMULLEN *et al.* were able to characterize the compound $Na_3(\mu_3\text{-}I)[Ni\{\mu_3\text{-}OSi(O\textit{t}Bu)_3\}_3I]$ (**18**, Scheme A10) representing an example of a more exotic multidentate bonding of the $OSi(O\textit{t}Bu)_3$ ligand to a transition metal (Scheme A9).[48]

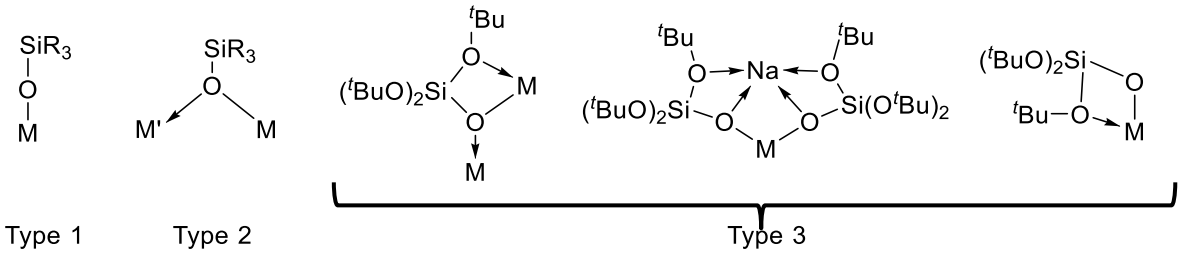

Scheme A9. Schematic display of different $OSiR_3$ and $OSi(OtBu)_3$ bonding modes and capabilities confirmed by structurally characterized complexes. (M = transition metal, rare earth metal)[41,49,50]

An example of a chromium compound including this bonding mode of the $OSi(OtBu)_3$ ligand is $[Cr\{OSi(OtBu)_3\}_2]_2$ (**19**, Scheme A10) generated from $[Cr\{N(SiMe_3)_2\}_2(thf)_2]$ and $HOSi(OtBu)_3$ in *n*-pentane at 25 °C in good yield. This compound was characterized by CONLEY et al. in 2014 in search of olefin polymerization catalysts.[51] Reacting **19** with N_2O generated compound **20** (Scheme A10). Further examples were found in the search for the structure of the TAKAI reagent by WERNER et. al.[26]

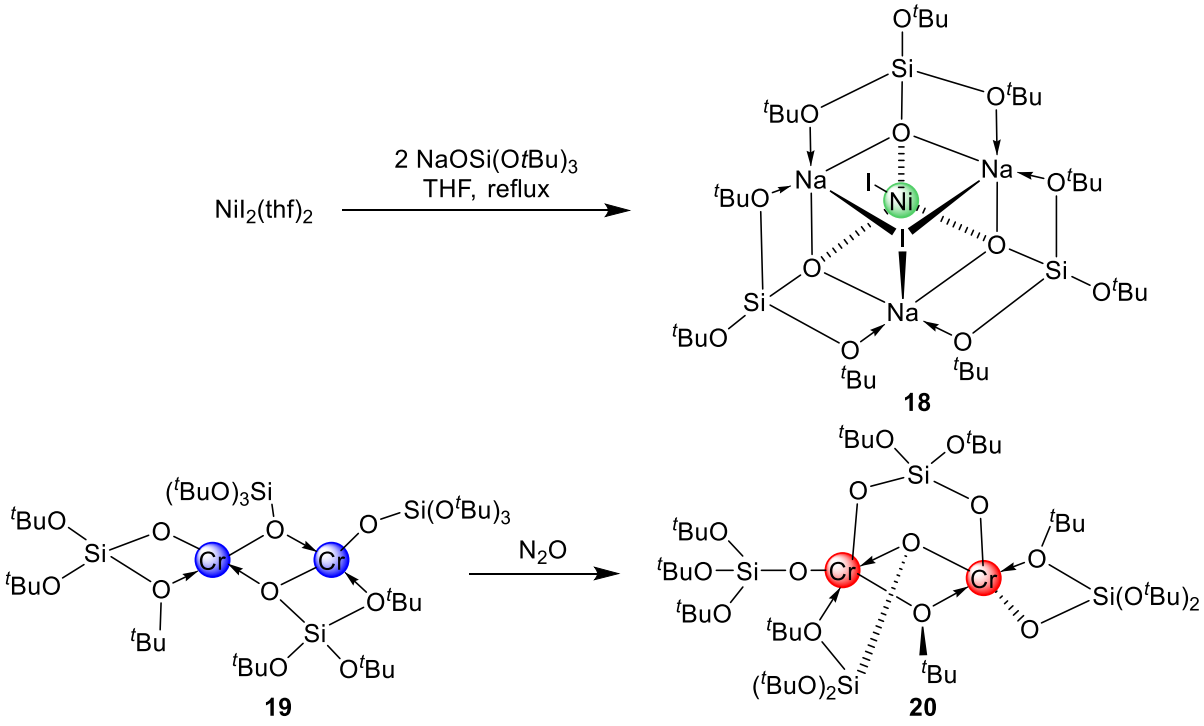

Scheme A10 Reaction of $NiI_2(thf)_2$ to **18** (top).[48] Reaction of **19** with N_2O to compound **20** (bottom).[51]

4 Molybdenum and Tungsten in the KAUFFMANN Reaction

4.1 Generation of Starting Materials: The Reactivity of $MoCl_5$ and WCl_6 with Ethers and Silylethers

The precursors for the KAUFFMANN reagents are mostly chlorides, oxy-dichlorides or dioxy-dichlorides of the form MO_xCl_y (M = Mo, W; x = 0-2; y = 2-6). These compounds can be generated through a variety of reactions. Direct reactions of molybdenum compounds with O_2 or $SOCl_2$ are feasible. On the laboratory scale, reactions of $MoCl_5$ or WCl_6 with ethers or silyl ethers are more viable.[52,53] These reactions have been extensively studied and their mechanism was partially explained.[54,55] Direct reaction of $MoCl_5$ with THF in aliphatic solvents or DCM produces $MoOCl_3(L)_x$ compounds (Scheme A11).[54] Problematic for reactions of this kind are the generated side products and impurities remaining in the product. This outcome can be circumvented by recrystallization or sublimation. Reactions of $MoCl_5$ with 1-2 equivalents of HMDSO (hexamethyldisiloxane) were shown to produce high purity $MoOCl_3(L)_x$ compounds by directly eliminating Me_3SiCl, through ether cleavage.[53] As the generated Me_3SiCl is volatile, application of vacuum leads to good yields of high purity products.

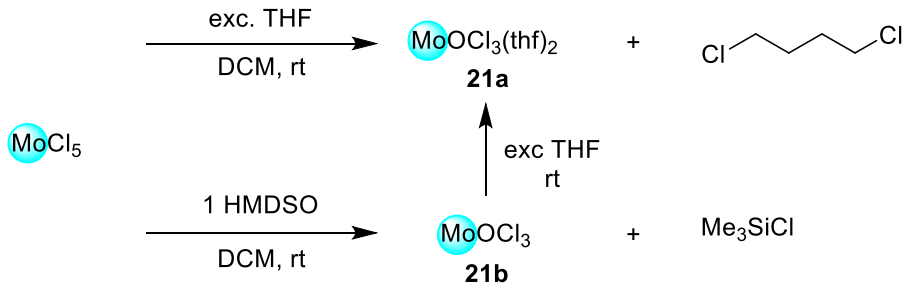

Scheme A11. Reaction of $MoCl_5$ to $MoOCl_3(thf)_2$ (**21a**) and $MoOCl_3$ (**21b**).[54]

For tungsten oxychlorides, the same reactions can be applied to generate $WO_xCl_y(L)_z$ (x = 1-2, y = 2-6, z= 1-2) compounds. Starting from WCl_6, the reaction with 1 equivalent of HMDSO in DCM generates $WOCl_4$ in good yield and high purity. Further reaction of $WOCl_4$ with another equivalent of HMDSO generates WO_2Cl_2 in good yield (Scheme A12). Addition of donating solvents or bidentate ligands produces the corresponding $WO_xCl_y(L)_z$ complexes.[53] Reactions of WCl_6 in cyclohexane with excess of THF lead to $WOCl_3(thf)_2$ in good yield and purity.[56]

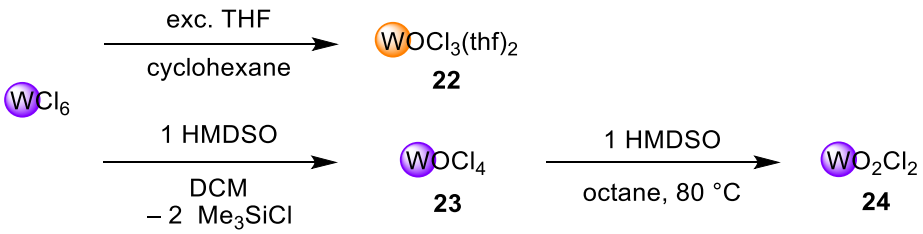

Scheme A12. Conversion of WCl_6 to $WOCl_3(thf)_2$ (**22**), $WOCl_4$ (**23**) and WO_2Cl_2 (**24**).

Furthermore, these complexes show the ability for subsequent ligand introduction or exchange.[57] $MO_2Cl_2(dme)$ (M = Mo, W) is directly accessible by reactions of MO_2Cl_2 with DME in DCM and can therefore be used as starting material for $MO_2Cl_2(tmeda)$ which is not directly accessible due to reduction.[58]

The Kauffmann Reaction

The KAUFFMANN reaction was first mentioned in 1983 and over the next years continuously studied.[25,59] Molybdenum or tungsten precursors of the form $MO_xCl_y(L)_z$ (M = Mo, W; x = 0-2; y = 2-6, z = 1-2) were reacted with alkylation reagents (MeLi, $AlMe_3$, $LiCH_2SiMe_3$) to generate a thermolabile alkylidene intermediate as the putative active species. Related tungsten and molybdenum carbenes have been intensively studied in the past, due to their applicability in olefin metathesis.[60,61] The formation and reaction mechanisms concerning these compounds were thoroughly investigated as molecular or surface-stabilized complexes.[62] Molybdenum and tungsten were shown to support a broad spectrum of reactions with alkylating reagents, with a multitude of characterized high oxidation state carbenes and carbynes.[61,63] The active species of the KAUFFMANN olefination were described as compounds with either terminal alkylidene groups or dimeric alkylidene-bridged complexes (Scheme A14).[64] The suggested terminal $M{=}CH_2$ theory was later dismissed due to different reactivity compared with SCHROCK carbenes and "replaced" by putative methyl compounds as intermediates.[24] The definite proof for the involvement of μ_2-CH_2 bridged molybdenum and tungsten compounds in these reactions has to this day not been accomplished through a solid state structure. A rare example for this coordination incorporating a μ_2-CH_2 bridge is the tungsten compound $(\eta_5\text{-}C_5Me_5)_2W_2O_2(\mu_2\text{-}CH_2)_2$ reported by GUZYR in 2000.[65] In the KAUFFMANN reaction reported in 1986, two equivalents of MeLi were reacted with $WOCl_3(thf)_2$ (**22**) in THF at −70 °C to produce thermolabile compounds which eliminate CH_4 upon heating to around 20 °C. This heating step, which was described as heating up to 80 °C in some experiments, generates the complexes active in carbonyl olefinations of aldehydes and ketones.[64]

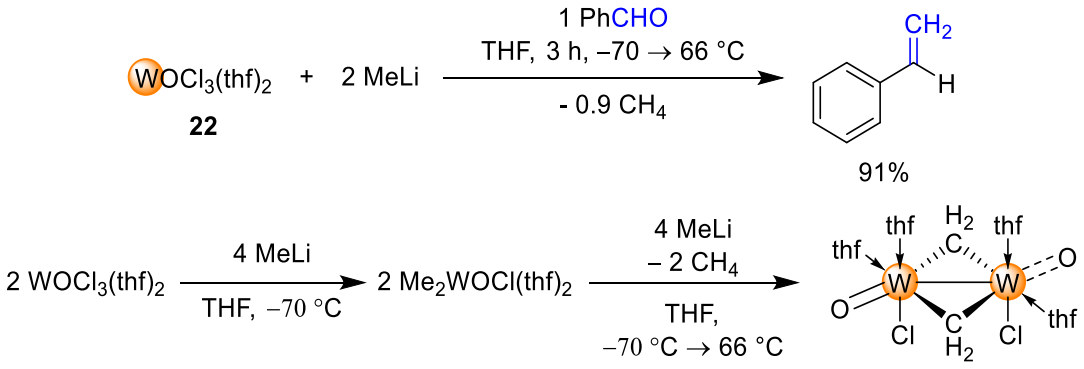

Scheme A13. Top: Original olefination with the KAUFFMANN reaction as published in 1986 by KAUFFMANN et al. Bottom: Schematic depiction of the formation mechanism of the reagent generated from $WOCl_3(thf)_2$ and MeLi. [24,64]

For molybdenum compounds, heating to 20 °C was sufficient to generate the active species, for tungsten compounds, heating to 45 °C was sufficient in some cases.[24] Below the temperature at which CH_4 was generated, compounds synthesized from $MoOCl_3$, $WOCl_3$ and $WOCl_4$ were not able to olefinate aldehydes and ketones. The reactions can be carried out in various solvents (THF, Et_2O, chlorobenzene, toluene, cyclohexane, and *n*-pentane). Compounds that are not coordinated by relatively strongly donating solvents like THF and Et_2O are able to react with C=C double bonds and allylic protons. These reactions either outperform the olefination or are secondary reactions following the olefination.[24,66] The compounds were not structurally characterized due to the high lability at elevated temperatures, but thoroughly investigated by NMR experiments. It was found that the signal for MeLi (δ = -1.98) could no longer be detected shortly after the start of the reactions. Two singlets were detected for each reagent generated from $MoCl_3(thf)_2$, $WOCl_3(thf)_2$ and $WOCl_4$ with two equivalents of MeLi (δ = 0.96/0.79, 0.92/0.69, and 0.95/0.73 ppm) indicating metal-bound methyl groups. These signals disappeared again when the temperature was raised, and peaks in the region of methane (0.23 ppm) emerged.[24] Upon addition of aldehydes and ketones, the ^1H and ^{13}C signals indicative of Mo and W cyclobutane complexes disappeared. Signals clearly indicating terminal CH_2 groups were not detected, but the observation of multiply coupled doublets in the δ = 9 – 11 ppm region in the ^1H spectrum (close to the signals typical for terminal CH_2 ligands) led to the assumption of putative interactions of one of the μ_2-CH_2 alkylidene protons with a donating THF ligand or bonded oxygen. This assumption was supported by various 1D and 2D (^1H and ^{13}C, DEPT) NMR experiments and the direct comparison with the μ_2-CH_2 signals detected in reactions of $WOCl_4$ with two equivalents of MeLi (3.5 ppm) and the signals for terminal $=CH_2$ found in $[(Me_3P)_2Cl_2(O)W=CH_2)]$ (12.34 and 11.47 ppm).[67,68] Another observation was the generation

of 0.75 to 0.96 μ_2-CH_2 ligands per generated molecule of CH_4 in these reactions.[24] The presence of metal-metal bonds in complexes generated from Mo(V) and W(V) chlorides with two equivalents of MeLi is suggested due to the diamagnetic behavior of the reaction mixtures. High instability of the compounds generated in these reactions made the isolation nearly impossible.

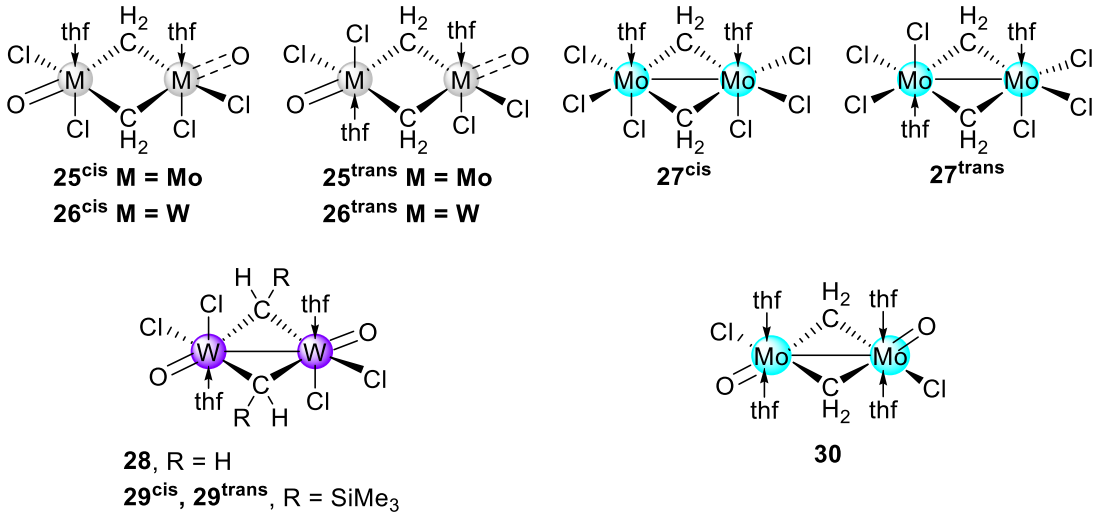

Scheme A14. Proposed structure of KAUFFMANN reagents generated by reaction of $MoOCl_4$ (**25**$^{cis/trans}$), $WOCl_4$ (**26**$^{cis/trans}$) or [Mo_5Cl_{10}] (**27**$^{cis/trans}$) with two equivalents of MeLi in THF (top). Proposed structure of compounds generated from $WOCl_3$ and two equivalents of MeLi (**28**) or $LiCH_2SiMe_3$ (**29**$^{cis/trans}$) and from $MoOCl_3(thf)_2$ and two equivalents of MeLi (**30**) (bottom).[24]

The formation of the various KAUFFMANN reagents generated with MeLi is thought to proceed *via* thermolabile intermediate M-CH_3 compounds which eliminate CH_4 upon temperature increase to generate the alkylidene (μ_2-CH_2) bridges.[24] The form of the complexes generated from Mo/W precursors and $AlMe_3$ is expected to be slightly more intricate. These compounds consist of coordinating $AlMe_x$ and coordinating oxygen ligands (Scheme A15). In reactions of $MoOCl_3$ or MoO_2Cl_2 with $AlMe_3$ in THF at –70°C, a different monomeric form of olefination reagent is generated. Crucial to this reaction is the addition of $AlMe_3$ at –70 °C to circumvent direct reaction of THF and $AlMe_3$. NMR experiments showed paramagnetic properties, therefore leading to the assumption of monomeric Mo and W complexes shown in Scheme A15. Other differences to the reagents generated from MeLi were described as well.[6] During the formation, roughly two equivalents of CH_4 were generated. The reagents showed high sensitivity to protons and were not suitable for reactions with hydroxy ketones, and lastly, the reagents showed similarities to the TEBBE reagent as their carbonylating activity could be

increased by adding bases like HMPA (HMPA = hexamethylphosphoric triamide) to the reaction mixtures.[4]

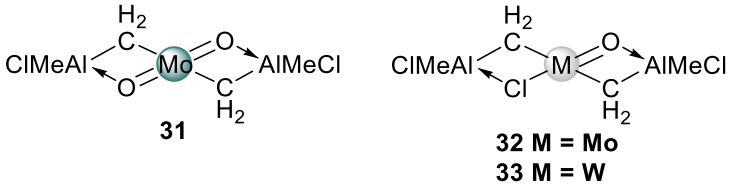

Scheme A15. Proposed structure of KAUFFMANN reagents generated by reaction of MoO_2Cl_2 (**31**) (left) or $MOCl_3(thf)_2$ (**32**) / $WOCl_3(thf)_2$ (**33**) and two equivalents of $AlMe_3$ (right).[4,27]

Reactions of ($MoCl_5$/Mo_2Cl_{10}) or $WOCl_3$ with two equivalents of $LiCH_2SiMe_3$ in THF at 20 °C and subsequent reaction with PhCHO only yielded low amounts of the olefination products, supposedly impeded by (single and double) α-H elimination and therefore generation of mixtures (alkylidene and alkylidyne compound) in comparison to the reaction with MeLi.[24,69]

Reactions of the active species with aldehydes or ketones is suggested to proceed *via* a cycloaddition cycloelimination mechanism shown in Scheme A16. This mechanism was suggested due to the high aldehyde selectivity of the studied compounds.[70]

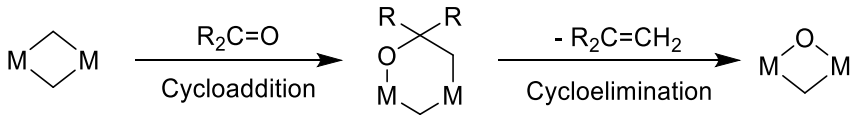

Scheme A16 Schematic depiction of the suggested mechanism of the KAUFFMANN olefination of aldehydes and ketones.[70]

For a long time, these reagents were not used in organic syntheses, but were recently applied to synthesize two natural products. SPRITZNER et al. used the reaction in the selective methylenation of precursor compounds to (+)-Axenol und (-)-Gleenol in 2002. The synthesis exploited the selectivity of the reagent and its low basicity as shown in Scheme A17.[16,17] Since 2002, many other applications of the KAUFFMANN reagents have been described.[18–20] As many multi-step syntheses require intense studies to find the most reliable/efficent reactions, these compounds have found their place in the repertoire of organic chemists.[21,22]

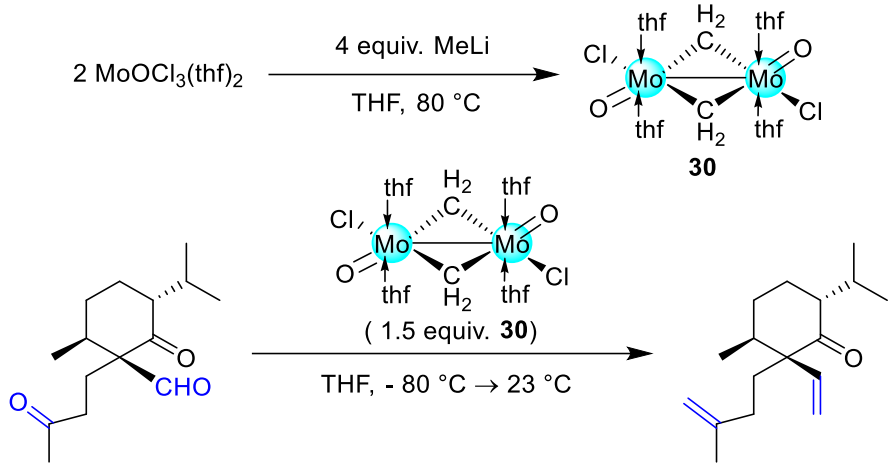

Scheme A17. Kauffmann reaction in the synthesis of (+)-Axenol as incorporated by SPRITZNER et al in 2002.[16]

Further applications of tailor-made KAUFFMANN reagent include highly selective mono-methylenation reactions. This reaction enables the selective methylenation in dialdehydes, diketones and triketones. By utilizing the reagent generated from two equivalents of MeLi and $MoOCl_3$ it was possible to selectively mono methylenate thiophen-2,5-dicarbaldehyde (**34a**) and 1H-pyrrol-2,5-dicarbaldehyde (**34b**). The reaction was also shown to selectively react with only one of the three carbonyl groups of triketones (e.g. reaction of 1H-indene-1,2,3-trione **35** with compound **30**) *via* a suggested quasi aromatic intermediate complex (**36**, Scheme A17).[24]

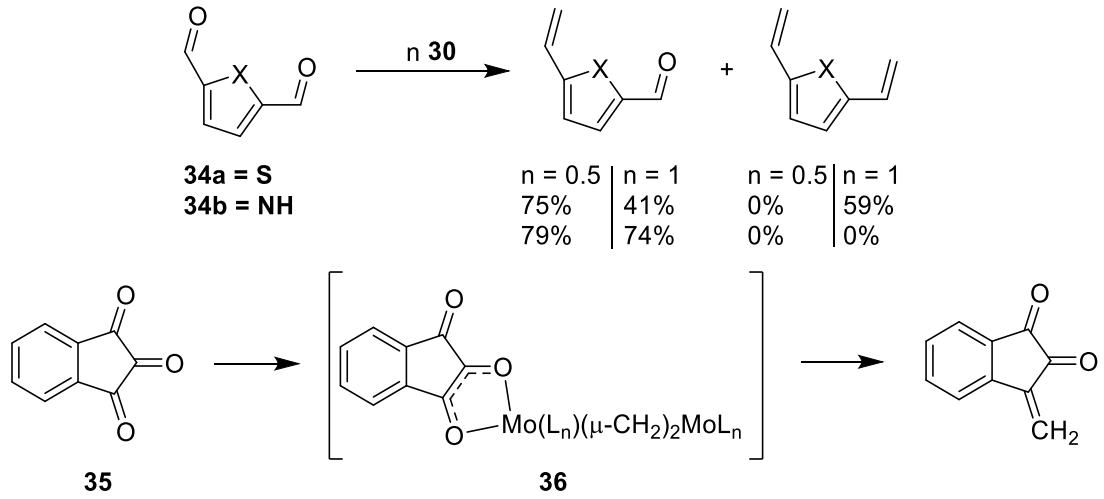

Scheme A18. Schematic depiction of the mono methylenation of **34a**, **34b** and **35** *via* the putative pseudoaromatic intermediate (**36**).[24]

These applications showcase the high selectivity through control of stoichiometries and selection of the right compound. Other possible applications are the methylenation of base-

sensitive ketones, methylenation in protic solvents and aldehyde/ ketone selective olefination.[24]

B

Summary of the Main Results

1 Synthesis, Derivatization and Characterization of Chromium(III) Alkylidynes

Chromium(III)-alkyl compounds are mainly generated over two routes. Transmetalation is the main approach to synthesize various organochromium compounds by reaction of common transmetalation reagents (Organolithium, GRIGNARD etc.) with pertinent chromium precursors. The TAKAI olefination reagent is accessed *via* the reduction of organic halides with $CrCl_2$ (Scheme B1).[28]

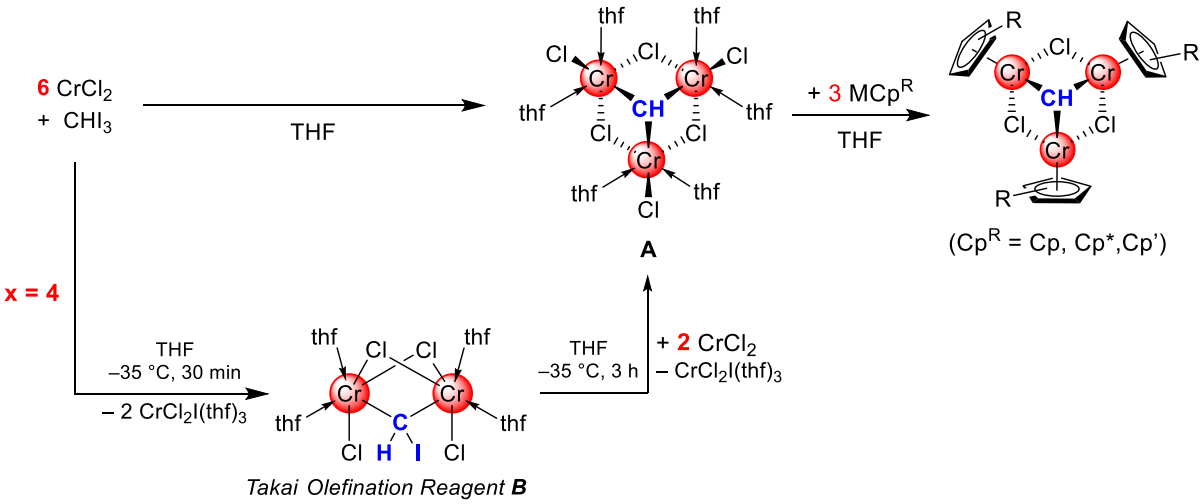

Scheme B1. Reaction of $CrCl_2$ and CHI_3 in different stoichiometries to either the TAKAI reagent or **A** together with the further derivatization by reaction with MCp^R compounds.

Reactions of $CrCl_2$ with CHI_3 in THF at −40 °C were shown to generate $[Cr_3(\mu_2\text{-}Cl)_3(\mu_3\text{-}CH)(thf)_6]$ **A** in up to 70% compound yield (*vide supra*). This compound has been published by TAKAI in 2021 as a side product, simultaneously to the findings of this work.[36] High sensitivity of this reaction to temperature and solvent made the optimization of this synthesis crucial. Even trace amounts of impurities in used solvents or starting materials led to the generation of various side products when targeting **A**. Identified side products were the related compounds $Cr_4Cl_4I_2(thf)_4$ (**C**$^{\mathbf{a}}$) and $Cr_4Cl_4I_2(thp)_4$ (**C**$^{\mathbf{b}}$) (Figure B1 and B2). Interestingly, compound **C**$^{\mathbf{b}}$ displayed one Cr^{III} center with one terminal iodido ligand in contrast to **C**$^{\mathbf{a}}$ with only Cr^{II} centers and bridging iodido ligands. Compound **A** was investigated regarding reactivity, stability and derivatisability (*vide infra*).

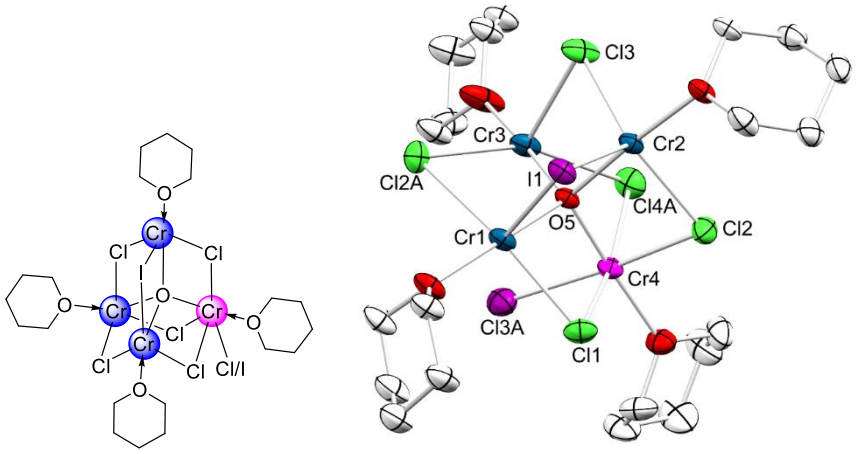

Figure B1. Chemdraw depiction (left) and crystal structure (right) of **C**[b], ellipsoids shown at 30% probability (**Paper I**).

Derivatization of **A** was achieved by reaction with three equivalents of sodium or lithium-cyclopentadienide compounds MR (R = C_5H_5, $C_5H_4SiMe_3$, C_5Me_5) (Scheme B1). $[(C_5H_5)_3Cr_3(\mu_2\text{-}Cl)_3(\mu_3\text{-}CH)]$ (**D**) has also been synthesized by RICHESON et al. in 1986 through decomposition of $[CpCr(\mu_2\text{-}Cl)Me]_2$ in toluene at 60 °C.[37] $[(C_5Me_5)_3Cr_3(\mu_2\text{-}Cl)_3(\mu_3\text{-}CH)]$ (**E**) and$[(C_5H_4SiMe_3)_3Cr_3(\mu_2\text{-}Cl)_3(\mu_3\text{-}CH)]$ (**F**) are new examples of this compound category involving Cr^{III}.

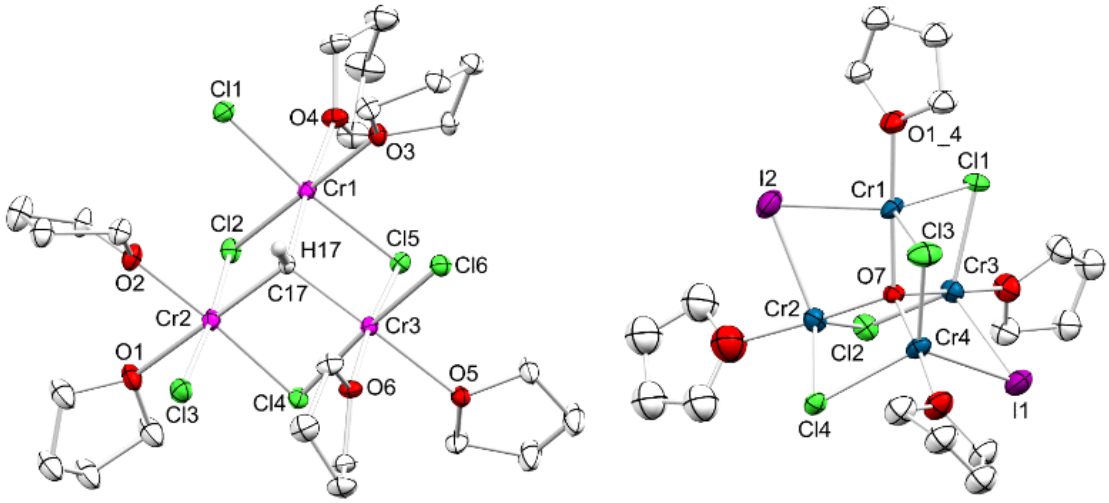

Figure B2. Crystal structures of $[Cr_3(\mu_2\text{-}Cl)_3(\mu_3\text{-}CH)(thf)_6]$ (**A**) and (**C**[a]) shown at 30% probability (**Paper I**).

Isolation of these compounds was impaired by decomposition of **A** *via* unknown pathways. Side products of these reactions contained high amounts of Cr^{II} compounds (e.g $Cr^{II}(Cp^R)_2$) leading to the assumption of a reductive pathway of decomposition. Other identified side

products of these reactions were Cp^*_2Cr, [(Cp*CrCl)(Cp*CrI)], [(Cp'$CrCl_3$)(Li(thf)$_2$] [Cp*$CrCl_2$(thf)], and $[CpCrCl]_2$. Compounds **E** and **F** were investigated regarding reactivity and stability, but unfortunately did not show the same reactivity as **A** with aldehydes or ketones. Compounds **E** and **F** show similar geometries with the core around the μ_3-CH moiety resembling a truncated triangle. Compound **E** is highly symmetric, compound **F** on the other hand shows slight asymmetry due to the multiple possible orientations of $CpSiMe_3$ ligands.

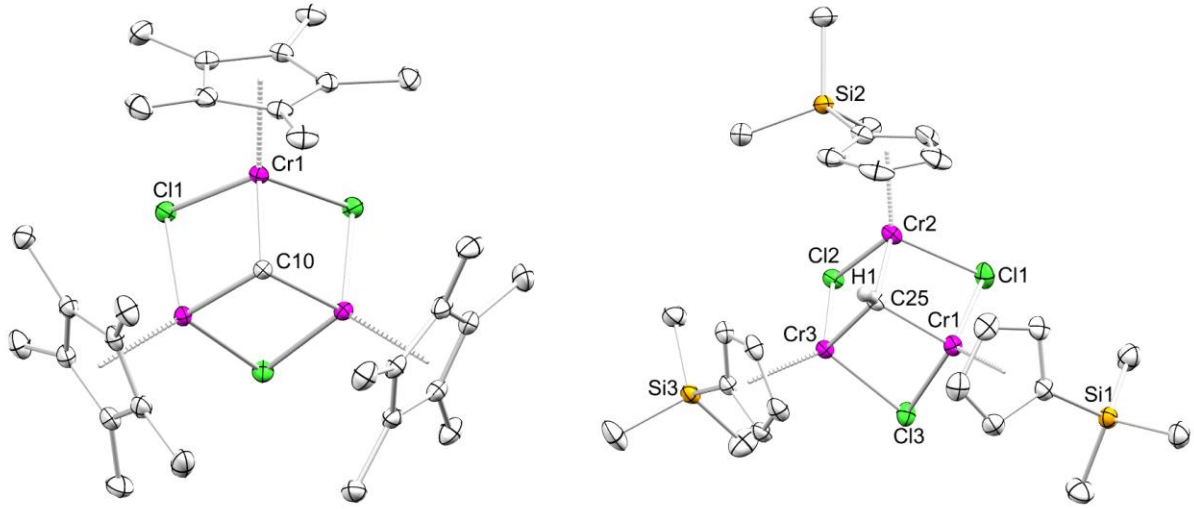

Figure B3. Crystal structures of [(C_5Me_5)$_3$$Cr_3$($\mu_2$-Cl)$_3$($\mu_3$-CH)] (**E**) and [($C_5H_4SiMe_3$)$_3$$Cr_3$($\mu_2$-Cl)$_3$($\mu_3$-CH)] (**F**), ellipsoids shown at 30% probability (**Paper I**).

The trinuclear half sandwich [Cr^{III}-μ_3-CH] compounds **D**, **E** and **F** also show interesting ^{1}H NMR spectra. Usually, the highly paramagnetic compounds cause a strong broadening of the ^{1}H resonances, but for these compounds, sharp signals were found. One signal of **D** was detected at 30.27 ppm, **E** shows a sharp singlet at – 5.8 ppm, **F** generates one signal at 0.49 ppm for the $SiMe_3$ groups and two signals at 30.39 and 35.35 ppm for the Cp protons (measured in THF-d_8). The newly generated compounds were also characterized by IR, UV/Vis and SQUID (SQUID = superconducting quantum interference device) magnetometer measurements. The composition and purity of the products was confirmed by microanalysis and the magnetic moment of solutions measured according to the Evans method. As the EVANS method only gives approximations of the real magnetic moments of these compounds, SQUID magnetometer measurements were conducted (Figure B4). These measurements revealed the high complexity of the magnetic coupling in these compounds. The magnetic moments at ambient temperature are shown in Table B1.

Table B1 Summary of measured magnetic moments with the EVANS method and SQUID magnetometer. (**a** = this work, **b** = literature measurement).[37]

Compound	μ_{eff} (EVANS)	μ_{eff} (SQUID)
$[Cr_3(\mu_2\text{-}Cl)_3(\mu_3\text{-}CH)(thf)_6]$ **A**	9.29 μ_B	9.11 μ_B
$[(C_5H_5)_3Cr_3(\mu_2\text{-}Cl)_3(\mu_3\text{-}CH)]$	3.19 μ_B[a] 3.58 μ_B[b]	-
$[(C_5H_4SiMe_3)_3Cr_3(\mu_2\text{-}Cl)_3(\mu_3\text{-}CH)]$	2.70 μ_B	-
$[(C_5Me_5)_3Cr_3(\mu_2\text{-}Cl)_3(\mu_3\text{-}CH)]$	3.63 μ_B	4.32 μ_B

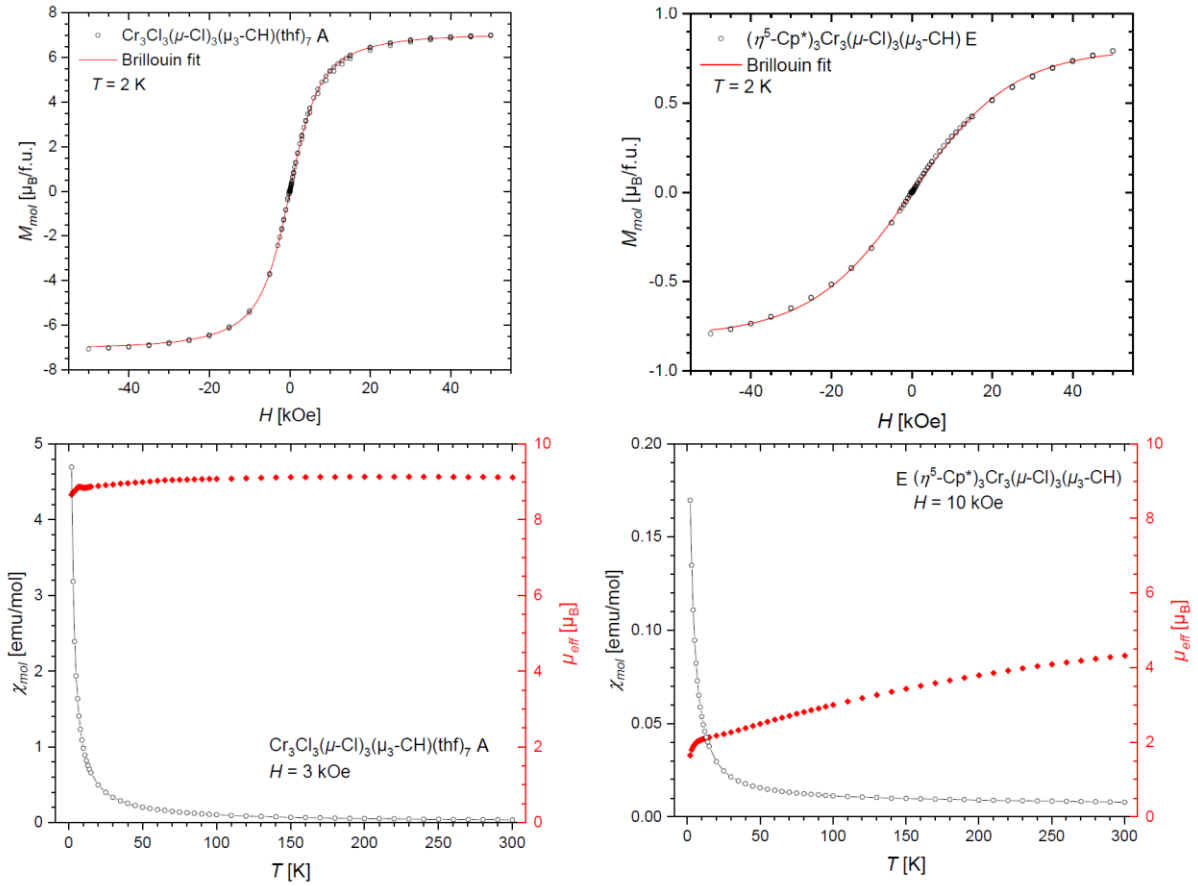

Figure B4. Top: Temperature-dependent molar magnetic susceptibility $\chi_{mol}(T)$ (black open circles; left ordinate) and effective magnetic moment $\mu_{eff}(T)$ (red filled diamonds; right ordinate) as obtained by SQUID magnetometric measurements on crystalline powder of **A** in an applied field H = 3 kOe. (for **E** H = 10 kOe). The $\chi_{mol}(T)$ data was corrected for diamagnetic contributions (**A**: $-7.243 \cdot 10^{-4}$ emu/mol; **E**: $-3.071 \cdot 10^{-4}$ emu/mol, calculated from Pascal's constants[71]), and a spin-only g factor of 2 was assumed in the calculation of $\mu_{eff}(T)$. Bottom: Field-dependent molar magnetization $M_{mol}(H)$ (black open circles) as obtained by SQUID magnetometric measurements on crystalline powder of **A** and **E** at a temperature T = 2 K. A fit of the data with a Brillouin function (red line; assuming a spin-only g factor of 2) yields a total spin quantum number S = 4.45(4) (**E**: S = 0.761(14)).

2 Reactivity of Chromium(III) Alkylidynes with Ketones and Aldehydes

Reactions of $[Cr_3(\mu_2\text{-}Cl)_3(\mu_3\text{-}CH)(thf)_6]$ (**A**) with aldehydes (benzaldehyde, pivalaldehyde) and ketones (cyclohexanone, benzophenone) were studied in THF-d_8 and monitored by ^1H and ^2D NMR experiments over several days and multiple heating steps. As these experiments only provided insufficient insight due to paramagnetic broadening and overlapping signals, samples were filtered over aluminum oxide to extract inorganic reaction products. This filtration made the observation of several organic moieties feasible, but the sheer number of signals still prevented clear identification of products. The measurement of generated product mixtures by GC/MS spectrometry (gas chromatography coupled with mass spectrometry) led to the discovery of several known organic products. Identified products of the reaction of **A** with one equivalent of benzaldehyde after 3 days in THF-d_8 at ambient temperature are shown in (Figure B5). When the same reaction of **A** in THF-d_8 was done with pivaldehyde, only 1-chloro-1,2,2-trimethyl-cyclopropane was identified as possible product by the software used to analyze the mass spectra. Other compounds could not be identified through ^1H NMR spectroscopy.

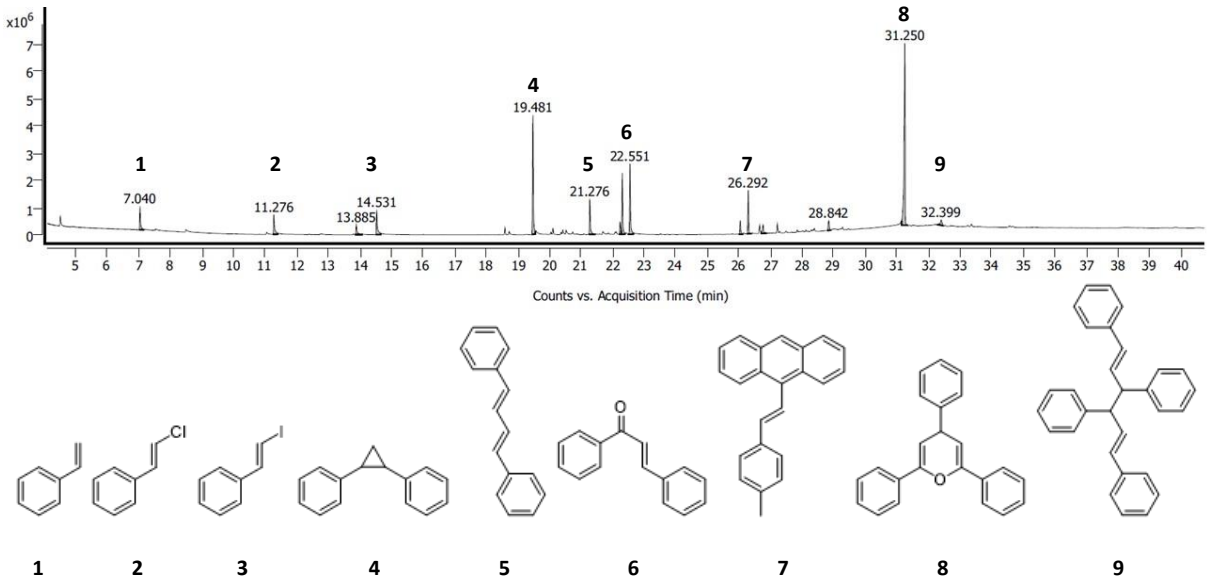

Figure B5. GC/MS spectrum with identified products of the reaction of $[Cr_3(\mu_2\text{-}Cl)_3(\mu_3\text{-}CH)(thf)_6]$ (**A**) with one equivalent of benzaldehyde in THF-d_8 after 3 days at ambient temperature, filtered over aluminum oxide. Displayed compounds were identified by MassHunter (GC/MS software).

Compounds **1** to **3** were probably generated from remaining impurities of $CrCl_2I(thf)_3$ or unreacted TAKAI reagent. Compounds **5**, **6**, **7** and **9** are putatively the outcome of radical generation and subsequent recombination (Scheme B2). Other compounds suggested were not explicable with generated data.

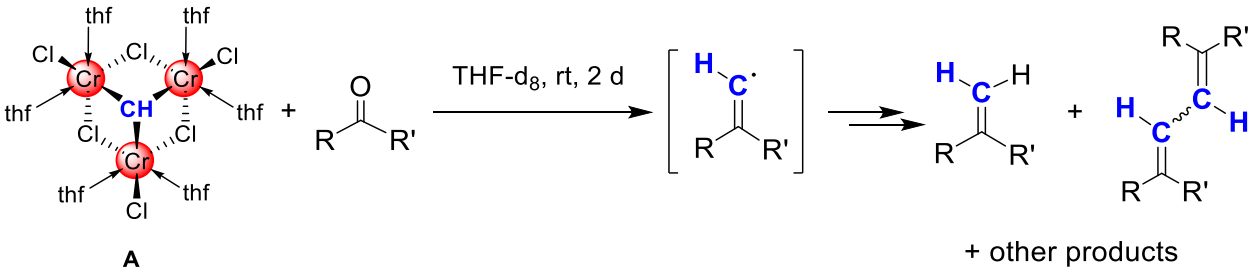

Scheme B2. Schematic display of the reaction of $[Cr_3(\mu_2\text{-}Cl)_3(\mu_3\text{-}CH)(thf)_6]$ (**A**) with aldehydes or ketones in THF. The generation of radicals is a suggestion based on the observed product compounds.

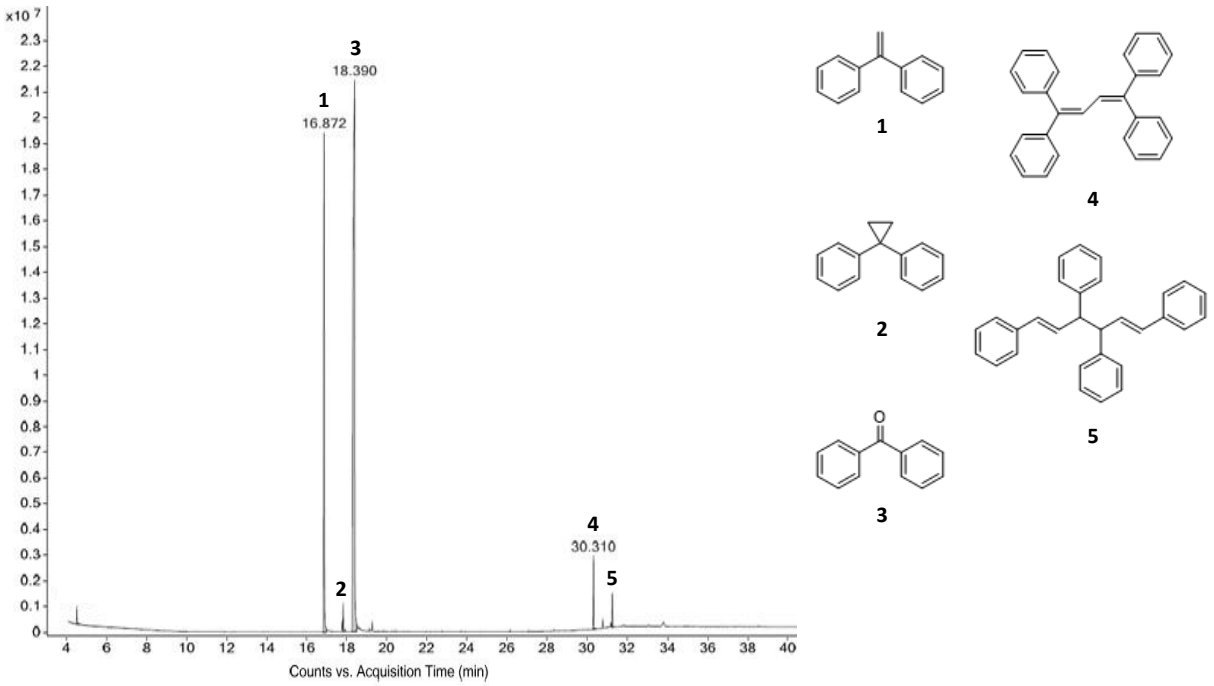

Figure B6. GC/MS spectrum with identified products of reaction of $[Cr_3(\mu_2\text{-}Cl)_3(\mu_3\text{-}CH)(thf)_6]$ (**A**) with one equivalent of benzophenone in THF-d_8 after 3 days at ambient temperature, filtered over aluminum oxide. Displayed compounds were identified by MassHunter (GC/MS software).

Identified products of the reaction of $[Cr_3(\mu_2\text{-}Cl)_3(\mu_3\text{-}CH)(thf)_6]$ (**A**) with one equivalent of benzophenone after 3 days in THF-d_8 at ambient temperature are shown in Figure B6. The results of the GC/MS measurements clearly indicated incomplete reaction after 3 days at ambient temperature. This observation was supported by the ^{1}H NMR signals of the starting

material. Identified compounds of this reaction suggest the same reactive pathway as for aldehydes but significantly decreased reaction rates probably due to steric hindrance.

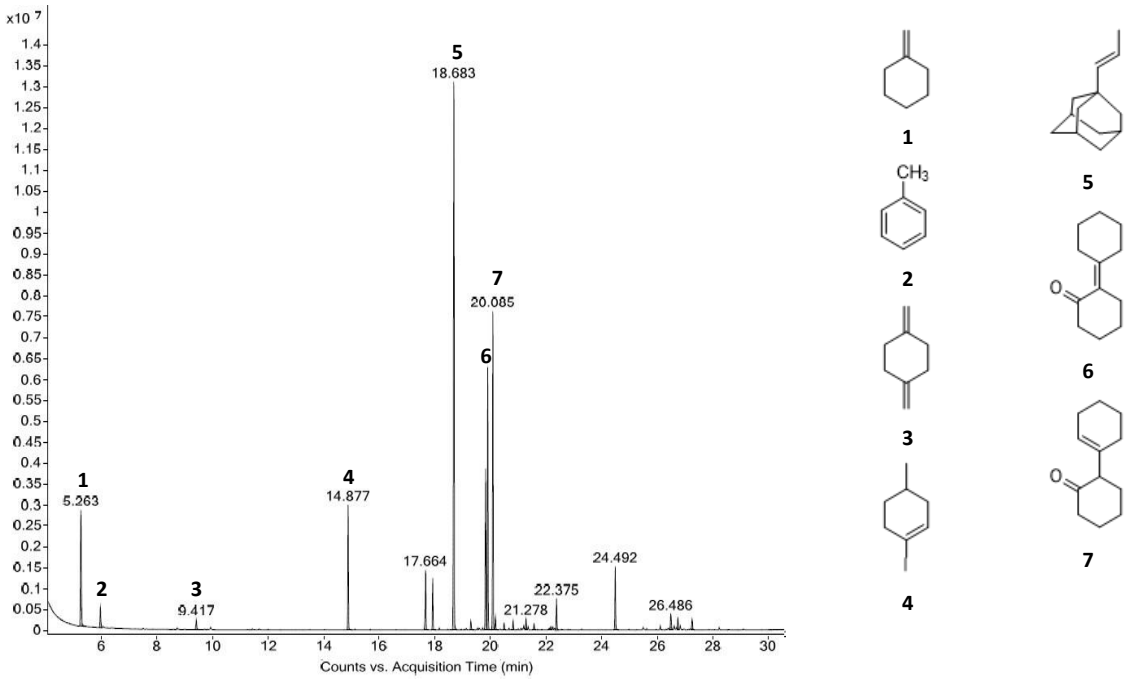

Figure B7. GC/MS spectrum with identified products of reaction of $[Cr_3(\mu_2\text{-}Cl)_3(\mu_3\text{-}CH)(thf)_6]$ (**A**) with one equivalent of cyclohexanone in THF-d_8 after 3 days at ambient temperature, filtered over aluminum oxide. Displayed compounds were identified by MassHunter (GC/MS software).

Identified products of the reaction of $[Cr_3(\mu_2\text{-}Cl)_3(\mu_3\text{-}CH)(thf)_6]$ (**A**) with one equivalent of cyclohexanone after 3 days in THF-d_8 at ambient temperature are shown in Figure B7. The results of the GC/MS measurements indicate complete reaction after 3 days at ambient temperature. The identified products show similar reactivity as observed for benzophenone, but faster conversion due to less steric hindrance and therefore higher reactivity of the starting material.

These results show the high complexity of the involved reaction mechanism of the μ_3-CH moiety with aldehydes or ketones and underline the problems found in the derivatization of **A** caused by impurities that could not be removed by standard techniques. Furthermore, the reactivity of **A** with standard substrates shows the importance of accurate application of stoichiometric amounts in the generation of the TAKAI reagent in organic syntheses.

3 Synthesis and Characterization of Chromium(II) Siloxide Compounds

In order to synthesize new suitable precursor compounds for the generation of TAKAI-like compounds, $Cr[N(SiMe_3)_2]_2(thf)_2$ (**G**) was reacted with silanols $HOSiR_3$ (R = Me, Et, *i*Pr, Ph, O*t*Bu). The products of these alcoholysis reactions were characterized and investigated regarding their reactivity and properties.

The reaction of $CrCl_2$ with $Na[N(SiMe_3)_2]$ in THF generated the silylamide **G** in good yield and purity. Treatment of **G** with two equivalents of $HOSi\mathit{i}Pr_3$ in THF at ambient temperature gave a color change from bright blue to purple (Scheme B3). Application of vacuum over several hours only led to a highly viscous purple residue. When this residue was dissolved in *n*-hexane or *n*-pentane, a color change to blue was observed. After addition of several drops of THF to this solution, the color change reversed to bright purple. Crystallization from *n*-pentane/THF gave crystals suitable for X-ray diffraction identified as dimeric $Cr_2(OSi\mathit{i}Pr_3)_2(\mu\text{-}OSi\mathit{i}Pr_3)_2(thf)_2$ (**H**, Figure B8). Compound **H** shows a slightly distorted tetrahedral geometry of the chromium centers, similar to the known $Cr_2(OSiPh_3)_2(\mu\text{-}OSiPh_3)_2(thf)_2$ published by QIU et al.

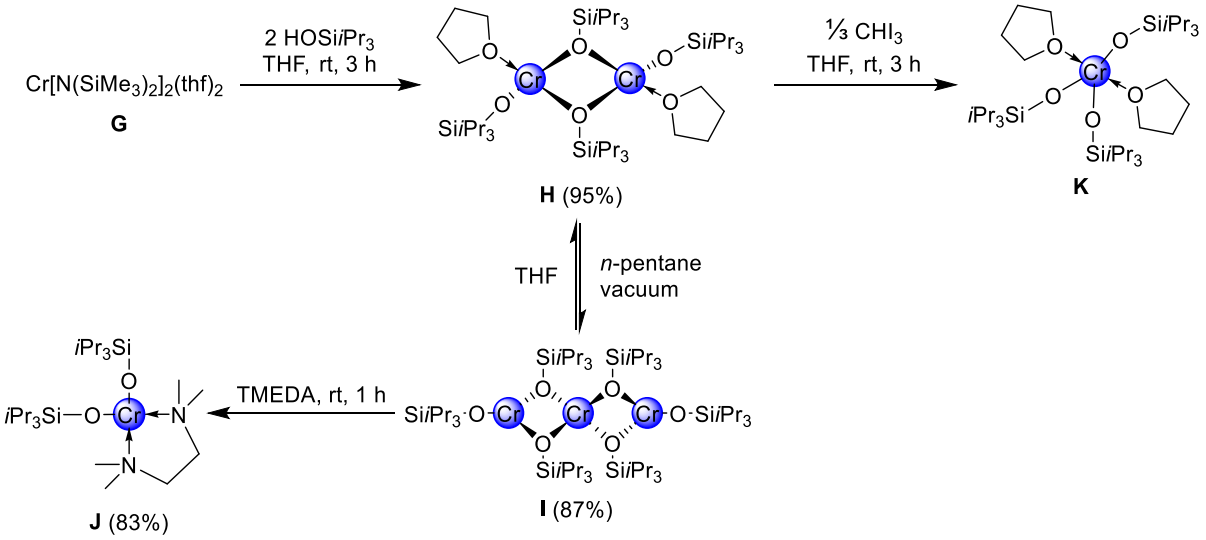

Scheme B3. Reaction of **G** to **H**, conversion of **H** to **I** by application of vacuum, reaction of **I** with donors to **J** and oxidation of **H** to **K**.

In an attempt to dry $Cr_2(OSi\mathit{i}Pr_3)_2(\mu\text{-}OSi\mathit{i}Pr_3)_2(thf)_2$ **H**, solutions in *n*-pentane were exposed to vacuum and the process was repeated several times (usually 4-6). With each repetition, the color

of the residue gradually changed to turquoise. When the process was completed, the bright turquoise powder was crystallized from *n*-pentane and yielded bright turquoise blocks suitable for X-ray diffraction. These crystals were identified as the donor-free trimeric $[Cr_3(OSi\mathit{i}Pr_3)_2(\mu\text{-}OSi\mathit{i}Pr_3)_4]$ (**I**, Figure B8). When **I** was exposed to TMEDA in *n*-pentane or *n*-hexane, a rapid color change to bright purple was observed. The product of this reaction was crystallized from a THF/*n*-hexane mixture and identified as the monomeric $Cr(OSi\mathit{i}Pr_3)_2(tmeda)$ (**J**).

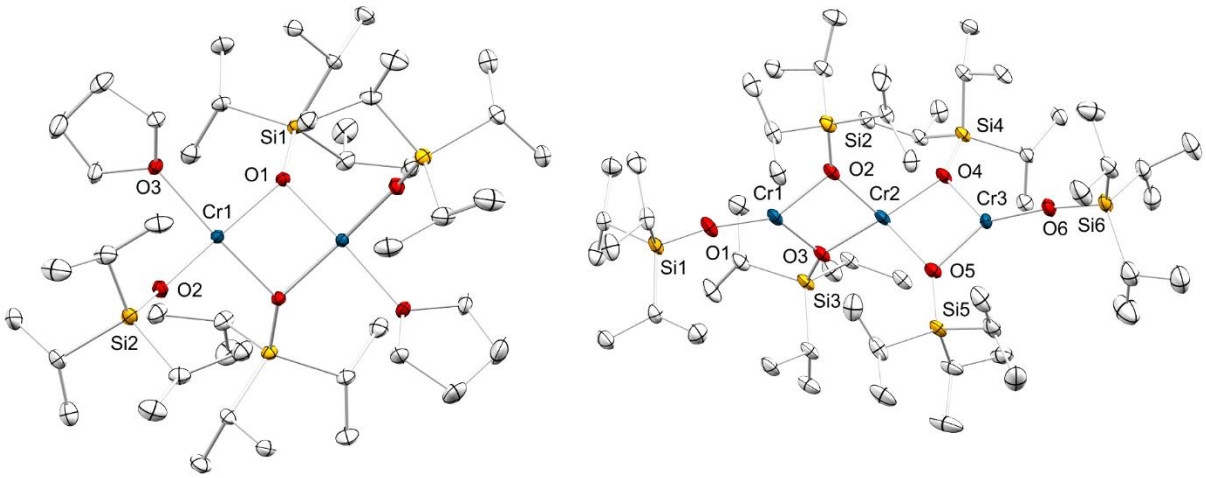

Figure B8. Crystal structures of $Cr_2(OSi\mathit{i}Pr_3)_2(\mu\text{-}OSi\mathit{i}Pr_3)_2(thf)_2$ (**H**, left) and $[Cr_3(OSi\mathit{i}Pr_3)_2(\mu\text{-}OSi\mathit{i}Pr_3)_4]$ (**I**, right).

Compound **H** could be oxidized by reaction with 1/3 equivalents of CHI_3, in an attempt to generate compounds similar to **A**. The found oxidization product was the highly unstable $Cr(OSi\mathit{i}Pr)_3(thf)_2$ (**K**, Scheme B3).

Attempted oxidization of $Cr_2(OSi\mathit{i}Pr_3)_2(\mu\text{-}OSi\mathit{i}Pr_3)_2(thf)_2$ with one equivalent of C_2Cl_6 in THF did not give **K** but led to the discovery of the asymmetrically coordinated $[Cr_2Cl_3(OSi\mathit{i}Pr_3)_3(thf)_3]$ (**L**). This compound was investigated regarding the loss of donor THF but it was not possible to crystallize the resulting green compound, assigned as putative **M** (Scheme B4).

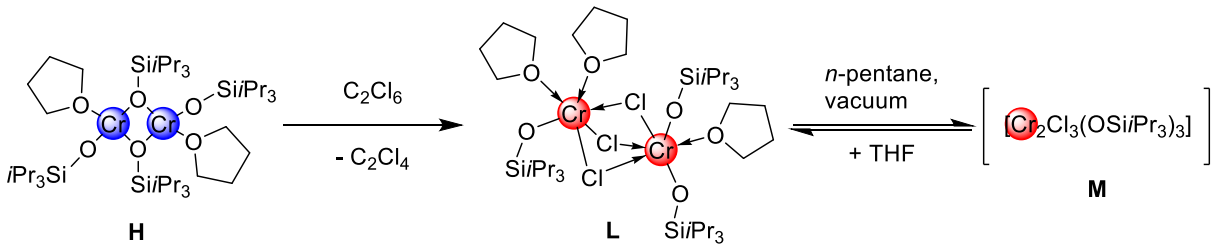

Scheme B4. Oxidation of **H** with C_2Cl_6 to **L** and subsequent conversion to **M**.

Intrigued by the versatility of these compounds and the controllable change in nuclearity, further protonolysis reactions of $Cr[N(SiMe_3)_2]_2(thf)_2$ were conducted with the smaller-sized $HOSiEt_3$. The two-equivalent reaction of $HOSiEt_3$ in THF gave purple solutions. Crystallization from *n*-pentane yielded trimeric $Cr_3(OSiEt_3)_2(\mu\text{-}OSiEt_3)_4(thf)_2$ (**N**, Figure B9), reflecting the lower steric demand of the $OSiEt_3$ ligand compared to $OSi\textit{i}Pr_3$ in dimeric **H**.

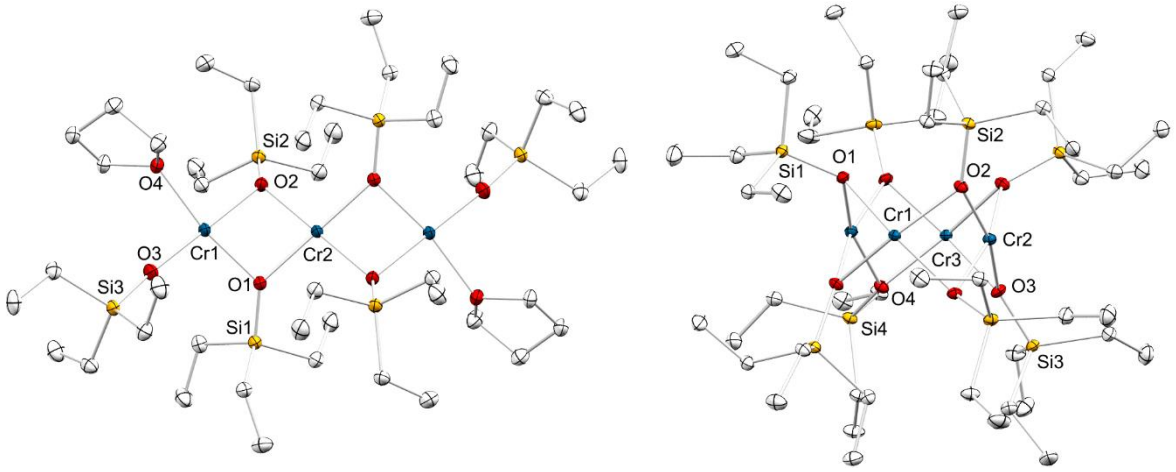

Figure B9. Crystal structures of $Cr_3(OSiEt_3)_2(\mu\text{-}OSiEt_3)_4(thf)_2$ (**N**, left) and $[Cr(\mu\text{-}OSiEt_3)_2]_4$ (**O**, right), ellipsoids shown at 30% probability (**Paper II**).

The peripheral chromium atoms in compound **N** display the same geometry as those in **H** but compound **N** incorporates a Cr^{II} forming a center of symmetry. When this compound was repeatedly dissolved in *n*-pentane or *n*-hexane and exposed to vacuum for several hours, a red-brown solid was obtained. Crystallization of this solid from *n*-pentane yielded crystals suitable for X-ray diffraction identified as tetrameric $[Cr(\mu\text{-}OSiEt_3)_2]_4$ (**O**, Scheme B5). This compound shows a crown like geometry similar to heteroleptic $[Cr(\mu_2\text{-}Cl)_4(\mu_2\text{-}OSi\textit{t}Bu_3)]_4$ published by SYDORA et al.[43]

It was also attempted to synthesize and isolate compounds $[Cr(OSiMe_3)_2]_n$ and $[\{Cr(OSi\textit{i}Ph_3)_2\}_2(thf)_2]$. The solids obtained from reactions of $Cr[N(SiMe_3)_2]_2(thf)_2$ in THF with two equivalents of $HOSiPh_3$ or $HOSiMe_3$, respectively, did not show the same properties due to instant precipitation from solutions probably due to agglomeration or polymerization. It was not possible to clearly identify any of these compounds by ^1H NMR because of the strong paramagnetic influence of Cr^{II}.

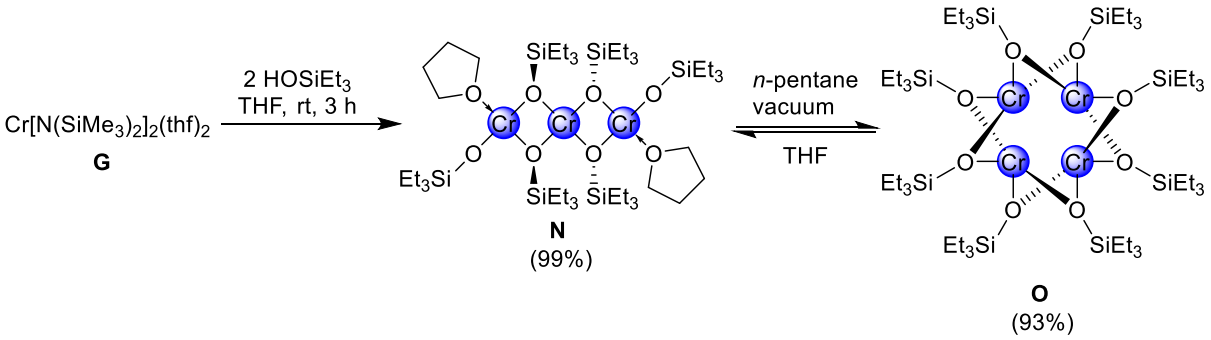

Scheme B5. Reaction of **G** to **N** and subsequent conversion to **O**.

Magnetic measurements with the EVANS method were performed and the results are shown in comparison to SQUID measurements in Table B2. SQUID magnetometer measurements of solid compounds **H**, **I**, and **O** were conducted to corroborate the magnetic moments in solution (Figure B10). The SQUID measurements showed temperature dependence. Overall lower values of μ_B compared to the expected (calculated) values were found. For high-spin configurations ($S = 2$) μ_{eff} of 4.90 μ_B (mononuclear), 6.93 μ_B (dinculear), 8.49 μ_B (trinuclear) and 9.80 μ_B (tetranuclear) are expected. For low-spin configurations ($S = 1$) μ_{eff} values of 2.83 μ_B (mononuclear), 4 μ_B (dinculear), 4.90 μ_B (trinuclear) and 5.66 μ_B (tetranuclear) would be expected.

The results of the SQUID measurements hinted at antiferromagnetic interactions between the Cr^{II} centres of multinuclear compounds **H**, **I**, and **O**, as they all showed a decrease of their effective magnetic moments upon cooling. Trinuclear complex **N** with $\mu_{eff} = 5.36$ μ_B (EVANS) shows similar behavior as the trimeric **I** with 5.22 μ_B (EVANS) and 5.68 μ_B (SQUID). The EVANS measurements also revealed a higher effective magnetic moment (μ_{eff}) of 5.1 μ_B for compound **J** compared to *trans*-heteroleptic monomer complexes. This was attributed to the *cis* coordination of heteroleptic **J**, as $Cr[OSi(OtBu)_3]_2(tmeda)$(5.73 μ_B)[26] shows similar magnetic behavior. Furthermore, **O** shows the highest reported magnetic moment for a tetranuclear Cr^{II} compound with 5.15 μ_B (EVANS) and 6.62 μ_B (SQUID). As the only comparable compound $[Cr(\mu_2\text{-}Cl)_4(\mu_2\text{-}OSitBu_3)]_4$ (1.1 μ_B)[43] is bridged by chlorido ligands, this behavior of **O** might originate in the different coupling mediation abilities of the siloxy ligands.

The found compounds increase the scope of the rare Cr^{II} siloxide compound class. As all characterized compounds can be synthesized in good yield and purity from standard chemicals with standard techniques, these compounds are predestined as precursors for further synthesis and research. Interesting and controllable geometries as well as the ability to introduce a

multitude of coordinating solvents and ligands could open a new and broad field of Cr^{II} siloxide complexes.

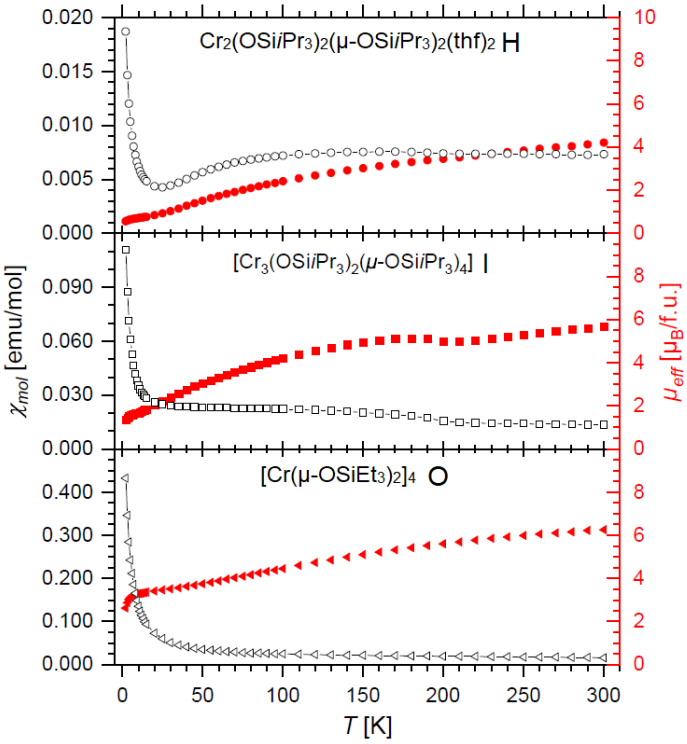

Figure B10. Temperature-dependent molar magnetic susceptibility $\chi_{mol}(T)$ (black open symbols; left ordinate) and effective magnetic moment $\mu_{eff}(T)$ (red filled symbols; right ordinate) as obtained by SQUID magnetic measurements on crystalline powder of **H** (top), **I** (middle) and **O** (bottom) in an applied field H = 10 kOe. The $\chi_{mol}(T)$ data was corrected for diamagnetic contributions (**H**: $-6.432 \cdot 10^{-4}$ emu/mol; **I**: $-8.438 \cdot 10^{-4}$ emu/mol; **O**: $-8.404 \cdot 10^{-4}$ emu/mol; calculated from Pascal's constants)[71], and a spin-only g factor of 2.0 was assumed in the calculation of $\mu_{eff}(T)$. **(Paper II)**

Table B2 Summary of measured magnetic moments with the EVANS method and SQUID magnetometer.

Compound	μ_{eff} (EVANS)	μ_{eff} (SQUID)
$[\{Cr(OSiEt_3)_2\}_3(thf)_2]$ (**N**)	5.36 μ_B	-
$[Cr(OSiEt_3)_2]_4$ (**O**)	5.15 μ_B	6.26 μ_B
$[\{Cr(OSi\textit{i}Pr_3)_2\}_2(thf)_2]$ (**H**)	4.88 μ_B	4.20 μ_B
$[\{Cr(OSi\textit{i}Pr_3)_2\}_2(tmeda)]$ (**J**)	5.13 μ_B	-
$[\{Cr(OSi\textit{i}Pr_3)_2\}_3]$ (**I**)	5.22 μ_B	5.68 μ_B

C

Unpublished Results

1 Reactions of Mo(V), W(V), and W(VI) Compounds with Methylating Reagents

Introduction

To elucidate the solid-state structures of the KAUFFMANN reagents, complexes derived from stabilizing siloxy/aryloxy-ligands (e.g., $OSi(O\mathit{t}Bu)_3$, $OC_6H_3Me_2$-2,6) should be synthesized and characterized. Alkylation of complexes should serve as proof of principle for the existence of the elusive μ_2-CH_2-bridged molybdenum and tungsten compounds which putatively are the reactive species of the KAUFFMANN olefination.

Results and Discussion

Treatment of $MoOCl_3(thf)_2$ with one or two equivalents of $[MOSi(O\mathit{t}Bu)_3]$ (M = Li, K) in THF or *n*-hexane generated a mixture of the two complexes $[MoOCl\{OSi(O\mathit{t}Bu)_3\}_2(thf)_2]$ (**P**$^{\mathbf{a}}$) and $[MoOCl\{OSi(O\mathit{t}Bu)_3\}_2(thf)]$ (**P**$^{\mathbf{b}}$). The co-generation of these two complexes was discovered because of their strongly differing color. **P**$^{\mathbf{a}}$ shows a pale green color and crystallized as platelets while **P**$^{\mathbf{b}}$ is pale orange colored and can be generated by applying vacuum to solutions of **P**$^{\mathbf{a}}$ in aliphatic solvents. It was not possible to completely transform either of the compounds into the mono or bis(thf) coordinated complex. Crystallization persistently gave small amounts of the corresponding other form. X-ray diffraction revealed an octahedral geometry of the Mo(V) center for **P**$^{\mathbf{a}}$, with a strong disorder of the oxy and chlorido ligands, resulting in only a connectivity assignment (Figure C1). Compound **P**$^{\mathbf{b}}$ shows a trigonal bipyramidal geometry with the coordinated THF molecule opposite (*trans*) to the chlorido ligand (Figure C1).

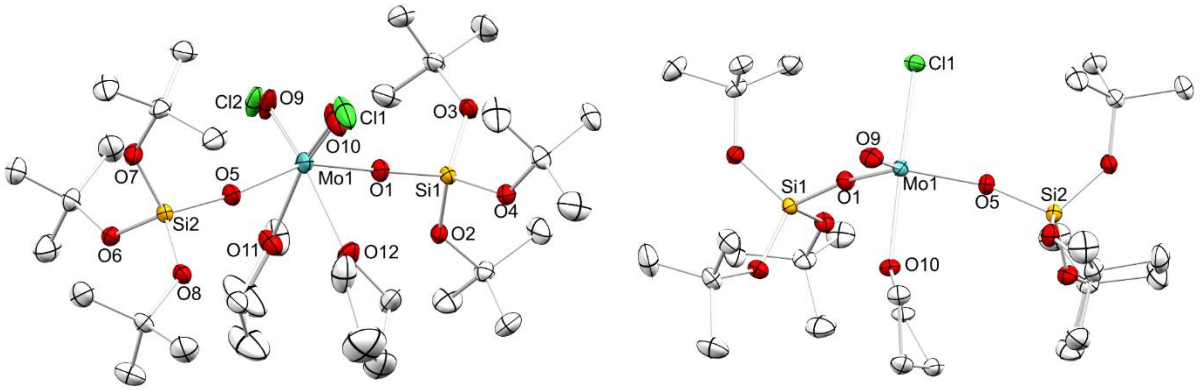

Figure C1. Connectivity of $[MoOCl\{OSi(O\mathit{t}Bu)_3\}_2(thf)_2]$ (**P**$^{\mathbf{a}}$)(left) and crystal structure of $[MoOCl\{OSi(O\mathit{t}Bu)_3\}_2(thf)]$ (**P**$^{\mathbf{b}}$) (right), ellipsoids shown at 30% probability.

The reactions of **P**[a] with varying equivalents of MeLi or $AlMe_3$ did neither lead to terminal Mo=CH_2 groups nor methylation of the compound, nor any other isolable product. NMR-scale reaction mixtures of **P**[a] and two equivalents of MeLi showed minimal olefination activity toward PhCHO in THF-d_8 (Figure C18). It could not be clarified, if this outcome was due to the generation of KAUFFMANN-like compounds.

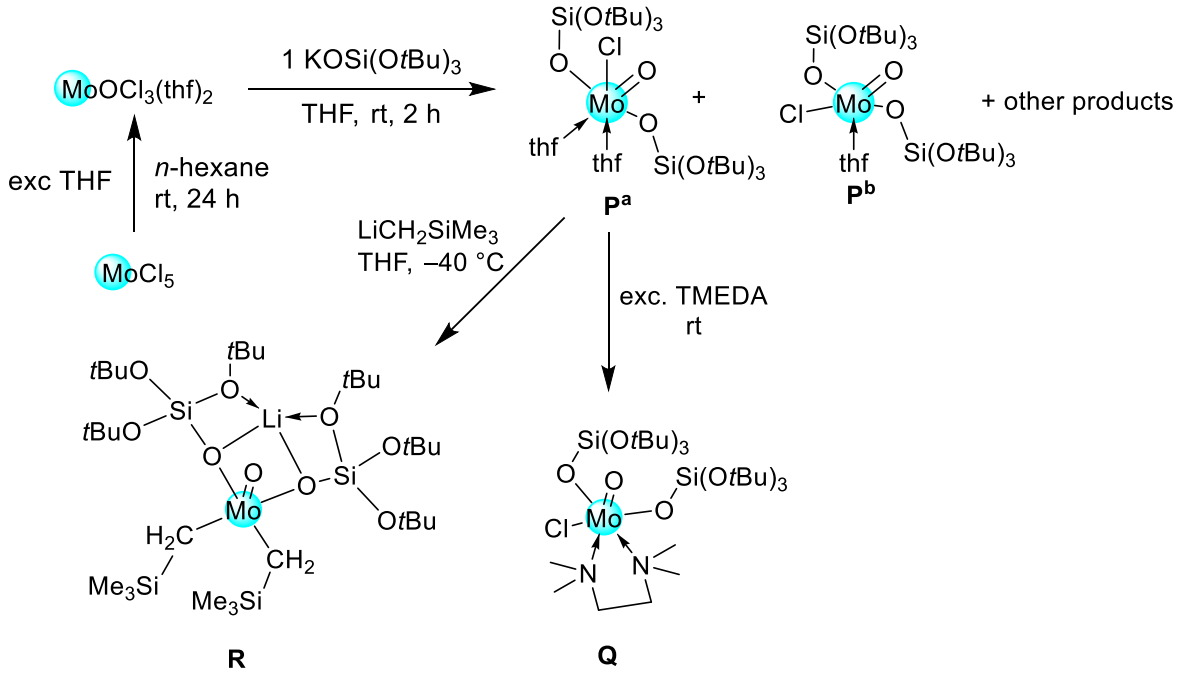

Scheme C 1. Schematic synthesis of molybdenum(V) compounds **P**[a]/**P**[b], **Q**, and **R**.

The reaction of **P**[a] with excess of TMEDA in *n*-hexane readily formed green [MoOCl{OSi(O*t*Bu)$_3$}$_2$(tmeda)] (**Q** Scheme C1) identified by X-ray diffraction and characterized by ^{1}H NMR spectroscopy and microanalysis. Reactions of **Q** with one equivalent of $LiCH_2SiMe_3$ in THF at – 40 °C gave intense yellow solutions. Unfortunately, it was not possible to identify any products of this reaction.

The reaction of **P**[a] with two equivalents of $LiCH_2SiMe_3$ in THF at -45 °C produced the ate complex [LiMoO(CH_2SiMe_3)$_2${OSi(O*t*Bu)$_3$}$_2$] (**R**, Scheme C1) in 52% yield. Compound **R** could be crystallized from *n*-hexane as blue-green blocks suitable for X-ray diffraction (Figure C2). The ^{1}H NMR spectrum of **R** shows a broadened signal at 1.6 ppm and a sharp singlet at 1.33 ppm. The ^{7}Li NMR spectrum shows one peak at 0.35 ppm.

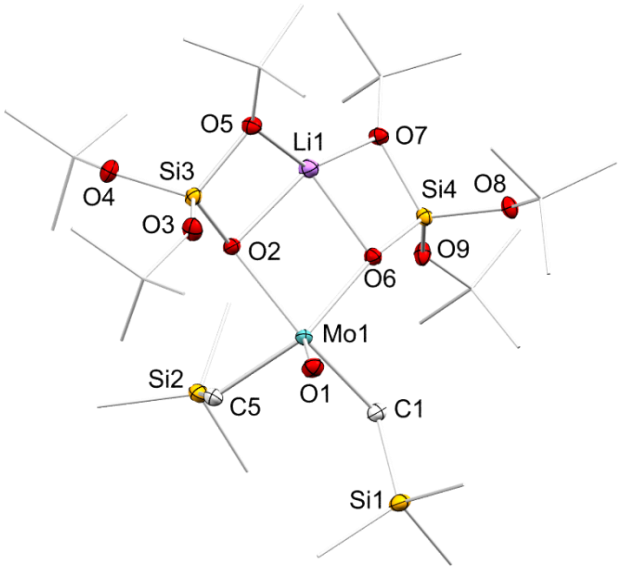

Figure C2. Crystal structure of $[LiMoO(CH_2SiMe_3)_2\{OSi(OtBu)_3\}_2]$ (**R**), partially wireframed to improve visibility, ellipsoids shown at 30% probability.

The reaction of WCl_6 with one equivalent of HMDSO in toluene generated bright orange $WOCl_4$. Treatment of $WOCl_4$ with two equivalents of $[MOSi(OtBu)_3]$ (M = Li, K) in THF gave $[WOCl_2\{OSi(OtBu)_3\}_2(thf)]$ (**S**, Scheme C2**)** in good yield (90%). The compound readily crystallized from *n*-hexane or THF solutions in colorless blocks. The ^{1}H NMR spectrum of **S** shows a sharp singlet at 1.44 ppm. The purity of **S** was confirmed by microanalysis. Subsequent reaction of **S** with two equivalents of $LiCH_2SiMe_3$ in THF at -45 °C yielded $[WO(CH_2SiMe_3)_2\{OSi(OtBu)_3\}_2]$ (**T**, Scheme C2**)** in low yield (38%). The compound was crystallized from *n*-hexane as orange blocks suitable for X-ray diffraction.

For comparison with other compounds, an exemplary NMR-scale experiment of the reaction of $WOCl_3(thf)_2$ with two equivalents of MeLi and 0.5 equivalents of PhCHO in THF-d_8 is shown in the experimental section (Figure C17). The signals clearly indicate the generation of small amounts styrene, but also show several other signals of unidentified side products. NMR-scale experiments of reactions of **R** and **T** with excess of PhCHO in THF-d_8 are shown in Figure C19 to C22. These experiments revealed the generation of methane (δ = 0.19 ppm, THF-d_8)[72], ethylene (δ = 5.36 ppm, THF-d_8)[72] and several unidentified side products after prolonged reaction at ambient temperature and heating to 50 °C for 1 hour to 1 day. It was not possible to clearly identify any olefination products due to the small amounts of a diverse set of generated compounds and their overlapping signals.

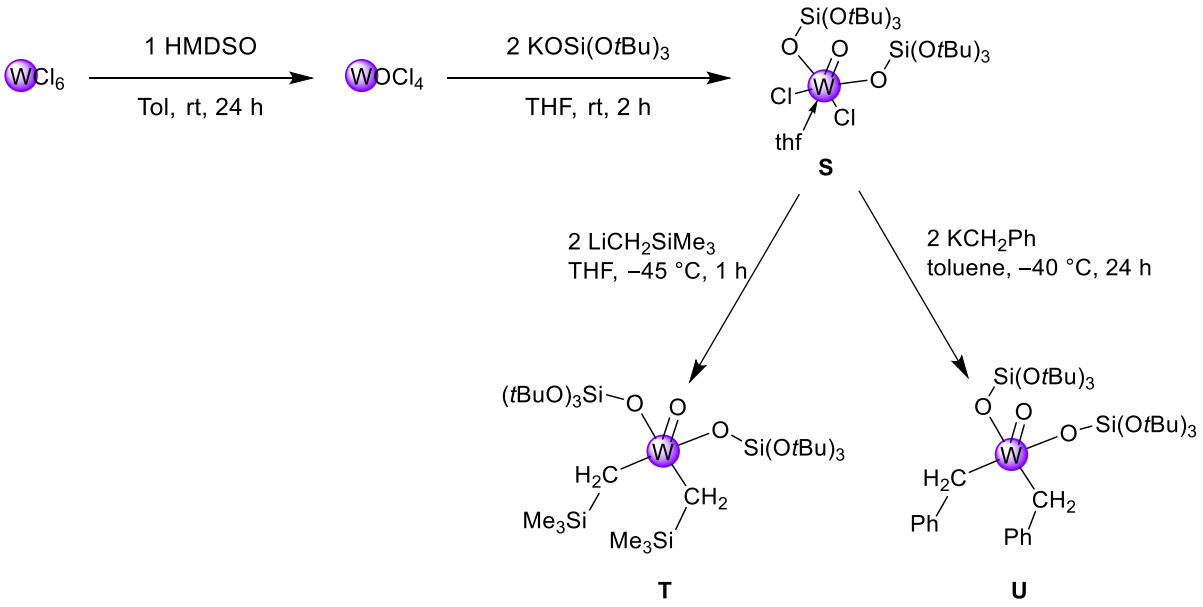

Scheme C2. Schematic synthesis of tungsten compounds **S**, **T**, and **U**.

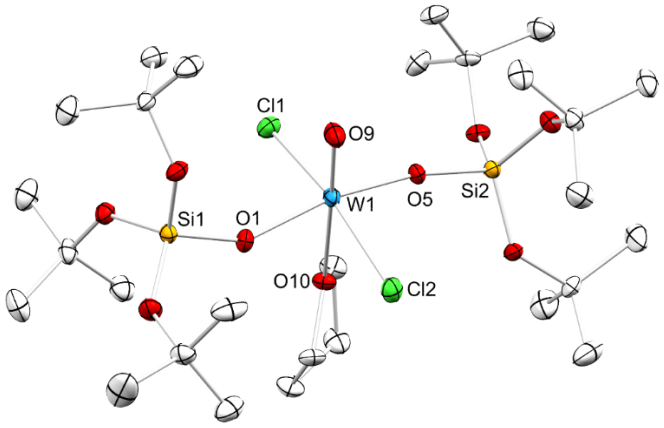

Figure C3. Crystal structure of $[WOCl_2\{OSi(OtBu)_3\}_2(thf)]$ (**S**), ellipsoids shown at 30% probability.

It was also possible to generate $[WO(CH_2Ph)_2\{OSi(OtBu)_3\}_2]$ (**U**, Scheme C2) in a similar reaction of **S** with two equivalents of KCH_2Ph in toluene at –40 °C. Compounds **V** and **S** show the possibility of forming terminal alkyl W^{VI} compounds in direct reactions with alkylation reagents. Unfortunately, this does not provide further evidence for the existence of M-μ_2-CHR-M compounds as supposed intermediates in the KAUFFMANN reaction.

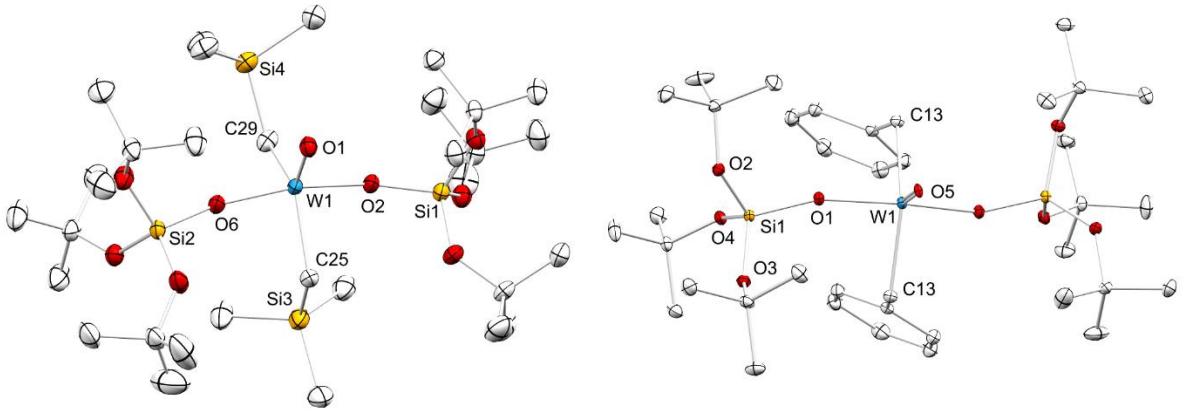

Figure C4. Crystal structure of $[WO(CH_2SiMe_3)_2\{OSi(OtBu)_3\}_2]$ (**T**, left) and $[WO(CH_2Ph)_2\{OSi(OtBu)_3\}_2]$ (**U**, right), ellipsoids shown at 30% probability.

Reactions of $[WOCl_2\{OSi(OtBu)_3\}_2(thf)]$ with two equivalents of $AlMe_3$ or $GaMe_3$ were conducted in *n*-hexane at −45 °C. Unfortunately, these reactions generated large amounts of $[\{Me_2Al(OSi(OtBu)_3)\}_2]$[73] (**V**) or $[\{Me_2Ga(OSi(OtBu)_3)\}_2]$[49,74] (**W**) (Scheme C5). These compounds are known from literature and were identified by a unit-cell check of crystals grown from *n*-hexane solutions. The reaction of $[WOCl_2\{OSi(OtBu)_3\}_2(thf)]$ with two equivalents of $GaMe_3$ conducted in *n*-hexane at −45 °C also produced low amounts of $[WO(CH_3)_2\{OSi(OtBu)_3\}_2(thf)]$ (**Z**) (Scheme C5). Compound **Z** crystallized as extremely temperature-sensitive orange needles after several separations from the colorless side product **W**. Compound **Z** is to the best of our knowledge the first structurally characterized methylated W(VI) oxo siloxide. The closest related and structurally characterized compound $[WO(n\text{-}Bu)_2(OSitBu)_2]_2$ was synthesized and published by *ROSENFELD* et. al. in 2006. The compound $[WO(CH_3)_2(OSitBu_3)_2]$ was also synthesized in a reaction of $WOCl_2(silox)_2$ with two equivalents of MeMgBr in Et_2O at −78 °C, but a crystal structure was not provided. [75]

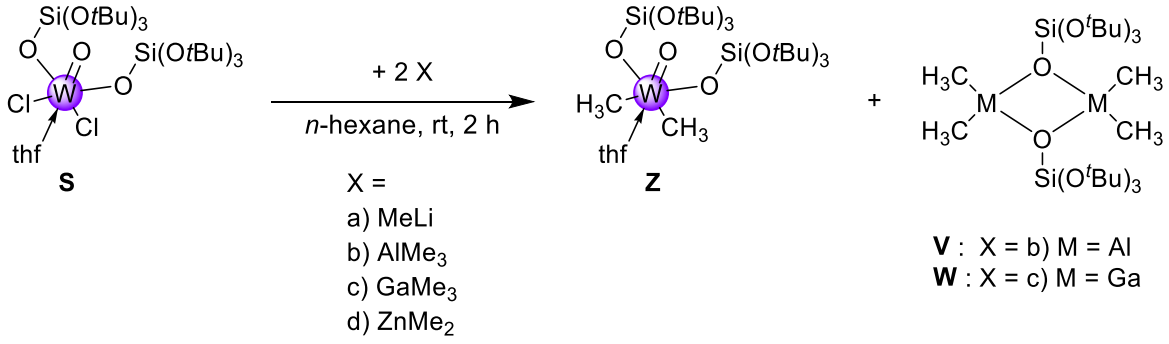

Scheme C5. Reaction of **S** with various methylation reagents X to **Z**, corresponding observed side products **V** or **W**.

Compound **Z** is structurally closely related to **T** and **U** but also incorporates one coordinating THF molecule (Figure C6). This THF coordination was crucial in attempts to isolate and crystallize compound **Z** as *n*-hexane solutions without the addition of small amounts of THF did not afford crystals and changed their color from orange to bright yellow upon removal of solvents. Elemental analysis of this yellow residue showed persistent levels of impurities due to similar solubility of **V** and **W**. The ^{1}H NMR spectrum of **Z** shows a singlet at 1.34 ppm assigned to the siloxy ligands but no signal clearly assignable to the methyl groups. As this compound is extremely sensitive to temperatures above −35 °C, no further analytics could be performed on this exact compound. NMR-scale reactions of **Z** with benzaldehyde in THF-d_8 at ambient temperature did not show olefination activity after 2 days. Reactions of **S** with two equivalents of $ZnMe_2$ in *n*-hexane at −45 °C gave yellow solutions, which crystallized as yellow blocks of poor quality. These crystals were not suitable for X-ray diffraction due to their poor diffraction properties. Recrystallization did not lead to better results. Attempts to separate the unidentified side product from this reaction failed.

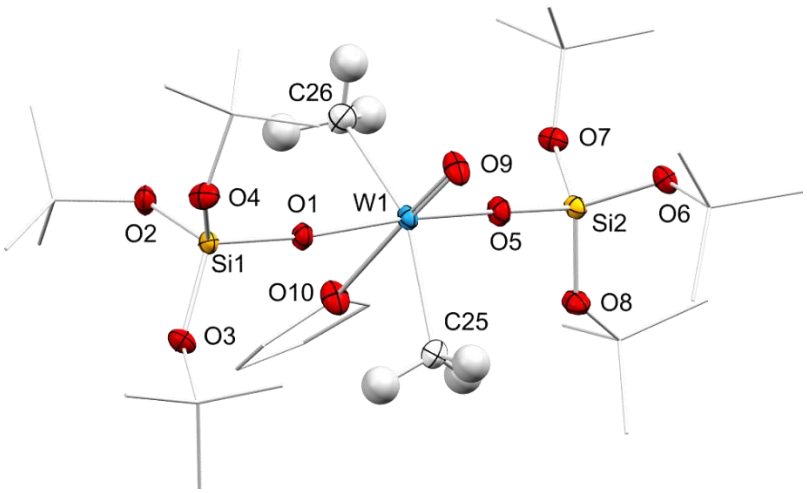

Figure C6. Crystal structure of $[WO(CH_3)_2\{OSi(OtBu)_3\}_2(thf)]$ (**Z**).

KAUFFMANN also researched alkoxides of tungsten and molybdenum and was able to prove their reactivity in the olefination of aldehydes and ketones. The research conducted was mainly performed on methoxides and ethoxides of W(VI) and Mo(V) in reactions with benzaldehyde.[4,24,67] The proposed active species and their structures are closely related to the oxychloride cyclobutene dimers shown in Scheme A14. Therefore, several aryloxide species were synthesized and investigated in methylation reactions. The higher steric hindrance of these compounds was expected to slow down the reaction and decomposition, as well as stabilize the active methylated species.

The reactions of $WOCl_4$ with aryloxides are known from literature.[76] GLENNY et. al. reported on the reactivity of $WOCl_4$ with 0.72 equivalents of $HOC_6H_3Me_2$-2,6 in Et_2O generating $[WOCl_3(OPh^{Me2})]_2$ (**AA**) in good yield. In an adapted synthesis $WOCl_4$ was treated with [(thf)NaOMes] (Mes = 2,4,6-trimethylphenyl) to examine the electronic and steric influence of a differently substituted aryloxy ligand on the system. The two-equivalent reaction in toluene at ambient temperature produced the monomeric compound $[WOCl_2(OMes)_2(thf)]$ (**BB**) in acceptable yield. Crystallization from concentrated *n*-hexane solutions gave crystals suitable for X-ray diffraction confirming the monomeric structure (Figure C7).

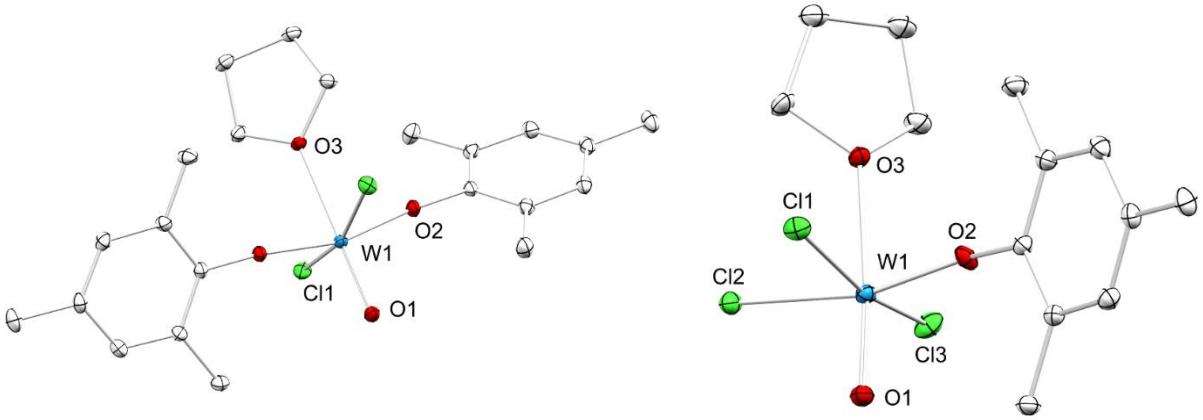

Figure C7. Crystal structures of compounds $[WOCl_2(OMes)_2(thf)]$ (**BB**, left) and $[WOCl_3(OMes)(thf)]$ (**CC**, right), ellipsoids shown at 30% probability.

Reactions of $WOCl_4$ with 0.7 equivalents of [(thf)NaOMes] in Et_2O gave the mono-substituted $[WOCl_3(OMes)(thf)]$ (**CC**) as a dark violet solid. Crystallization of this solid from *n*-hexane produced dark violet crystals. X-ray diffraction measurements again revealed a monomeric structure for **CC** (Figure C7). When this reaction was repeated with 0.7 equivalents [(thf)NaOPh^{Me_2}], the found product was identified as the monomeric $[WOCl_3(OPh^{Me_2})(thf)]$ (**DD**) (Scheme C7). This discovery led to the assumption of thf preventing dimerization. KAUFFMANN also observed a reduced reactivity of Lewis acidic reagents in THF and mentioned the reduced selectivity for ketones due to strongly bonded, donating THF.[24,77] Unfortunately, no products could be isolated from reactions of **DD** and two equivalents of MeLi in THF. A ^{1}H NMR investigation did not show peaks indicating dimerization which would provide first insight into this system, reaffirming this suggestion. To further clarify the influence of donor solvents and especially THF on these complexes, more research is needed.

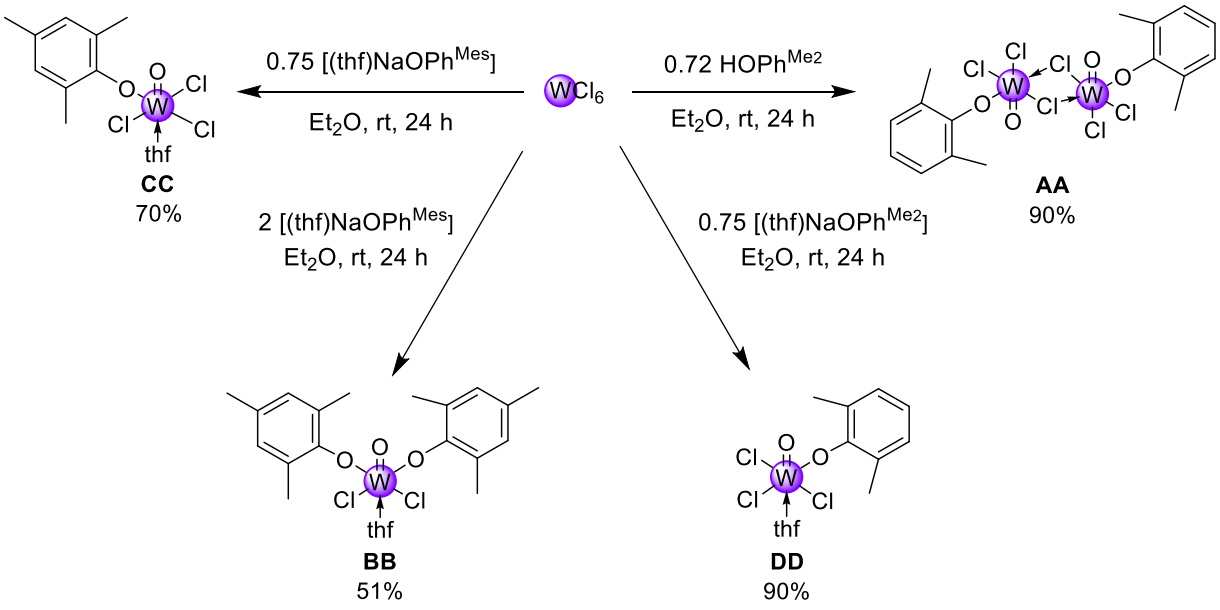

Scheme C8. Reaction of $WOCl_4$ to $[WOCl_3(OPh^{Me2})]_2$ (**AA**), $[WOCl_2(OMes)_2(thf)]$ (**BB**), $[WOCl_3(OMes)(thf)]$ (**CC**), and $[WOCl_3(OPh^{Me2})(thf)]$ (**DD**).

Experimental Section

General Procedures. All manipulations were performed under an inert atmosphere (Ar) using a glovebox (*MBraun* 200B; <0.1 ppm O_2, <0.1 ppm H_2O), or according to standard Schlenk techniques in oven-dried glassware. The solvents were purified with Grubbs-type columns (*MBraun* SPS, solvent purification system) and stored in a glovebox. MoO_2Cl_2, WCl_6, $MoCl_5$ were purchased from *Sigma-Aldrich* and used as received. C_6D_6 and THF-d_8 were purchased from *Sigma Aldrich* and pre-dried over NaK alloy and filtered off prior use, THF-d_8 was re-condensed. NMR spectra were recorded at 26 °C with a Bruker AVII+400 (^{1}H: 400.13 MHz) or a *Bruker* AVIIIHD-300 (^{1}H: 300.13 MHz, ^{7}Li 116.64 MHz) using J. Young valve NMR spectroscopy tubes. ^{1}H shifts are referenced to a solvent resonance and reported in parts per million (ppm) relative to tetramethylsilane. Analyses of NMR spectra were performed with *Bruker* TOPSPIN (version 3.6.1). Infrared spectra were recorded on a *ThermoFisher Scientific* NICOLET 6700 FTIR ($\tilde{\nu}$= 4000 – 400 cm^{-1}) spectrometer using a DRIFTS chamber with dry KBr/sample mixtures and KBr windows. Elemental analysis (C, H, N) was performed on an *Elementar vario MICRO cube*.

[$MoOCl_3(thf)_2$]. [$MoCl_5$] (0.592 g, 2.16 mmol) was stirred in *n*-hexane (10 mL) and ~ 2 mL of THF added to the suspension at –45 °C. After stirring for 24 h at ambient temperature, volatiles were removed under reduced pressure. The green precipitate was washed 3 times with 2 mL of *n*-hexane and dried in vacuo. Crystallization from concentrated THF solutions gave [$MoOCl_3(thf)_2$] as bright green crystals. Yield: 0.655 g (1.81 mmol, 83%). ^{1}H NMR (THF-d_8, 400.13 MHz, 26 °C) δ = no signals detected; IR (DRIFT): $\tilde{\nu}$ = 2985 (s), 2903 (m), 1454 (w), 1344 (w) 1247 (vw), 1177 (vw), 1045 (vw), 1007 (sh), 985 (vs), 956 (vw), 924 (w), 835 (s), 675 (vw).cm^{-1}; elemental analysis (%) calcd. for $C_8H_{16}Cl_3MoO_3$ (362.51): C 26.51, H 4.45; found: C 26.69, H 4.24.

[$WOCl_4$]. [WCl_6] (0.298 g, 0.75 mmol) was suspended in 3 mL toluene, and HMDSO (0.12 g, 0.74 mmol) added at –45 °C. After stirring for 24 h at ambient temperature, the supernatant solution was discarded. The orange precipitate was washed 3 times with 2 mL of *n*-hexane and dried in vacuo. Sublimation at 90 °C yielded orange needles of [$WOCl_4$]. Yield: 0.23 g (0.67 mmol, 89%).

[$MoOCl\{OSi(O\mathit{t}Bu)_3\}_2(thf)_2$] ($\mathbf{P^a}$) / [$MoOCl\{OSi(O\mathit{t}Bu)_3\}_2(thf)$] ($\mathbf{P^b}$). KOSi(O*t*Bu)$_3$ (0.05 g, 0.12 mmol) in 0.5 mL THF was added to a stirred bright green solution of [$MoOCl_3(thf)_2$] (0.04 g, 0.12 mmol) in 0.5 mL THF which led to a change of color to pale red. After stirring for 1 h at ambient temperature, volatiles were removed in vacuo and the residue was extracted with *n*-hexane. Drying of this *n*-hexane solution yielded a brown-green solid mixture of $\mathbf{P^a}$ and $\mathbf{P^b}$. Crystallization from *n*-hexane with low content of THF (2-5 drops) gave pale green platelets of $\mathbf{P^a}$ with minor contamination of $\mathbf{P^b}$. Yield: 0.43 g (0.06 mmol, 46%). ^{1}H NMR (THF-d_8,400.13 MHz, 26 °C) δ = 1.63 (br s) ppm. elemental analysis (%) calcd. for $C_{28}H_{62}ClMoO_{11}Si_2$ (818.47): C 46.96, H 8.62; found: C 46.63, H 8.32.

[$MoOCl\{OSi(O\mathit{t}Bu)_3\}_2$(tmeda)] (Q). To a stirred solution of [$MoOCl\{OSi(O\mathit{t}Bu)_3\}_2(thf)_2$] (0.07 g, 0.09 mmol) in 0.5 mL *n*-hexane, TMEDA (~0.1 mL) was added. The solution changed color from pale red to green. After stirring for 0.5 h at ambient temperature, volatiles were removed under reduced

pressure, giving a pale yellow solid. Extraction of this yellow solid with *n*-hexane yielded violet **Q**. Crystallization from concentrated THF gave violet blocks of **Q**. Yield: 0.06 g (0.08 mmol, 87%). ^{1}H NMR (THF-d_8, 400.13 MHz, 26 °C) δ = 1.55 (br s, 54H,*t*Bu), 1.33 (s, 4 H,-CH_2-), 1.29 (s, 12 H, -Me) ppm. elemental analysis (%) calcd. for $C_{30}H_{70}ClMoN_2O_9Si_2$ (790.47): C 45.58, H 8.93, N 3.54; found: C 45.65, H 8.24, N 3.55.

[LiMoO(CH$_2$SiMe$_3$)$_2${OSi(O*t*Bu)$_3$}$_2$] (R). $LiCH_2SiMe_3$ (0.02 g, 0.17 mmol) in 0.2 mL THF was added to a stirred solution of [MoOCl{OSi(O*t*Bu)$_3$}$_2$(thf)$_2$] (0.07 g, 0.08 mmol) in 0.5 mL THF at –45 °C. Immediately the color changed from pale green to orange. After stirring for 1 h at ambient temperature, volatiles were removed under reduced pressure yielding a yellow solid. Extraction of the residue with *n*-hexane gave an orange solution. Crystallization from this concentrated *n*-hexane solution gave blue-green blocks of **R** suitable for X-ray diffraction. Yield: 0.03 g (0.04 mmol, 52%). ^{1}H NMR (THF-d_8, 400.13 MHz, 26 °C) δ =1.66 (br s), 1.33 (s) ppm.^{7}Li NMR (THF-d_8, 300.13 MHz, 26 °C) δ = 0.351 ppm. IR (DRIFT): $\tilde{\nu}$ = 2975 (vs), 2931 (m), 2904 (m), 2873 (m), 1473 (m) 1389 (s), 1364 (s), 1246 (s), 1212 (m), 1190 (s), 1065 (vs), 1055 (vs), 1027 (s), 986 (m), 940 (s), 895 (vs), 889 (vs), 883 (vs), 844 (vs), 751 (w), 703 (s), 530 (m), 490 (m), 449 (m), 440 (m), 433 (m).cm^{-1}; elemental analysis (%) calcd. for $C_{32}H_{76}LiMoO_9Si_4$ (820.18): C 46.86, H 9.34; found: C 47.00, H 9.27.

[WOCl$_2${OSi(O*t*Bu)$_3$}$_2$(thf)] (S). $KOSi(OtBu)_3$ (0.18 g, 0.59 mmol) in 0.2 THF was added to a stirred bright orange solution of $WOCl_4$ (0.10 g, 0.29 mmol) in 0.5 mL THF. Immediately, the color changed from bright orange to pale yellow. After stirring for 3 h at ambient temperature, the volatiles were removed, and the residue was redissolved in *n*-hexane. Filtration and drying under reduced pressure yielded a colorless solid. Yield: 0.23 g (0.26 mmol, 89%). ^{1}H NMR (THF-d_8, 400.13 MHz, 26 °C) δ = 1.44 (s, 54 H, *t*Bu) ppm; elemental analysis (%) calcd. for $C_{28}H_{62}Cl_2O_{10}Si_2W$ (869.7): C 38.67, H 7.19; found: C 38.83, H 7.19.

[WO(CH$_2$SiMe$_3$)$_2${OSi(O*t*Bu)$_3$}$_2$] (T). $LiCH_2SiMe_3$ (0.02 g, 0.18 mmol) in 0.2 mL THF was added to a stirred solution of [WOCl$_2${OSi(O*t*Bu)$_3$}$_2$(thf)] (0.08 g, 0.09 mmol) in 0.5 mL THF at –45 °C. Immediately the color changed from colorless over green to orange. After stirring for 1 h at ambient temperature, volatiles were removed under reduced pressure. Extraction of the residue with *n*-hexane gave a dark green solution. Crystallization from concentrated *n*-hexane solution gave orange blocks of **T** suitable for X-ray diffraction. Yield: 0.03 g (0.03 mmol, 38%). ^{1}H NMR (THF-d_8, 400.13 MHz, 26 °C) δ =1.39 (s), 1.38 (s), 0.23 (s) ppm. IR (DRIFT): $\tilde{\nu}$ = 2975 (vs), 2931 (m), 2904 (m), 2873 (w), 1473 (m), 1389 (s), 1364 (vs), 1246 (vs), 1190 (vs), 1065 (vs), 1027 (s), 986 (m), 940 (s), 895 (s), 833 (s), 751 (w), 703 (s), 530 (m), 490 (w), 483 (w), 470 (w), 457 (w), 440 (w), 433 (w) cm^{-1}; elemental analysis (%) calcd. for $C_{32}H_{76}LiMoO_9Si_4$ (900.13): C 42.65, H 8.50; found: C 42.23, H 8.35.

[WO(CH$_2$Ph)$_2${OSi(O*t*Bu)$_3$}$_2$] (U). Benzylpotassium (0.02 g, 0.12 mmol) in 0.2 mL toluene was added to a stirred solution of [WOCl$_2${OSi(O*t*Bu)$_3$}$_2$(thf)] (0.05 g, 0.06 mmol) in 0.5 mL toluene at –45 °C. After stirring for 1 h at ambient temperature, volatiles were removed under reduced pressure, yielding a yellow solid. Extraction of the residue with *n*-hexane gave a red-brown solution. Crystallization from concentrated *n*-hexane solution gave violet blocks of **U** suitable for X-ray diffraction. Yield: 5.4 mg

(0.01 mmol, 10%). ^{1}H NMR (THF-d_8, 400.13 MHz, 26 °C) δ =7.2-6.9 (m, Ar-*H*), 3.23 (s), 2.87 (s), 1.41 (s), 1.35 (s), 1.29 (s) ppm.

[WO(CH$_3$)$_2$({OSi(O*t*Bu)$_3$}$_2$(thf)] (Z). GaMe$_3$ (0.01 g, 0.12 mmol) in 0.2 mL *n*-hexane was added to a stirred solution of (0.05 g, 0.06 mmol) [WOCl$_2$}{OSi(O*t*Bu)$_3$}$_2$(thf)] in 0.5 mL *n*-hexane at −45 °C. The colorless reaction mixture slowly changed colour to a turbid orange. The solution was stirred for 1.5 h at ambient temperature. Filtration yielded a bright orange solution. Crystallization of this solution yielded colorless crystals of [{Me$_2$Ga(OSi(O*t*Bu)$_3$)}$_2$] (**V**). These colorless crystals were discarded and the remaining concentrated *n*-hexane solution was crystallized yielding a mixture of orange needles of [WO(CH$_3$)$_2$({OSi(O*t*Bu)$_3$}$_2$(thf)] and [{Me$_2$Ga(OSi(O*t*Bu)$_3$)}$_2$]. Yield could not be calculated due to persistent co-crystallization of impurities. ^{1}H NMR (THF-d_8, 400.13 MHz, 26 °C) δ =1.34 (s, 27H, *t*Bu) ppm. Further analytics could not be conducted due to thermal sensitivity.

[WOCl$_2$(OMes)$_2$(thf)] (BB). Following a modified literature synthesis[76]. [Na(OMes)(thf)] (0.14 g, 0.6 mmol) in 0.5 mL toluene was added to a stirred orange-brown solution of WOCl$_4$ (0.10 g, 0.3 mmol) in 0.5 mL toluene. Immediately the color changed from orange to red. After stirring for 24 h at ambient temperature, the red solution was filtered, and all volatiles removed under reduced pressure. Extraction of the dark red residue with *n*-hexane yielded a dark red solution. Crystallization from *n*-hexane gave red needles of [WOCl$_2$(OMes)$_2$(thf)]. Yield: 0.09 g (0.15 mmol, 51%). ^{1}H NMR (THF-d_8, 400.13 MHz, 26 °C) δ = 6.9 (s, Ar-*H*), 6.7 (s), 2.13 (s, CH$_3$) ppm; elemental analysis (%) calcd. for C$_{22}$H$_{30}$Cl$_2$O$_3$W (613.2): C 43.09, H 4.93; found: C 43.27.28, H 5.07.

[WOCl$_3$(OMes)(thf)] (CC). Following a modified literature synthesis[76]. [Na(OMes)(thf)] (0.03 g, 0.11 mmol) in 0.2 mL Et$_2$O was added to a stirred bright orange solution of WOCl$_4$ (0.05 g, 0.15 mmol) in 0.5 mL Et$_2$O. Immediately, the color changed from bright orange to dark red. After stirring for 3 h the now dark violet solution was filtered, and all volatiles were removed under reduced pressure. Crystallization from *n*-hexane gave violet needles. Yield: 0.05 g (0.11 mmol, 70%). ^{1}H NMR (THF-d_8, 400.13 MHz, 26 °C) δ = 2.16 (s, Ar-*CH$_3$*) ppm; elemental analysis (%) calcd. for C$_{13}$H$_{19}$Cl$_3$O$_3$W (513.5): C 30.41, H 3.73; found: C 28.28, H 3.84.

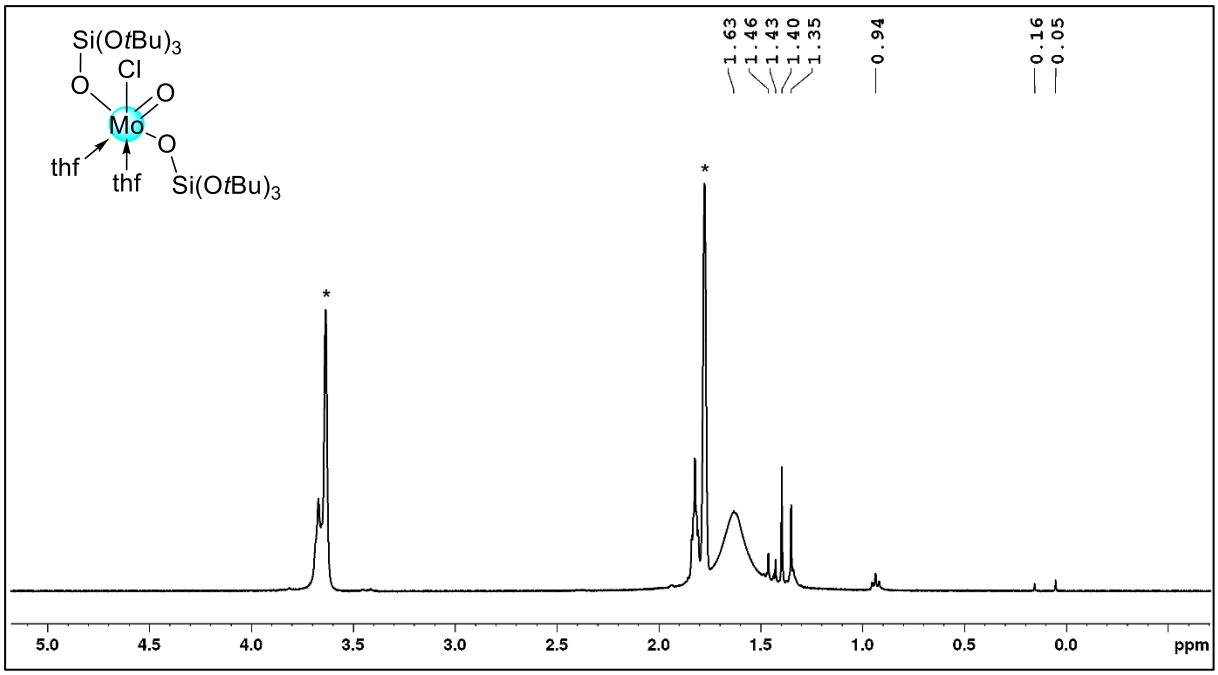

Figure C9. ^{1}H NMR spectrum (THF-d_8, 400.13 MHz, 26 °C) of [MoOCl{OSi(O*t*Bu)$_3$}$_2$(thf)x] (**P^{a}/P^{b}**).

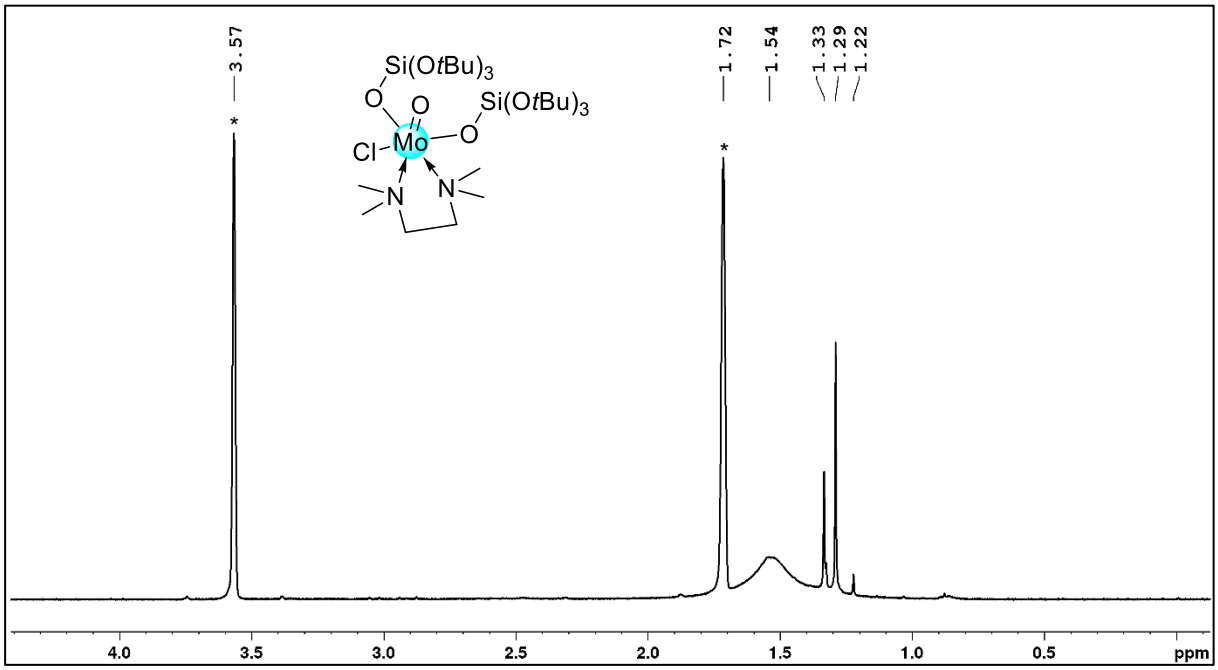

Figure C10. ^{1}H NMR spectrum (THF-d_8, 400.13 MHz, 26 °C) of [MoOCl{OSi(O*t*Bu)$_3$}$_2$(tmeda)] (**Q**).

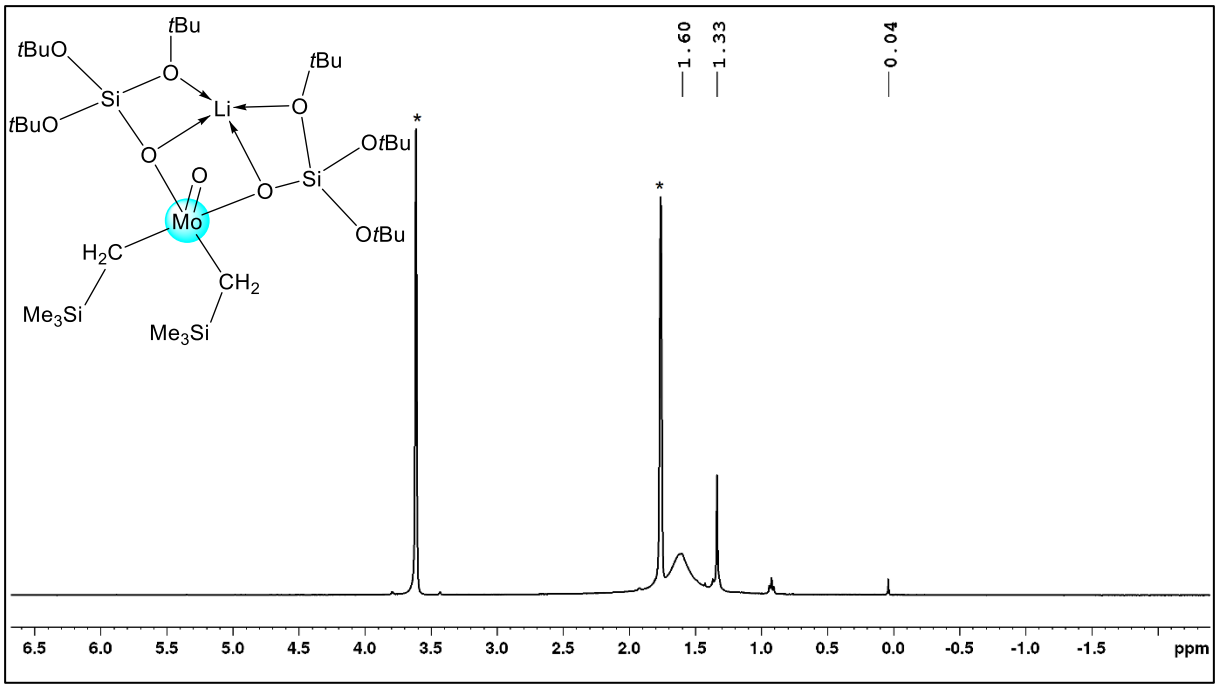

Figure C11. ^{1}H NMR spectrum (THF-d_8, 400.13 MHz, 26 °C) of [LiMoO(CH$_2$SiMe$_3$)$_2${OSi(O*t*Bu)$_3$}$_2$] (**R**).

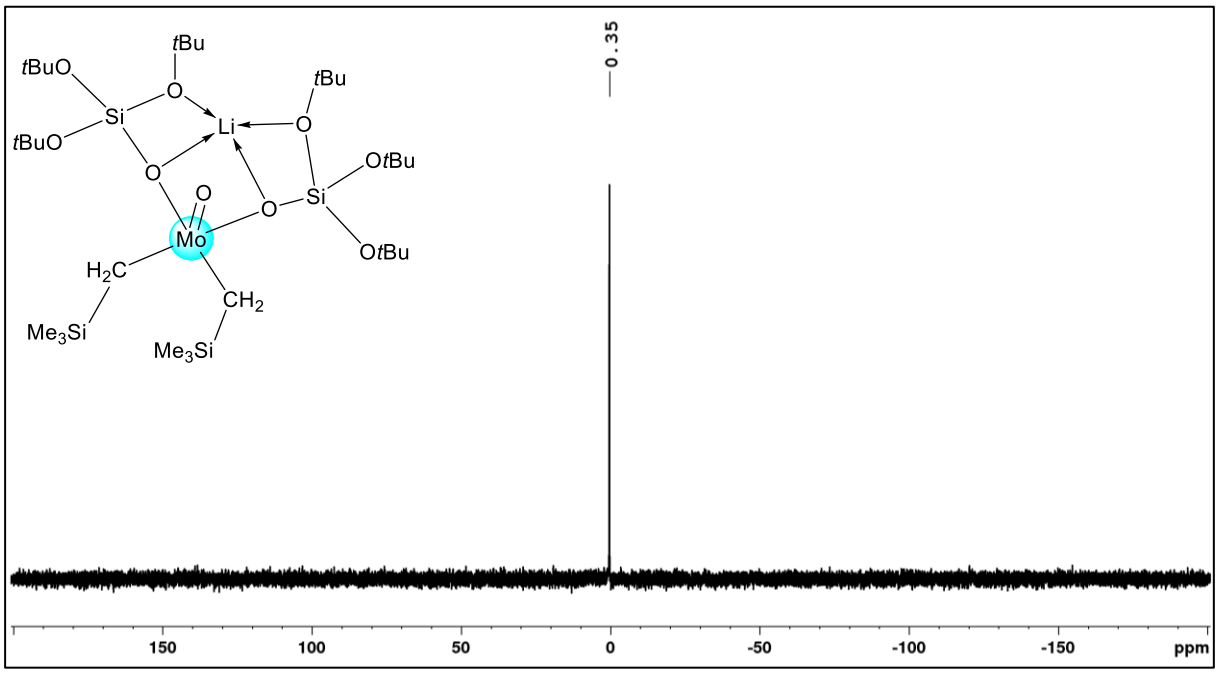

Figure C12. ^{7}Li NMR spectrum (THF-d_8, 116.64 MHz, 26 °C) of [LiMoO(CH$_2$SiMe$_3$)$_2${OSi(O*t*Bu)$_3$}$_2$] (**R**).

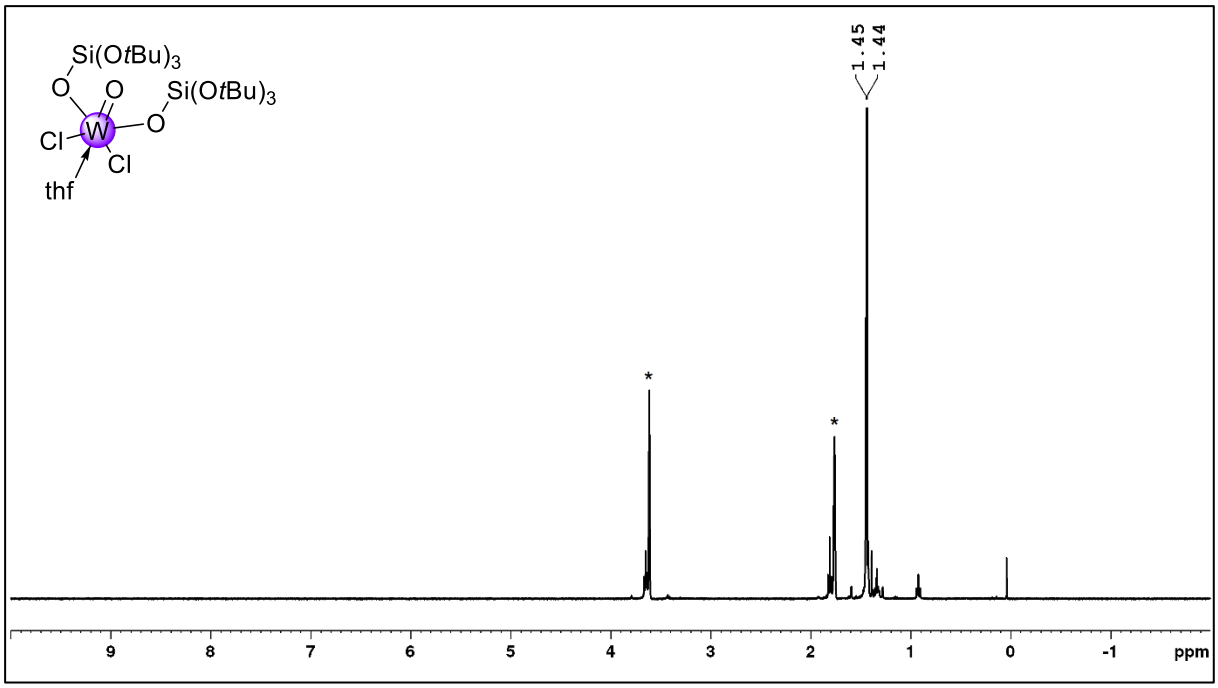

Figure C13. ^{1}H NMR spectrum (THF-d_8, 400.13 MHz, 26 °C) of [$WOCl_2${$OSi(OtBu)_3$}$_2$(thf)] (**S**).

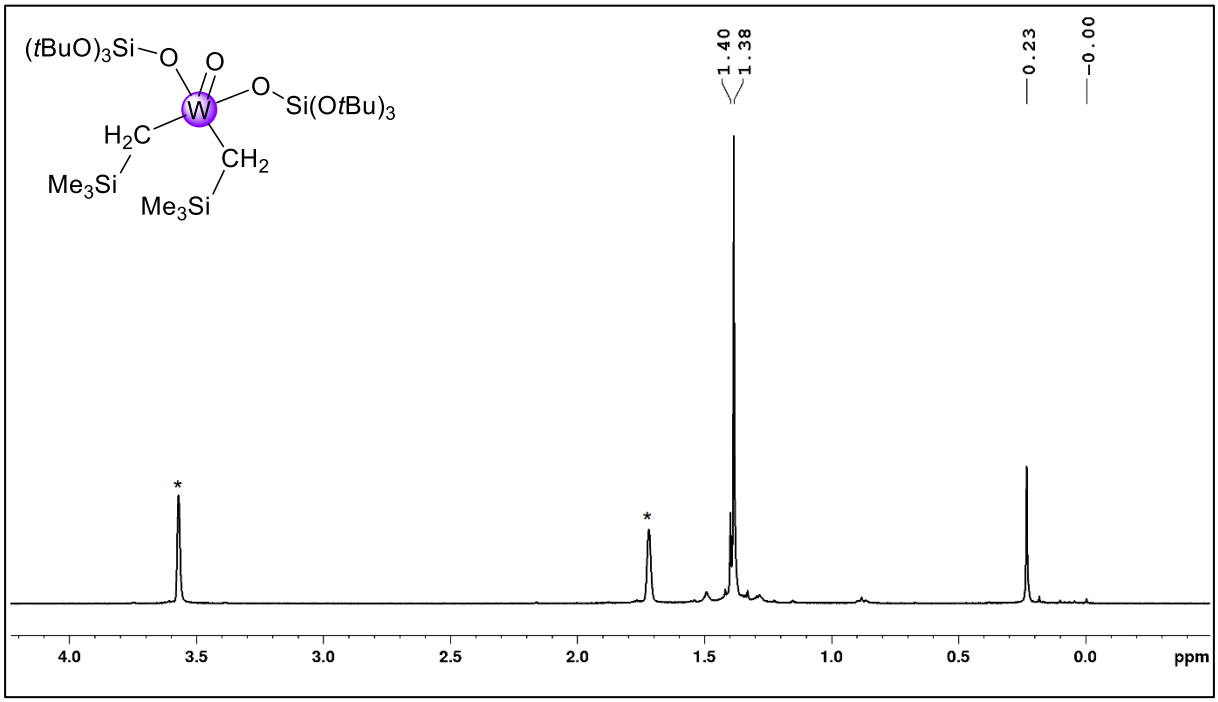

Figure C14. ^{1}H NMR spectrum (THF-d_8, 400.13 MHz, 26 °C) of [$WO(CH_2SiMe_3)_2${$OSi(OtBu)_3$}$_2$] (**T**).

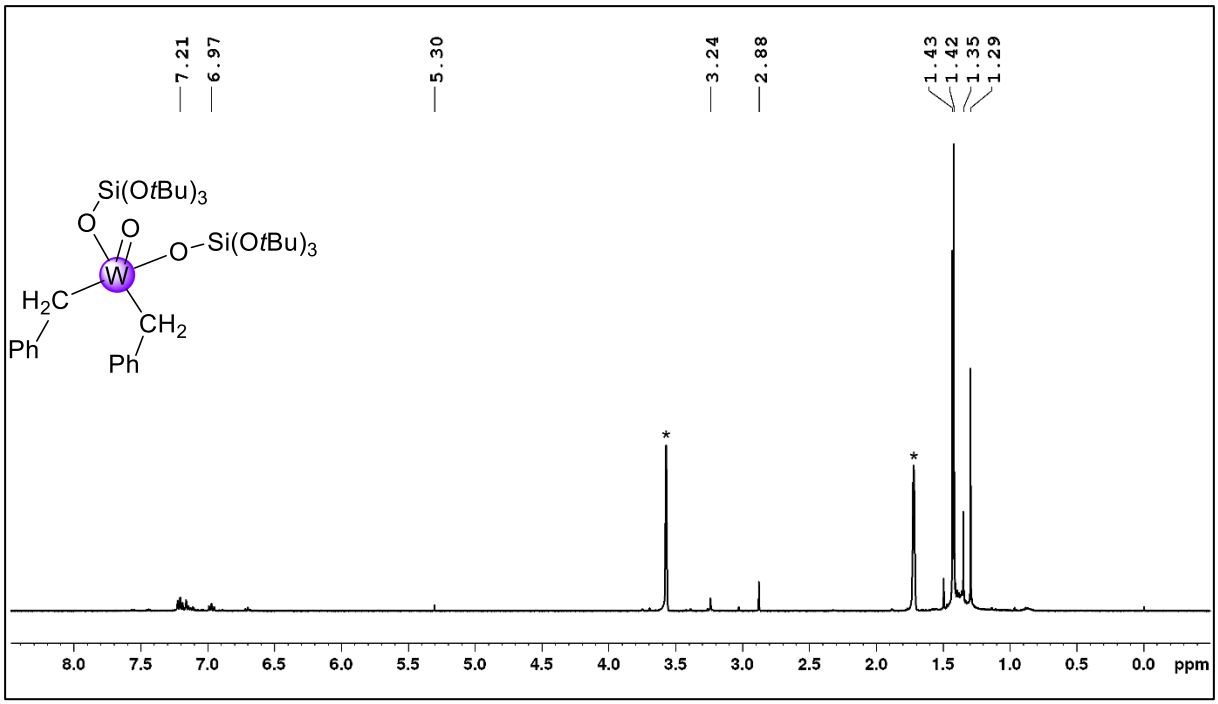

Figure C15. ^{1}H NMR spectrum (THF-d_8, 400.13 MHz, 26 °C) of [WO(CH$_2$Ph)$_2${OSi(O*t*Bu)$_3$}$_2$] (**U**).

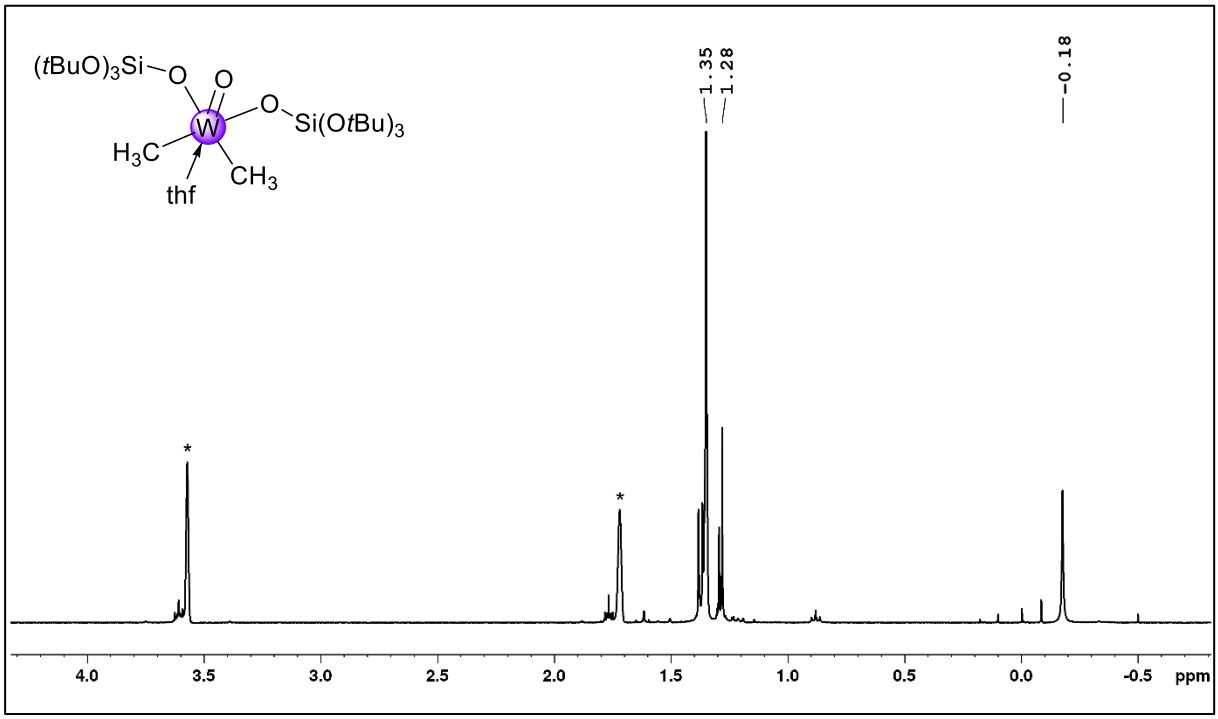

Figure C16. ^{1}H NMR spectrum (THF-d_8, 400.13 MHz, 26 °C) of [WO(CH$_3$)$_2${OSi(O*t*Bu)$_3$}$_2$] (**Z**).

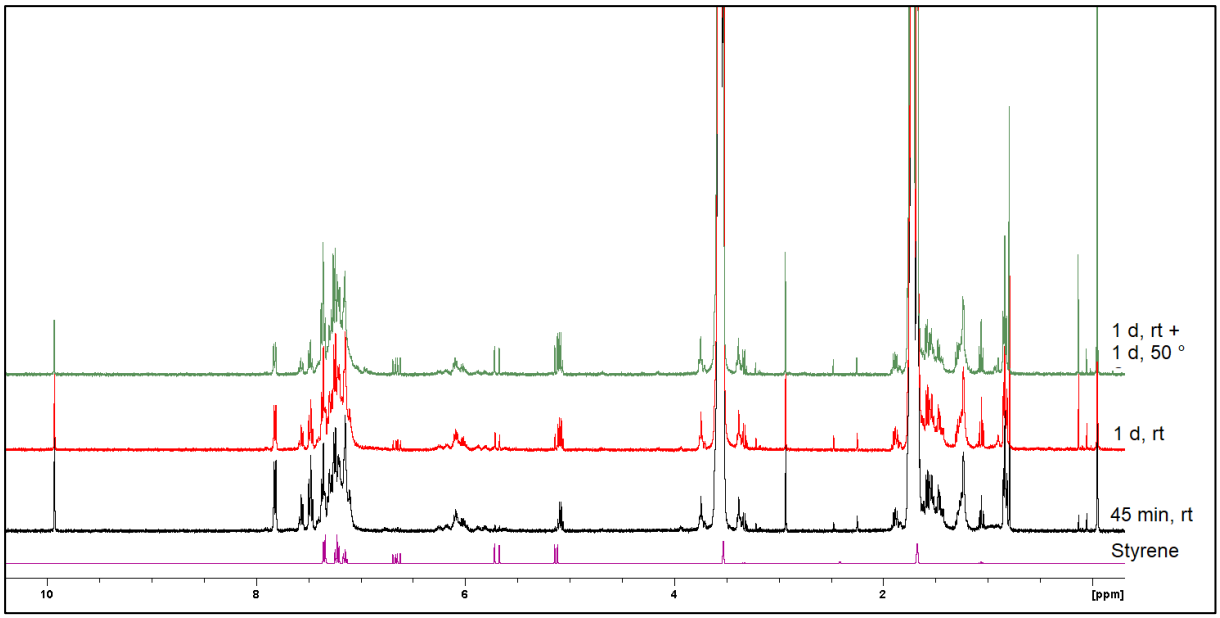

Figure C17. ^{1}H NMR spectra (THF-d_8, 400.13 MHz, 26 °C) of the reaction of $WOCl_3(thf)_2$ with two equivalents of MeLi and 0.5 equivalents of PhCHO in THF-d_8 over several heating intervals. Styrene is shown at the bottom (purple) for comparison.

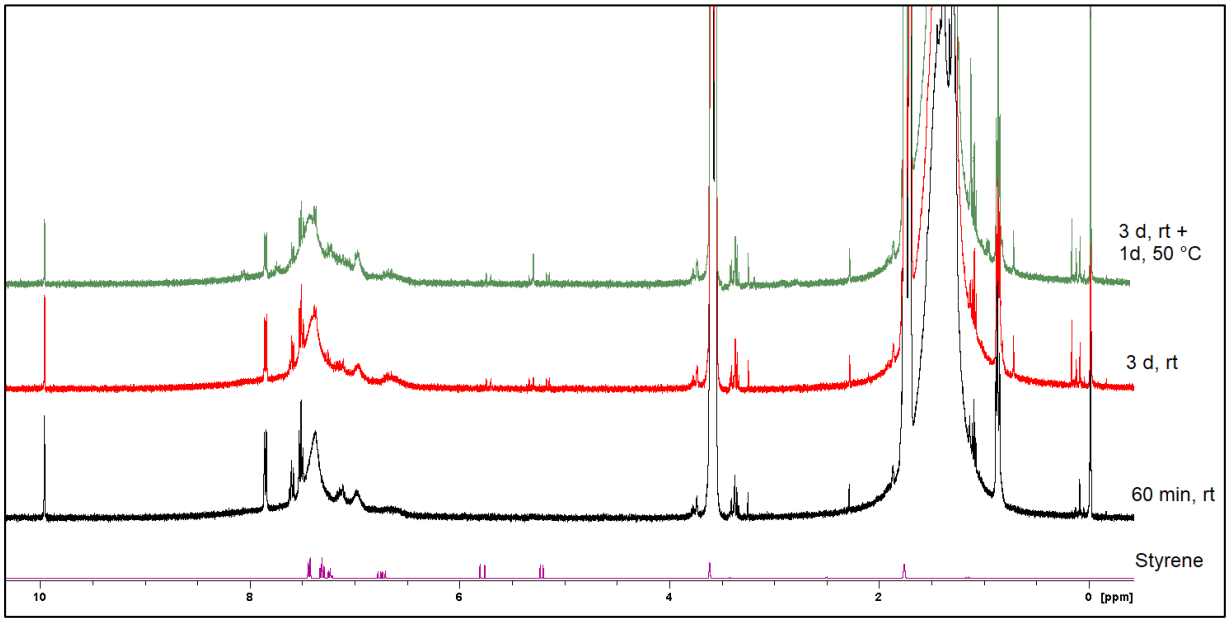

Figure C18. ^{1}H NMR spectra (THF-d_8, 400.13 MHz, 26 °C) of the reaction of **P^{a}** with two equivalents of MeLi and excess of PhCHO in THF-d_8 over several heating intervals. Styrene is shown at the bottom (purple) for comparison.

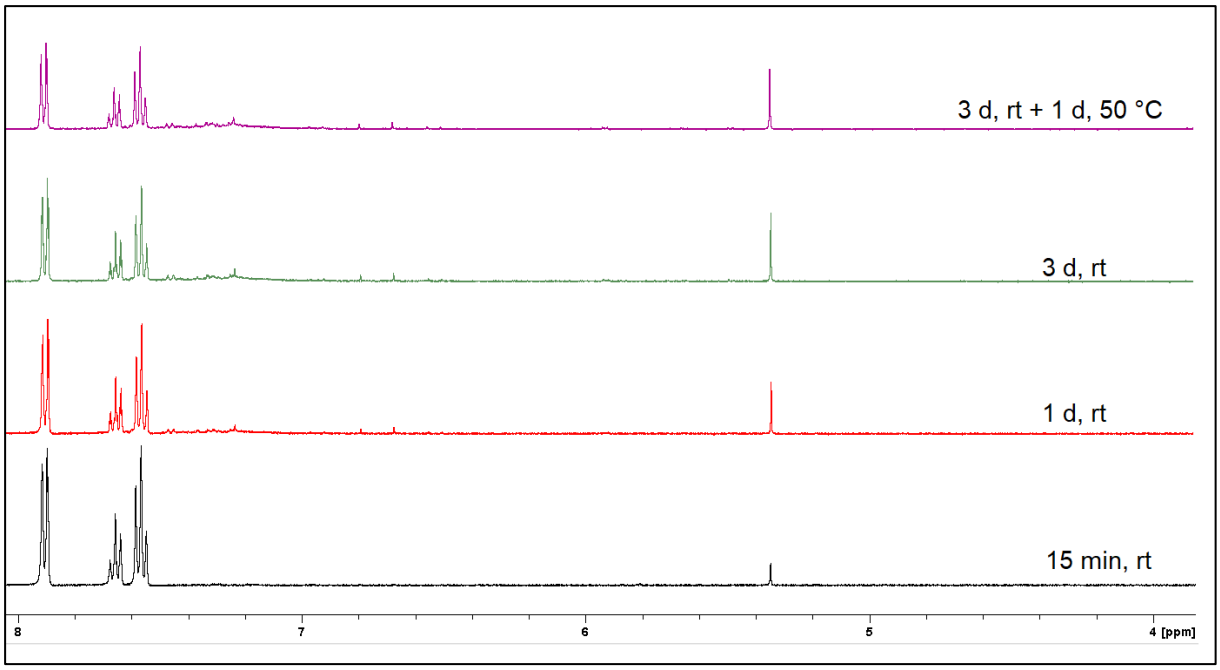

Figure C19. ^{1}H NMR spectra (THF-d_8, 400.13 MHz, 26 °C) of the reaction of [LiMoO(CH$_2$SiMe$_3$)$_2${OSi(O*t*Bu)$_3$}$_2$] (**R**) with excess of PhCHO in THF-d_8 over several heating intervals.

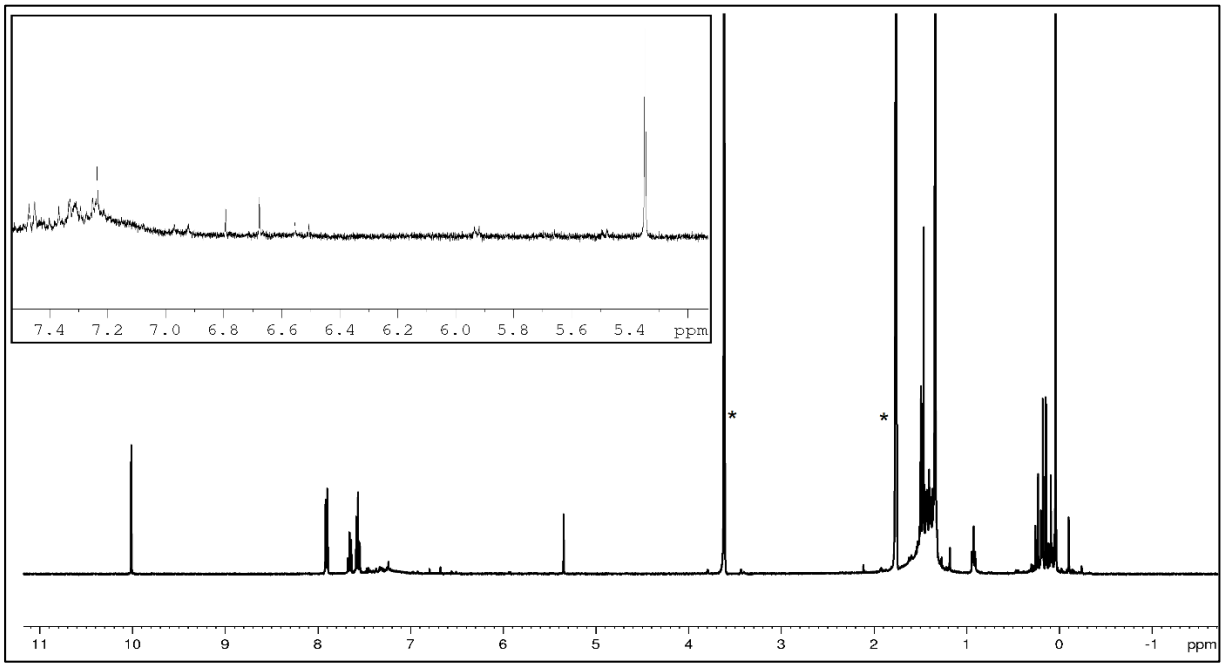

Figure C20. ^{1}H NMR spectra (THF-d_8, 400.13 MHz, 26 °C) of the reaction of [LiMoO(CH$_2$SiMe$_3$)$_2${OSi(O*t*Bu)$_3$}$_2$] (**R**) with excess of PhCHO in THF-d_8 after heating to rt for 3 days and to 50 °C for 1 day.

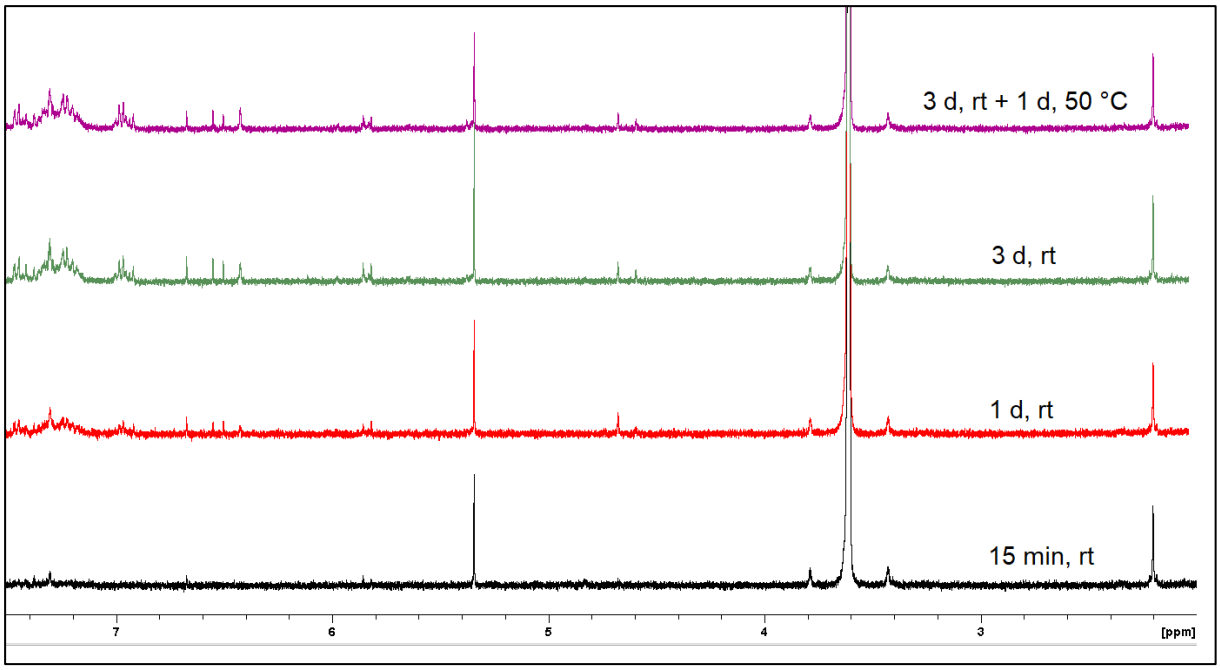

Figure C21. ^{1}H NMR spectra (THF-d_8, 400.13 MHz, 26 °C) of the reaction of $[WO(CH_2SiMe_3)_2\{OSi(OtBu)_3\}_2]$ (**T**) with excess of PhCHO in THF-d_8 over several heating intervals.

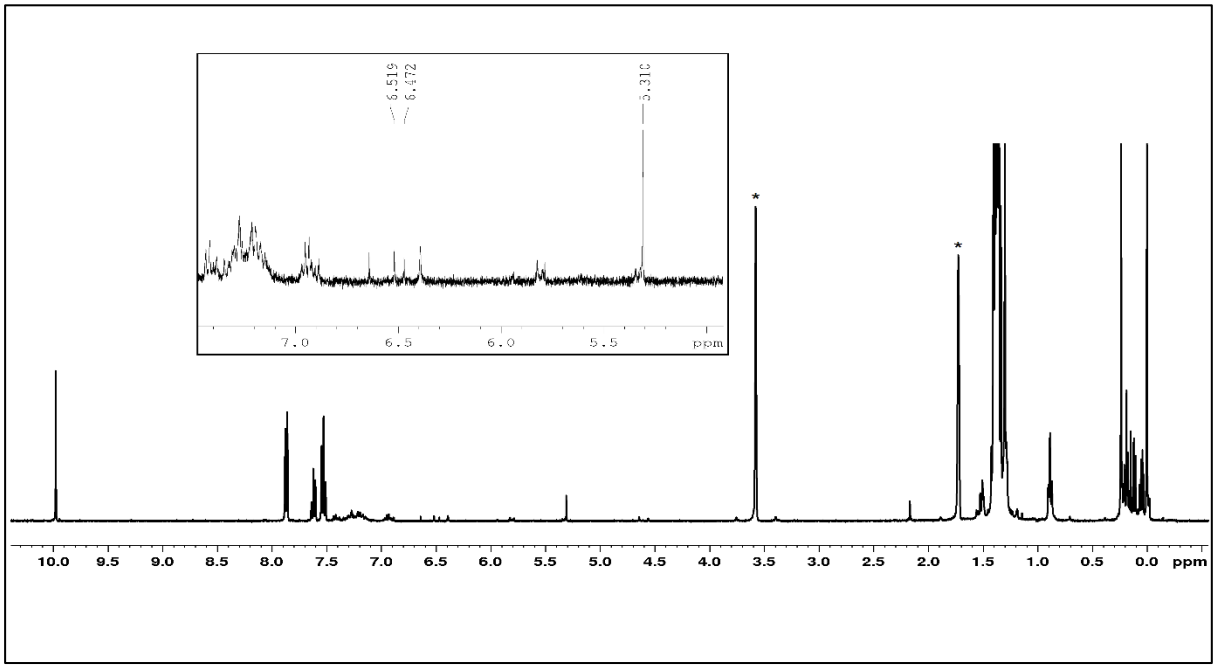

Figure C22. ^{1}H NMR spectrum of the reaction of $[WO(CH_2SiMe_3)_2\{OSi(OtBu)_3\}_2]$ (**T**) with excess of PhCHO in THF-d_8 after heating to rt for 3 days and to 50 °C for 1 day.

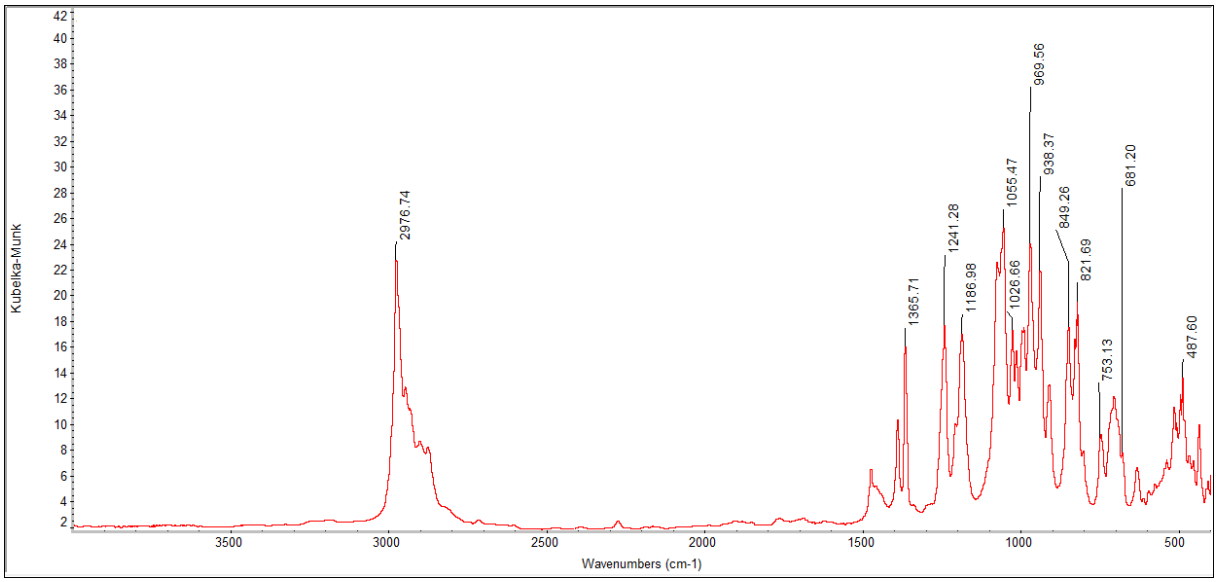

Figure C23. DRIFT spectrum of $[WO(CH_2SiMe_3)_2\{OSi(O\textit{t}Bu)_3\}_2]$ (**T**).

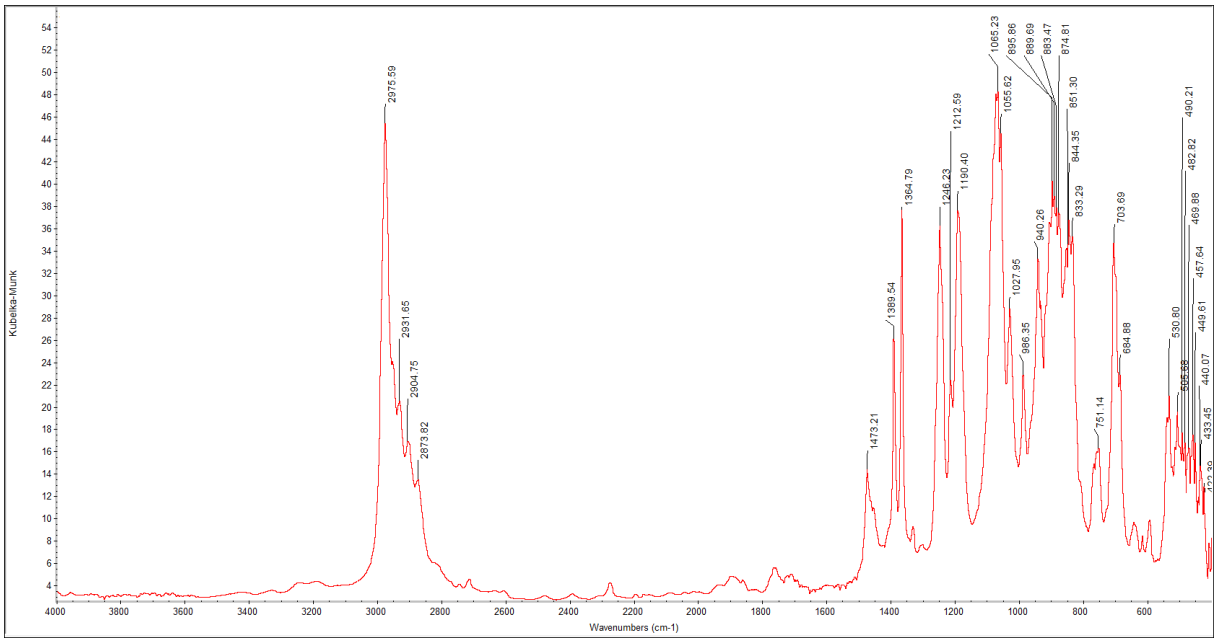

Figure C24. DRIFT spectrum of $[LiMoO(CH_2SiMe_3)_2\{OSi(O\textit{t}Bu)_3\}_2]$ (**R**).

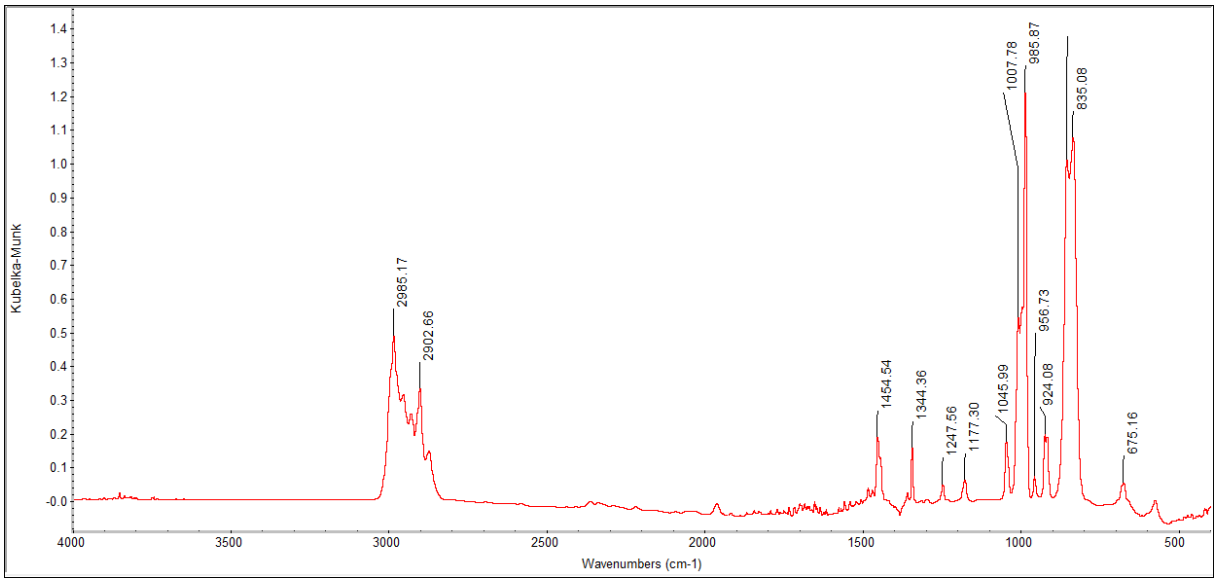

Figure C25. DRIFT spectrum of $[MoOCl_3(thf)_2]$.

.

Table C1. Crystallographic data for compounds **P**, **Q**, **R** and **S**.

	P[a]	**Q**	**R**	**S**
formula	$C_{28}H_{62}ClMoO_{10}Si_2$	$C_{30}H_{70}ClMoN_2O_9Si_2$	$C_{32}H_{76}LiMoO_9Si_4$	$C_{28}H_{62}Cl_2O_{10}Si_2W$
M [g·mol^{-1}]	746.34	790.45	820.16	869.70
λ [Å]	0.71073	0.71073	0.71073	0.71073
color	orange	green	blue-green	colourless
crystal dimensions [mm]	0.269 x 0.262 x 0.202	0.455 x 0.134 x 0.067	0.515 x 0.355 x 0.284	0.413 x 0.163 x 0.152
crystal system	Orthorhombic	Monoclinic	Monoclinic	Monoclinic
space group	P212121	C2/c	$P2_1/n$	$P2_1$
a [Å]	9.8954(8)	54.734(4)	13.2717(5)	9.4265(7)
b [Å]	14.1813(11)	9.0987(7)	24.3484(8)	14.6292(10)
c [Å]	27.775(2)	17.2786(14)	15.3466(5)	14.5922(10)
α [°]	90	90	90	90
β [°]	90	97.844(3)	109.2450(10)	99.4520(10)
γ [°]	90	90	90	90
V [Å^3]	3897.7(5)	8524.4(12)	4682.0(3)	1985.0(2)
Z	4	8	4	2
F(000)	1588	3384	1764	892
T [K]	100(2)	180(2)	100(2)	100(2)
ρ_{calcd} [g·cm^{-3}]	1.272	1.232	1.164	1.455
μ[mm^{-1}]	0.511	0.471	0.423	3.150
Data / restraints / parameters	11874 / 0 / 398	7874 / 879 / 521	14233 / 90 / 479	10059 / 1 / 407
Goodness of fit	1.034	1.172	1.057	0.790
R_1 (I > 2σ (I))[a]	0.0232	0.0645	0.0280	0.0226
ωR_2 (all data)[b]	0.0563	0.1651	0.0725	0.0490

[a] $R_1 = \Sigma(||F0|-|Fc||)/\Sigma|F0|, F0> 4s(F0)$. $\omega R_2 = \{\Sigma[w(F02-Fc2)2/\Sigma[w(F02)^2]\}^{1/2}$

Table C2. Crystallographic data for compounds **T**, **U**, **Z**, **BB** and **CC**.

	T	**U**	**Z**	**BB**	**CC**
formula	$C_{32}H_{76}O_9Si_4W$	$C_{38}H_{68}O_9Si_2W$	$C_{30}H_{68}O_{10}Si_2W$	$C_{22}H_{30}Cl_2O_4W$	$C_{13}H_{19}Cl_3O_3W$
M [g·mol^{-1}]	901.13	908.95	828.87	613.21	513.48
λ [Å]	0.71073	0.71073	0.71073	0.71073	0.71073
color	yellow?	violet	orange	violet	red
crystal dimensions [mm]	0.244 x 0.162 x 0.071	0.338 x 0.168 x 0.098	0.723 x 0.374 x 0.252	0.265 x 0.100 x 0.055	0.250 x 0.098 x 0.077
crystal system	Monoclinic	Monoclinic	Monoclinic	Monoclinic	Triclinic
space group	P21/n	C2/c	P21	C2/c	P-1
a [Å]	9.8087(6)	28.668(2)	9.47267(10)	14.1377(6)	8.0507(2)
b [Å]	36.900(2)	9.4042(8)	14.54009(16)	9.3582(4)	8.2812(2)
c [Å]	13.5402(8)	16.6194(14)	15.19034(16	17.8562(7)	12.9888(4)
α [°]	90	90	90	90	73.8070(10)
β [°]	110.2070(10)	104.1670(10)	100.1990(10)	99.1170(10)	83.6290(10)
γ [°]	90	90	90	90	81.9480(10)
V [Å^3]	4599.1(5)	4344.3(6)	2059.16(4)	2332.59(17)	821.05(4)
Z	4	4	2	4	2
F(000)	1880	1880	860	1208	492
T [K]	100(2)	100(2)	150(2)	100(2)	100(2)
ρ_{calcd} [g·cm^{-3}]	1.301	1.390	1.337	1.746	2.077
μ[mm^{-1}]	2.657	2.761	2.907	5.206	7.525
Data / restraints / parameters	14090 / 1 / 452	8274 / 0 / 244	17585 / 823 / 486	3259 / 0 / 136	4997 / 0 / 184
Goodness of fit	1.171	1.109	0.999	1.096	1.096
R_1 (I > 2σ (I))[a]	0.0359	0.0171	0.0251	0.0152	0.0253
ωR_2 (all data)[b]	0.0728	0.0433	0.0584	0.0371	0.0591

[a] $R_1 = \Sigma(||F0|-|Fc||)/\Sigma|F0|, F0> 4s(F0)$. $\omega R_2 = \{\Sigma[w(F02-Fc2)2/\Sigma[w(F02)^2]\}^{1/2}$

D

Bibliography

[1] a) G. Wittig, G. Geissler, *Justus Liebigs Ann. Chem.* **1953**, *580*, 44–57; b) L. Horner, H. Hoffmann, H. G. Wippel, *Chem. Ber.* **1958**, *91*, 64–67; c) D. J. Peterson, *J. Org. Chem.* **1968**, *33*, 780–784; d) J. E. Mc Murry, M. P. Fleming, *J. Am. Chem. Soc.* **1974**, *96*, 4708–4709; e) F. N. Tebbe, G. W. Parshall, G. S. Reddy, *J. Am. Chem. Soc.* **1978**, *100*, 3611–3613.

[2] a) L. E. Overman, *Organic reactions*, Wiley, Hoboken, NJ, **2001**; b) T. Takeda, *Modern Carbonyl Olefination*, Wiley, **2003**; c) M. G. Moloney (Ed.) *Organic reaction mechanisms*, *Vol. 54*, Wiley, Chichester, West Sussex, **2021**.

[3] K. Takai, K. Nitta, K. Utimoto, *J. Am. Chem. Soc.* **1986**, *108*, 7408–7410.

[4] T. Kauffmann, M. Enk, P. Fiegenbaum, U. Hansmersmann, W. Kaschube, M. Papenberg, E. Toliopoulos, S. Welke, *Chem. Ber.* **1994**, *127*, 127–135.

[5] T. Kauffmann, B. Ennen, J. Sander, R. Wieschollek, *Angew. Chem. Int. Ed. Engl.* **1983**, *22*, 244–245.

[6] L. A. Wessjohann, G. Scheid, *Synthesis* **1999**, *1999*, 1–36.

[7] a) D. A. Evans, W. C. Black, *J. Am. Chem. Soc.* **1993**, *115*, 4497–4513; b) E. Matoušová, P. Koukal, B. Formánek, M. Kotora, *Org. Lett.* **2016**, *18*, 5656–5659; c) B. M. Trost, J. D. Knopf, C. S. Brindle, *Chem. Rev.* **2016**, *116*, 15035–15088; d) L. C. Dias, E. C. de Lucca, *J. Org. Chem.* **2017**, *82*, 3019–3045.

[8] B. Saikia, T. J. Devi, N. C. Barua, *Org. Biomol. Chem.* **2013**, *11*, 905–913.

[9] M. Tortosa, N. A. Yakelis, W. R. Roush, *J. Am. Chem. Soc.* **2008**, *130*, 2722–2723.

[10] P. Liu, E. N. Jacobsen, *J. Am. Chem. Soc.* **2001**, *123*, 10772–10773.

[11] T. Okazoe, K. Takai, K. Utimoto, *J. Am. Chem. Soc.* **1987**, *109*, 951–953.

[12] K. Takai, S. Toshikawa, A. Inoue, R. Kokumai, *J. Am. Chem. Soc.* **2003**, *125*, 12990–12991.

[13] M. Murai, R. Taniguchi, N. Hosokawa, Y. Nishida, H. Mimachi, T. Oshiki, K. Takai, *J. Am. Chem. Soc.* **2017**, *139*, 13184–13192.

[14] M. Murai, C. Mizuta, R. Taniguchi, K. Takai, *Org. Lett.* **2017**, *19*, 6104–6107.

[15] M. Murai, R. Taniguchi, C. Mizuta, K. Takai, *Org. Lett.* **2019**, *21*, 2668–2672.

[16] K. Oesterreich, D. Spitzner, *Tetrahedron* **2002**, *58*, 4331–4334.

[17] K. Oesterreich, I. Klein, D. Spitzner, *Synlett* **2002**, *10*, 1712–1714.

[18] P. Schär, P. Renaud, *Org. Lett.* **2006**, *8*, 1569–1571.

[19] S. Cren, P. Schär, P. Renaud, K. Schenk, *J. Org. Chem.* **2009**, *74*, 2942–2946.

[20] A. C. Wright, C. W. Lee, B. M. Stoltz, *Org. Lett.* **2019**, *21*, 9658–9662.

[21] N. Marinus, N. Tahiri, M. Duca, L. M. C. M. Mouthaan, S. Bianca, M. van den Noort, B. Poolman, M. D. Witte, A. J. Minnaard, *Org. Lett.* **2020**, *22*, 5622–5626.

[22] M. Haider, G. Sennari, A. Eggert, R. Sarpong, *J. Am. Chem. Soc.* **2021**, *143*, 2710–2715.

[23] T. Kauffmann, J. Baune, P. Fiegenbaum, U. Hansmersmann, C. Neiteler, M. Papenberg, R. Wieschollek, *Chem. Ber.* **1993**, *126*, 89–96.

[24] T. Kauffmann, *Angew. Chem. Int. Ed. Engl.* **1997**, *36*, 1258–1275.

[25] T. Kauffmann, B. Ennen, J. Sander, R. Wieschollek, *Angew. Chem. Int. Ed. Engl.* **1983**, *22*, 222–227.

[26] D. Werner, R. Anwander, *J. Am. Chem. Soc.* **2018**, *140*, 14334–14341.

[27] T. Kauffmann, M. Enk, W. Kaschube, E. Tolipoulos, D. Wingbermühle, *Angew. Chem. Int. Ed. Engl.* **1986**, *25*, 910–911.

[28] K. Takai in *Organic reactions*, Wiley Online Library, [Hoboken, N.J.], **2004**, 253–612.

[29] K. Takai, M. Hirano, S. Toshikawa, *Synlett* **2004**, *8*, 1347–1350.

[30] J. K. Kochi, P. E. Mocadlo, *J. Am. Chem. Soc.* **1966**, *88*, 4094–4096.

[31] a) S. Nakatsukasa, K. Takai, K. Utimoto, *J. Organomet. Chem.* **1986**, *51*, 5045–5046; b) *1.06 Organochromium Reagents A2 - Knochel, Paul. In Comprehensive Organic Synthesis II, 2nd ed.; Elsevier: Amsterdam, 2014; pp 159– 203.*

[32] K. Takai, R. Kokumai, T. Nobunaka, *Chem. Commun.* **2001**, 1128–1129.

[33] K. Takai, S. Toshikawa, A. Inoue, R. Kokumai, M. Hirano, *J. Organomet. Chem.* **2007**, *692*, 520–529.

[34] a) C. E. Castro, W. C. Kray, *J. Am. Chem. Soc.* **1963**, *85*, 2768–2773; b) J. K. Kochi, D. D. Davis, *J. Am. Chem. Soc.* **1964**, *86*, 5264–5271; c) R. Sneeden, H. P. Throndsen, *J. Organomet. Chem.* **1966**, *6*, 542–550; d) J. K. Kochi, J. W. Powers, *J. Am. Chem. Soc.* **1970**, *92*, 137–146.

[35] S. M. Geddis, C. E. Hagerman, W. R. J. D. Galloway, H. F. Sore, J. M. Goodman, D. R. Spring, *Beilstein J Org Chem* **2017**, *13*, 323–328.

[36] T. Kurogi, K. Irifune, T. Enoki, K. Takai, *Chem. Commun.* **2021**, *57*, 5199–5202.

[37] D. S. Richeson, S. W. Hsu, N. H. Fredd, G. van Duyne, K. H. Theopold, *J. Am. Chem. Soc.* **1986**, *108*, 8273–8274.

[38] a) J. Andrez, J. Pécaut, P.-A. Bayle, M. Mazzanti, *Angew. Chem. Int. Ed. Engl.* **2014**, *53*, 10448–10452; b) J. Friedrich, C. Maichle-Mössmer, R. Anwander, *Chem. Commun.* **2017**, *53*, 12044–12047; c) R. P. Kelly, L. Maron, R. Scopelliti, M. Mazzanti, *Angew. Chem. Int. Ed. Engl.* **2017**, *56*, 15663–15666; d) J. Friedrich, Y. Qiao, C. Maichle-Mössmer, E. J. Schelter, R. Anwander, *Dalton Trans.* **2018**, *47*, 10113–10123; e) S. N. König, C. Maichle-Mössmer, K. W. Törnroos, R. Anwander, *Z. Naturforsch. B* **2014**, *69*, 1375–1383.

[39] T. Auvray, O. Nachtigall, W. W. Brennessel, W. D. Jones, E. M. Matson, *Dalton Trans.* **2021**, *50*, 4300–4310.

[40] P. T. Wolczanski, *Polyhedron* **1995**, *14*, 3335–3362.

[41] C. Krempner, *Eur. J. Inorg. Chem.* **2011**, *2011*, 1689–1698.

[42] J. K. Kochi, D. M. Singleton, L. J. Andrews, *Tetrahedron* **1968**, *24*, 3503–3515.

[43] O. L. Sydora, P. T. Wolczanski, E. B. Lobkovsky, C. Buda, T. R. Cundari, *Inorg. Chem.* **2005**, *44*, 2606–2618.

[44] O. L. Sydora, D. S. Kuiper, P. T. Wolczanski, E. B. Lobkovsky, A. Dinescu, T. R. Cundari, *Inorg. Chem.* **2006**, *45*, 2008–2021.

[45] P. Qiu, R. Cheng, B. Liu, B. Tumanskii, R. J. Batrice, M. Botoshansky, M. S. Eisen, *Organometallics* **2011**, *30*, 2144–2148.

[46] D. R. Neithamer, R. E. LaPointe, R. A. Wheeler, D. S. Richeson, G. D. van Duyne, P. T. Wolczanski, *J. Am. Chem. Soc.* **1989**, *111*, 9056–9072.

[47] L. Barluzzi, M. Falcone, M. Mazzanti, *Chem. Commun.* **2019**, *55*, 13031–13047.

[48] A. K. McMullen, T. D. Tilley, A. L. Rheingold, S. J. Geib, *Inorg. Chem.* **1990**, *29*, 2228–2232.

[49] N. Dettenrieder, H. M. Dietrich, C. Maichle-Mössmer, R. Anwander, *Chem. Eur. J.* **2016**, *22*, 13189–13200.

[50] G. Lapadula, M. P. Conley, C. Copéret, R. A. Andersen, *Organometallics* **2015**, *34*, 2271–2277.

[51] M. P. Conley, M. F. Delley, G. Siddiqi, G. Lapadula, S. Norsic, V. Monteil, O. V. Safonova, C. Copéret, *Angew. Chem. Int. Ed. Engl.* **2014**, *53*, 1872–1876.

[52] C. A. McAuliffe, A. Werfali, W. E. Hill, D. Minahan, *Inorg. Chim. Acta* **1982**, *60*, 87–91.

[53] V. C. Gibson, T. P. Kee, A. Shaw, *Polyhedron* **1990**, *9*, 2293–2298.

[54] L. Favero, F. Marchetti, G. Pampaloni, S. Zacchini, *Dalton Trans.* **2014**, *43*, 495–504.

[55] a) S. Dolci, F. Marchetti, G. Pampaloni, S. Zacchini, *Dalton Trans.* **2010**, *39*, 5367–5376; b) C. Vitzthumecker, F. Robinson, A. Pfitzner, *Monatsh Chem* **2017**, *148*, 629–633; c) F. Marchetti, G. Pampaloni, S. Zacchini, *Dalton Trans.* **2013**, *42*, 15226–15234.

[56] W. Levason, C. A. McAuliffe, F. P. McCullough, *Inorg. Chem.* **1977**, *16*, 2911–2916.

[57] D. E. Smith, W. Levason, J. Powell, G. Reid, *Dalton Trans.* **2021**, *50*, 4380–4389.

[58] a) K. Dreisch, C. Andersson, C. Sta»handske, *Polyhedron* **1992**, *11*, 2143–2150; b) K. Dreisch, C. Andersson, C. St»lhandske, *Polyhedron* **1991**, *10*, 2417–2421.

[59] T. Kauffmann, P. Fiegenbaum, R. Wieschollek, *Angew. Chem. Int. Ed. Engl.* **1984**, *23*, 531–532.

[60] a) O. Fujimura, G. C. Fu, P. W. K. Rothemund, R. H. Grubbs, *J. Am. Chem. Soc.* **1995**, *117*, 2355–2356; b) R. R. Schrock, *Angew. Chem. Int. Ed. Engl.* **2006**, *45*, 3748–3759; c) R. R. Schrock, *Chem. Rev.* **2002**, *102*, 145–179.

[61] R. R. Schrock, *Chem. Rev.* **2009**, *109*, 3211–3226.

[62] a) N. Calderon, E. A. Ofstead, W. A. Judy, *Angew. Chem. Int. Ed. Engl.* **1976**, *88*, 433–442; b) D. Gajan, N. Rendón, K. M. Wampler, B. Jean-Marie, C. Copéret, A. Lesage, L. Emsley, R. R. Schrock, *Dalton Trans.* **2010**, *39*, 8547–8551; c) L. C. H. Gerber, R. R. Schrock, P. Müller, M. K. Takase, *J. Am. Chem. Soc.* **2011**, *133*, 18142–18144; d) K. W. Chan, E. Lam, V. D'Anna, F. Allouche, C. Michel, O. V. Safonova, P. Sautet, C. Copéret, *J. Am. Chem. Soc.* **2018**, *140*, 11395–11401.

[63] a) M. R. Churchill, A. L. Rheingold, H. J. Wasserman, *Inorg. Chem.* **1981**, *20*, 3392–3399; b) P. R. Sharp, S. J. Holmes, R. R. Schrock, M. R. Churchill, H. J. Wasserman, *J. Am. Chem. Soc.* **1981**, *103*, 965–966; c) J. H. Wengrovius, J. Sancho, R. R. Schrock, *J. Am. Chem. Soc.* **1981**, *103*, 3932–3934; d) S. J. Holmes, D. N. Clark, H. W. Turner, R. R. Schrock, *J. Am. Chem. Soc.* **1982**, *104*, 6322–6329; e) S. L. Latesky, J. P. Selegue, *J. Am. Chem. Soc.* **1987**, *109*, 4731–4733; f) J. C. Peters, A. L. Odom, C. C. Cummins, *Chem. Commun.* **1997**, 1995; g) R. L. Miller, P. T. Wolczanski, A. L. Rheingold, *J. Am. Chem. Soc.* **1993**, *115*, 10422–10423; h) J. Manna, R. J. Kuk, R. F. Dallinger, M. D. Hopkins, *J. Am. Chem. Soc.* **1994**, *116*, 9793–9794; i) L. M. Atagi, S. C. Critchlow, J. M. Mayer, *J. Am. Chem. Soc.* **1992**, *114*, 1483–1484; j) M. H. Chisholm, K. Folting, D. M. Hoffman, J. C. Huffman, *J. Am. Chem. Soc.* **1984**, *106*, 6794–6805.

[64] T. Kauffmann, R. Abeln, S. Welke, D. Wingbermühle, *Angew. Chem. Int. Ed. Engl.* **1986**, *25*, 909–910.

[65] O. I. Guzyr, J. Prust, H. W. Roesky, C. Lehmann, M. Teichert, F. Cimpoesu, *Organometallics* **2000**, *19*, 1549–1555.

[66] *Advances in Organometallic Chemistry*. *Advances in Organometallic Chemistry , ed. P. J. Pérez , Elsevier , 1976 , vol. 14*, **1976**.

[67] T. Kauffmann, P. Fiegenbaum, M. Papenberg, R. Wieschollek, D. Wingbermühle, *Chem. Ber.* **1993**, *126*, 79–87.

[68] a) R. Schrock, S. Rocklage, J. Wengrovius, G. Rupprecht, J. Fellmann, *J. Mol. Catal.* **1980**, *8*, 73–83; b) J. H. Wengrovius, R. R. Schrock, *Organometallics* **1982**, *1*, 148–155.

[69] R. A. Andersen, M. H. Chisholm, J. F. Gibson, W. W. Reichert, I. P. Rothwell, G. Wilkinson, *Inorg. Chem.* **1981**, *20*, 3934–3936.

[70] T. Kauffmann, P. Fiegenbaum, M. Papenberg, R. Wieschollek, J. Sander, *Chem. Ber.* **1992**, *125*, 143–148.

[71] G. A. Bain, J. F. Berry, *J. Chem. Educ.* **2008**, *85*, 532.

[72] G. R. Fulmer, A. J. M. Miller, N. H. Sherden, H. E. Gottlieb, A. Nudelman, B. M. Stoltz, J. E. Bercaw, K. I. Goldberg, *Organometallics* **2010**, *29*, 2176–2179.

[73] E. Le Roux, Y. Liang, K. W. Törnroos, F. Nief, R. Anwander, *Organometallics* **2012**, *31*, 6526–6537.

[74] K. Samedov, Y. Aksu, M. Driess, *ChemPlusChem* **2012**, *77*, 663–674.

[75] D. C. Rosenfeld, D. S. Kuiper, E. B. Lobkovsky, P. T. Wolczanski, *Polyhedron* **2006**, *25*, 251–258.

[76] M. W. Glenny, A. J. Nielson, C. E. Rickard, *Polyhedron* **1998**, *17*, 851–856.

[77] a) T. Kauffmann, T. Abel, M. Schreer, D. Wingbermühle, *Tetrahedron* **1987**, *43*, 2021–2028; b) M. T. Reetz, S. H. Kyung, M. Hüllmann, *Tetrahedron* **1986**, *42*, 2931–2935.

E

Publications

Paper I

Beyond Takai´s Olefination Reagent: Persistent Dehalogenation Emerges in a Chromium(III)-μ_3-Methylidyne Complex

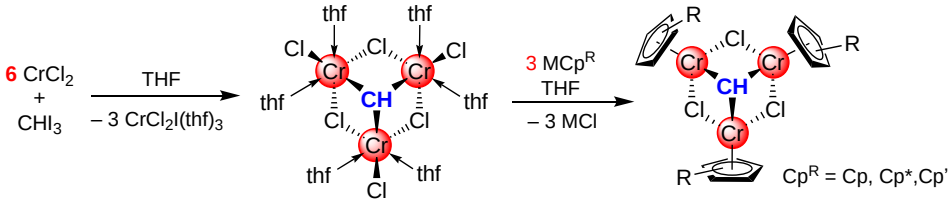

How to cite: *Angew. Chem. Int. Ed.* **2021**, *60*, 20049–20054
International Edition: doi.org/10.1002/anie.202106608
German Edition: doi.org/10.1002/ange.202106608

Coordination Chemistry

Beyond Takai's Olefination Reagent: Persistent Dehalogenation Emerges in a Chromium(III)-μ_3-Methylidyne Complex

Simon Trzmiel, Jan Langmann, Daniel Werner, Cäcilia Maichle-Mössmer, Wolfgang Scherer, and Reiner Anwander**

Abstract: *Reaction of CHI_3 with six equivalents of $CrCl_2$ in THF at low temperatures affords $[Cr_3Cl_3(\mu_2\text{-}Cl)_3(\mu_3\text{-}CH)(thf)_6]$ as the first isolable high-yield Cr^{III} μ_3-methylidyne complex. Substitution of the terminal chlorido ligands via salt metathesis with alkali-metal cyclopentadienides generates isostructural half-sandwich chromium(III)-μ_3-methylidynes $[Cp^R{}_3Cr_3(\mu_2\text{-}Cl)_3(\mu_3\text{-}CH)]$ ($Cp^R = C_5H_5$, C_5Me_5, $C_5H_4SiMe_3$). Side and decomposition products of the Cl/Cp^R exchange reactions were identified and structurally characterized for $[Cr_4(\mu_2\text{-}Cl)_4(\mu_2\text{-}I)_2(\mu_4\text{-}O)(thf)_4]$ and $[(\eta^5\text{-}C_5H_4SiMe_3)CrCl(\mu_2\text{-}Cl)_2Li(thf)_2]$. The Cl/$Cp^R$ exchange drastically changed the ambient-temperature effective magnetic moment μ_{eff} from 9.30/9.11 μ_B (solution/solid) to 3.63/4.32 μ_B ($Cp^R = C_5Me_5$). Reactions of $[Cr_3Cl_3(\mu_2\text{-}Cl)_3(\mu_3\text{-}CH)(thf)_6]$ with aldehydes and ketones produce intricate mixtures of species through oxy/methylidyne exchange, which were partially identified as radical recombination products through GC/MS analysis and ^1H NMR spectroscopy.*

Introduction

Carbyne or alkylidyne moieties display archetypal ligands in organo(transition)metal chemistry.[1] In particular, alkylidyne complexes of the high-oxidation-state heavier group 6 metals molybdenum and tungsten emerged as eminent alkyne metathesis catalysts.[2] Such discrete complexes feature multiply bonded terminal moieties of the type M≡CR (M = Mo, W) and have been studied comprehensively.[3,4] On the other hand, derivatives of the first-row homologue chromium are very rare. While molecules $[X_3Cr{\equiv}CH]$ (X = F, Cl) have been observed in an argon matrix (8 K),[5] heteroatom-substituted carbyne derivatives such as $[(C_5Me_5)Cr(\equiv CN\textit{i}Pr_2)(CN\textit{t}Bu)_3][PF_6]_2$[6] and the trimetallic cluster $[Cp_3Cr_3(\mu_2\text{-}Cl)_3(\mu_3\text{-}CH)]$ (**A**)[7] display crystalline compounds.[7] Purple trivalent **A** has remained the only structurally characterized methylidyne complex of chromium.[7,8] On the other hand, the $M_3(\mu_3\text{-}CH)$ entity exhibits a common structural motif detected throughout *d*-transition metal chemistry (Ti, Fe, Co, Ru, Re and Os).[9] Prominent examples of the μ_3-alkylidyne compound class are tricobalt nonacarbonyl clusters, which were investigated comprehensively by Seyferth et al.[10] Methylidyne complexes structurally related to **A** comprise $[\{Cp^*Ti(\mu_2\text{-}O)\}_3(\mu_3\text{-}CH)]$[11] and $[Cp^*{}_3Mo_3(\mu_2\text{-}O)_2(\mu_2\text{-}CH_2)(\mu_3\text{-}CH)]$[12] the reactivity of which has been investigated as well.

Complex **A** has been obtained by thermal treatment (60 °C) of $[CpCr(CH_3)(\mu_2\text{-}Cl)]_2$ via multiple abstraction of hydrogen from a methyl ligand,[13] while its reactivity was not commented on.[7] Dehalogenation of organic halides features another viable pathway to alkylidyne/methylidyne complexes.[14] Both pathways can proceed via intermediate alkylidene/methylidene species. For chromium, well-defined alkylidene species are just as rare as alkylidyne complexes.[15,16] The most prominent chromium alkylidene complex is Takai's olefination/cyclopropanation reagent $[Cr_2Cl_2(\mu_2\text{-}Cl)_2(\mu_2\text{-}CHI)(thf)_4]$ (**B**, shown in Scheme 1).[16] The active reagent is routinely generated in situ applying the dehalogenation protocol, with $CrCl_2$ and CHX_3 (X = Cl, Br, I) as the main components in varying ratios.[17] Recently, we succeeded in determining the solid-state structure of the Takai haloalkylidene complex **B**,[18] only confirming the connectivity originally proposed by Takai. By taking a closer look at the formation of the Takai olefination reagent, we have now uncovered the chromium(III) methylidyne species $[Cr_3Cl_3(\mu_2\text{-}$

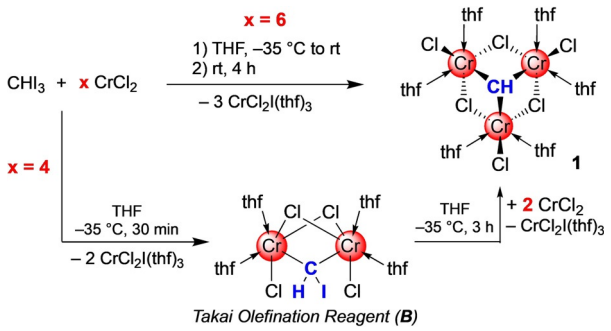

Scheme 1. Synthesis of methylidyne complex **1**, directly (upper path) or via the Takai olefination reagent **B** (lower path).

[*] S. Trzmiel, Dr. D. Werner, Dr. C. Maichle-Mössmer, Prof. Dr. R. Anwander
Institut für Anorganische Chemie, Eberhard-Karls-Universität Tübingen
Auf der Morgenstelle 18, 72076 Tübingen (Germany)
E-mail: reiner.anwander@uni-tuebingen.de
J. Langmann, Prof. Dr. W. Scherer
Institut für Physik, Universität Augsburg
Universitätsstr. 1, 86159 Augsburg (Germany)
E-mail: wolfgang.scherer@physik.uni-augsburg.de
Supporting information and the ORCID identification number(s) for the author(s) of this article can be found under: https://doi.org/10.1002/anie.202106608.

$Cl)_3(\mu_3\text{-}CH)(thf)_6]$ (**1**) as the ultimate product of the $CrCl_2$/CHI_3 reaction. Interestingly, complex **1** engages in selective halogenido exchange reactions, preserving the $M_3(\mu_3\text{-}CH)$ entity. Preliminary conversions of aldehydes or ketones revealed reaction pathways involving radical intermediates.

Results and Discussion

Formation of Methylidyne Complex $[Cr_3Cl_3(\mu_2\text{-}Cl)_3(\mu_3\text{-}CH)(thf)_6]$ (1) in the Reaction of Chromium(II) Chloride with Iodoform

The Takai olefination reagent is routinely generated in situ via a 3:1 mixture of $CrCl_2$ and CHX_3 (Scheme 1). The original report also mentioned the use of a 4:1 ratio in case of bromoform which did not significantly affect the yield and *E*/*Z* ratio of the alkenyl halide product.[17] Therefore we pondered about whether use of excessive $CrCl_2$ would affect, if at all, the formation of Takai reagent **B**. Surprisingly, the reaction of $CrCl_2$ with CHI_3 in a 6:1 molar ratio at −35 °C in THF afforded the red methylidyne complex $[Cr_3Cl_3(\mu_2\text{-}Cl)_3(\mu_3\text{-}CH)(thf)_6]$ (**1**) in up to 70% yield (Scheme 1, Figure 1) along with the precipitation of three equivalents of $CrCl_2I(thf)_3$.

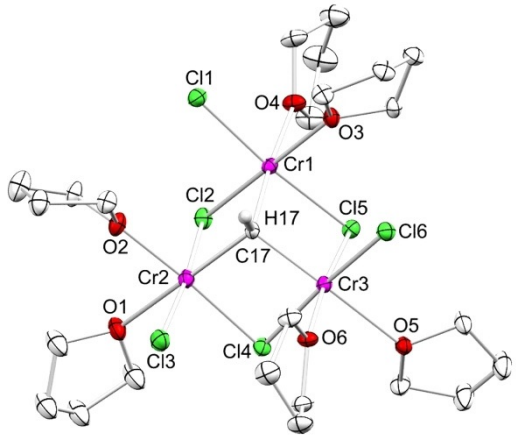

Figure 1. Crystal structure of **1**, ellipsoids shown at 50% probability, THF lattice solvent and hydrogen atoms are omitted for clarity. Selected interatomic distances/angles are listed in the Supporting Information (ESI, Figure S17).[32]

Compound **1** is also accessible via **B** and addition of another two equivalents of $CrCl_2$ (Scheme 1). Crystallization from the THF solution at −35 °C yielded compound **1** as a microcrystalline solid. Repeated crystallization increased the overall yield, but to the expense of co-crystallizing $CrCl_2I(thf)_3$. Crystallization from less concentrated solutions gave red plates suitable for X-ray diffraction (XRD) analysis. The crystal structure of **1** shows the known tetrahedral $M_3(\mu_3\text{-}CH)$ structural motif, with three chromium atoms forming a nearly equilateral triangle (Figure 1). Three μ_2-bridging chlorido ligands complement the cluster core, resembling a truncated cube. One terminal chlorido and two THF molecules each complete the slightly distorted octahedral coordination of the Cr^{III} atoms.[19]

The Cr−(μ_3-CH) distances in **1** of 2.018(3)/2.019(3)/2.022(3) Å appear slightly longer than those in Theopold's compound $[Cp_3Cr_3(\mu_2\text{-}Cl)_3(\mu_3\text{-}CH)]$ (**A**; 1.935(10) and 1.949(14) Å), as are the bridging Cr−Cl distances (2.3328(7) to 2.4186(7) Å versus 2.348(4) to 2.360(4) Å).[7] The average Cr—Cr distance of 3.167 Å is also considerably longer than in **A** (2.82 Å), which has been referred to as an unusually short contact (range for Cr−Cr single bonds: 2.65–2.97 Å).[7] Correspondingly, both the Cr-Cl-Cr and Cr-C-Cr angles are more flat in **1** (81.88(2)–82.96(2)°; 102.72(12)–103.66(12)°) than in **A** (73.0(1) and 73.9(1)°; 92.4(6) and 93.8(5)°).

The ^1H NMR spectroscopic investigation of **1** in $[D_8]$THF did not reveal any signal for the μ_3-CH proton in the range of −500 to 500 ppm, presumably caused by paramagnetic broadening.[20] Also, any distinct μ_3-CH vibration band was not detectable by IR-spectroscopy (ESI, Figure S26). The effective magnetic moment of **1** in dissolved and solid form was determined by the Evans method[21] and SQUID magnetic measurements, respectively. Both methods consistently point to ferro- or ferrimagnetic coupling between the individual Cr^{III} centers already at ambient temperature. The derived values of μ_{eff} (Evans method: 9.30 μ_B; SQUID: 9.11 μ_B) are significantly larger than those expected for three uncoupled Cr^{III} centers (6.71 μ_B). Notably, the effective moment of solid **1** is nearly temperature independent down to 2 K (Figure 2, Figure S30). A fit of the field-dependent molar magnetization $M_{mol}(H)$ at 2 K with a Brillouin function (the Landé *g*-factor was assumed to be 2.0) yields a spin quantum number of S = 4.45(4) which is in line with a S = 9/2

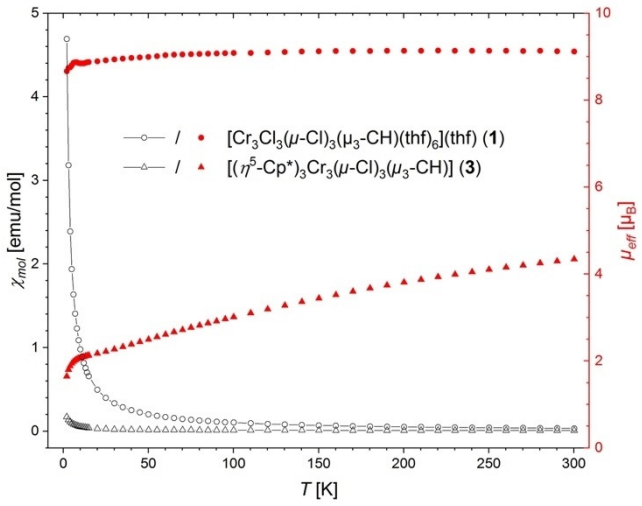

Figure 2. Temperature-dependent molar magnetic susceptibility $\chi_{mol}(T)$ (black open symbols; left ordinate) and effective magnetic moment $\mu_{eff}(T)$ (red filled symbols; right ordinate) as obtained by SQUID magnetic measurements on crystalline powders of **1** and **3** in applied fields $H = 3$ kOe and 10 kOe, respectively. The $\chi_{mol}(T)$ data were corrected for diamagnetic contributions (**1**: -4.243×10^{-4} emu mol^{-1}; **3**: -3.071×10^{-4} emu mol^{-1}; calculated from Pascal's constants),[23] and a spin-only *g* factor of 2.0 was assumed in the calculation of $\mu_{eff}(T)$. Note, that **1** contains an additional THF solvent molecule per formula unit in the crystal packing.

ground state (Figure S32). A similar large μ_{eff} value of 9.61 was found for the related chromium chlorocarbyne complex $[Cr_3Cl_3(\mu_2\text{-}Cl)_3(\mu_3\text{-}CCl)(thf)_6]$ assuming an $S = 9/2$ ground state.[8] We note, that also the tetranuclear Cr^{III}/Cr^{II} complex $[Cp^R{}_4Cr_4(\mu_2\text{-}H)_5(\mu_3\text{-}H)_2]$ ($Cp^R = \eta^5$-tetramethyl-ethyl-cyclopentadienyl) displays a temperature-independent high μ_{eff} of 8.1 μ_B with $S = 3.4(2)$ which is due to intramolecular ferrimagnetic couplings and in line with a $S = 7/2$ ground state.[22]

Compound **1** was found to be infinitely stable in the solid state, while high purity samples showed minor decomposition in THF at −35 °C over several weeks. Thermal decomposition of **1** in THF occurred rapidly above 40 °C (as indicated by a gradual color change from red to yellow). Similarly, progressive decomposition of **1** was observed in non-coordinating solvents like toluene as indicated by the formation of a precipitate as well as decoloration. Utilization of high-purity reactants is crucial for the successful synthesis of **1**, as water-containing solvents or oxygen-containing impurities of iodoform or $CrCl_2$ (99.99 % trace metal basis, anhydrous $CrCl_2$) led to partially inseparable decomposition/side products, as evidenced for the serendipitous identification of $[Cr_4(\mu_2\text{-}Cl)_4(\mu_2\text{-}I)_2(\mu_4\text{-}O)(thf)_4]$ (**2a**) and mixed-valent $[Cr_4Cl(\mu_2\text{-}Cl)_4(\mu_2\text{-}I)_2(\mu_4\text{-}O)(thp)_4]$ (**2b**, thp = tetrahydropyran) by XRD analysis. As complexes **2** were obtained in minute amounts and the crystals were of poor quality, the crystal structures represent only connectivities (Figures 3/S18/S19). The molecular structure of **2a** is isostructural to $[Cr_4(\mu_2\text{-}Cl)_6(\mu_4\text{-}O)(thf)_4]$ reported by Cotton et al. with two iodido ligands instead of chloridos.[24] The core of complexes **2** features a $[M_4O]^{6+}$ entity with the central oxygen tetrahedrally coordinated by the metal atoms. Each 5-coordinate chromium(II) engages further in two chlorido and one iodido bridge, and the coordination of a THF molecule. The single 6-coordinate chromium(III) in **2b** is additionally coordinated by a terminal chlorido ligand. Compounds **2** probably formed at an early stage of the reaction, most likely due to solvent water impurities. However, neither **2a** nor **2b** could be reproduced by the admittance of deliberate amounts of water to the reaction mixture.

Formation of Half-Sandwich Methylidyne Complexes $[Cp^R{}_3Cr_3(\mu_2\text{-}Cl)_3(\mu_3\text{-}CH)(thf)_6]$ via Selective Cl/Cp^R Exchange

With compound **1** accessible in decent yields, we targeted the selective exchangeability of the terminal chlorido ligands. As the cyclopentadienyl ligand proved a stabilizing ligand for the $M_3(\mu_3\text{-}CH)$ entity in general, and specifically for compound **A**, we probed the reactivity of **1** toward NaCp (Cp = C_5H_5) and the substituted cyclopentadienides LiCp* and LiCp′ (Cp* = C_5Me_5, Cp′ = $[C_5H_4(SiMe_3)]$) (Scheme 2).

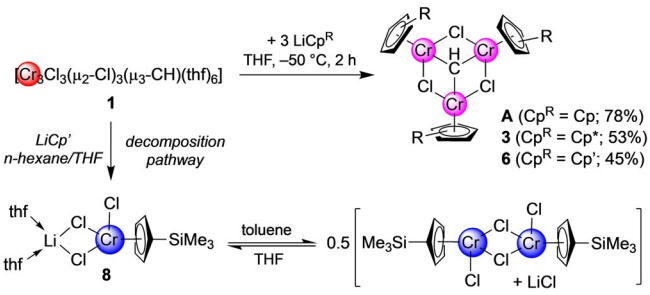

Scheme 2. Synthesis of trimetallic half-sandwich methylidyne complexes; representation of the suggested equilibrium of ate complex **8** in solution.

Reaction of **1** with three equivalents of NaCp in THF at −50 °C yielded a clear dark purple solution. Crystallization from *n*-pentane gave purple needles of $[Cp_3Cr_3(\mu_2\text{-}Cl)_3(\mu_3\text{-}CH)]$ (**A**) in good yield (78 %). Lower yields at elevated temperatures and absence of metathesis salt most likely result from the instability of **1** dissolved in THF and its partial decomposition during the reaction, through unknown reduction pathways. Moreover, chromocene $[Cp_2Cr]$ could be identified as a major impurity by ^{1}H NMR spectroscopy ($[D_8]$THF, $\delta = 319.4$ ppm) being separable by sublimation at 40 °C. Other Cr^{II} and Cr^{III} species present in reaction mixtures, even at −50 °C, were not assignable by NMR spectroscopy (distinct signals in the range 10 to 50 ppm), but could be removed by crystallization. The ^{1}H NMR spectrum

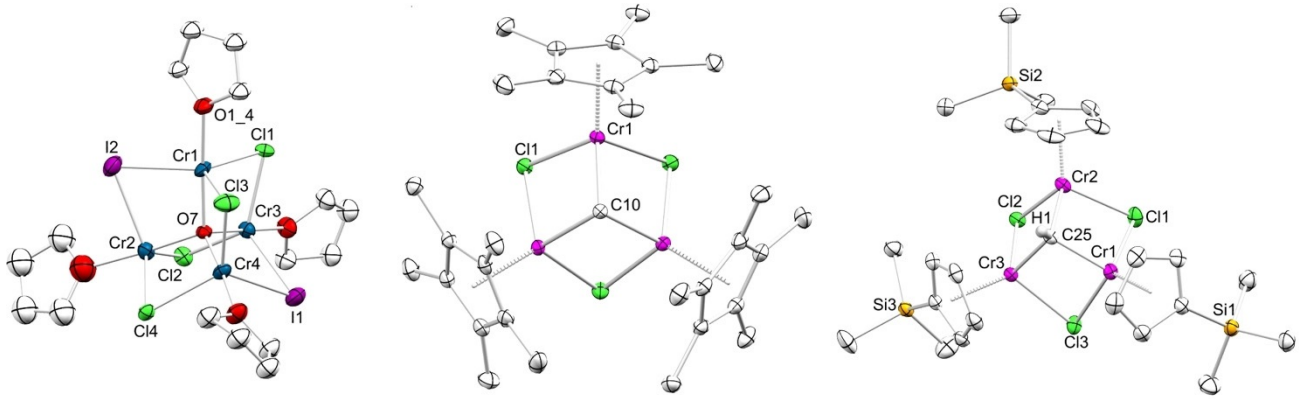

Figure 3. Connectivity of $[Cr_4(\mu_2\text{-}Cl)_4(\mu_2\text{-}I)_2(\mu_4\text{-}O)(thf)_4]$ (**2a**, left), ellipsoids shown at 30 % probability, lattice solvent and hydrogen atoms are omitted for clarity. Crystal structures of $[(\eta^5\text{-}Cp^*)_3Cr_3(\mu_2\text{-}Cl)_3(\mu_3\text{-}CH)]$ (**3**, middle) and $[(\eta^5\text{-}Cp')_3Cr_3(\mu_2\text{-}Cl)_3(\mu_3\text{-}CH)]$ (**6**, right), ellipsoids shown at 50 % probability, lattice solvent and hydrogen atoms (except for the methylidyne hydrogen atom in **6**) are omitted for clarity. Selected interatomic distances/angles are listed in the Supporting Information (Figures S18/S20/S23).[32]

of **A** measured in [D$_8$]THF at ambient temperature shows a broad singlet at $\delta = 30.27$ ppm (in $CDCl_3$ at $\delta = 31.05$ ppm), in agreement with the literature.[7]

The 3-equivalent reaction of **1** with LiCp* in THF at −50 °C led to an instant color change from dark red to dark green. Crystallization from concentrated toluene/*n*-hexane mixtures gave dark green crystals of [(η^5-Cp*)$_3$Cr$_3$(μ_2-Cl)$_3$(μ_3-CH)] (**3**) featuring a structural motif similar to **1** (Figure 1) and **A**. Compound **3** crystallizes in the trigonal space group *R3* and displays a local symmetry of C_3 with Cr—Cr distances of 2.9103(5) Å, slightly longer than in **A**. The Cr−Cl distances of 2.3416(5) to 2.3615(5) Å as well as the Cr-C-Cr angles involving the central μ_3-CH moiety (92.71(11)°) match those in **A**. The ^{1}H NMR spectrum of crystalline **3** in [D$_8$]THF at ambient temperature shows a slightly broadened singlet at $\delta = -5.8$ ppm assignable to $C_5(CH_3)_5$. The ambient-temperature magnetic moment drastically changed upon Cl/Cp^R exchange as evidenced by the Evans method in solution ($\mu_{eff} = 3.63\ \mu_B$) and in the solid state by SQUID measurements ($\mu_{eff} = 4.32\ \mu_B$). These values are in accordance with the results obtained for dissolved **A** (Evans method: $\mu_{eff} = 3.55\ \mu_B$)[7] and substantially below the effective magnetic moment expected in case of three uncoupled Cr^{III} centers ($\mu_{eff} = 6.71\ \mu_B$). A possible explanation may be the establishment of antiferromagnetic interactions causing the observed gradual decrease of μ_{eff} for solid **3** upon cooling (Figure 2, Figures S31/S33).[7] A similar temperature-dependent decrease of the effective magnetic moment upon cooling has been observed earlier in the related complex **A** and considered as an evidence for antiferromagnetic couplings between the chromium ions.[7] A further analogy to **A** is that reaction mixtures of **3** show a multitude of paramagnetically shifted proton signals, due to partial reduction and decomposition of complex **1**. Identified side products comprise Cp*$_2$Cr ($\delta = -6.2$ ppm, [D$_8$]THF)[25] and [Cp*CrCl$_2$]$_2$ ($\delta = -71.5$ ppm, $CDCl_3$).[26] Overall, the synthesis of such half-sandwich complexes is extremely sensitive toward change of reaction conditions and choice of precursor. While switching the solvent from THF to toluene led to the isolation of trivalent [Cp*CrCl$_2$(thf)] (**4**), probing the direct synthesis of **3** from [Cp*Cr(μ_2-Cl)]$_2$/CHI_3 gave only partial halogenido exchange in [(Cp*Cr)$_2$(μ_2-Cl)(μ_2-I)] (**5**) (synthesis details and crystal structures, see Supporting Information).

Salt metathesis of **1** with three equivalents of LiCp′ in THF at −50 °C gave a dark red/violet solution. After several extraction steps, crystallization from *n*-hexane yielded dark purple needles of [(η^5-Cp′)$_3$Cr$_3$(μ_2-Cl)$_3$(μ_3-CH)] (**6**). The crystal structure of **6** is isostructural to **A** and **3** (Figure 3), with similar Cr−Cl distances of 2.3243(4) Å to 2.3519(4) Å. Not unexpectedly, the Cr—Cr distances of 2.8192(3) Å to 2.8363(3) Å match those in **A**. The ^{1}H NMR spectrum of **6** recorded in [D$_8$]THF at ambient temperature shows two broadened signals at $\delta = 35.35$ and 30.39 ppm for the aromatic protons of the Cp′ ligands, and one sharp singlet at $\delta = 0.49$ ppm for the SiCH_3 protons ($\mu_{eff} = 2.70\ \mu_B$). Again, the ^{1}H NMR spectrum of the reaction mixture of **6** shows numerous other signals. To prove similar reaction/decomposition behavior as found for **A** and **3**, chromocene Cp′$_2$Cr (**7**) was synthesized independently from $CrCl_2$ and LiCp′. Crystallization of **7** from *n*-hexane produced orange crystals suitable for an X-ray diffraction study (Figure S24). The ^{1}H NMR spectrum of **7** measured in [D$_8$]THF at ambient temperature displays signals at $\delta = 322.33$ ppm, 249.42 ppm, and −3.32 ppm (Figure S5). Half-sandwich ate complex [(η^5-Cp′)CrCl(μ_2-Cl)$_2$Li(thf)$_2$] (**8**) could be crystallized as another side product from reactions in THF. The crystal structure of deep blue **8** proved the existence of an intramolecular ate complex (Figure S25). Compound **8** provides further evidence for the equilibrium theory proposed by Rojas et al. (Scheme 2) and explains the virtually non-existent (non-separable) amount of metathesis salt in the reaction mixtures of **1** and compounds MCp^R.[27] Nearly identical solubilities of the side products clearly counteract the isolation of these compounds. In general, the proneness of **1** to reduction (and the formation of Cp$^R_2$Cr^{II}) can be minimized by performing the reactions at low temperatures in less polar solvents. In THF, the reactions proceeded with minor impurities only at −50 °C, while in *n*-hexane and *n*-pentane acceptable results were obtained at −35 °C. Toluene is unsuitable as a solvent, since decomposition of **1** was significant within minutes, even at low temperatures.

Reactivity of Methylidyne Complex 1 toward Aldehydes and Ketones

The Takai and Takai-Utimoto olefination reagents engage in (*E*)-selective olefinations of aldehydes, with high functional group tolerance.[28,29] Later, reagent extensions involved the formation of (heteroatom-)substituted cyclopropane products.[30] It was of interest how the methylidyne complex **1** would affect such olefination reactions. Direct NMR-scale reactivity studies turned out difficult to interpret because of paramagnetic shifting and broadening. However, filtration of the reaction mixtures over aluminum oxide facilitated the observation of organic products via ^{1}H NMR spectroscopy. The conversions of benzaldehyde and pivaldehyde with **1** in [D$_8$]THF were complete after 1 h at ambient temperature.[31] During this period, the mixtures changed color from deep red to turbid green brown, leading to a multitude of products as detected by GC/MS analysis (see Figures S34 to S43). Most of these compounds are suggested to be formed by radical recombination, involving transient olefinic radical, as a result from methylidyne/oxy exchange (Scheme 3). 1D and 2D NMR spectroscopies could not resolve the observed overlapping signals of the product mixtures (Figures S6 to S12). For example, the benzaldehyde reaction revealed the forma-

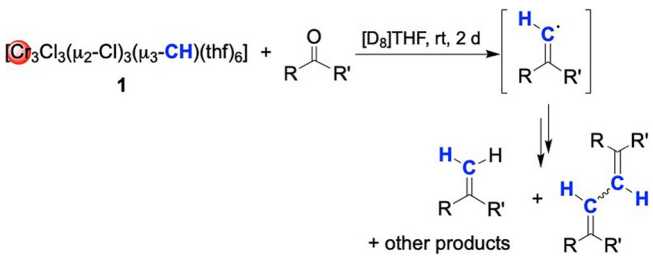

Scheme 3. Reactions of **1** with aldehydes and ketones.

tion of styrene as the only component identifiable by ^{1}H NMR spectroscopy. Striking was the observation of trace amounts of (2-iodoethenyl)-benzene by GC/MS analysis. As the synthesis of **1** produces a substantial amount of the iodinated side product $CrCl_2I(thf)_3$ (approximate solubility of 1 mg mL^{-1} in THF at 17 °C), product contamination with iodine seems inevitable. ICP (Inductively Coupled Plasma) analysis of recrystallized samples of compound **1** indicated a persistent iodine content of roughly 3.3 %.

Other causes for the iodine contamination could be the presence of decomposition product **2** or non-reacted Takai reagent $[Cr_2Cl_2(\mu_2\text{-}Cl)_2(\mu_2\text{-}CHI)(thf)_4]$ (**B**), which are both easily soluble in THF and hence difficult to separate via crystallization.

Compound **1** did not show any reactivity toward alkynes HC≡CSiMe$_3$, HC≡CPh and PhC≡CPh, neither alkyne metathesis nor insertion/addition-type reactions. The latter investigations were carried out in [D$_8$]THF and monitored by ^{1}H NMR spectroscopy over several hours, also by heating to the decomposition temperature of **1**. Finally, the reactivity of $[(\eta^5\text{-}Cp^*)_3Cr_3(\mu_2\text{-}Cl)_3(\mu_3\text{-}CH)]$ (**3**) toward benzaldehyde or benzophenone was examined under similar conditions, but the ^{1}H NMR spectra were inconclusive and only indicated decomposition of the methylidyne complex. Further research is needed to elucidate the reactivity of the organometallic compounds.

Conclusion

The chromium(III) μ_3-methylidyne complex $[Cr_3Cl_3(\mu_2\text{-}Cl)_3(\mu_3\text{-}CH)(thf)_6]$ features the ultimate C-X cleavage product in the dehalogenation sequence of haloforms CHX_3(here: $CrCl_2/CHI_3$ mixture). The decent yields of the methylidyne complex enabled a series of reactivity studies. The terminal chlorido ligands can be selectively displaced via salt metathesis with alkali-metal cyclopentadienides to afford rare examples of half-sandwich chromium(III) methylidynes, $[(\eta^5\text{-}Cp^R)_3Cr_3(\mu_2\text{-}Cl)_3(\mu_3\text{-}CH)]$. Despite the paramagnetic nature of Cr^{III}, these compounds exhibit only slightly broadened signals in the ^{1}H NMR spectra, facilitating the observation of in situ derivatizations. Treatment of $[Cr_3Cl_3(\mu_2\text{-}Cl)_3(\mu_3\text{-}CH)(thf)_6]$ with ketones and aldehydes led to olefination, entailing the formation of various products probably formed by radical recombination. The methylidyne complexes under study do not promote alkyne metathesis reactions or insertions/additions with acetylenes, but display exceptional magnetic behavior. Finally, our study underlines the importance of complying with correct $CrCl_2$/haloform ratios for efficient olefination reactions.

Acknowledgements

We thank the German Science Foundation for financial support (Grant: AN 238/15-2). Open access funding enabled and organized by Projekt DEAL.

Conflict of Interest

The authors declare no conflict of interest.

Keywords: chromium · cylopentadienyl · magnetism · methylidyne · olefination

[1] C. Elschenbroich, *Organometallics*, Wiley-VCH, Weinheim, **2006**.
[2] a) R. R. Schrock, *Chem. Rev.* **2002**, *102*, 145 – 179; b) A. Fürstner, P. W. Davies, *Chem. Commun.* **2005**, 2307 – 2320; c) A. Fürstner, *Angew. Chem. Int. Ed.* **2013**, *52*, 2794 – 2819; *Angew. Chem.* **2013**, *125*, 2860 – 2887; d) Y. Jin, Q. Wang, P. Taynton, W. Zhang, *Acc. Chem. Res.* **2014**, *47*, 1575 – 1586; e) H. Ehrhorn, M. Tamm, *Chem. Eur. J.* **2019**, *25*, 3190 – 3208.
[3] For examples, see: a) J. H. Wengrovius, J. Sancho, R. R. Schrock, *J. Am. Chem. Soc.* **1981**, *103*, 3932 – 3934; b) J. C. Peters, A. L. Odom, C. C. Cummins, *Chem. Commun.* **1997**, *118*, 1995 – 1996; c) A. Fürstner, C. Mathes, C. W. Lehmann, *J. Am. Chem. Soc.* **1999**, *121*, 9453 – 9454; d) S. Beer, C. G. Hrib, P. G. Jones, K. Brandhorst, J. Grunenberg, M. Tamm, *Angew. Chem. Int. Ed.* **2007**, *46*, 8890 – 8894; *Angew. Chem.* **2007**, *119*, 9047 – 9051; e) E. F. van der Eide, W. E. Piers, M. Parvez, R. McDonald, *Inorg. Chem.* **2007**, *46*, 14 – 21; f) R. R. Thompson, M. E. Rotella, P. Du, X. Zhou, F. R. Fronczek, R. Kumar, O. Gutierrez, S. Lee, *Organometallics* **2019**, *38*, 4054 – 4059; g) J. Hillenbrand, M. Leutzsch, A. Fürstner, *Angew. Chem. Int. Ed.* **2019**, *58*, 15690 – 15696; *Angew. Chem.* **2019**, *131*, 15837 – 15843; h) A. Haack, J. Hillenbrand, M. Leutzsch, M. van Gastel, F. Neese, A. Fürstner, *J. Am. Chem. Soc.* **2021**, *143*, 5643 – 5648.
[4] For a terminally bonded niobium(V) methylidyne, see: T. Kurogi, P. J. Carroll, D. J. Mindiola, *J. Am. Chem. Soc.* **2016**, *138*, 4306 – 4307.
[5] J. T. Lyon, H.-G. Cho, L. Andrews, *Organometallics* **2007**, *26*, 6373 – 6387.
[6] A. C. Filippou, B. Lungwitz, K. M. A. Wanninger, E. Herdtweck, *Angew. Chem. Int. Ed. Engl.* **1995**, *34*, 924 – 927; *Angew. Chem.* **1995**, *107*, 1007 – 1010.
[7] D. S. Richeson, S. W. Hsu, N. H. Fredd, G. van Duyne, K. H. Theopold, *J. Am. Chem. Soc.* **1986**, *108*, 8273 – 8274.
[8] Parallel to our work, the isostructural trinuclear chromium chlorocarbyne complex $[Cr_3Cl_3(\mu\text{-}Cl)_3(\mu_3\text{-}CCl)(thf)_6]$ has been obtained from carbon tetrachloride and ca. 7 equivalents of $CrCl_2$, along with compound **1** as a decomposition/hydrolysis product: T. Kurogi, K. Irifune, T. Enoki, K. Takai, *Chem. Commun.* **2021**, *57*, 5199 – 5202.
[9] a) A. G. Orpen, T. F. Koetzle, *Acta Crystallogr. Sect. B* **1984**, *40*, 606 – 612; b) T. Kakigano, H. Suzuki, M. Igarashi, Y. Morooka, *Organometallics* **1990**, *9*, 2192 – 2194; c) D. Lentz, H. Michael, *Chem. Ber.* **1990**, *123*, 1481 – 1483; d) U. Flörke, H.-J. Haupt, *Z. Kristallogr. Cryst. Mater.* **1993**, *204*, 292 – 294; e) V. Moberg, M. A. Mottalib, D. Sauer, Y. Poplavskaya, D. C. Craig, S. B. Colbran, A. J. Deeming, E. Nordlander, *Dalton Trans.* **2008**, 2442 – 2453; f) M. González-Moreiras, M. Mena, A. Pérez-Redondo, C. Yélamos, *Chem. Eur. J.* **2017**, *23*, 3558 – 3561; g) Y. Takahashi, Y. Nakajima, H. Suzuki, T. Takao, *Organometallics* **2017**, *36*, 3539 – 3552.
[10] D. Seyferth, J. E. Hallgren, P. L. K. Hun, *J. Organomet. Chem.* **1973**, *50*, 265 – 275.
[11] M. Gómez-Pantoja, P. Gómez-Sal, A. Hernán-Gómez, A. Martín, M. Mena, C. Santamaría, *Inorg. Chem.* **2012**, *51*, 8964 – 8972.
[12] O. I. Guzyr, J. Prust, H. W. Roesky, C. Lehmann, M. Teichert, F. Cimpoesu, *Organometallics* **2000**, *19*, 1549 – 1555.
[13] Thermal degradation of $[Cp^*TiMe_3]$ gave $[Cp^*Ti(\mu_3\text{-}CH)]_4$: R. Andrés, P. Gómez-Sal, E. de Jesús, A. Martin, M. Mena, C.

Yélamos, *Angew. Chem. Int. Ed. Engl.* **1997**, *36*, 115 – 117; *Angew. Chem.* **1997**, *109*, 72 – 74.
[14] a) W. T. Dent, L. A. Duncanson, R. G. Guy, W. H. B. Reed, B. L. Shaw, *Proc. Chem. Soc.* **1961**, 169; b) G. Bor, L. Markó, B. Markó, *Chem. Ber.* **1962**, *95*, 333 – 340; c) D. Seyferth, R. J. Spohn, M. R. Churchill, K. Gold, F. R. Scholer, *J. Organomet. Chem.* **1970**, *23*, 237 – 255; d) R. Bejot, A. He, J. R. Falck, C. Mioskowski, *Angew. Chem. Int. Ed.* **2007**, *46*, 1719 – 1722; *Angew. Chem.* **2007**, *119*, 1749 – 1752.
[15] a) S. K. Noh, R. A. Heintz, C. Janiak, S. C. Sendlinger, K. H. Theopold, *Angew. Chem. Int. Ed. Engl.* **1990**, *29*, 775 – 777; *Angew. Chem.* **1990**, *102*, 805 – 807; b) S. Hao, J.-I. Song, P. Berno, S. Gambarotta, *Organometallics* **1994**, *13*, 1326 – 1335; c) R. A. Heintz, S. Leelasubcharoen, L. M. Liable-Sands, A. L. Rheingold, K. H. Theopold, *Organometallics* **1998**, *17*, 5477 – 5485; d) P. Wei, D. W. Stephan, *Organometallics* **2003**, *22*, 1712 – 1717; e) P. Wei, D. W. Stephan, *Organometallics* **2003**, *22*, 1992 – 1994; f) S. Licciulli, K. Albahily, V. Fomitcheva, I. Korobkov, S. Gambarotta, R. Duchateau, *Angew. Chem. Int. Ed.* **2011**, *50*, 2346 – 2349; *Angew. Chem.* **2011**, *123*, 2394 – 2397; g) P. Wu, G. P. A. Yap, K. H. Theopold, *J. Am. Chem. Soc.* **2018**, *140*, 7088 – 7091; h) P. Wu, G. P. A. Yap, K. H. Theopold, *Organometallics* **2019**, *38*, 4593 – 4600; i) P. K. R. Panyam, L. Stöhr, D. Wang, W. Frey, M. R. Buchmeiser, *Eur. J. Inorg. Chem.* **2020**, 3673 – 3681; j) N. Wei, D. Yang, J. Zhao, T. Mei, Y. Zhang, B. Wang, J. Qu, *Organometallics* **2021**, *40*, 1434 – 1442.
[16] a) M. Murai, R. Taniguchi, N. Hosokawa, Y. Nishida, H. Mimachi, T. Oshiki, K. Takai, *J. Am. Chem. Soc.* **2017**, *139*, 13184 – 13192; b) M. Murai, R. Taniguchi, T. Kurogi, M. Shunsuke, K. Takai, *Chem. Commun.* **2020**, *56*, 9711 – 9714.
[17] K. Takai, K. Nitta, K. Utimoto, *J. Am. Chem. Soc.* **1986**, *108*, 7408 – 7410.
[18] D. Werner, R. Anwander, *J. Am. Chem. Soc.* **2018**, *140*, 14334 – 14341.
[19] For further comparison, a mixed methyl/iodido chromium complex was obtained by oxidative addition of CH_3I to a Cr–Cr quintuple bond: A. Noor, S. Schwarz, R. Kempe, *Organometallics* **2015**, *34*, 2122 – 2125.
[20] a) K. H. Theopold, *Acc. Chem. Res.* **1990**, *23*, 263 – 270; b) F. H. Köhler, C. Krüger, H. J. Zeh, *Organomet. Chem.* **1990**, *386*, C13 – C15; c) M. Enders, *Macromol. Symp.* **2006**, *236*, 38 – 47.
[21] D. F. Evans, *J. Chem. Soc.* **1959**, 2003 – 2005.
[22] R. A. Heintz, T. F. Koetzle, R. L. Ostrander, A. L. Rheingold, K. H. Theopold, P. Wu, *Nature* **1995**, *378*, 359 – 362.
[23] G. A. Bain, J. F. Berry, *J. Chem. Educ.* **2008**, *85*, 532 – 536.
[24] F. A. Cotton, C. A. Murillo, I. Pascual, *Inorg. Chem.* **1999**, *38*, 2746 – 2749.
[25] F. H. Koehler, B. Metz, W. Strauss, *Inorg. Chem.* **1995**, *34*, 4402 – 4413.
[26] B. Bräunlein, F. H. Köhler, W. Strauß, H. Zeh, *Z. Naturforsch. B* **1995**, *50*, 1739 – 1747.
[27] R. Rojas, M. Valderrama, *J. Organomet. Chem.* **2004**, *689*, 2268 – 2272.
[28] a) L. A. Wessjohann, G. Scheid, *Synthesis* **1999**, 1 – 36; b) "Olefination of Carbonyl Compounds by Zinc and Chromium Reagents": S. Matsubara, K. Oshima, in *Modern Carbonyl Olefination* (Ed.: T. Takeda), Wiley-VCH, Weinheim, **2003**, pp. 200 – 222.
[29] T. Okazoe, K. Takai, K. Utimoto, *J. Am. Chem. Soc.* **1987**, *109*, 951 – 953.
[30] a) K. Takai, S. Toshikawa, A. Inoue, R. Kokumai, *J. Am. Chem. Soc.* **2003**, *125*, 12990 – 12991; b) K. Takai, S. Toshikawa, A. Inoue, R. Kokumai, M. Hirano, *J. Organomet. Chem.* **2007**, *692*, 520 – 529; c) M. Murai, C. Mizuta, R. Taniguchi, K. Takai, *Org Lett.* **2017**, *19*, 6104 – 6107; d) M. Murai, R. Taniguchi, C. Mizuta, K. Takai, *Org. Lett.* **2019**, *21*, 2668 – 2672.
[31] Compound **1** proved comparatively less reactive toward ketones resulting in predominant recovery of the unreacted educts after 2 to 3 days (e.g., 88 % for benzophenone, see Figure S7; quantifications for reactions with 9-fluorenone and cyclohexanone were infeasible). For the reactions of **1** with benzophenone and 9-fluorenone, the alkylidene exchange products 1,1-diphenyl-ethylene (Figure S45) and 9-methylene-9*H*-fluorene (Figure S50) were found as the only product species identifiable by ^{1}H NMR spectroscopy (Figures S7 to S10). GC/MS analysis revealed trace amounts of numerous other compounds in the product solutions, among them iodinated olefination products as well as radical recombination products.
[32] Deposition Numbers 2084204, 2084205, 2084206, 2084207, 2084208, 2084209, 2084210, 2084211 and 2084212 contain the supplementary crystallographic data for this paper. These data are provided free of charge by the joint Cambridge Crystallographic Data Centre and Fachinformationszentrum Karlsruhe Access Structures service www.ccdc.cam.ac.uk/structures.

Manuscript received: May 17, 2021
Revised manuscript received: July 1, 2021
Accepted manuscript online: July 2, 2021
Version of record online: August 1, 2021

Angewandte Chemie
Eine Zeitschrift der Gesellschaft Deutscher Chemiker

Supporting Information

Beyond Takai's Olefination Reagent: Persistent Dehalogenation Emerges in a Chromium(III)-μ_3-Methylidyne Complex

Simon Trzmiel, Jan Langmann, Daniel Werner, Cäcilia Maichle-Mössmer, Wolfgang Scherer, and Reiner Anwander**

anie_202106608_sm_miscellaneous_information.pdf

Table of Contents

SUPPORTING INFORMATION

Experimental Procedures

General Procedures. All manipulations were performed using a glovebox (MBraun 200B; <0.1 ppm O_2, <0.1 ppm H_2O) or Schlenk line techniques under an atmosphere of purified argon in oven dried glassware. Solvents (THF, *n*-hexane, *n*-pentane and toluene) were purified over Grubbs-type columns (MBraun SPS, solvent purification system) and stored in a glovebox. THF and THP were further stored over 3 Å molecular sieve. Chromium(II) chloride was purchased from Abcr (99.99% pure, trace metal basis) and used as received. Iodoform was purchased from Sigma-Aldrich and sublimed before use. Benzaldehyde was purchased from Sigma-Aldrich, purified by distillation, and stored over pre-dried 3 Å molecular sieve. Pivalaldehyde, benzophenone, 9-fluorenone, trimethylsilylacetylene, phenylacetylene, 1,2-diphenylacetylene, *n*-butyllithium (1.6 M in *n*-hexane), 1,2,3,4,5-pentamethylcylopentadiene, and cyclohexanone were purchased from Sigma-Aldrich and used as received. LiCp* was synthesized from *n*-BuLi and HCp*. $[Cp^*CrCl]_2$ was synthesized according to a literature procedure.[1] The NMR spectra of air and moisture sensitive compounds were performed in pre-dried (over NaK alloy) benzene-d_6, chloroform-d_3, or THF-d_8, with J. Young valved NMR-spectroscopy tubes. NMR spectra were recorded on a Bruker AVII+400 (^{1}H: 400.13 MHz, ^{13}C: 100.16 MHz) at 26 °C. ^{1}H shifts are referenced to a solvent resonance and reported in parts per million (ppm) relative to tetramethylsilane.[2] ^{1}H NMR measurements were performed with a scan range of 1000 ppm (–500 – 500 ppm). Analyses of the NMR spectra were performed with Bruker TOPSPIN (version 3.6.1). The Evans method has been carried out on a Bruker AVII+400 at 298 K in THF/THF-d_8, with hexamethyldisiloxane as reference.[3] Concentrations of the complexes in THF solution ranged from 7-10 mg/mL. Additional measurements of the DC magnetic moment in solid samples were performed using the SQUID magnetometer Quantum Design MPMS-XL. The temperature dependence of the magnetic moment was determined between 2 K and 300 K in applied magnetic fields of 3 kOe or 10 kOe. Additional field-dependent data were collected between -50 kOe and 50 kOe at a temperature of 2 K. The samples were supplied in powdered crystalline form and held by gelatin capsules packed into surrounding plastic straws. All sample containers showed a minor magnetic moment in the range of 10^{-5} emu in the temperature range between 2 K and 300 K at an applied field of 10 kOe. Continuous inert conditions were ensured by sample preparation in a glovebox under argon atmosphere and subsequent transfer to the magnetometer in an air-tight transport vessel. UV-Vis measurements were performed on a PG Instruments T60 UV-Vis spectrophotometer as dilute THF solutions. Infrared spectra were recorded on a Thermo Fisher Scientific NICOLET 6700 FTIR ($\tilde{\nu}$= 4000 – 400 cm^{-1}), using a DRIFT chamber with dry KBr/sample mixtures and KBr windows. Elemental analyses (C, H, N) were performed on an Elementar vario MICRO cube. GC/MS was performed on an Agilent Q 5973 with electron impact ionization, and the obtained mass spectral data analyzed with Agilent MassHunter (version 10.0.368)[4] and compared to Main EI MS Library (mainlib)[5].

Syntheses

Synthesis of $[Cr_3Cl_3(\mu\text{-}Cl)_3(\mu_3\text{-}CH)(thf)_6]$ (1). $CrCl_2$ (500.0 mg, 4.068 mmol) was stirred in THF (5 mL) at −35 °C, giving a grey slurry. A solution of CHI_3 (267.0 mg, 0.678 mmol) was slowly added dropwise at −35 °C. Upon warming to ambient temperature over half an hour, the solution turned deep red, and orange $CrCl_2I(thf)_3$ precipitated from the solution. The mixture was stirred at ambient temperature for 4 h and then cooled to −35 °C prior to centrifugation. After filtration the solution was concentrated and stored at −35 °C, giving a red microcrystalline solid and a dark red supernatant solution. Repeating this process gave **1** as a red microcrystalline solid (387 mg, 70%). ^{1}H NMR (26 °C, 400.00 MHz, THFd_8): did not show any signals in the range of −500 to 500 ppm due to the paramagnetic behavior of the compound. $\chi^{mol} = 3.58x10^{-3}$ cm^3 mol^{-1}, $\mu_{eff} = 9.24$ μ_B. IR (DRIFT): $\tilde{\nu}$ = 2970 (s), 2900 (s), 1455 (m), 13635 (vw), 1340 (w), 1315 (w), 1295 (w), 1245 (w), 1175 (w), 1025 (s), 1015 (s), 9201 (s), 860 (s), 680 (w) cm^{-1}. UV-vis (THF solution, λ_{max}, nm): 344, 527. Elemental analysis calcd. (%) for $C_{25}H_{49}Cl_6Cr_3O_6$ (814,35 g mol^{-1}, dry solid **1**): C 36.87, H 6.07; found: C 36.56, H 5.98.

When the supernatant reddish brown solution from the synthesis of **1** was re-crystallized, small amounts of **2a** were separable as emerald green crystal. These crystals only formed in the presence of THF which was not thoroughly dried prior to use. The same crystals could be isolated from reactions of **1** with benzaldehyde in THF. After stirring the reaction mixture 3 to 18 h at rt, the orange

solution was filtered and the precipitate discarded. The resulting green solution was concentrated and crystalline **2a** could be harvested as emerald green blocks.

In an attempt to synthesize the tetrahydropyrane (THP) derivative $[Cr_3Cl_3(\mu\text{-}Cl)_3(\mu_3\text{-}CH)(thp)_6]$, mixed-valent complex **2b** could be isolated: $CrCl_2$ (200 mg, 1.627 mmol) was suspended in THP at –35 °C and CHI_3 (106.8 mg, 0.271 mmol) suspended in THP at –35 °C added. The color slowly changed from grey to orange over 1 h. The solution was warmed to ambient temperature and stirred for additional 18 h. The formed dark red suspension was filtered and the orange precipitate was discarded. The resulting dark red solution was concentrated and crystallized giving red to brown blocks of $[Cr_4Cl(\mu\text{-}Cl)_4(\mu\text{-}I)_2(\mu_4\text{-}O)(thp)_4]$ (**2b**) after one night at –35 °C.

Synthesis of $[\eta^5\text{-}Cp_3Cr_3(\mu\text{-}Cl)_3(\mu_3\text{-}CH)]$ (A). $[Cr_3Cl_3(\mu\text{-}Cl)_3(\mu_3\text{-}CH)(thf)_6]$ (**1**) (184 mg, 0.226 mmol) was dissolved in THF and cooled to−50 °C. Addition of solid $Na(C_5H_5)$ (60.0 mg, 0.681 mmol) and stirring the reaction mixture at −50 °C for 2 h gave a deep red/purple solution. The solvent was removed under reduced pressure and the solid residue extracted with *n*-pentane to separate Cp_2Cr. The dark violet residue of this extraction was redissolved in toluene. Filtration and drying of this solution gave a dark purple residue. Heating of this residue on a magnetic stirrer to 45 °C led to the sublimation of remaining Cp_2Cr. Crystallization of the dark purple solid residue from *n*-pentane through slow-evaporation at 17 °C yielded purple needles of **A** (83 mg, 78%). ^{1}H NMR (26 °C, 400.00 MHz, thf-d_8): δ = 30.25 (s, 5 H; Ar-H); elemental analysis calcd (%) for $C_{16}H_{16}Cl_3Cr_3$: C 40.83, H 3.43; found: C 39.89, H 3.63.

Synthesis of $[(\eta^5\text{-}C_5Me_5)_3Cr_3(\mu\text{-}Cl)_3(\mu_3\text{-}CH)]$ (3). $[Cr_3Cl_3(\mu\text{-}Cl)_3(\mu_3\text{-}CH)(thf)_6]$ (**1**) (126.5 mg, 0.155 mmol) was dissolved in THF at –50 °C and solid $Li(C_5Me_5)$ (66.3 mg, 0.466 mmol) was added. The mixture turned from dark red to dark green within seconds. Centrifugation, filtration, and drying of the filtrate under reduced pressure gave a dark green residue. The dark green solid was then redissolved in toluene, concentrated, and filtered. Crystallization from a toluene/*n*-hexane mixture yielded dark green crystals of **3** (56 mg, 53%). ^{1}H NMR (26 °C, 400.00 MHz, THF-d_8): δ = −5.8 (s, 15 H; Ar-CH_3). χ^{mol} = 5.53x10^{-4} cm^3 mol^{-1}, μ_{eff} = 3.63 μ_B. IR (DRIFT): $\tilde{\nu}$ = 2909 (vs), 1456 (m), 1375 (s), 1023 (m), 729 (vw), 494 (w), 436 (w) cm^{-1}. UV-vis (THF solution, λ_{max}, nm): 600. Elemental analysis calcd (%) for $C_{31}H_{46}Cl_3Cr_3$: C 54.67, H 6.81; found: C 53.80, H 6.82.

Attempt to synthesize **3** in toluene solution: $[Cr_3Cl_3(\mu\text{-}Cl)_3(\mu_3\text{-}CH)(thf)_6]$ (**1**) (50.0 mg, 61.6 μmol) was suspended in toluene at –35 °C. LiCp* (26.2 mg, 184.2 μmol) was added as a solid. The suspension was stirred at –35 °C for 30 minutes, centrifuged, and filtered. The resulting dark green solution was dried in *vacuo* and the black residue extracted with Et_2O. The resulting dark blue-green solution was concentrated and filtered again. The resulting clear dark blue-green solution was dried in *vacuo* and recrystallized from THF at –35 °C over several days, giving several dark blue blocks handpicked and identified as $[Cp^*CrCl_2(thf)]$ (**4**) by XRD analysis. The yield was not calculated due to other impurities.

Attempt to synthesize **3** directly from $[Cp^*Cr(\mu\text{-}Cl)]_2$ and CHI_3: $[Cp^*Cr(\mu\text{-}Cl)]_2$ (29.1 mg, 65.3 μmol) was suspended in *n*-hexane and CHI_3 (4.3 mg, 10.9 μmol) was added as a suspension in *n*-hexane. The color of the solution changed to turbid green. After stirring at ambient temperature for 2 h, the solution was filtered, and the resulting dark green nearly black solution was concentrated. Crystallization of this solution at –35 °C over several days resulted in dark blue blocks of $[(Cp^*Cr)_2(\mu\text{-}Cl)(\mu\text{-}I)]$ (**5**), identified by XRD analysis. The yield could not be calculated.

Synthesis of $[(\eta^5\text{-}C_5H_4SiMe_3)]_3Cr_3(\mu\text{-}Cl)_3(\mu_3\text{-}CH)]$ (6). $[Cr_3Cl_3(\mu\text{-}Cl)_3(\mu_3\text{-}CH)(thf)_6]$ (**1**) (64.7 mg, 79 μmol) was dissolved in THF, cooled to –50 °C, and $Li(C_5H_4SiMe_3)$ (21.0 mg, 0.238 mmol) added as a solid. After stirring the mixture at –50 °C for 2.5 h the solvent was removed under reduced pressure giving a purple slurry. Addition of toluene and filtration gave a clear purple solution. Drying of this solution under reduced pressure and crystallization from *n*-hexane yielded dark violet needles of **4** (25 mg, 45%). ^{1}H NMR (26 °C, 400.00 MHz, thf-d_8): δ = 35.35 (s, 2 H; Ar-H), 30.39 (s, 2 H; Ar-H), 0.49 ppm (s, 9 H; $SiMe_3$). χ^{mol} = 3.06x10^{-4} cm^3 mol^{-1}, μ_{eff} = 2.70 μ_B. IR (DRIFT): $\tilde{\nu}$ = 2949 (s), 2894 (w), 1365 (w), 12456 (s), 1168 (s), 1043 (s), 902 (s), 838 (vs), 756 (m), 694 (vw), 632 (w) cm^{-1}. UV-vis (THF solution, λ_{max}, nm): 445 (sh), 564, 655 (sh). Elemental analysis calcd (%) for $C_{25}H_{40}Cl_3Cr_3Si_3$: C 43.70, H 5.87; found: C 43.92, H 5.84.

Synthesis of $[(\eta^5\text{-}C_5H_4SiMe_3)_2Cr]$ (7). $CrCl_2$ (53.0 mg, 0.431 mmol) was suspended in THF and $Li(C_5H_4SiMe_3)$ (61.0 mg, 0.423 mmol, 0.98 equiv.) added as a THF solution. The grey slurry turned red over 10 minutes. After stirring at ambient temperature for 4 h, the turbid red solution was filtered, and the solvent removed under reduced pressure. The residue was extracted several times with *n*-

pentane. Crystallization from concentrated *n*-pentane yielded orange needles of **5** (58 mg, 89%). ^{1}H NMR (26 °C, 400.00 MHz, THF-d_8): δ = 322.32 (s, 2 H; Ar-H), 249.42 (s, 2 H; Ar-H), -3.23 ppm (s, 9 H; $SiMe_3$). IR (DRIFT): $\tilde{\nu}$ = 3087 (w), 2953 (s), 2895 (m), 1413 (w), 1246 (s), 1169 (s), 1150 (s), 1029 (m), 892 (m), 838 (s), 799 (s), 752 (s), 691 (m), 628 (m), 574 (m) cm^{-1}. UV-vis (THF solution, λ_{max}, nm): 348, 452. Elemental analysis calcd (%) for $C_{16}H_{26}CrSi_2$: C 58.85, H 8.03; found: C 58.81, H 7.71.

Attempt to synthesize **6** in *n*-hexane solution: $[Cr_3Cl_3(\mu\text{-}Cl)_3(\mu_3\text{-}CH)(thf)_6]$ (**1**) (128 mg, 0.157 mmol) was suspended in *n*-hexane and cooled to – 35 °C. LiCp' (41.5 mg, 0.472 mmol) was added as a suspension in *n*-hexane at –35 °C. The color of the suspension changed from pale red to brown. After stirring at –35 °C for 1.5 h, the suspension was centrifugated and the precipitate was discarded. The supernatant brown solution was dried in vacuo and the residue extracted with THF, giving a green solution. This green solution was crystallized yielding colorless $CrCl_2(thf)_2$ (identified by XRD analysis). The crystals were discarded, and the residue redissolved in thf yielding a dark blue solution. Crystallization of this blue solution yielded several blue crystals identified as $[(\eta^5\text{-}C_5H_4SiMe_3)CrCl(\mu\text{-}Cl)_2Li(thf)_2]$ (**8**) by XRD analysis. The yield could not be calculated due to co-crystallization of several other unidentified compounds and impurities.

Reactivity Studies

General procedure for reactions of $[Cr_3Cl_3(\mu\text{-}Cl)_3(\mu_3\text{-}CH)(thf)_6]$ (1) with Ketones and Aldehydes.

$[Cr_3Cl_3(\mu\text{-}Cl)_3(\mu_3\text{-}CH)(thf)_6]$ (**1**, 20.0 mg, 24.6 µmol) was dissolved in thf-d_8. Benzophenone (4.4 mg, 24.1 µmol, 1 equivalent) was added and the mixture stirred at ambient temperature for 3 days. After complete reaction, the solution was filtered through a small Al_2O_3 column and the colorless product mixture analyzed by ^{1}H NMR spectroscopy. The product mixture was then used for further product identification via GCMS analysis.

General procedure for reactions of $[Cr_3Cl_3(\mu\text{-}Cl)_3(\mu_3\text{-}CH)(thf)_6]$ (1) with Acetylenes.

$[Cr_3Cl_3(\mu\text{-}Cl)_3(\mu_3\text{-}CH)(thf)_6]$ (**1**, 10.0 mg, 12.3 µmol) was dissolved in thf-d_8 and transferred to a J.Young-valved NMR tube. Between 1 and 2 equivalents (12.3 to 25 µmol) of acetylene were added and the tube shaken to ensure even distribution of reactants. The NMR tube was then sealed, the mixture heated to 50 °C and the reaction monitored *via* ^{1}H NMR spectroscopy over several h.

NMR Spectra

Solvent signals are marked with *.

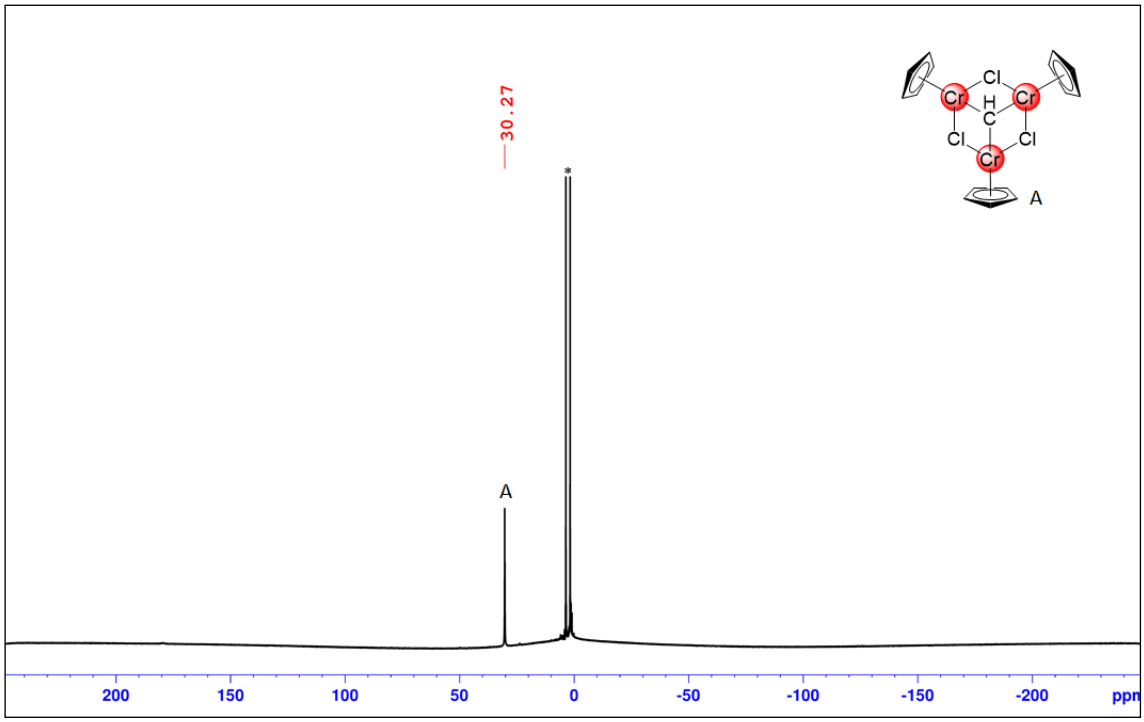

Figure S1. ^{1}H NMR spectrum (26 °C, 400.13 MHz, thf-d_8) of [(η^5-C_5H_5)Cr_3(μ_2-Cl)$_3$(μ_3-CH)] (**A**).

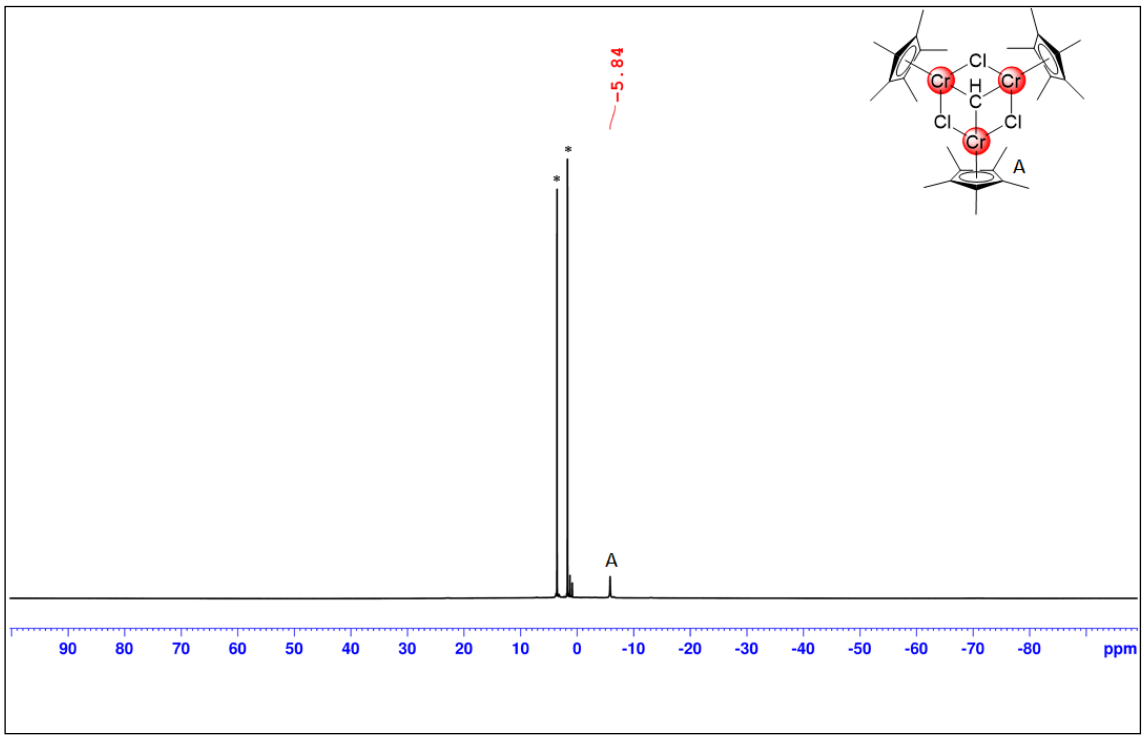

Figure S2. ^{1}H NMR spectrum (26 °C, 400.13 MHz, thf-d_8) of [(η^5-C_5Me_5)Cr_3(μ_2-Cl)$_3$(μ_3-CH)] (**3**).

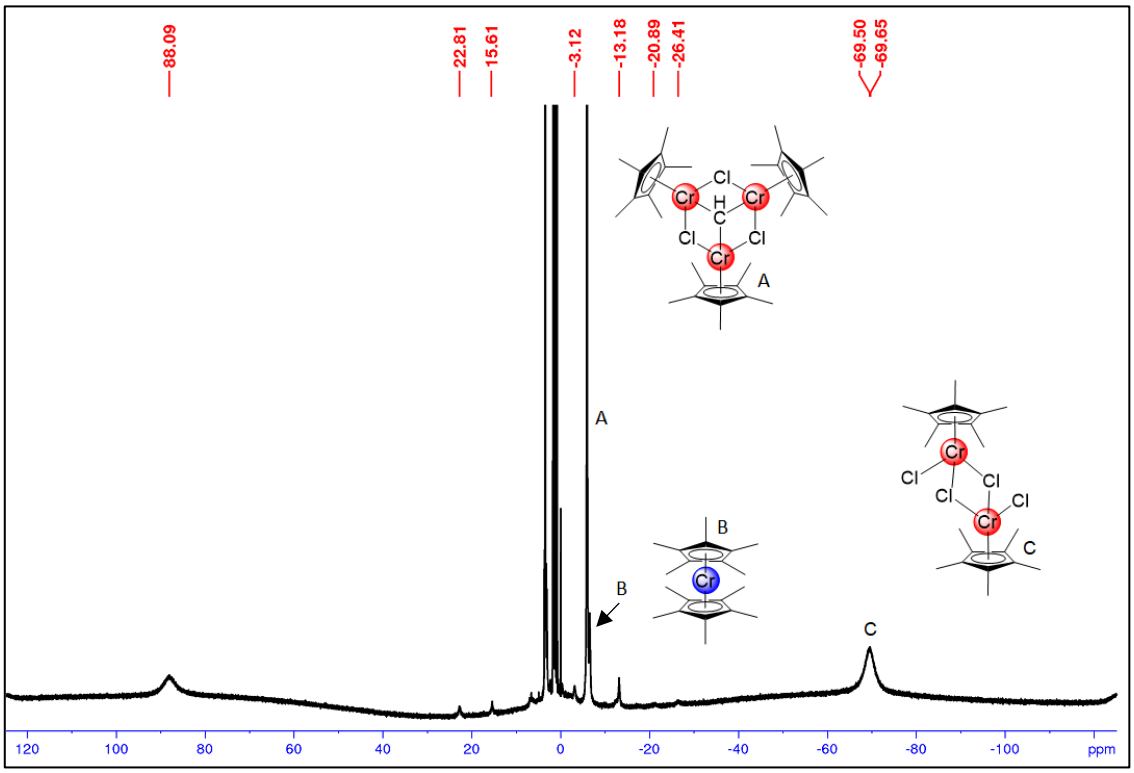

Figure S3. ^{1}H NMR spectrum (26 °C, 400.13 MHz, thf-d_8) of the reaction of **1** with 3 equivalents of LiCp* in THF at –35 °C after 1.5 h without workup. Displayed are the proposed compounds found in the mixture.

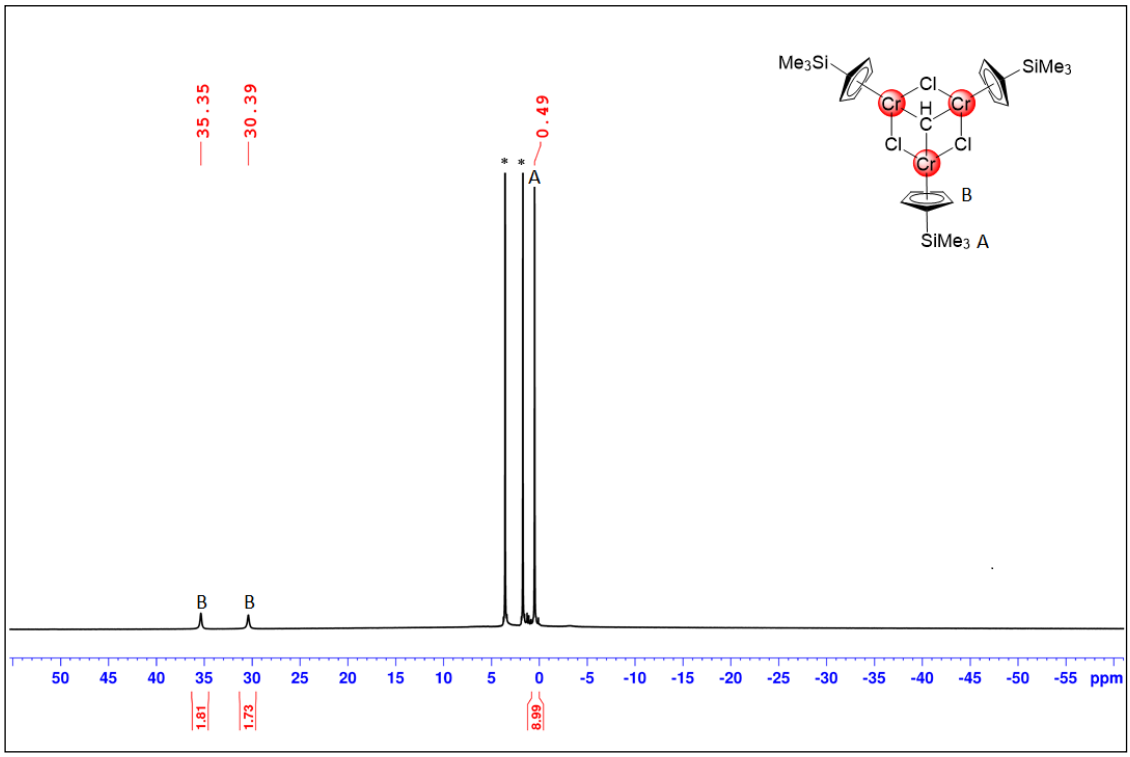

Figure S4. ^{1}H NMR spectrum (26 °C, 400.13 MHz, thf-d_8) of [(η^5-$C_5H_4SiMe_3$)Cr_3(μ_2-Cl)$_3$(μ_3-CH)] (**6**).

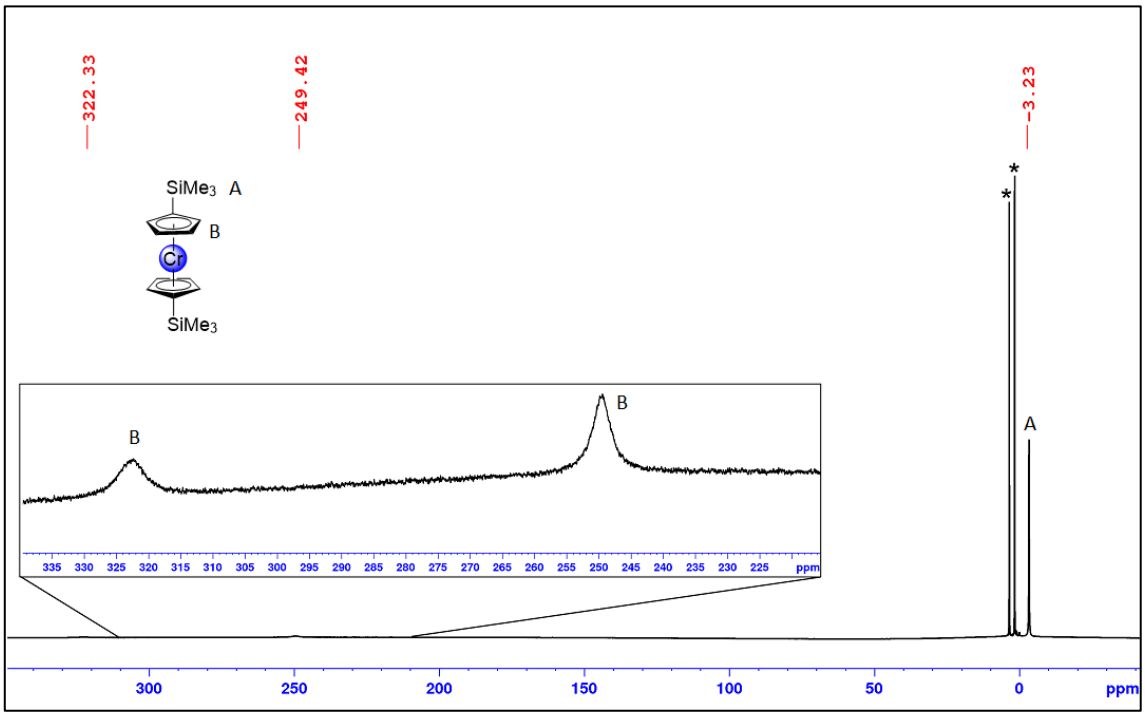

Figure S5. ^{1}H NMR spectrum (26 °C, 400.13 MHz, thf-d_8) of [(η^5-$C_5H_4SiMe_3$)$_2$Cr] (**7**).

Reactions of 1 with Aldehydes and Ketones.

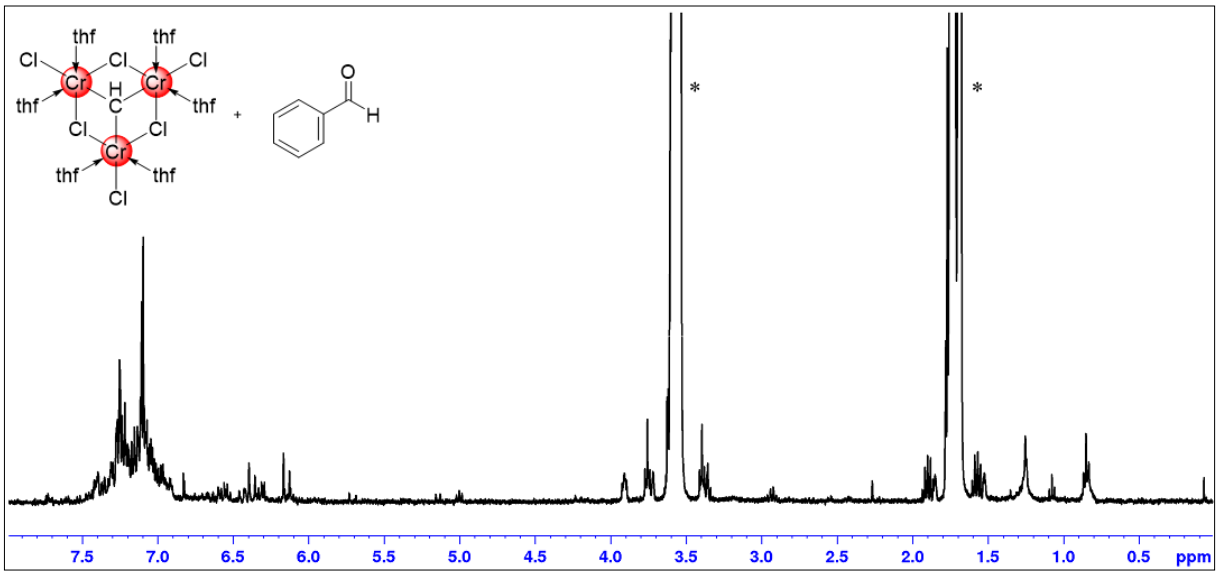

Figure S6. ^{1}H NMR spectrum (26 °C, 400.13 MHz, thf-d_8) of the product mixture of the reaction of **1** and benzaldehyde (1:1) in THF-d_8 at ambient temperature for 6 d, filtered over Al_2O_3.

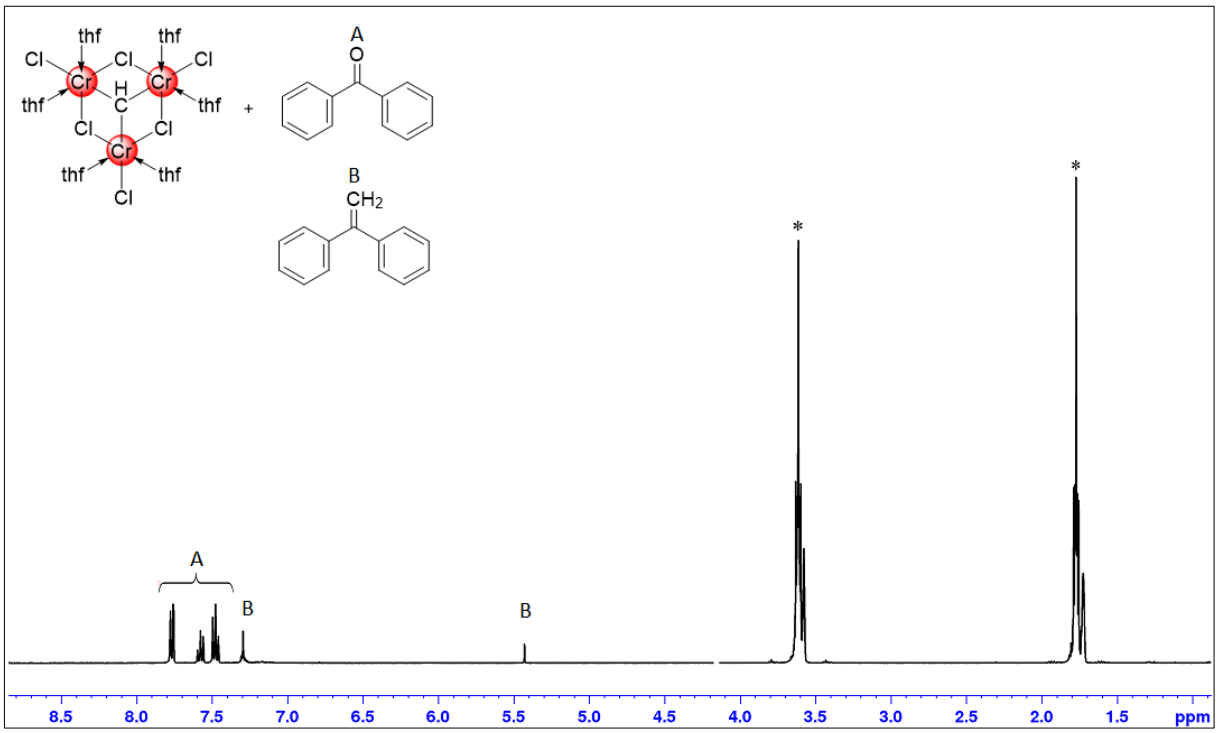

Figure S7. ^{1}H NMR spectrum (26 °C, 400.13 MHz, thf-d_8) of the product mixture of the reaction of **1** and benzophenone (1:1) in THF-d_8 at ambient temperature for 3 d, filtered over Al_2O_3.

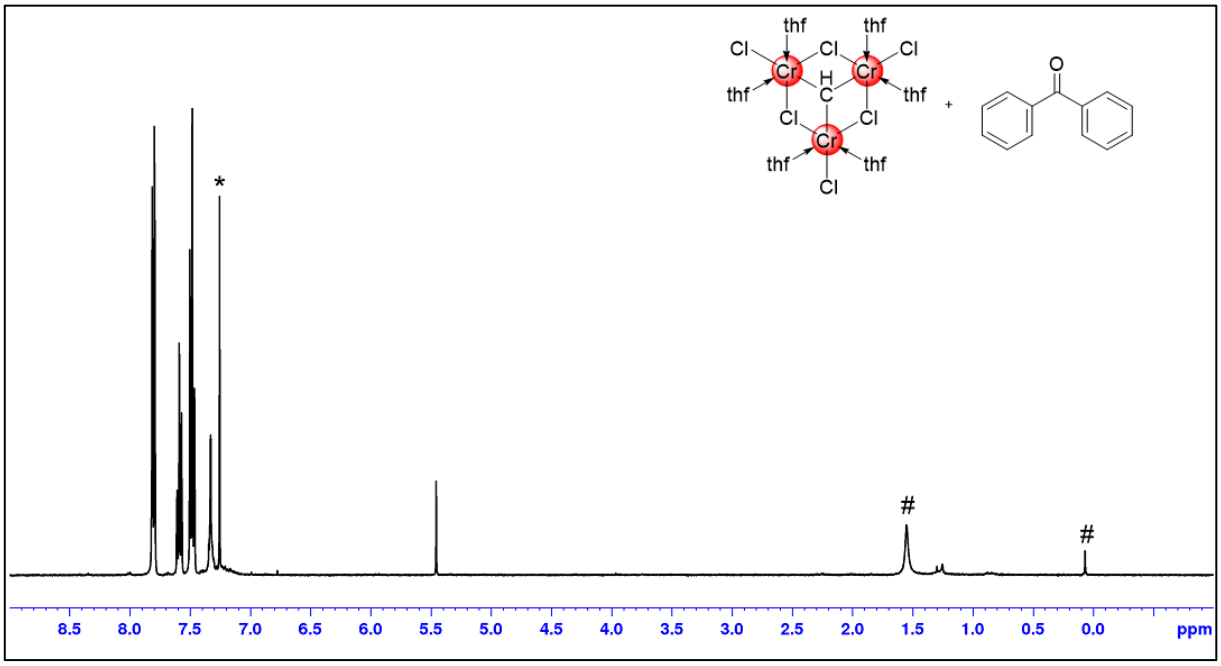

Figure S8. ^{1}H NMR spectrum (26 °C, 400.13 MHz, chloroform-d_3) of the product mixture of the reaction of **1** and benzophenone (1:1) in THF-d_8 at ambient temperature for 3 d, filtered over Al_2O_3. (Solvent impurities marked by #).

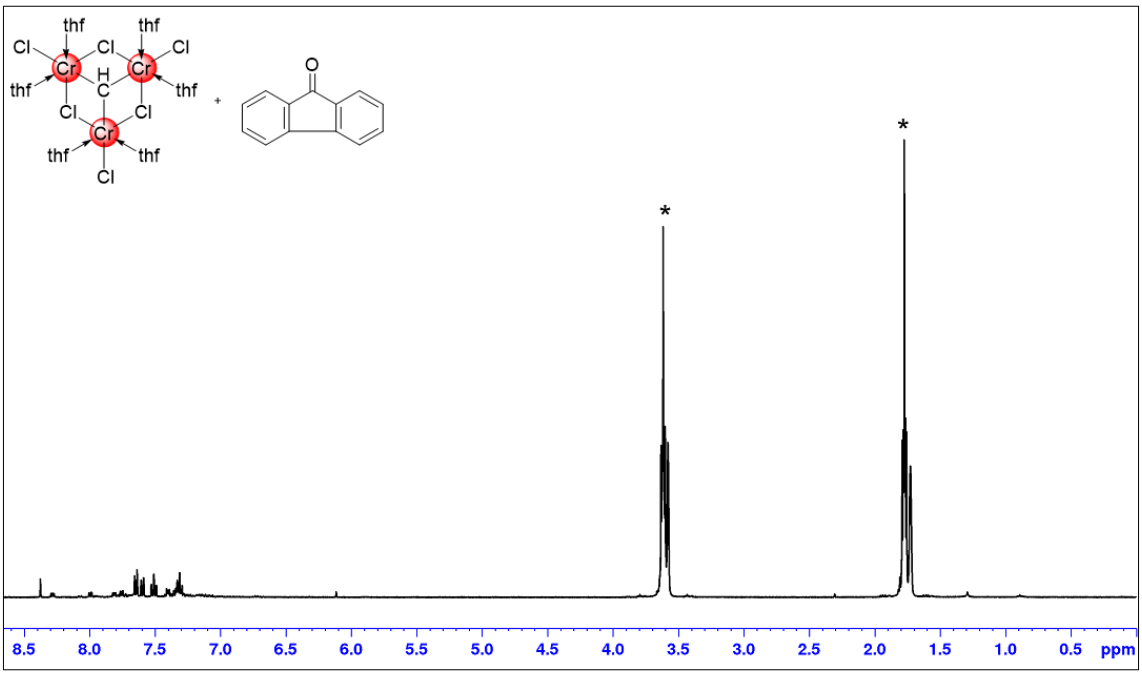

Figure S9. ^{1}H NMR spectrum (26 °C, 400.13 MHz, THF-d_8) of the product mixture of the reaction of **1** and 9-fluorenone (1:1) in THF-d_8 at ambient temperature for 3 d, filtered over Al_2O_3.

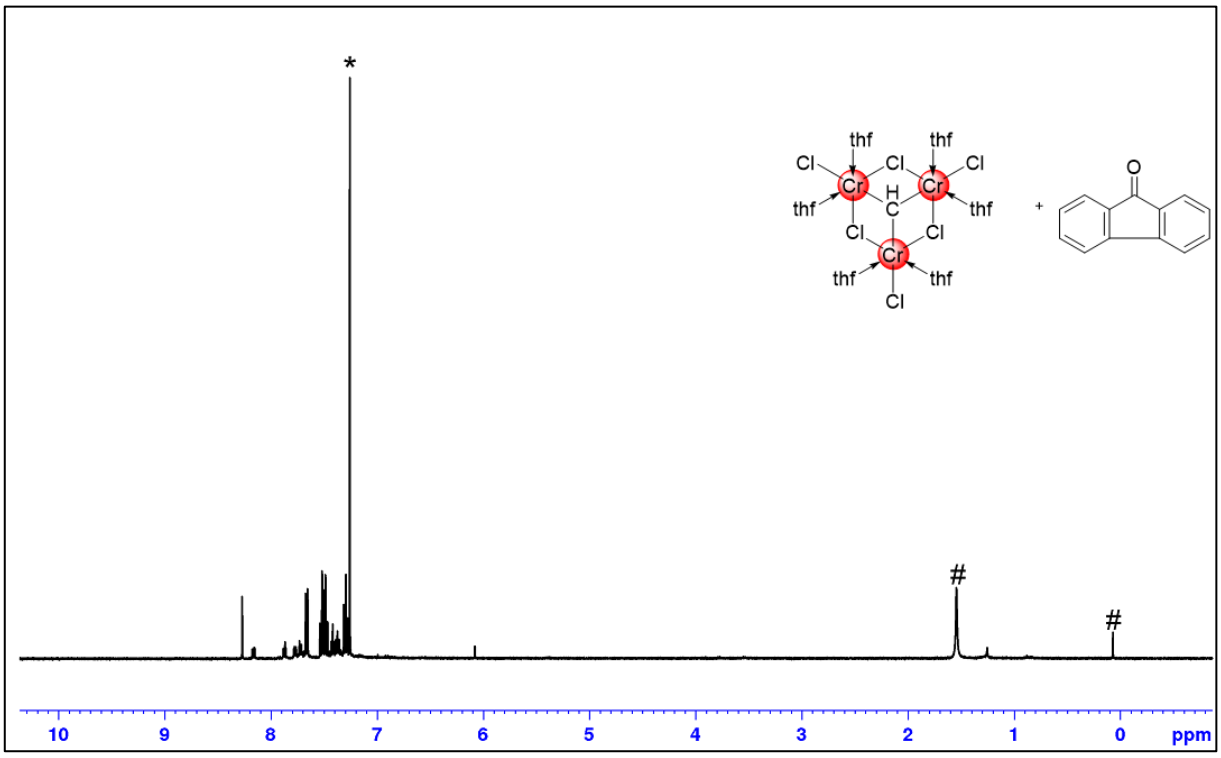

Figure S10. ^{1}H NMR spectrum (26 °C, 400.13 MHz, chloroform-d_3) of the product mixture of the reaction of **1** and 9-fluorenone (1:1) in THF-d_8 at ambient temperature for 3 d, filtered over Al_2O_3.(Solvent impurities marked by #)

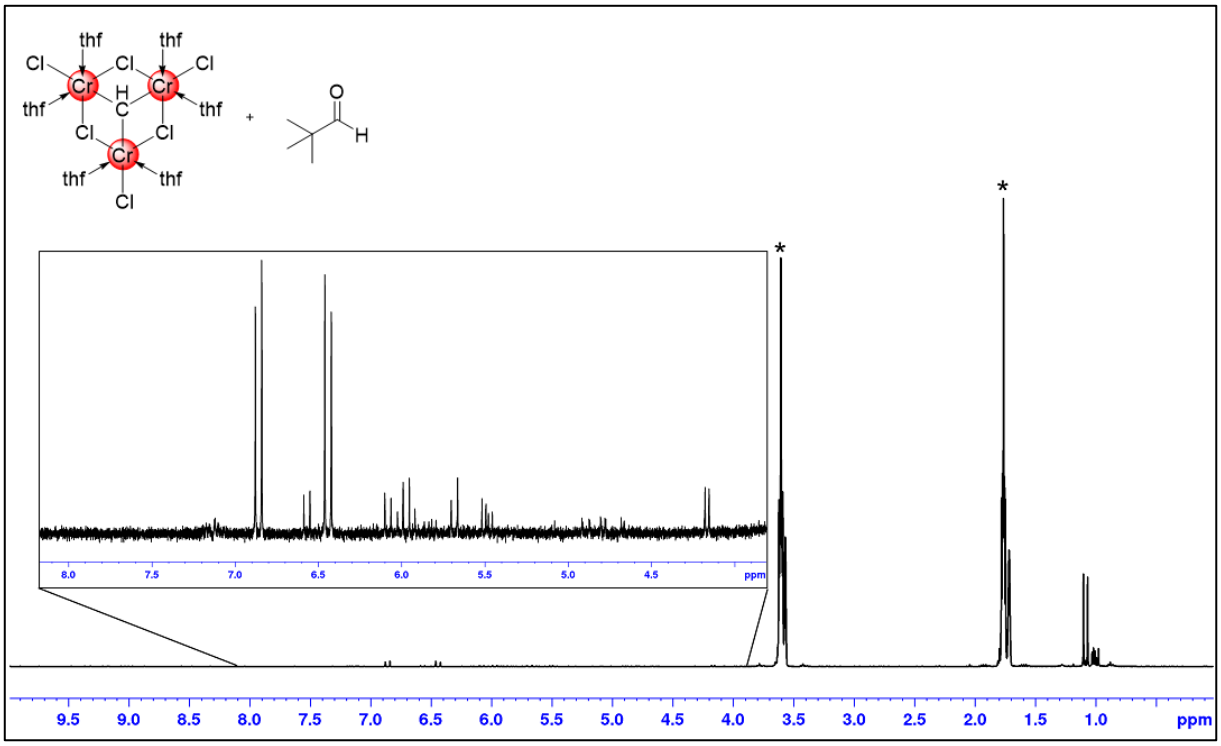

Figure S11. ^{1}H NMR spectrum (26 °C, 400.13 MHz, THF-d_8) of the product mixture of the reaction of **1** and pivalaldehyde (1:1) in THF-d_8 at ambient temperature for 3 d, filtered over Al_2O_3.

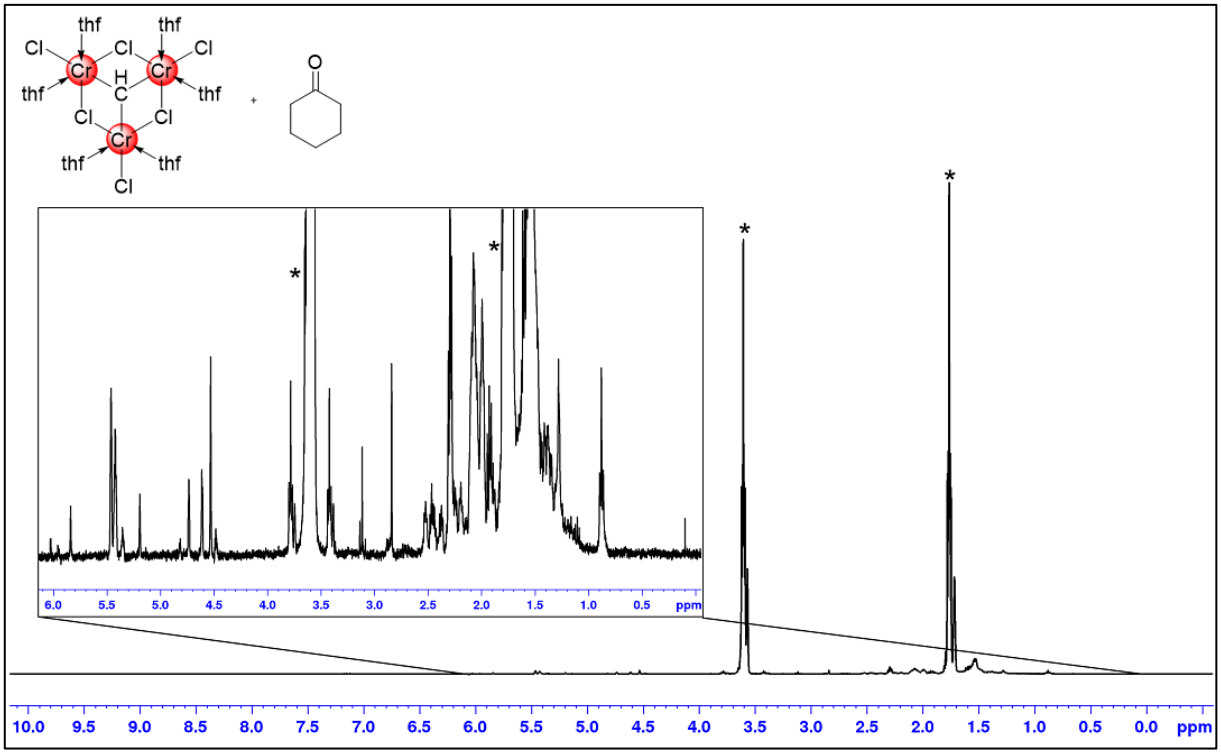

Figure S12. ^{1}H NMR spectrum (26 °C, 400.13 MHz, THF-d_8) of the product mixture of the reaction of **1** and cyclohexanone (1:1) in THF-d_8 at ambient for 3 d, filtered over Al_2O_3.

UV/Vis Spectra

Steps/artifacts at 360 nm are due to a switch of light sources of the spectrometer.

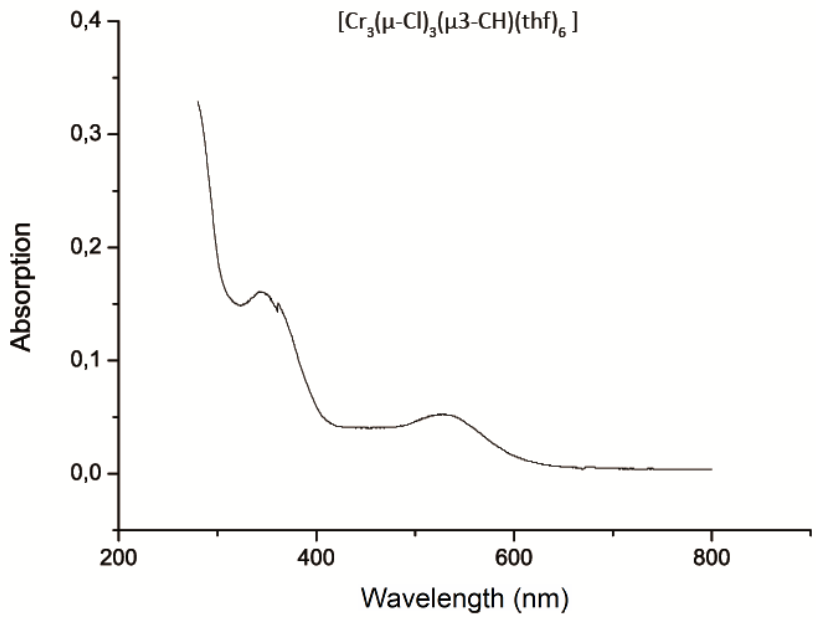

Figure S13. UV/Vis spectrum of **1** in THF at 20 °C.

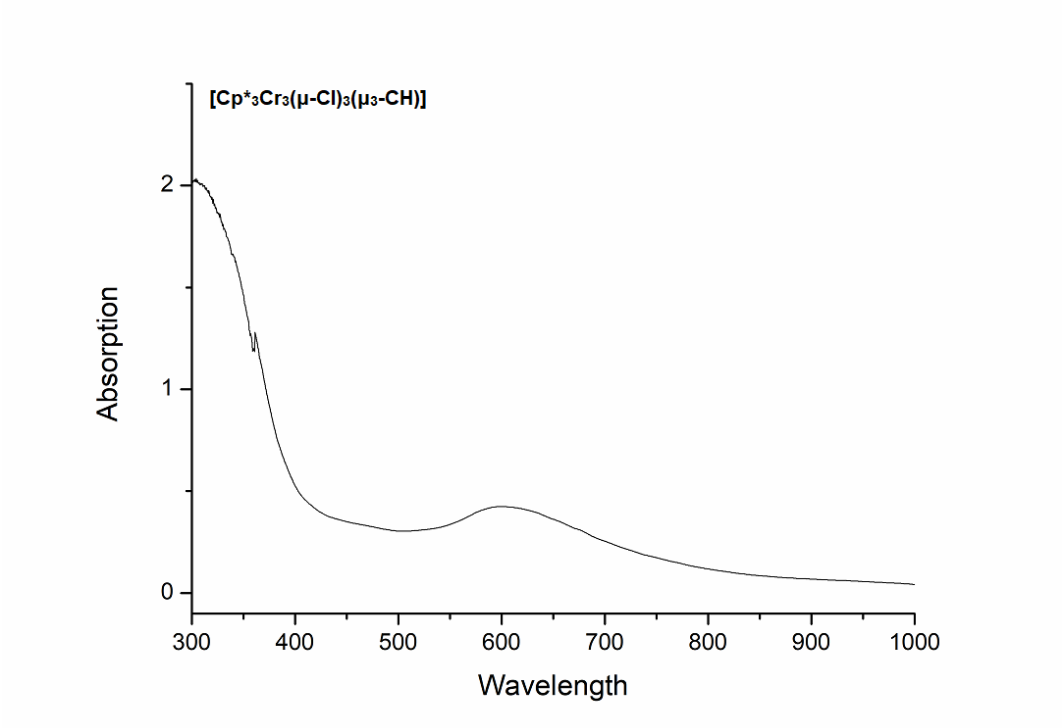

Figure S14. UV/Vis spectrum of **3** in THF at 20 °C.

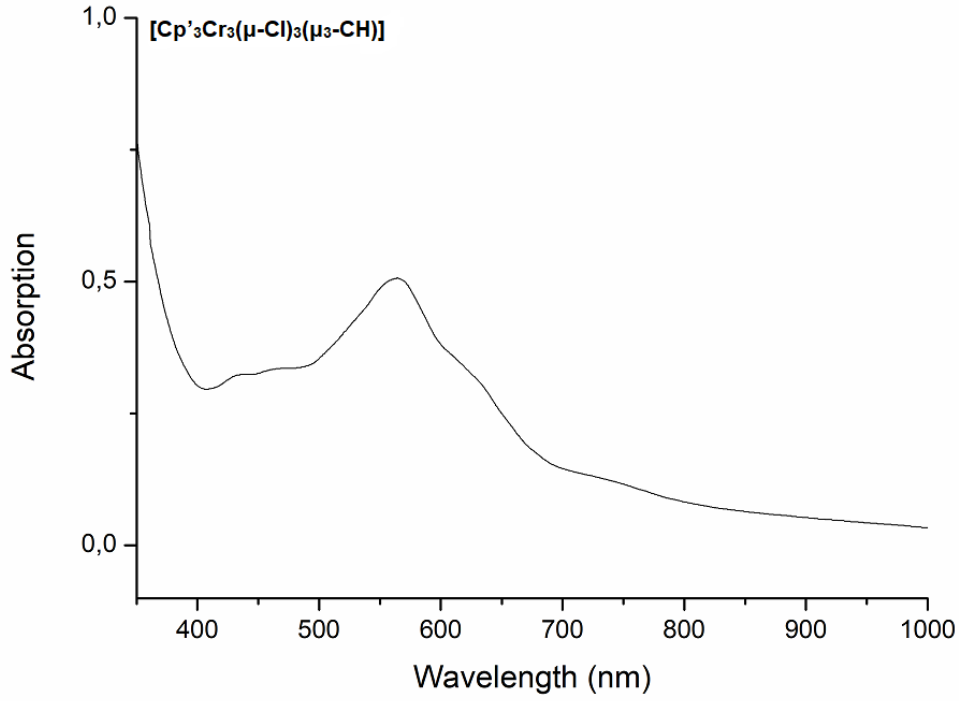

Figure S15. UV/Vis spectrum of **6** in THF at 20 °C.

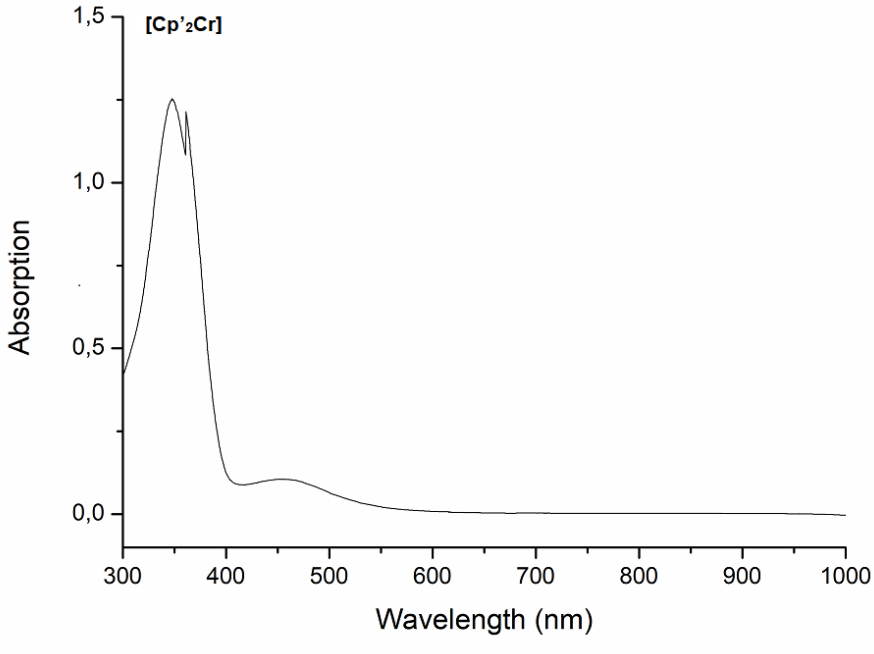

Figure S16. UV/Vis spectrum of **7** in THF at 20 °C.

SUPPORTING INFORMATION

Crystallographic Details

X-Ray Crystallography and Crystal Structure Determinations. Crystals for XRD analysis were grown from saturated solutions of toluene, thf, *n*-hexane or *n*-pentane. Suitable crystals were handpicked in a glovebox, coated with Parabar 10312, and stored on microscope slides before mounting outside the glovebox onto a micro loop. Data collection were done on a Bruker APEX II Duo diffractometer by using QUAZAR optics and Mo K_α (λ = 0.71073 Å). The data collection strategy was determined using COSMO[6] employing ω scans. Raw data were processed by APEX 3[7] and SAINT,[8] corrections for absorption effects were applied using SADABS.[9] Structure **2b** was refined as a twin and for absorption correction TWINABS[10] has been applied. The structures were solved by direct methods and refined against all data by full-matrix least-squares methods on F^2 using SHELXTL[11] and SHELXLE.[12] All atoms except hydrogen atoms were refined anisotropically. Disorders were modelled using DSR,[13] a program for refinement of disordered structures with SHELXL. Plots were generated by using CCDC Mercury 3.19.1.[14] Further details regarding the refinement and crystallographic data are listed in Tables S1 and S2, and in the CIF files.

For compound **2a**, **2b**, and **5** complete refinement of the structure was not possible, due to bad crystal quality. Only a connectivity is given for all three crystal structures. For compound **1** and **6**, the methylidyne hydrogen atoms were found in the Fourier map. The one in compound **3** is located on a three-fold axis and therefore was calculated using HFIX13.

Table S1. Crystallographic data for compound **1**, **2a**, **2b, 3** and **4**

	$[Cr_3Cl_3(\mu\text{-}Cl)_3(\mu_3\text{-}CH)(thf)_6]$ (1)	$[Cr_4(\mu\text{-}Cl)_4(\mu\text{-}I)_2(\mu_4\text{-}O)(thf)_4]$ (2a)	$[Cr_4(\mu\text{-}Cl)_{4.4}(\mu\text{-}I)_{2.6}(\mu_4\text{-}O)(thp)_4]$ (2b)	$[Cp^*_3Cr_3(\mu\text{-}Cl)_3(\mu_3\text{-}CH)]$ (3)	$[Cp^*CrCl_2(thf)]$ (4)
Formula	$C_{29}H_{57}Cl_6Cr_3O_7$	$C_{20}H_{40}Cl_4Cr_4I_2O_6$	$C_{25}H_{50}Cl_{4.4}Cr_4I_{2.6}O_6$	$C_{31}H_{46}Cl_3Cr_3$	$C_{14}H_{23}Cl_2CrO_1$
CCDC	2084207	2084206	2084205	2084204	2084210
M_r [g mol^{-1}]	886.44	980.12	1140.57	681.03	330.22
color	red/ plates	green/ block	green/ blocks	green/	blue/block
crystal system	triclinic	monoclinic	monoclinic	trigonal	monoclinic
space group	$P\bar{1}$	Cc	$P2_1/c$	R3	Pc
a [Å]	11.5732(3)	21.388(4)	15.8809(10)	18.1645(6)	12.2585(14)
b [Å]	12.3378(3)	13.308(3)	12.2956(7)	18.1645(6)	17.595(2)
c [Å]	14.2492(3)	14.340(3)	20.7392(12)	7.8855(3)	15.0197(17)
α [°]	106.3760(10)	90	90	90	90
β [°]	101.9940(10)	109.833(2)	104.5370(10)	90	103.544(2)
γ [°]	93.0250(10)	90	90	120	90
V [Å^3]	1895.97(8)	3839.52	3920.0(4)	2253.24(17)	3149.5(6)
Z	2	8	4	3	8
T [K]	100(2)	170(2)	100(2)	173(2)	100(2)
ρ_{calcd} [g cm^{-3}]	1.553			1.506	1.393
μ [mm^{-1}]	1.309			1.353	1.053
F (000)	922			1065	1384
total reflns	68227			17191	41526
unique reflns	8347			2813	12856
Data/restrains/parameter	8347 / 194 / 400			2813 / 1 / 118	12856 / 192 / 716
R_1(I>2σ)[a]	0.0396			0.0189	0.0630
ωR_2 (I>2σ)[a]	0.0963			0.0483	0.1674
R_1 (all data)	00570			0.0193	0.0846
ωR_2 (all data)	0.1064			0.0486	0.1867
GOF	1.038			1.091	1.062

[a] $R_1 = \Sigma(||F_0|-|F_c||)/\Sigma|F_0|, F_0 > 4\sigma(F_0)$. $wR_2 = \{\Sigma[w(F_0^2-F_c^2)^2/\Sigma[w(F_0^2)^2]\}^{1/2}$.

Table S2. Crystallographic data for compound **5**, **6**, **7** and **8**

	[Cp*Cr(μ-Cl)(μ-I)]$_2$ (5)	**[Cp'$_3$Cr$_3$(μ-Cl)$_3$(μ$_3$-CH)] (6)**	**[Cp'$_2$Cr] (7)**	**{(Cp'CrCl$_3$)[Li(thf)$_2$]} (8)**
Formula	$C_{20}H_{30}Cl_{10.83}Cr_2I_{1.17}$	$C_{25}H_{40}Cl_3Cr_3Si_3$	$C_{16}H_{26}CrSi_2$	$C_{16}H_{29}Cl_3CrLiO_2Si$
CCDC	2084212	2084208	2084209	2084211
M$_r$ [g mol^{-1}]	552.79	687.19	326.55	446.77
color	blue/ block	violet/ needles	orange	blue
crystal system	monoclinic	monoclinic	monoclinic	orthorhombic
space group	$P2_1/n$	$P2_1/c$	$P2_1/c$	$Pna2_1$
a [Å]	11.145(4)	13.2665(6)	6.1193(11)	29.821(2)
b [Å]	13.403(6)	18.3676(8)	8.0476(14)	10.1555(10)
c [Å]	14.649	13.6325(6)	17.290(3)	20.468(2)
α [°]	90	90	90	90
β [°]	101.542(6)	107.6150(10)	94.932(2)	90
γ [°]	90	90	90	90
V [Å^3]	2143.9(15)	3166.1(2)	848.(3)	4328.0(8)
Z	4	4	2	8
T [K]	173(2)	100(2)	173(2)	100(2)
ρ$_{calcd}$ [g cm^{-3}]		1.442	1.278	1.371
μ [mm^{-1}]		1.392	0.802	0.960
F (000)		1420	348	1864
total reflns		84588	9415	45447
unique reflns		8510	2225	10157
Data/restrains/parameter		8510 / 0 / 320	2225 / 0 / 91	10157 / 1 / 439
R_1(I>2σ)[a]		R_1 = 0.0261	R1 = 0.0376	R1 = 0.0399
ωR_2 (I>2σ)[a]		ωR_2 = 0.0670	ωR_2 = 0.0933	ωR_2 = 0.0863
R_1 (all data)		R_1 = 0.0307	R1 = 0.0477	R_1 = 0.0531
ωR_2 (all data)		ωR_2 = 0.0702	ωR_2 = 0.1009	ωR_2 = 0.0940
GOF		1.051	1.053	1.027

[a] $R_1 = \Sigma(||F_0|-|F_c||)/\Sigma|F_0|, F_0 > 4\sigma(F_0)$. $wR_2 = \{\Sigma[w(F_0^2-F_c^2)^2/\Sigma[w(F_0^2)^2]\}^{1/2}$.

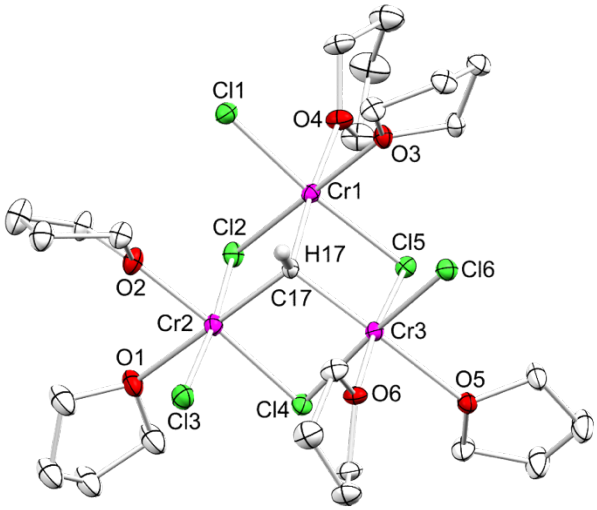

Figure S17. MERCURY representation (50% probability ellipsoids) of $[Cr_3Cl_3(\mu\text{-}Cl)_3(\mu_3\text{-}CH)(thf)_6]$ (**1**). Hydrogen atoms (except for H17) and co-crystallized solvent molecules (thf) are omitted for clarity. Selected interatomic distances (Å) and angles (°): Cr1–C17 2.022(3), Cr2–C17 2.019(3), Cr3–C17 2.018(3), C17–H17 0.84(3), Cr1–O3 2.0433(18), Cr1–O4 2.2409(19), Cr1–Cl1 2.3328(7), Cr1–Cl2 2.3876(7),Cr1–Cl5 2.4186(7), Cr2–Cl2 2.4159(8), Cr2–Cl3 2.3291(8), Cr2–Cl4 2.3769(7), Cr3–Cl4 2.4071(7),Cr3–Cl5 2.3975(7), Cr3–Cl6 2.3141(7), C17–H17 0.84(3); Cr1–C17–Cr2 103.66(12), Cr1–C17–Cr3 102.72(12), Cr2–C17–Cr3 103.43(12), Cr1–Cl2–Cr2 82.83(2), Cr2–Cl4–Cr3 82.96(2), Cr3–Cl5–Cr1 81.88(2).

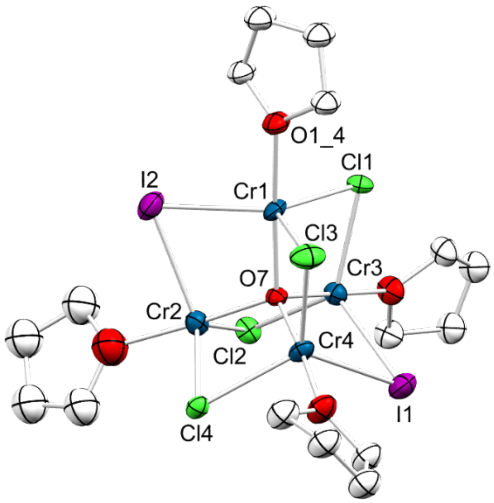

Figure S18. MERCURY representation of the connectivity (30% probability ellipsoids) of $[Cr_4(\mu\text{-}Cl)_4(\mu\text{-}I)_2(\mu_4\text{-}O)(thf)_4]$*thf (**2a**). Hydrogen atoms and lattice solvent (thf) are omitted for clarity.

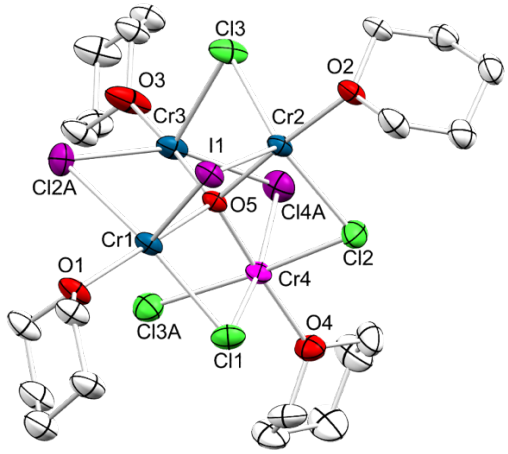

Figure S19. MERCURY representation (50% probability ellipsoids) of $[Cr_4Cl(\mu\text{-}Cl)_4(\mu\text{-}I)_2(\mu_4\text{-}O)(thp)_4]$ (**2b**). Hydrogen atoms and co-crystallized solvent molecules (THP) are omitted for clarity.

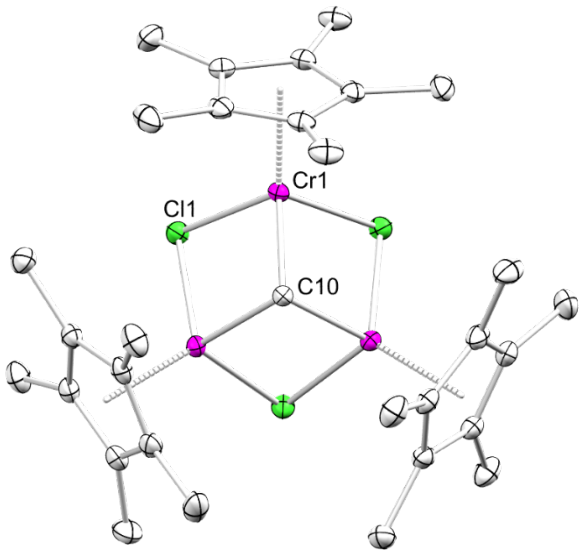

Figure S20. MERCURY representation (50% probability ellipsoids) of $[(\eta_5\text{-}C_5Me_5)_3Cr_3(\mu\text{-}Cl)_3(\mu_3\text{-}CH)]$ (**3**). Hydrogen atoms are omitted for clarity. Selected interatomic distances (Å) and angles (°): Cr1–C10 2.0109(19), Cr1–Cl1 2.3416(5), Cr1–Cr1' 2.9103(5), Cr1–Cr1'' 2.9103(5), Cr1''–Cl1 2.3615(5), Cr1–$Cp_{centroid}$ 1.903 (calculated with Mercury); C10–Cr1–Cl1 95.73(6), C10–Cr1–Cl1' 95.11(6), C10–Cr1–Cr1' 43.65(5), Cl1–Cr1–Cl1' 92.15(2), Cl1'–Cr1–Cr1' 96.046(13), Cl1'–Cr1–Cr1' 51.46(13), C10–Cr1–Cr1'' 43.65(5), Cr1'–Cr1–Cr1'' 60.002(1), Cr1–Cl1–Cr1'' 76.456(18).

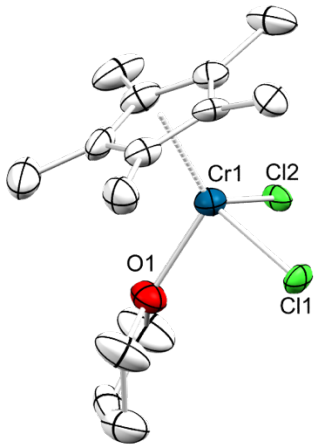

Figure S21. MERCURY representation (50% probability ellipsoids) of [Cp*$CrCl_2$(thf)] (**4**). Hydrogen atoms and the three additional molecules in the unit cell are omitted for clarity. Selected interatomic distances (Å) and angles (°): Cr1–Cl1 2.388(3), Cr1–Cl2 2.349(3), Cr1–O1 2.060(8), Cr1–$Cp_{centroid}$ 1.878 (calculated with Mercury); Cl1–Cr1–Cl2 98.44(11).

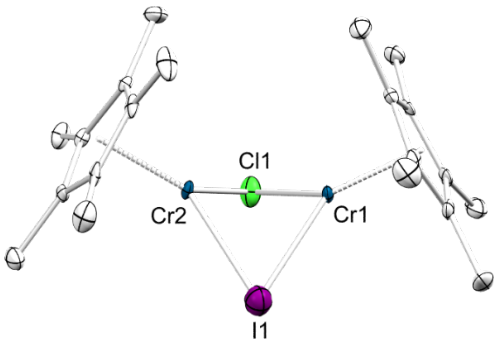

Figure S22. MERCURY representation (50% probability ellipsoids) of [$(Cp^*Cr)_2$(μ-Cl)(μ-I)] (**5**). Hydrogen atoms and the second molecule in the unit cell are omitted for clarity. Selected interatomic distances (Å) and angles (°): Cr1–I1 2.929(1), Cr2–I1 2.627(1), Cr1–Cl1 2.32(1), Cr2–Cl1 2.33(2),Cr1–$Cp_{centroid}$ 1.909, Cr2–$Cp_{centroid}$ 1.920 (calculated with Mercury); Cr1–I1–Cr2 58.60(3), Cr1–Cl1–Cr2 67.2(4), I1–Cr2–Cl1 95.4(4).

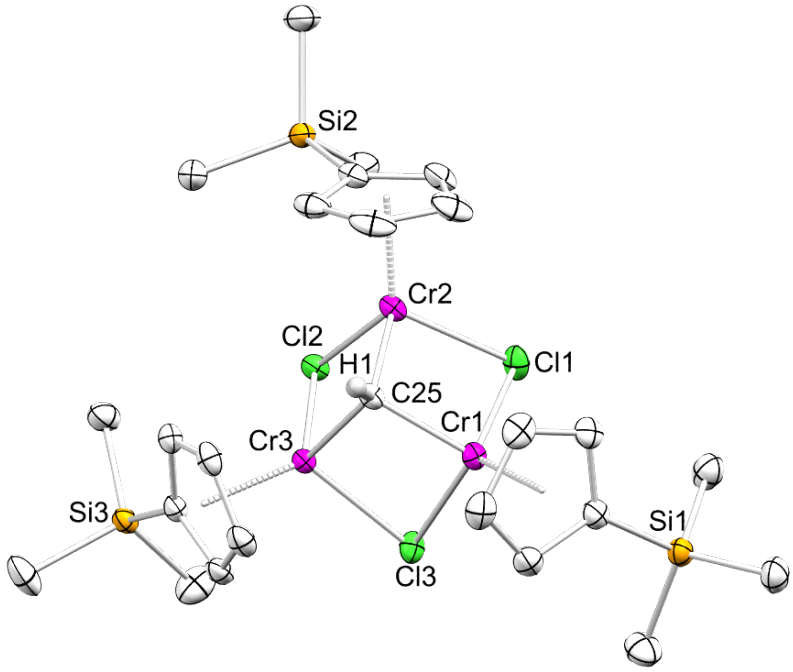

Figure S23. MERCURY representation (50% probability ellipsoids) of [(η_5-$C_5H_4SiMe_3$)$_3$$Cr_3$($\mu$-Cl)$_3$($\mu_3$-CH)] (**6**). Hydrogen atoms (except for H1) are omitted for clarity. Selected interatomic distances (Å) and angles (°): Cr1–C25 1.9846(15), Cr2–C25 1.9806(14), Cr3–C25 1.9822(14), Cr1–Cr2 2.8193(3), Cr1–Cr3 2.8318(3), Cr2–Cr3 2.8363(3), Cr3–Cl2 2.3316(4), Cr3–Cl3 2.3519(4), Cr1–Cl1 2.3243(4), Cr2–Cl1 2-3270(4), Cr2–Cl2 2.3355(4), Cr1–Cl3 2.3479(4), C25–H1 0.965(19), Cr1–$Cp_{centroid}$ 1.873, Cr2–$Cp_{centroid}$ 1.871, Cr3–$Cp_{centroid}$ 1.868 (calculated with Mercury); Cr(1)–Cl(1)–Cr(2) 74.621(13), Cr(1)–Cl(3)–Cr(3) 74.102(13), Cr(3)–Cl(2)–Cr(2) 74.850(12), Cl(1)–Cr(1)–Cl(3) 93.396(16), Cl(2)–Cr(3)–Cl(3) 93.783(15), Cl(1)–Cr(2)–Cl(2) 91.652(15), C(25)–Cr(1)–Cl(1) 97.36(4), C(25)–Cr(2)–Cl(2) 96.82(4), C(25)–Cr(3)–Cl(3) 97.31(4), C(25)–Cr(1)–Cl(3) 97.37(4), C(25)–Cr(2)–Cl(1) 97.38(4), C(25)–Cr(3)–Cl(2) 96.90(4), Cr(2)–C(25)–Cr(3) 91.41(6), Cr(2)–C(25)–Cr(1) 90.64(6), Cr(3)–C(25)–Cr(1) 91.10(6).

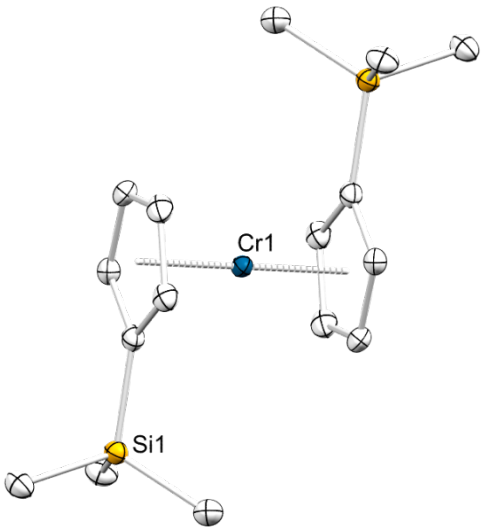

Figure S24. MERCURY representation (50% probability ellipsoids) of [(η^5-$C_5H_4SiMe_3$)$_2$Cr] (**7**). Hydrogen atoms are omitted for clarity. Selected interatomic distances (Å) and angles (°): Cr1–C1 2.1343(18), Cr1–C2 2.1331(17), Cr1–C3 2.1905(18), Cr1–C4 2.2106(18), Cr1–C5 2.159(2), Cr1–$Cp_{centroid}$ 1.798 (calculated with Mercury), Si1–C1 1.8602(19); Cr1–C1–Si1 127.56(9).

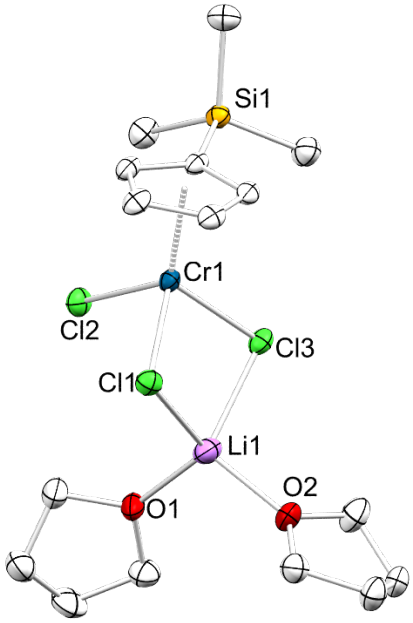

Figure S25. MERCURY representation (50% probability ellipsoids) of [(η^5-$C_5H_4SiMe_3$)$CrCl(\mu$-Cl)$_2$Li(thf)$_2$] (**8**). Hydrogen atoms and the second molecule in the unit cell are omitted for clarity. Selected interatomic distances (Å) and angles (°): Cr1–Cl1 2.3524(12), Cr1–Cl2 2.2928(13), Cr1–Cl3 2.3387(12), Cr1–$Cp_{centroid}$ mean1.794 (calculated with Mercury), Li1–O1 1.899(9), Li1–O2 1.939(9), Li1–Cl3 2.401(8), Li1–Cl1 2.362(8), Li1–Cl3 2.401(8); Cr1–Cl1–Li1 85.8(2), Cr1–Cl3–Li1 85.3(2), Cl2–Cr1–Cl3 95.36(5), Cl2–Cr1–Cl1 97.92(5), Cl3–Cr1–Cl1 92.18(5).

Infrared Spectra

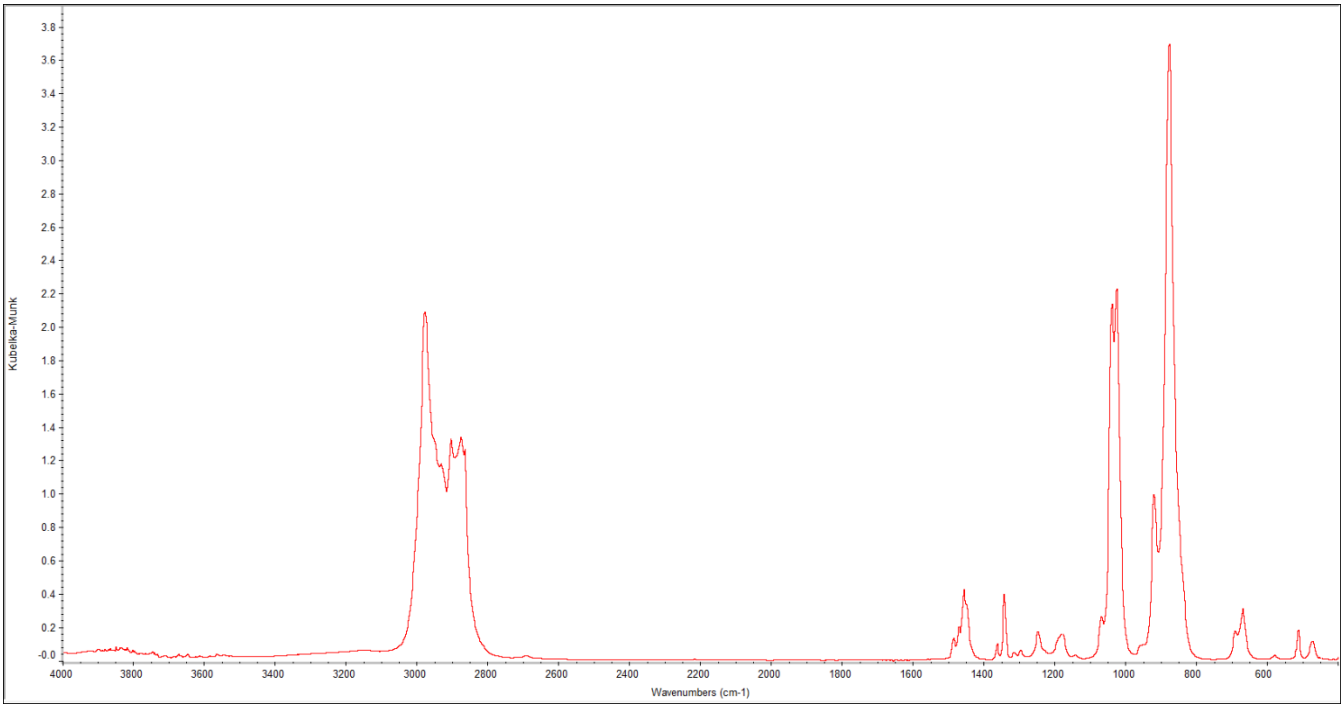

Figure S26. DRIFT spectrum of $[Cr_3(\mu_2\text{-}Cl)_3Cl_3(\mu_3\text{-}CH)(thf)_6]$ (**1**) at 25 °C.

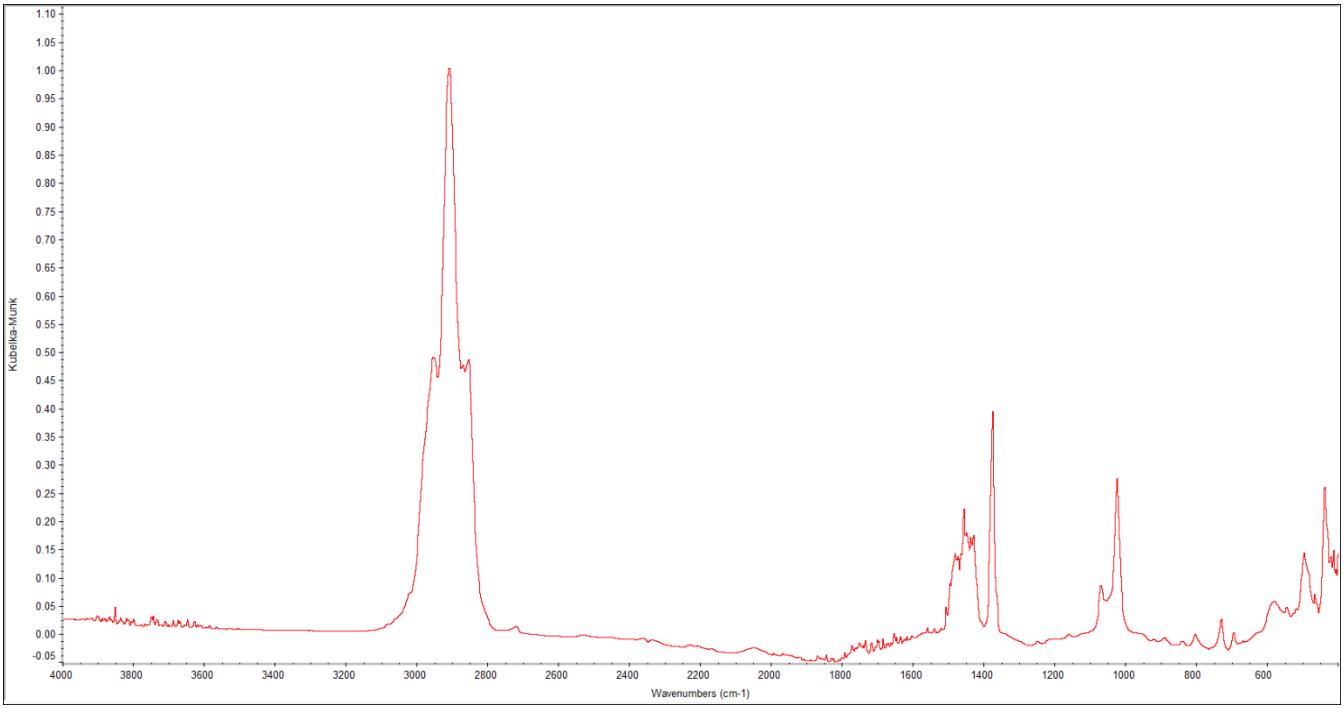

Figure S27. DRIFT spectrum of $[(\eta^5\text{-}C_5Me_5)_3Cr_3(\mu_2\text{-}Cl)_3(\mu_3\text{-}CH)]$ (**3**) at 25 °C.

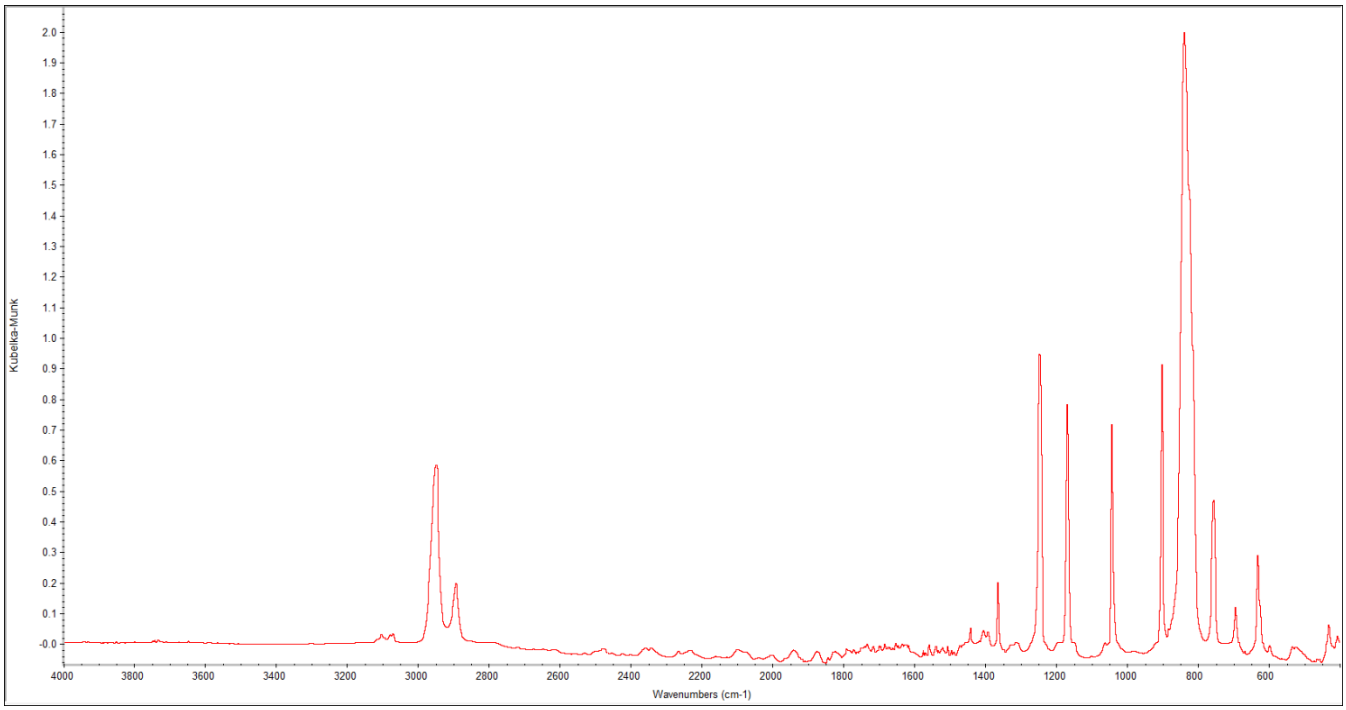

Figure S28. DRIFT spectrum of [(η^5-$C_5H_4SiMe_3$)Cr_3(μ_2-Cl)$_3$(μ_3-CH)] (**6**) at 25 °C.

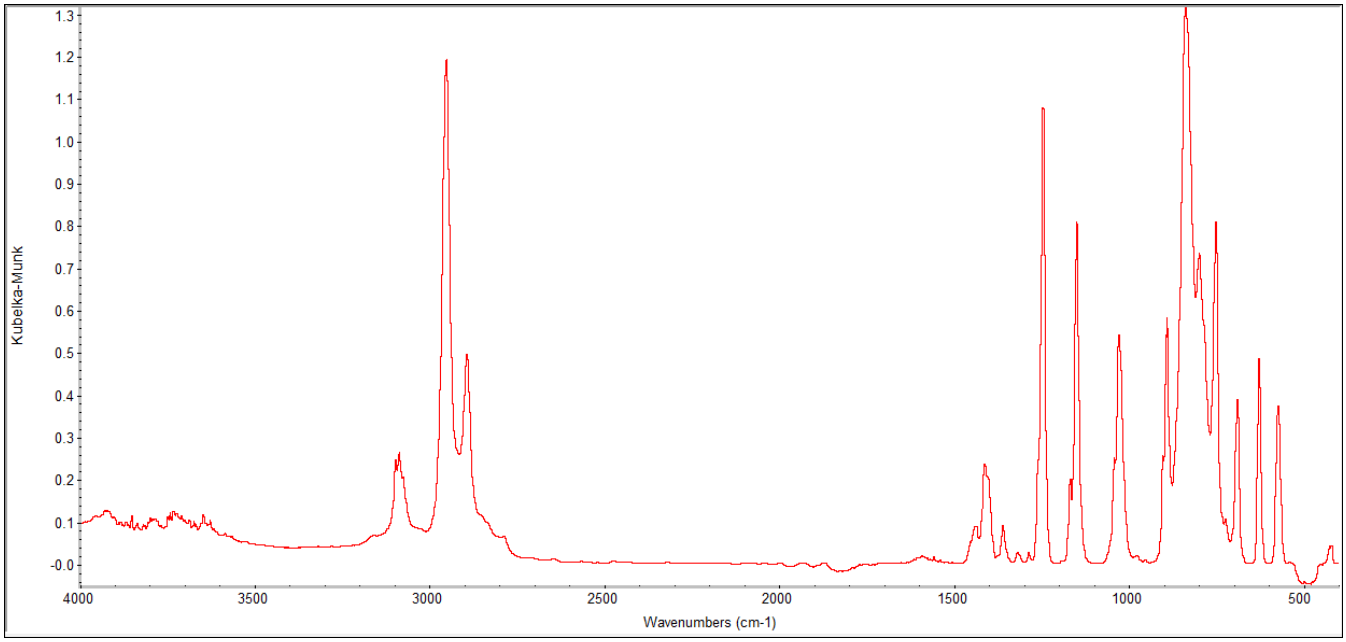

Figure S29. DRIFT spectrum of [(η^5-$C_5H_4SiMe_3$)$_2$Cr] (**7**) at 25 °C.

SQUID Measurements

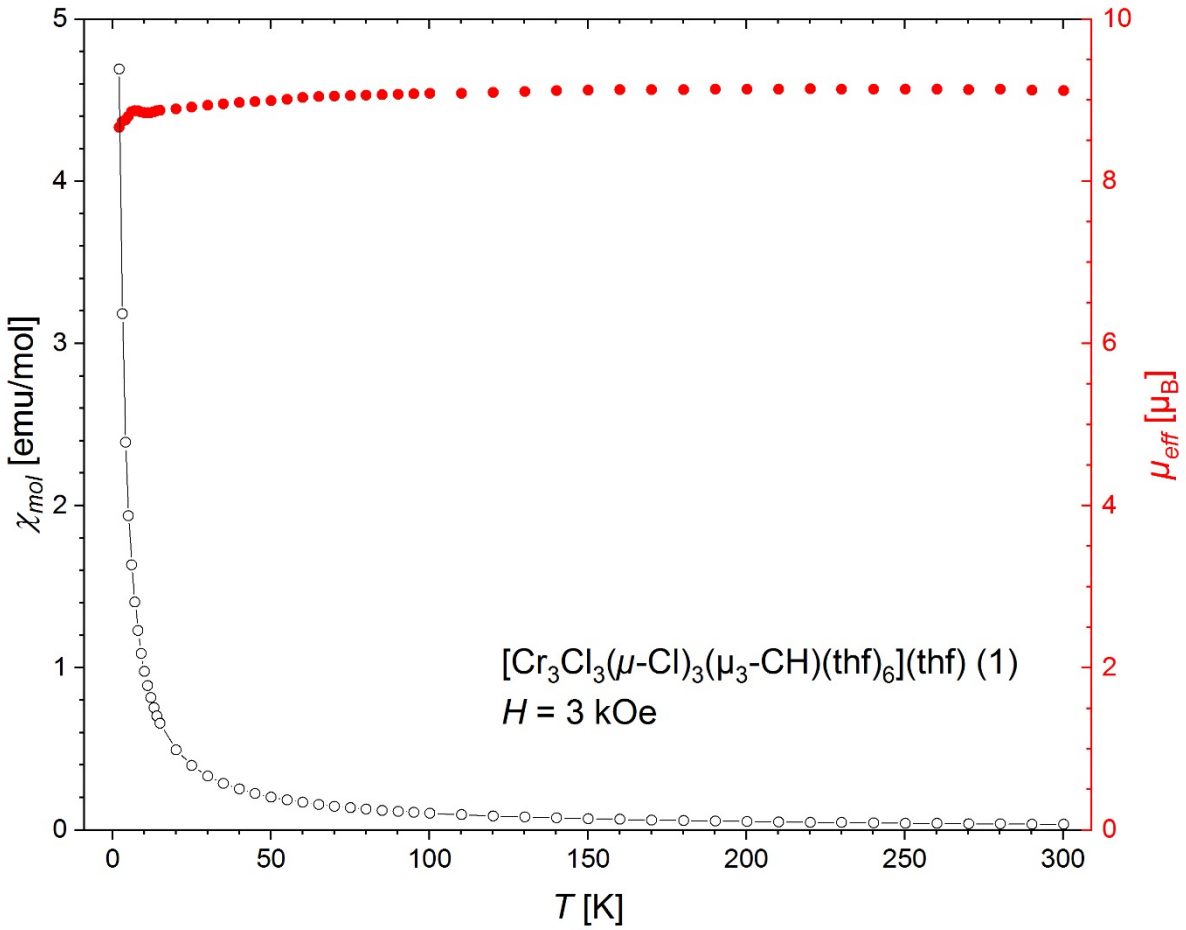

Figure 30. Temperature-dependent molar magnetic susceptibility $\chi_{mol}(T)$ (black open circles; left ordinate) and effective magnetic moment $\mu_{eff}(T)$ (red filled circles; right ordinate) as obtained by SQUID magnetic measurements on crystalline powder of **1** in an applied field H = 3 kOe. The $\chi_{mol}(T)$ data was corrected for diamagnetic contributions ($-7.243 \cdot 10^{-4}$ emu/mol; calculated from Pascal's constants),[15] and a spin-only g factor of 2.0 was assumed in the calculation of $\mu_{eff}(T)$. Note, that **1** contains an additional THF solvent molecule per formula unit in the crystal packing.

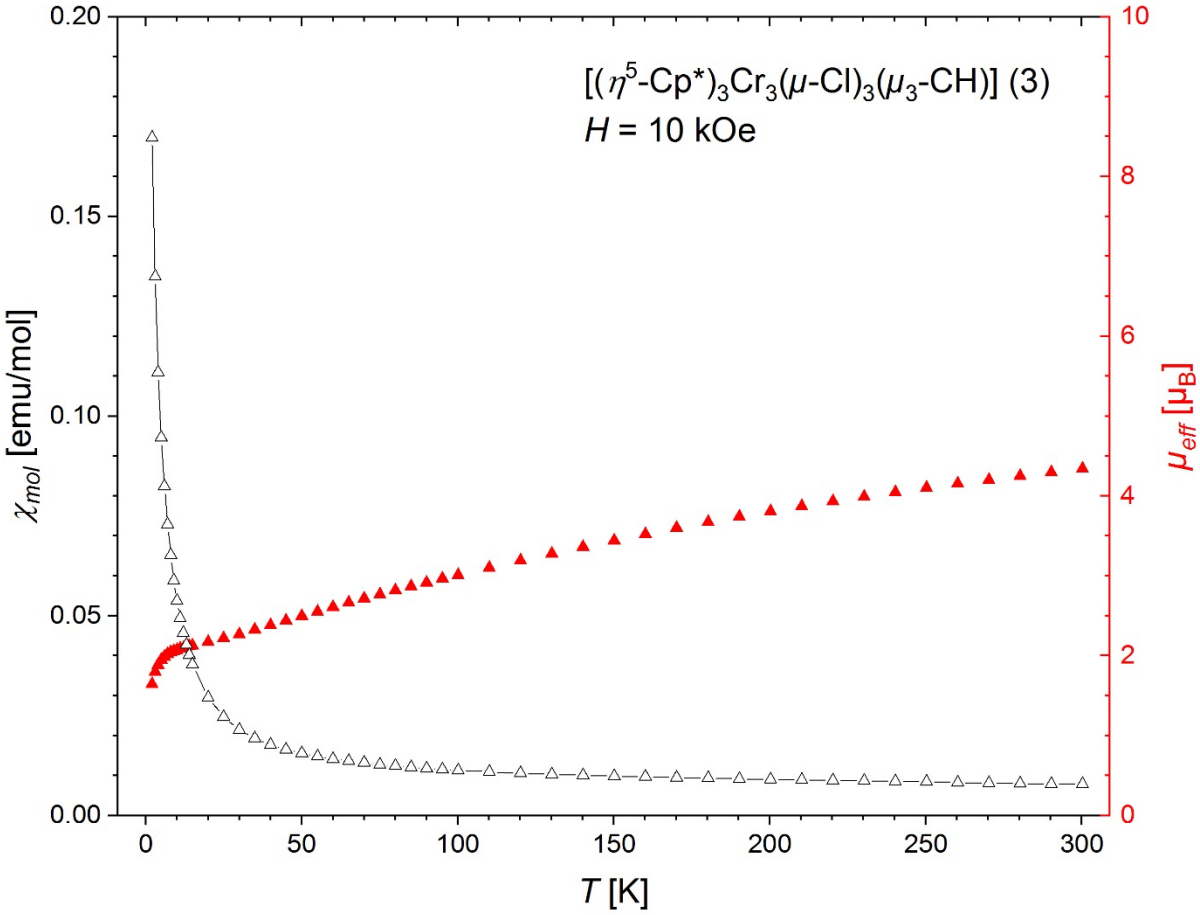

Figure 31. Temperature-dependent molar magnetic susceptibility $\chi_{mol}(T)$ (black open triangles; left ordinate) and effective magnetic moment $\mu_{eff}(T)$ (red filled triangles; right ordinate) as obtained by SQUID magnetic measurements on crystalline powder of **3** in an applied field H = 10 kOe. The $\chi_{mol}(T)$ data was corrected for diamagnetic contributions ($-3.071 \cdot 10^{-4}$ emu/mol; calculated from Pascal's constants),[15] and a spin-only g factor of 2.0 was assumed in the calculation of $\mu_{eff}(T)$.

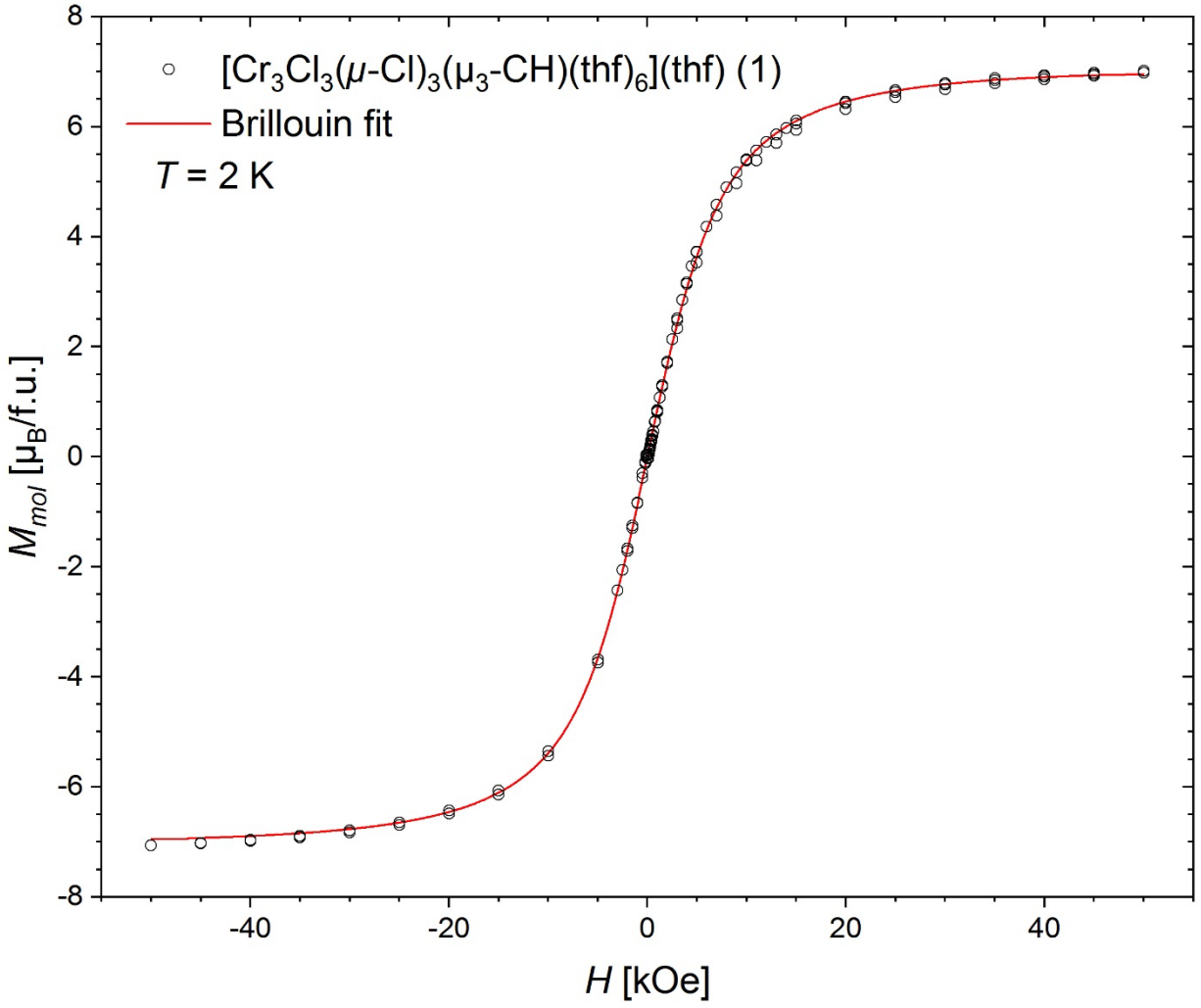

Figure 32. Field-dependent molar magnetization $M_{mol}(H)$ (black open circles) as obtained by SQUID magnetic measurements on crystalline powder of **1** at a temperature T = 2 K. A fit of the data with a Brillouin function (red line; assuming a spin-only g factor of 2.0) yields a total spin quantum number S = 4.45(4). Note, that **1** contains an additional THF solvent molecule per formula unit in the crystal packing.

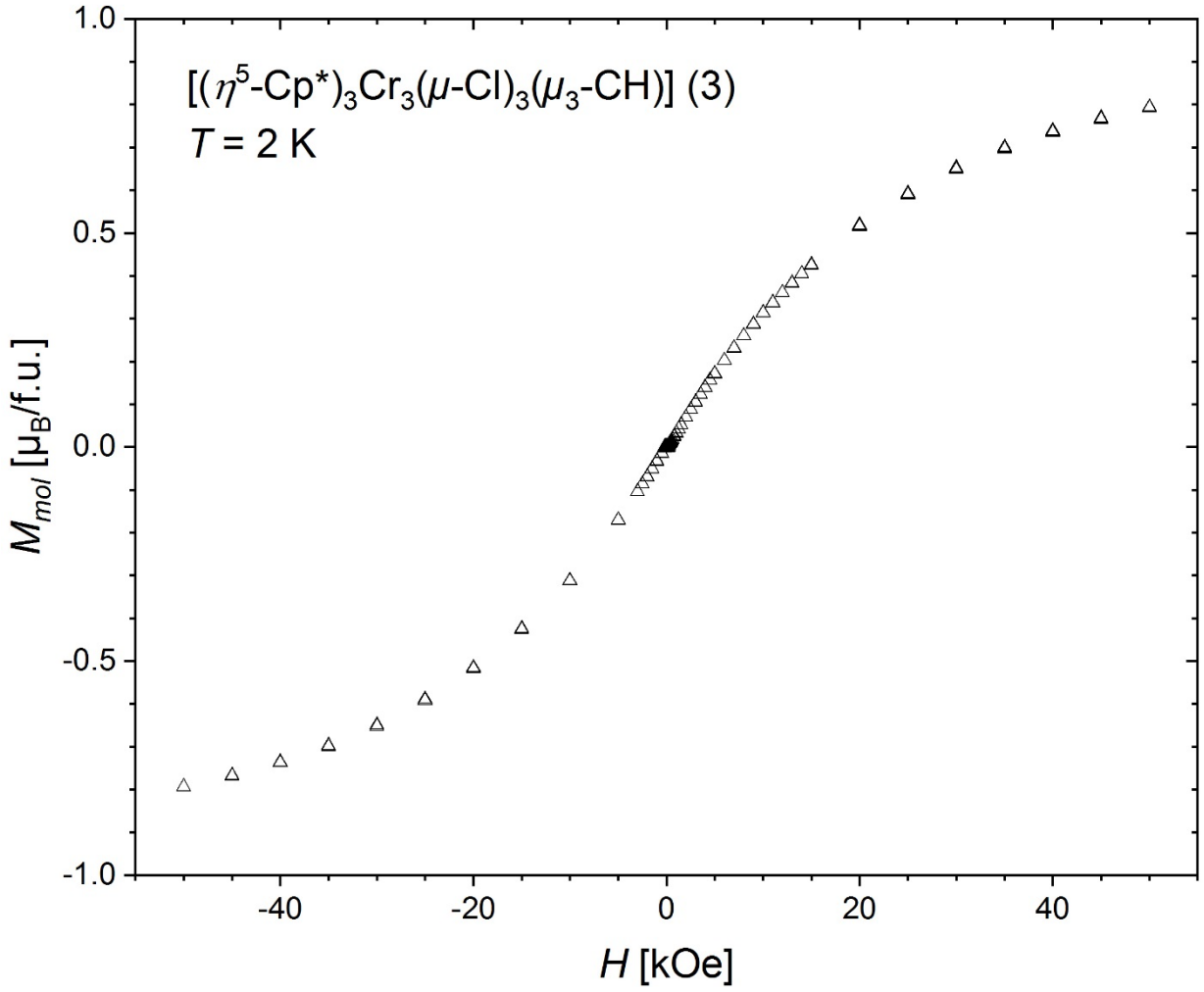

Figure S33. Field-dependent molar magnetization $M_{mol}(H)$ (black open circles) as obtained by SQUID magnetic measurements on crystalline powder of **3** at a temperature T = 2 K.

SUPPORTING INFORMATION

Gas Chromatography – Mass Spectrometry

GC/MS was performed on an *Agilent* Q 5973 with electron impact ionization.The obtained mass spectral data were analyzed with *Agilent* MassHunter (version 10.0.368) and compared to Main EI MS Library (mainlib). Further product suggestions for found compounds are based on plausible isostructural known compounds, that are not listed in the databases used by *Agilent* MassHunter and are marked by square brackets.

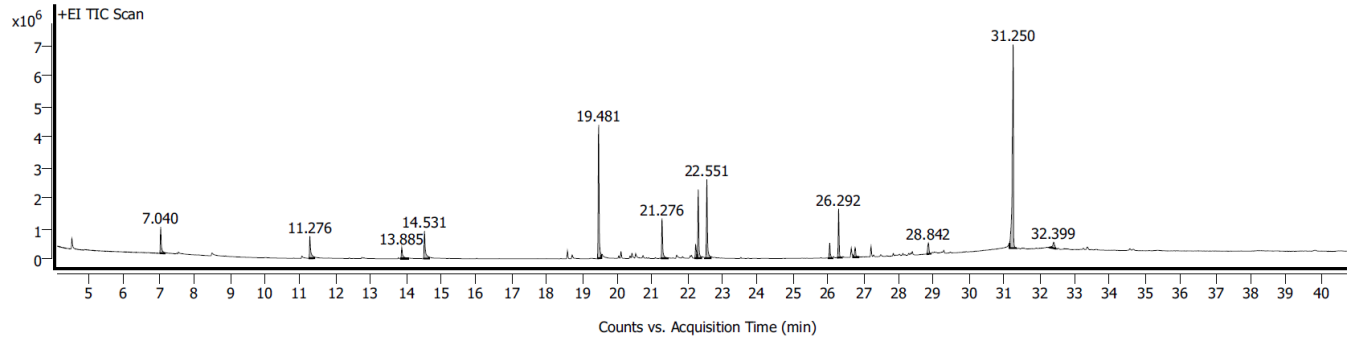

Figure S34. Gas chromatogram of the filtered reaction mixture of **1** with 1 equivalent of benzaldehyde in THF-d_8 at ambient temperature for 6 d.

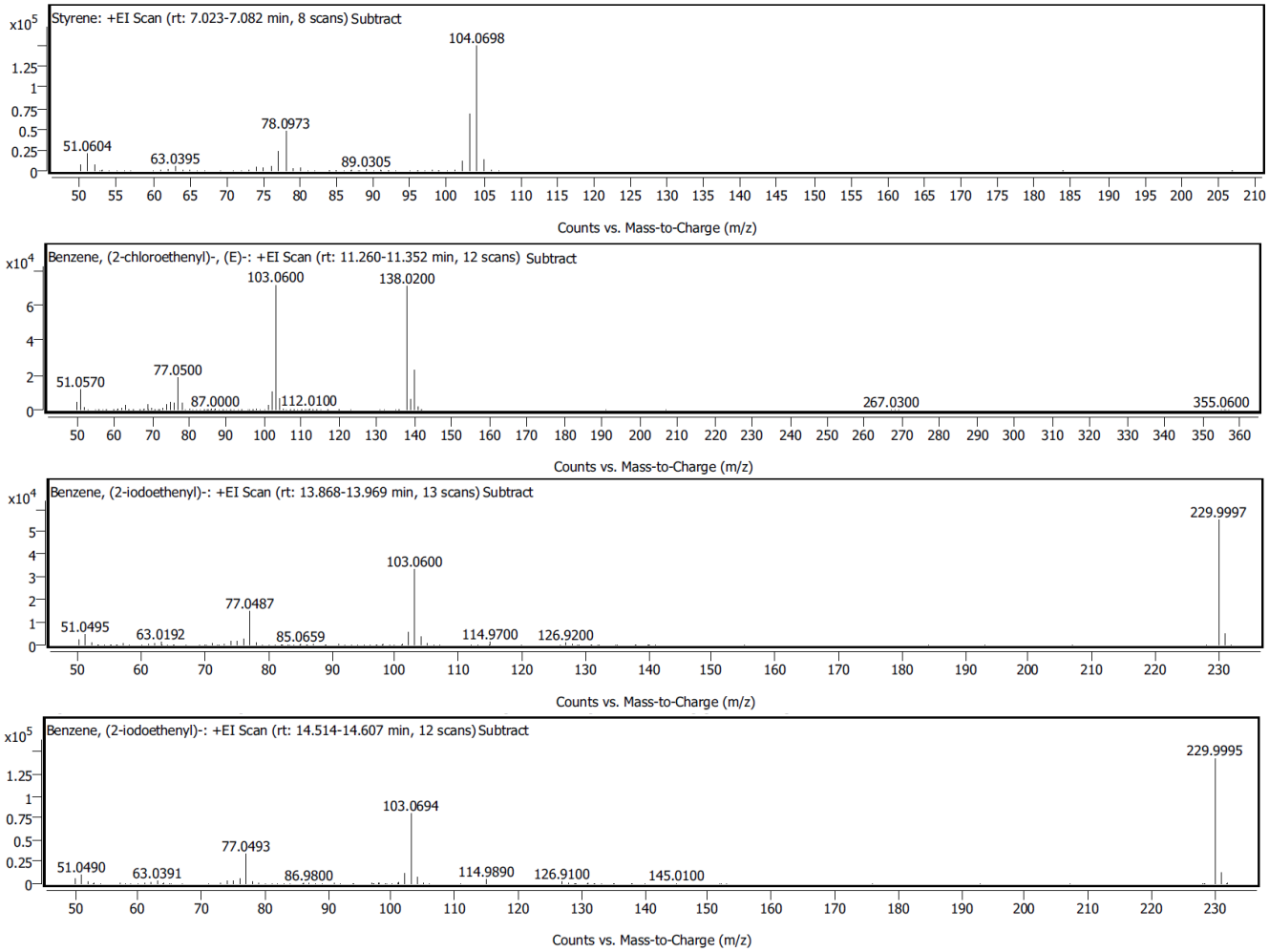

Figure S35. EI-mass spectra of the GC peaks of the filtered reaction mixture of **1** with 1 equivalent of benzaldehyde in THF-d_8 at ambient temperature for 6 d from 7.023 min to 14.607 min, evaluated by *Agilent* MassHunter.

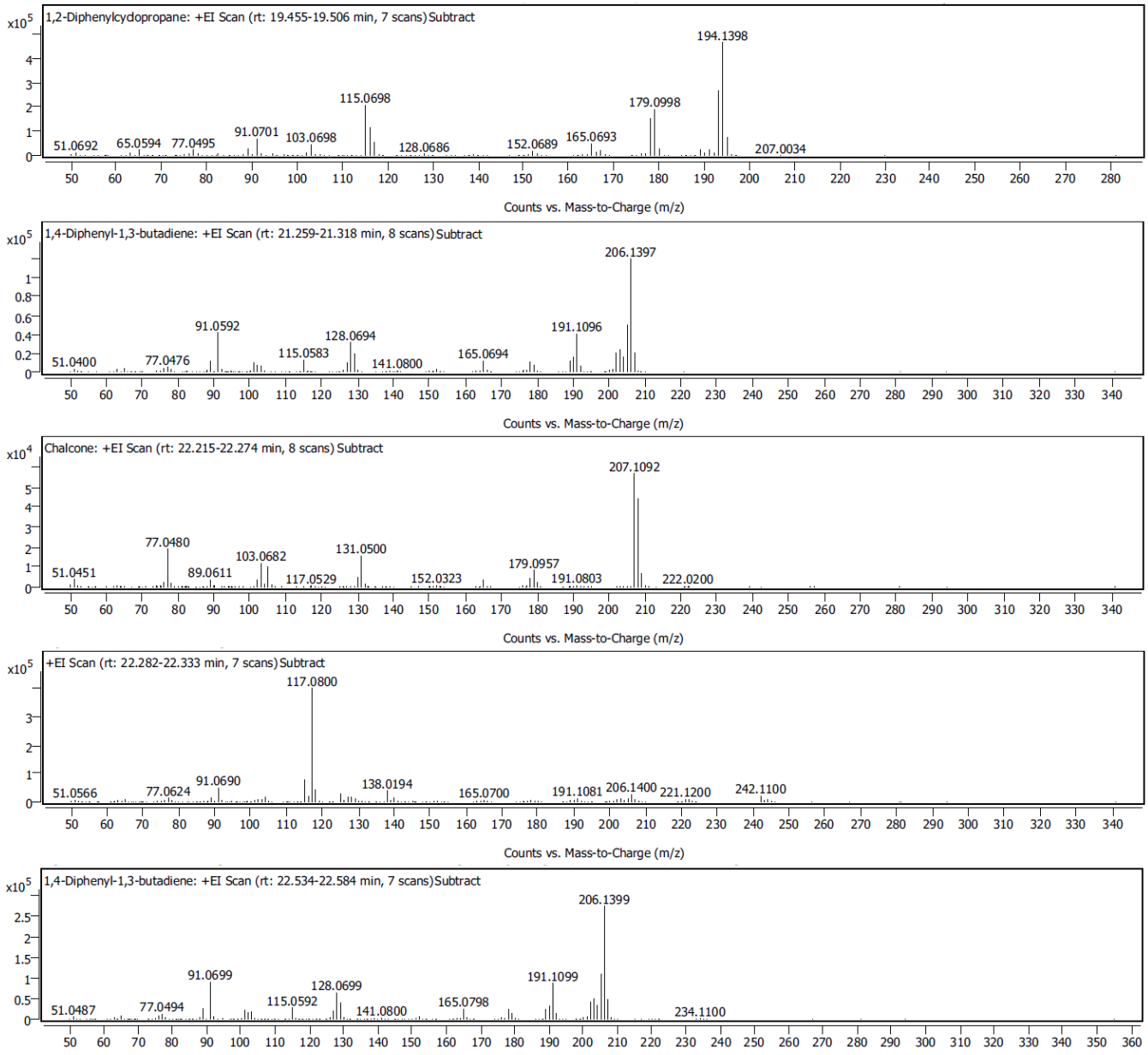

Figure S36. EI-mass spectra of the GC peaks of the filtered reaction mixture of **1** with 1 equivalent of benzaldehyde in $THFd_8$ at ambient temperature for 6 d from 19.455 min to 22.584 min, evaluated by *Agilent* MassHunter.

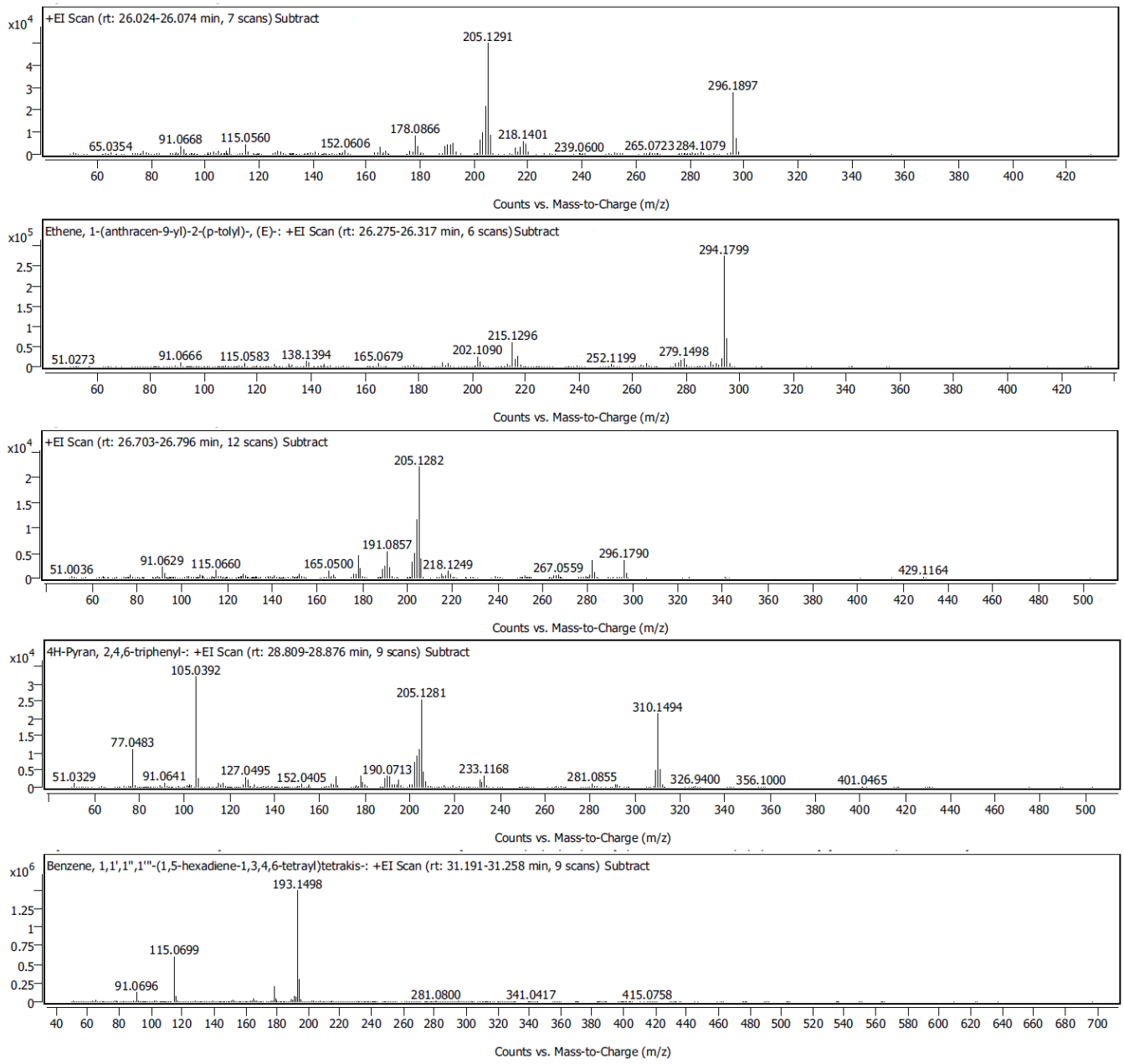

Figure S37. EI-mass spectra of the GC peaks of the filtered reaction mixture of **1** with 1 equivalent of benzaldehyde in THF-d_8 at ambient temperature for 6 d from 26.024 min to 31.258 min, evaluated by *Agilent* MassHunter.

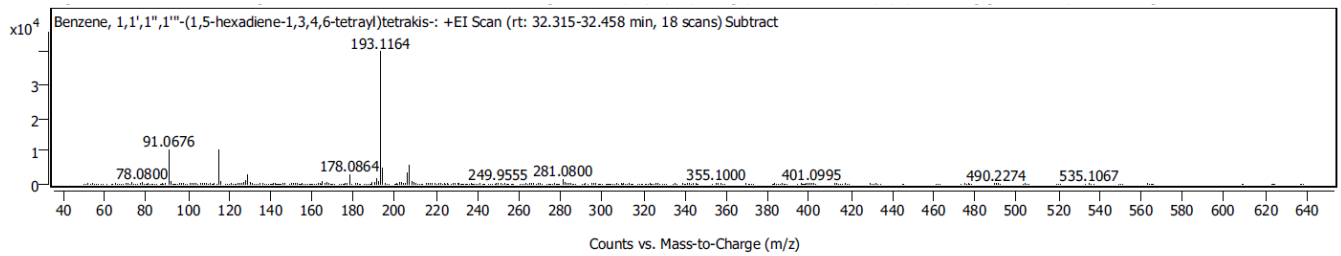

Figure S38. EI-mass spectra of the GC peaks of the filtered reaction mixture of **1** with 1 equivalent of benzaldehyde in THF-d_8 at ambient temperature for 6 d at 32.315-32.458 min, evaluated by *Agilent* MassHunter.

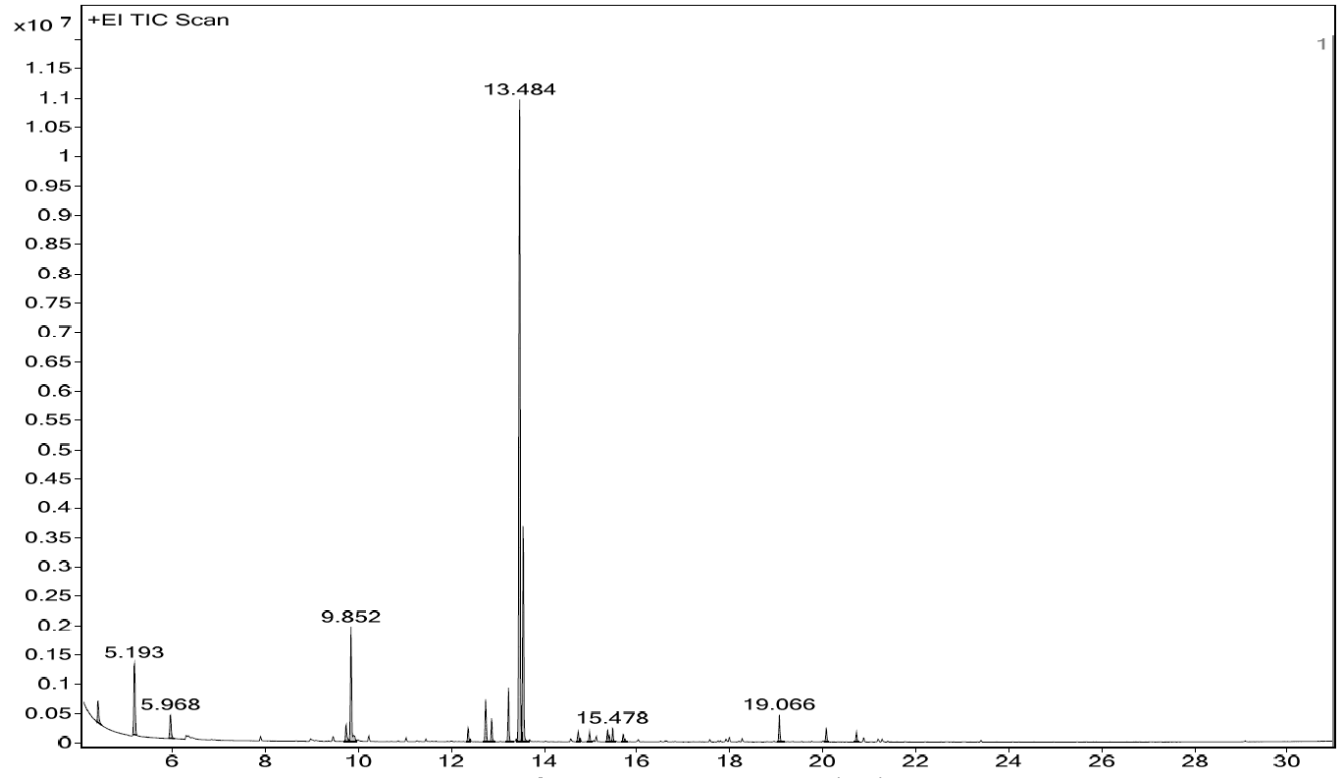

Figure S39. Gas chromatogram of the filtered reaction mixture of **1** with 1 equivalent of pivalaldehyde in THF-d_8 at ambient temperature for 3 d.

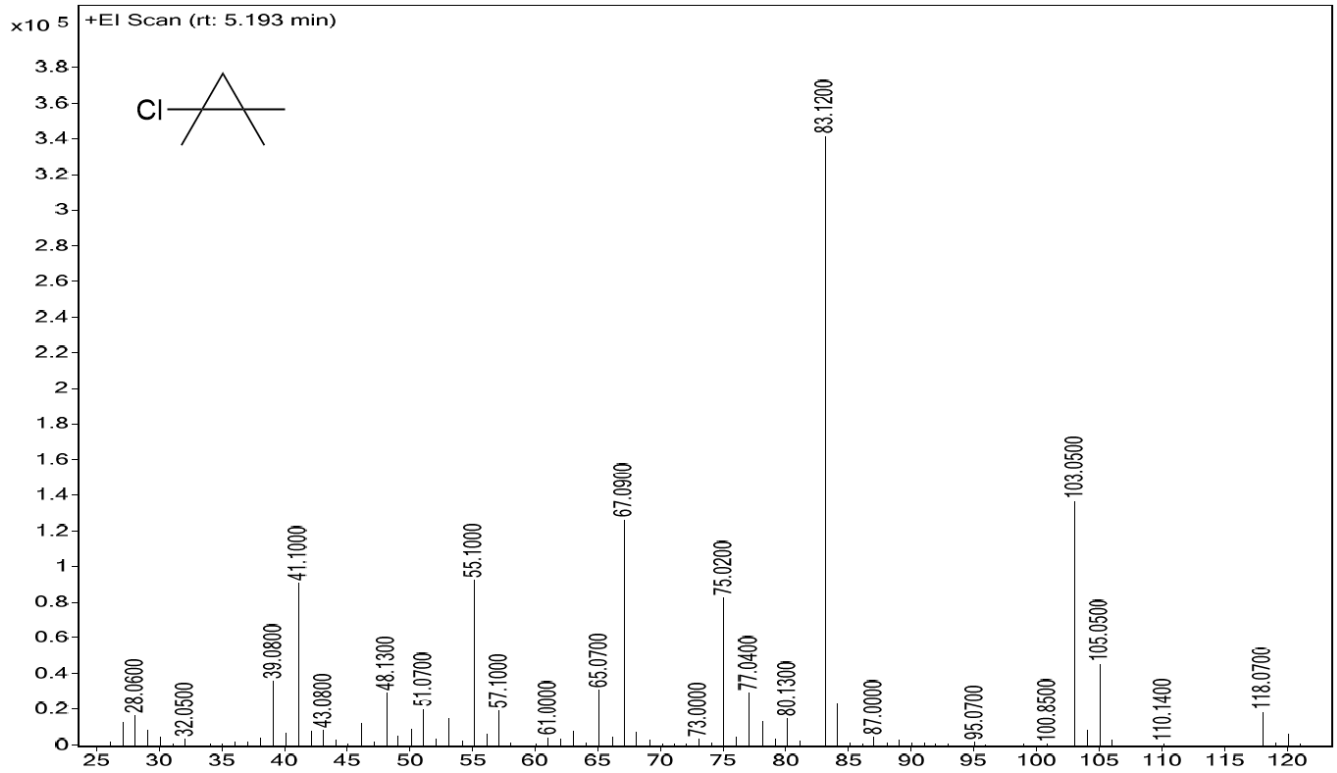

Figure S40. Mass spectrum (EI) of the GC peak of the filtered reaction mixture of **1** with 1 equivalent of pivalaldehyde in THF-d_8 at ambient temperature for 3 d at 5.193 min, suggested compound (mainlib), 1-chloro-1,2,2-trimethylcyclopropane.

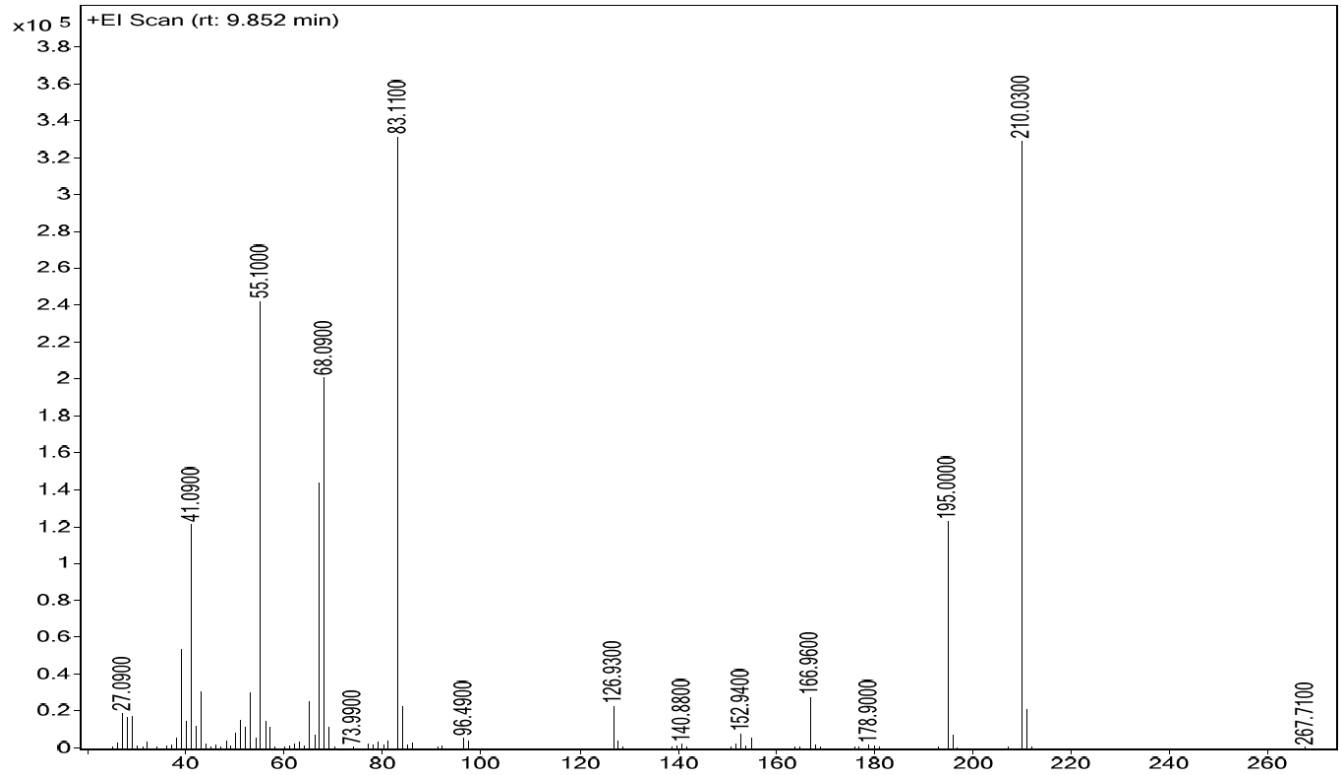

Figure S41. Mass spectrum (EI) of the GC peak of the filtered reaction mixture of **1** with 1 equivalent of pivalaldehyde in THF-d_8 at ambient temperature for 3 d at 9.852 min.

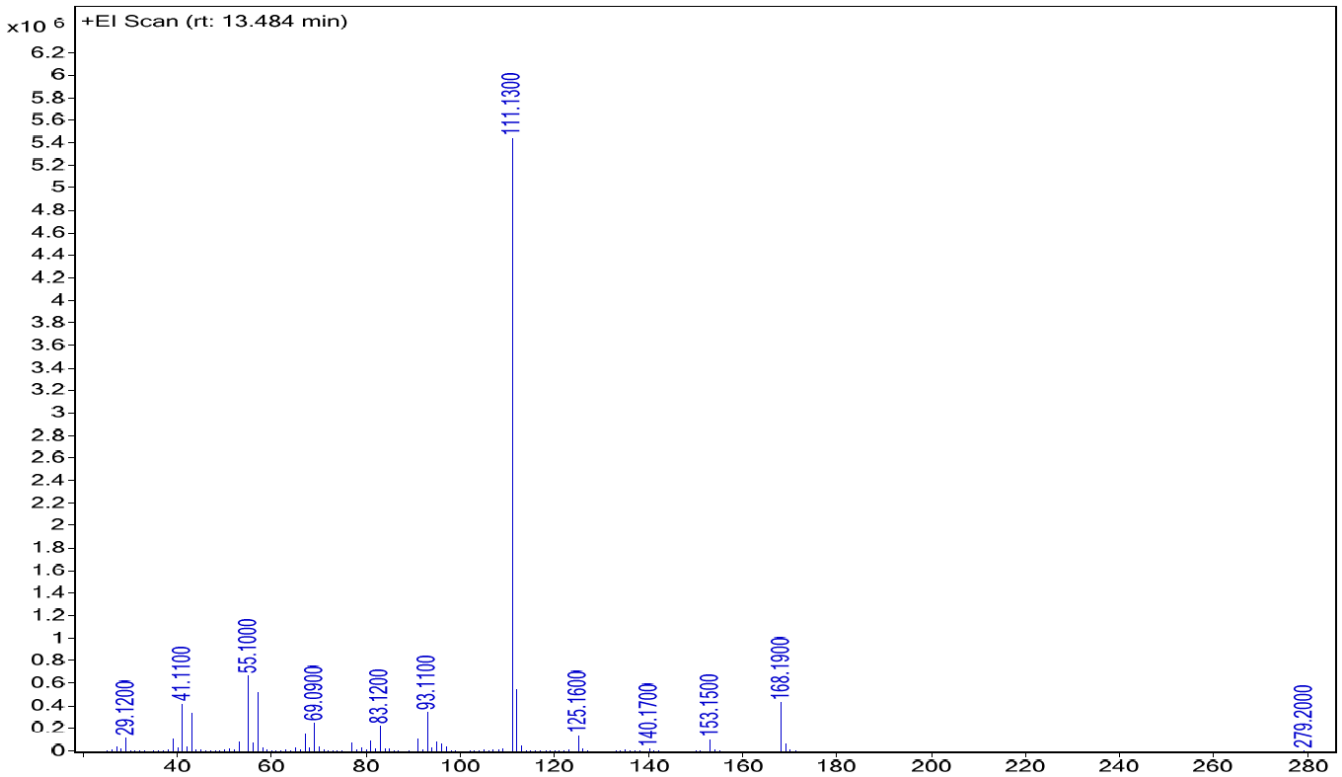

Figure S42. Mass spectrum (EI) of the GC peak of the filtered reaction mixture of **1** with 1 equivalent of pivalaldehyde in THF-d_8 at ambient temperature for 3 d at 13.484 min.

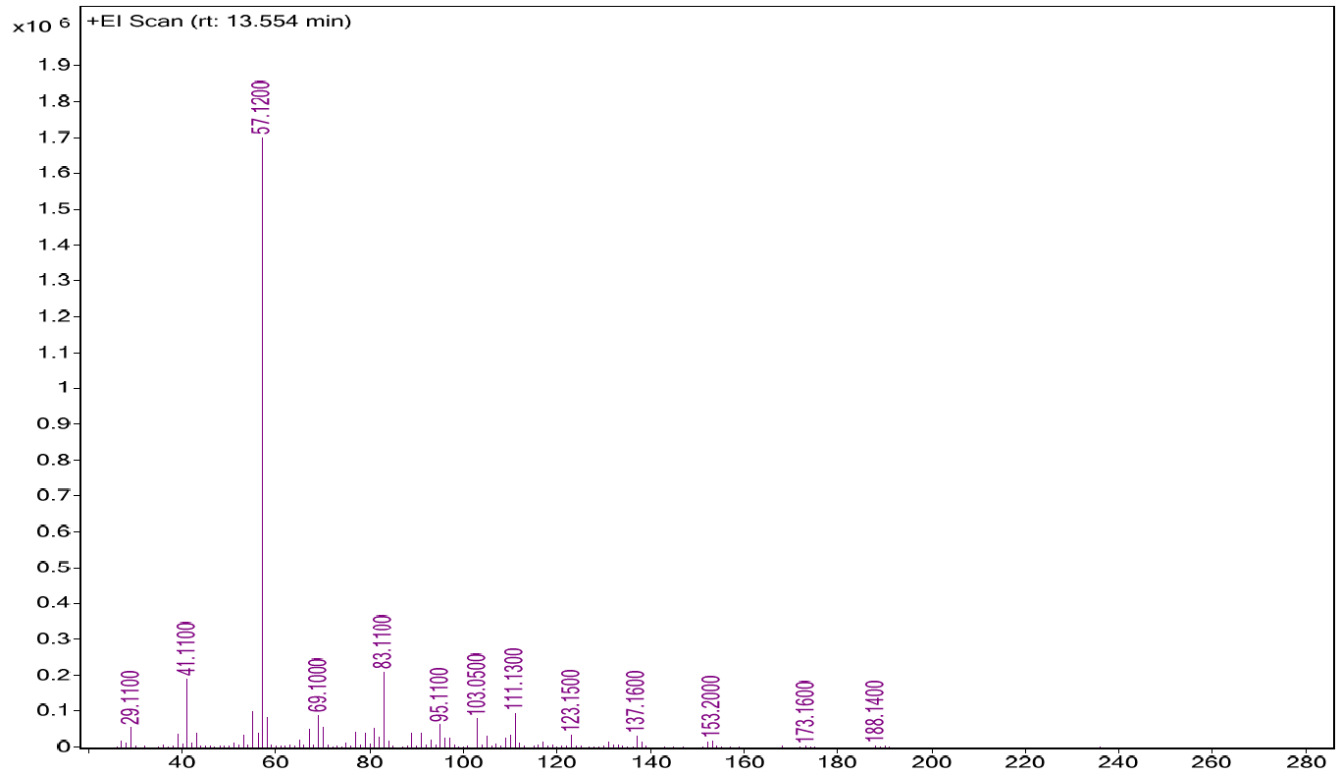

Figure S43. Mass spectrum (EI) of the GC peak of the filtered reaction mixture of **1** with 1 equivalent of pivalaldehyde in THF-d_8 at ambient temperature for 3 d at 13.554 min.

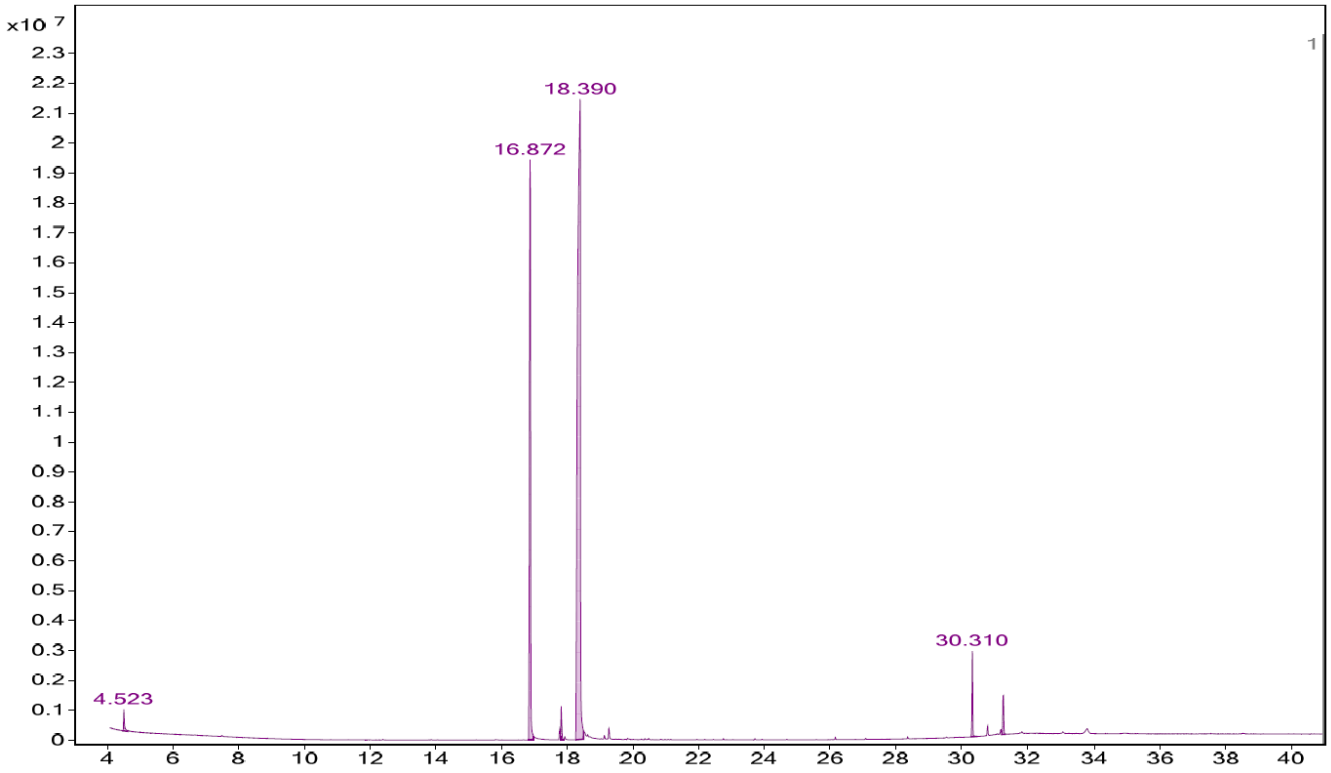

Figure S44. Gas chromatogram of the filtered reaction mixture of **1** with 1 equivalent of benzophenone in THF-d_8 at ambient temperature for 3 d.

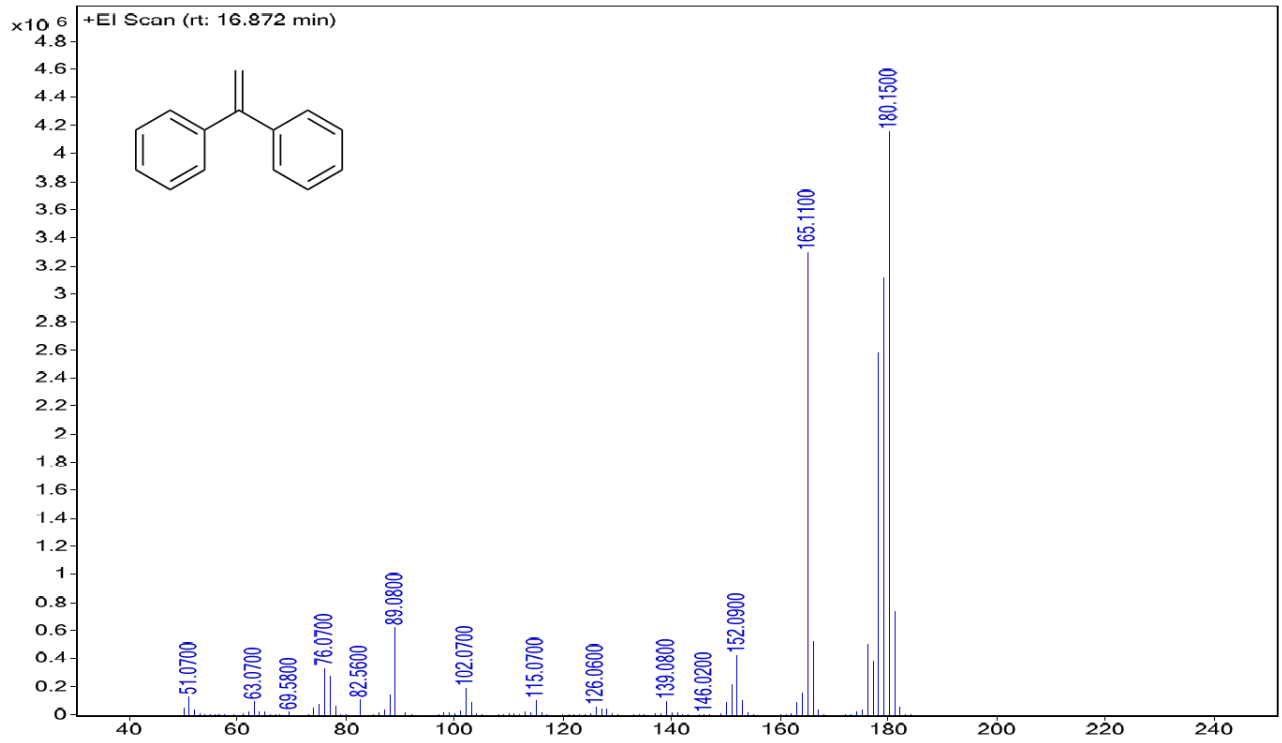

Figure S45. Mass spectrum of the GC peak of the filtered reaction mixture of **1** with 1 equivalent of benzophenone in THF-d_8 at ambient temperature for 3 d at 16.872 min, suggested compound (mainlib) 1,1-diphenylethylene.

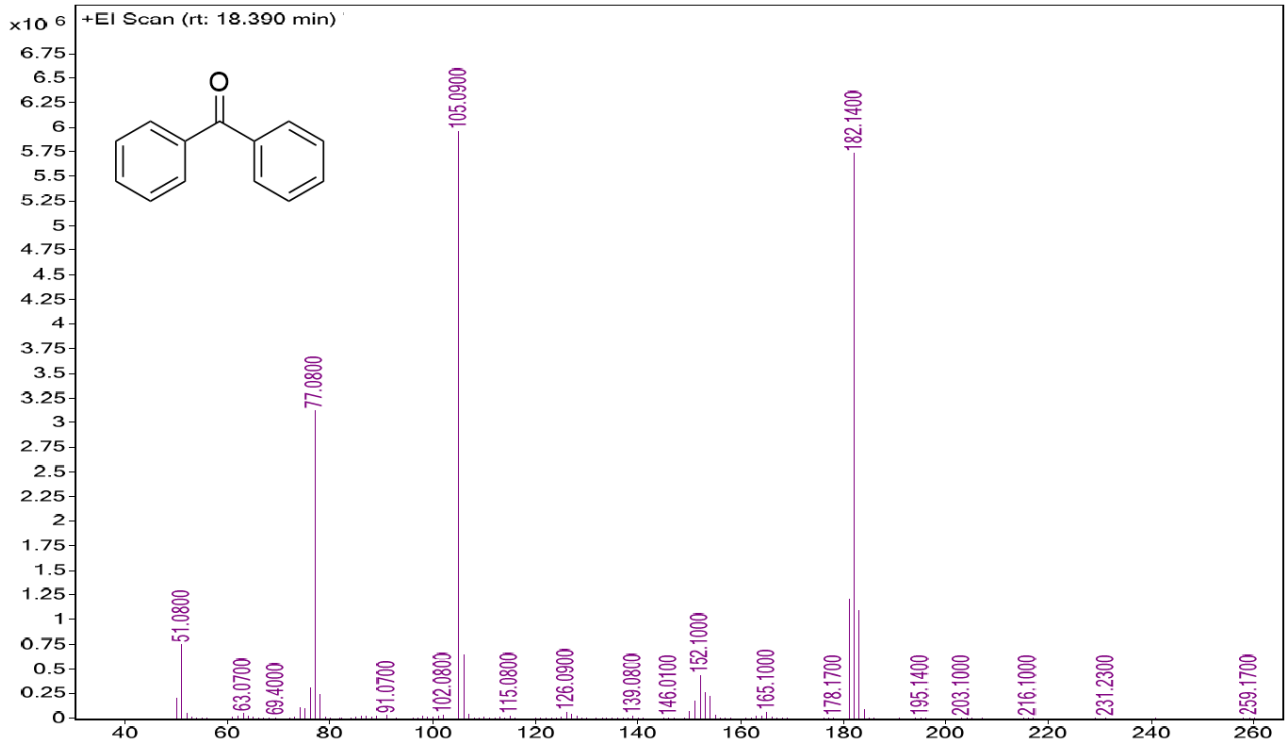

Figure S46. Mass spectrum of the GC peak of the filtered reaction mixture of **1** with 1 equivalent of benzophenone in THF-d_8 at ambient temperature for 3 d at 18.390 min, suggested compound (mainlib) benzophenone.

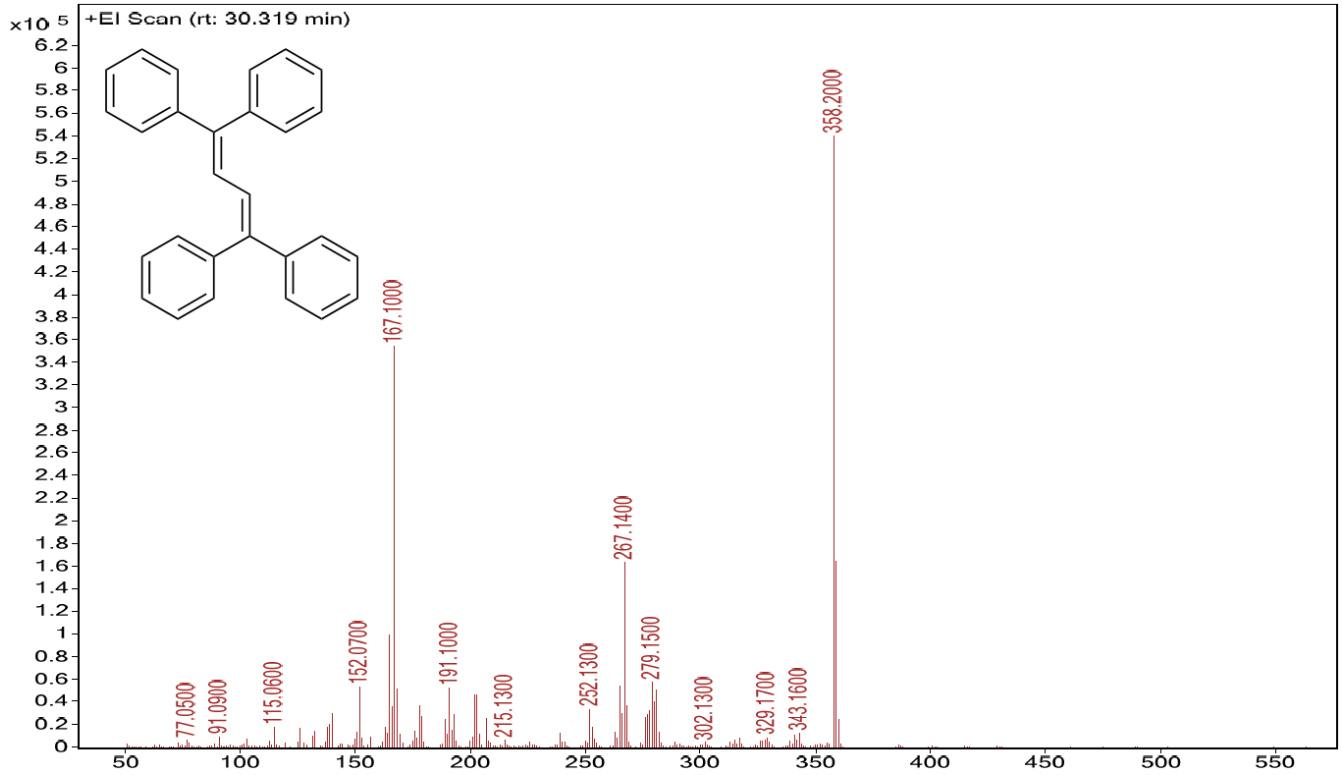

Figure S47. Mass spectrum of the GC peak of the filtered reaction mixture of (**1**) with 1 equivalent of benzophenone inTHF-d_8 at ambient temperature for 3 d at 30.319 min, suggested compound (mainlib) 1,1',1'',1'''-(1,3-butadiene-1,4-diylidene)tetrakis(benzene).

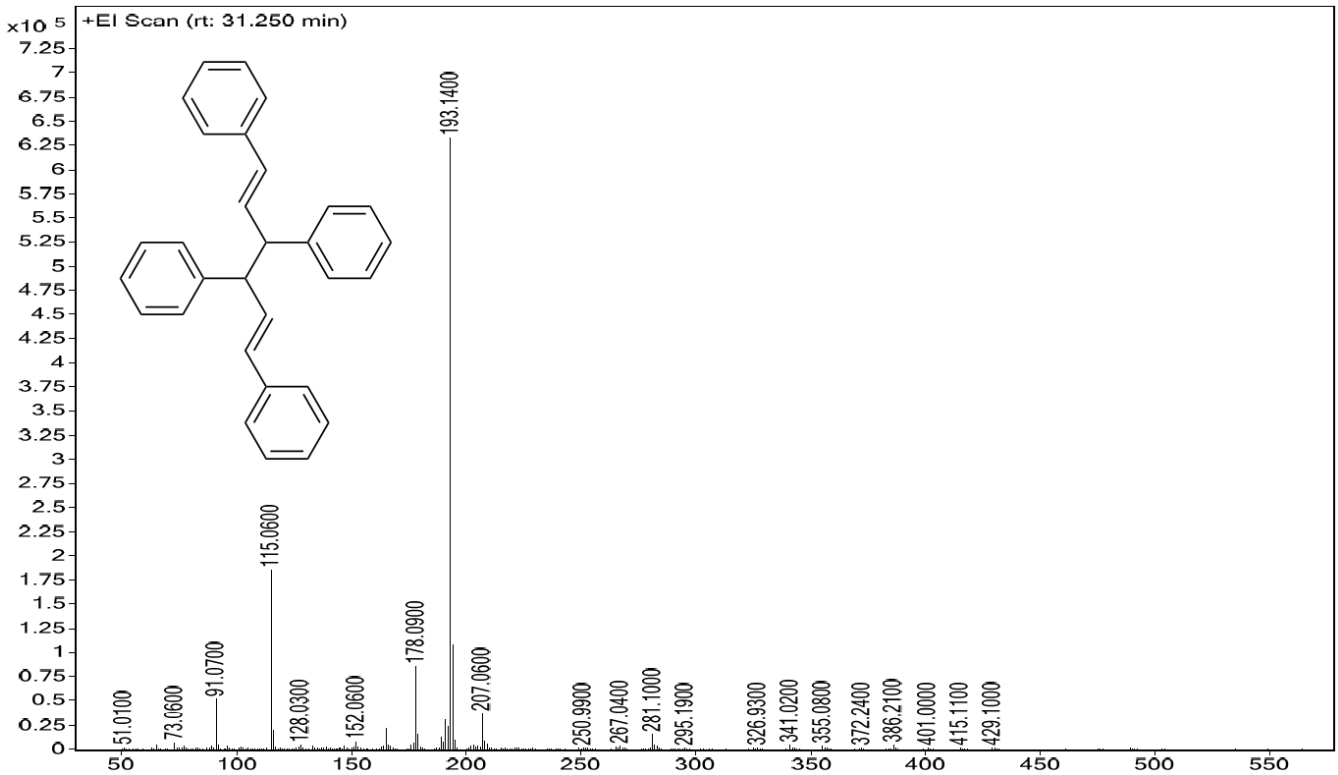

Figure S48. Mass spectrum of the GC peak of the filtered reaction mixture of (**1**) with 1 equivalent of benzophenone in THF-d_8 at ambient temperature for 3 d at 31.250 min, suggested compound (mainlib) 1,1'1'',1'''-(1,5-hexadiene-1,3,4,6-tetrayl)tetrakis(benzene).

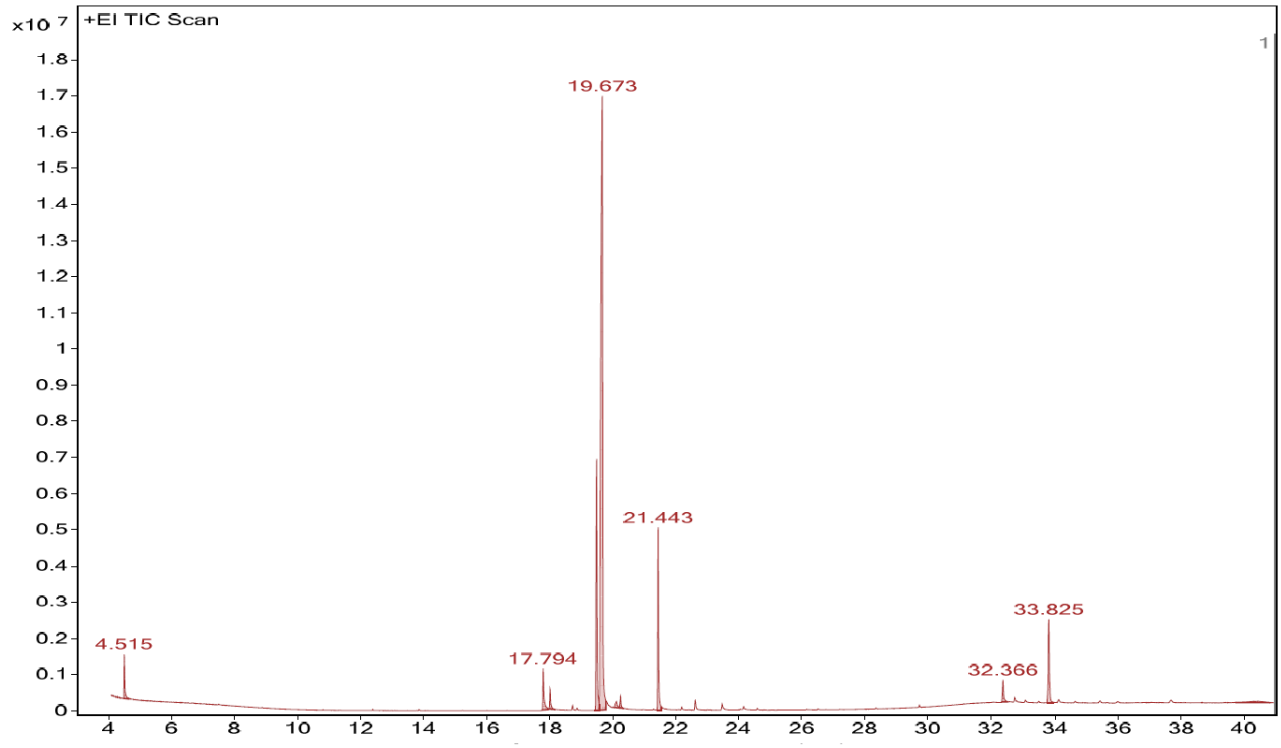

Figure S49. Gas chromatogram of the filtered reaction mixture of **1** with 1 equivalent of 9-fluorenone in THF-d_8 at ambient temperature for 3 d.

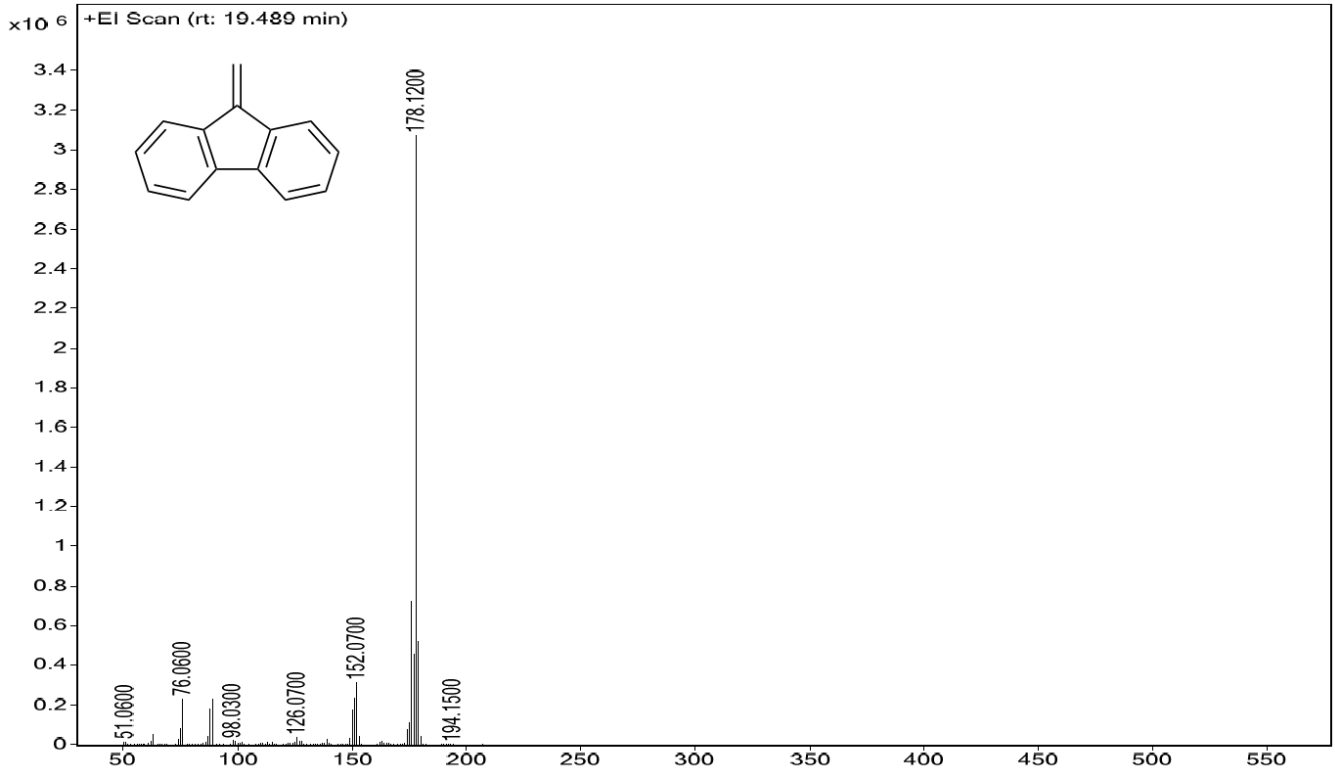

Figure S50. Mass spectrum (EI) of the GC peak of the filtered reaction mixture of **1** with 1 equivalent of 9-fluorenone in THF-d_8 at ambient temperature for 3 d at 19.489 min, suggested compound (mainlib) 9-methylene-9H-fluorene.

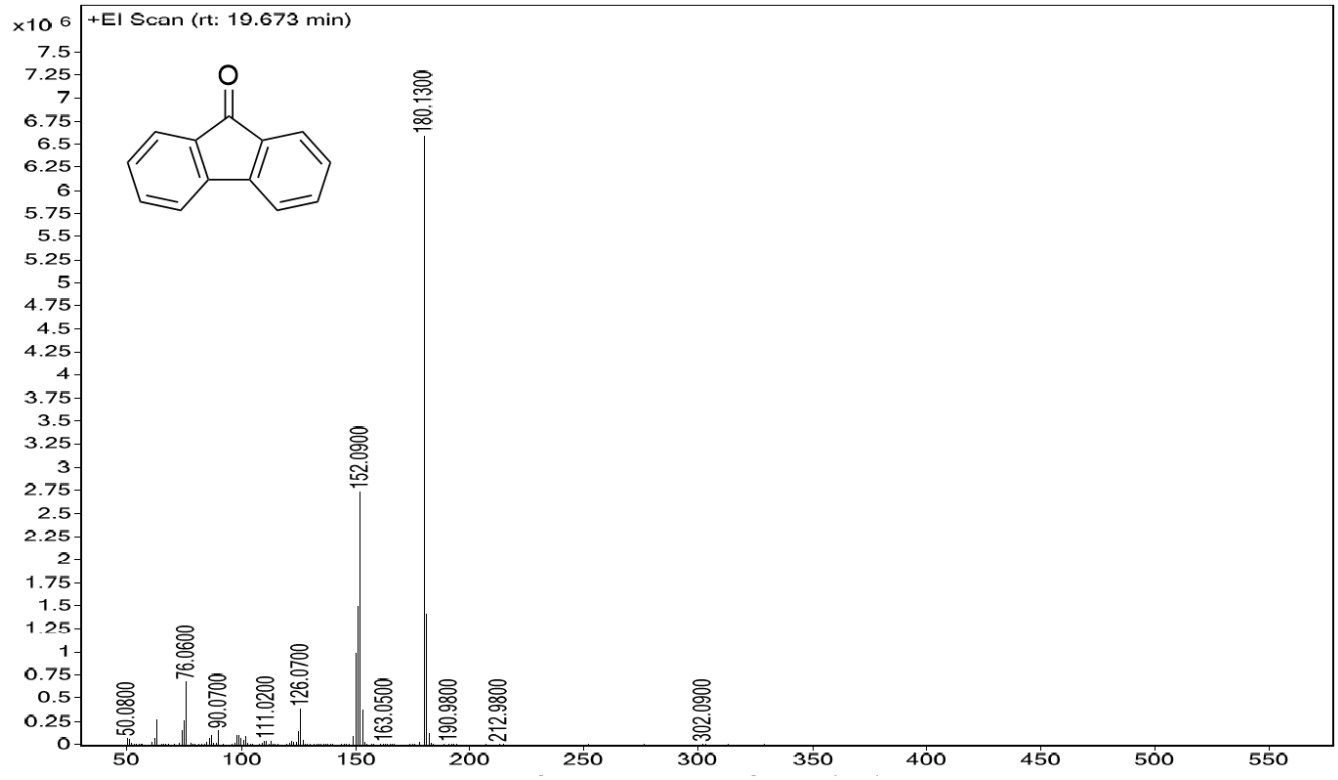

Figure S51. Mass spectrum (EI) of the GC peak of the filtered reaction mixture of **1** with 1 equivalent of 9-fluorenone in THF-d_8 at ambient temperature for 3 d at 19.673 min, suggested compound (mainlib) 9H-fluoren-9-one.

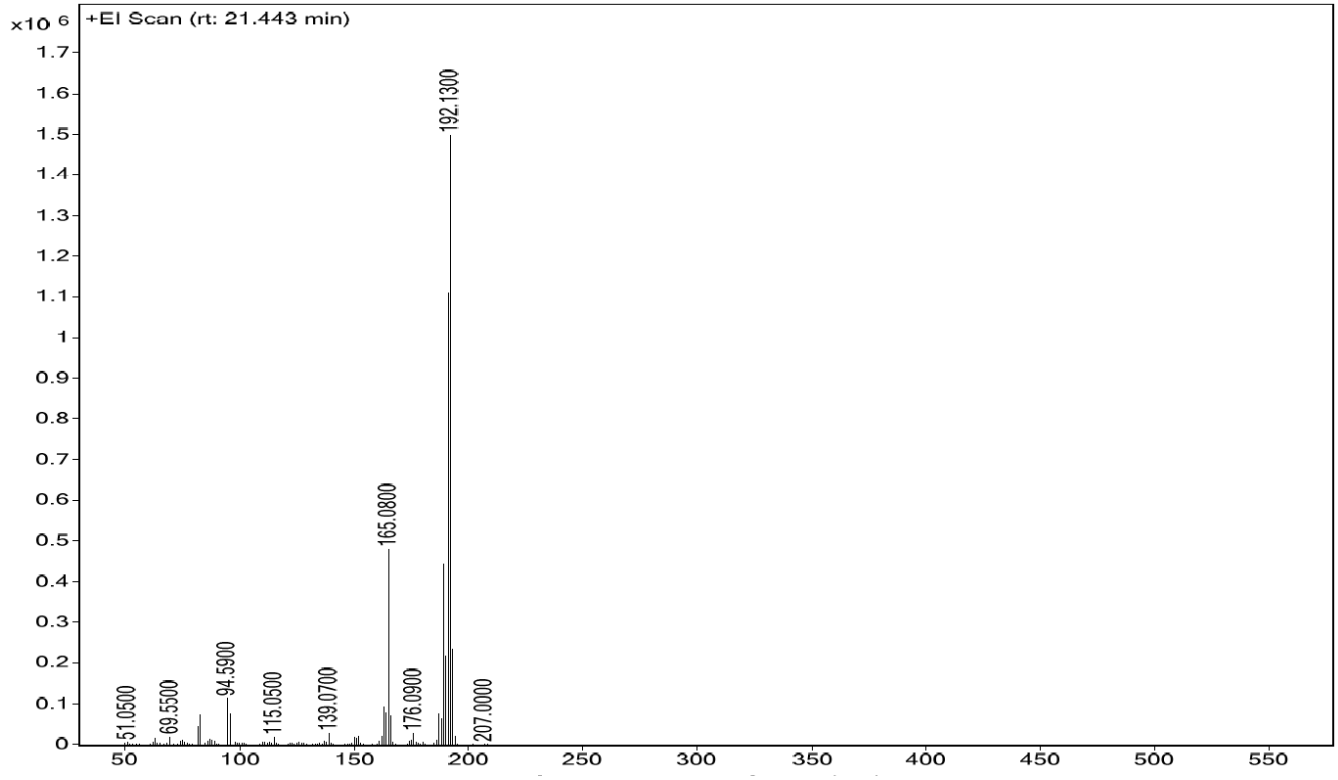

Figure S52. Mass spectrum (EI) of the GC peak of the filtered reaction mixture of **1** with 1 equivalent of 9-fluorenone in THF-d_8 at ambient temperature for 3 d at 21.443 min.

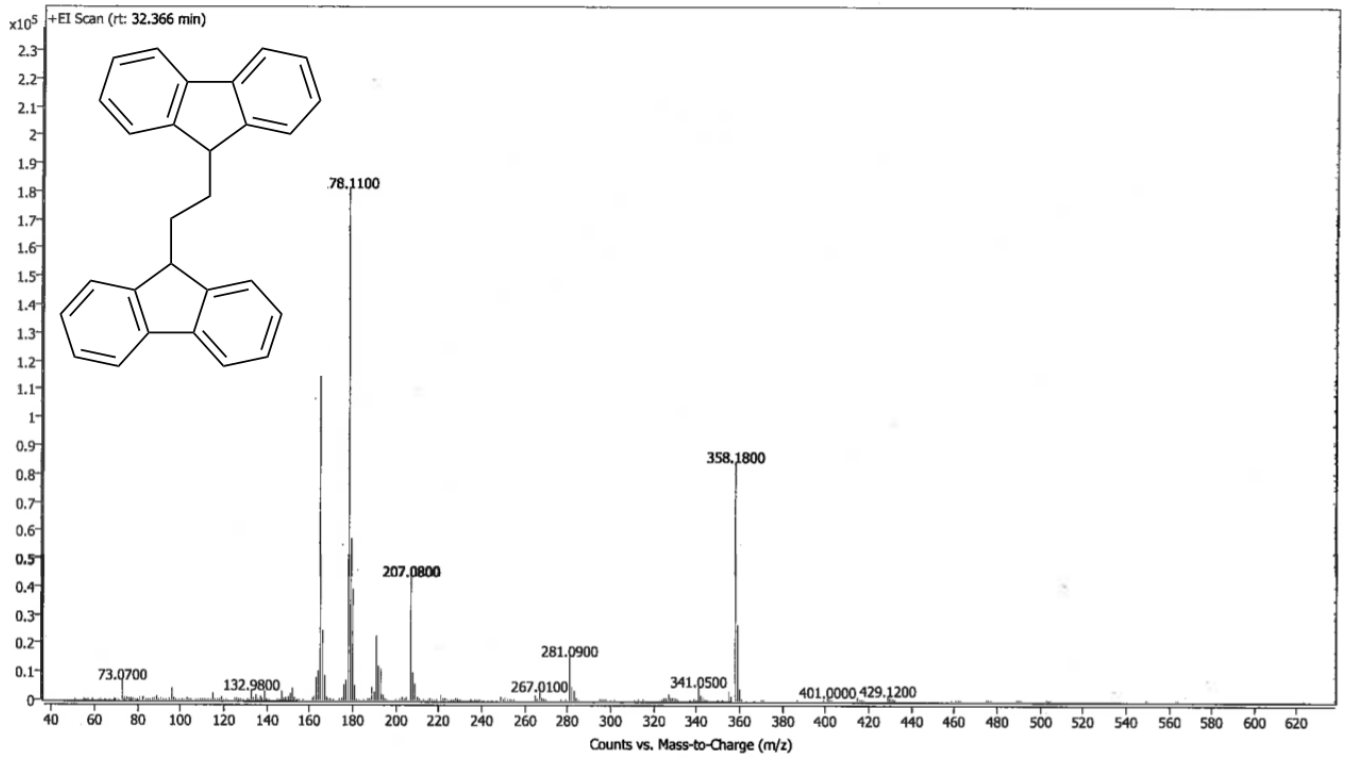

Figure S53. Mass spectrum (EI) of the GC peak of the filtered reaction mixture of **1** with 1 equivalent of 9-fluorenone in THF-d_8 at ambient temperature for 3 d at 32.366 min, suggested compound (mainlib) 1,2-di(9-fluorenyl)ethane.

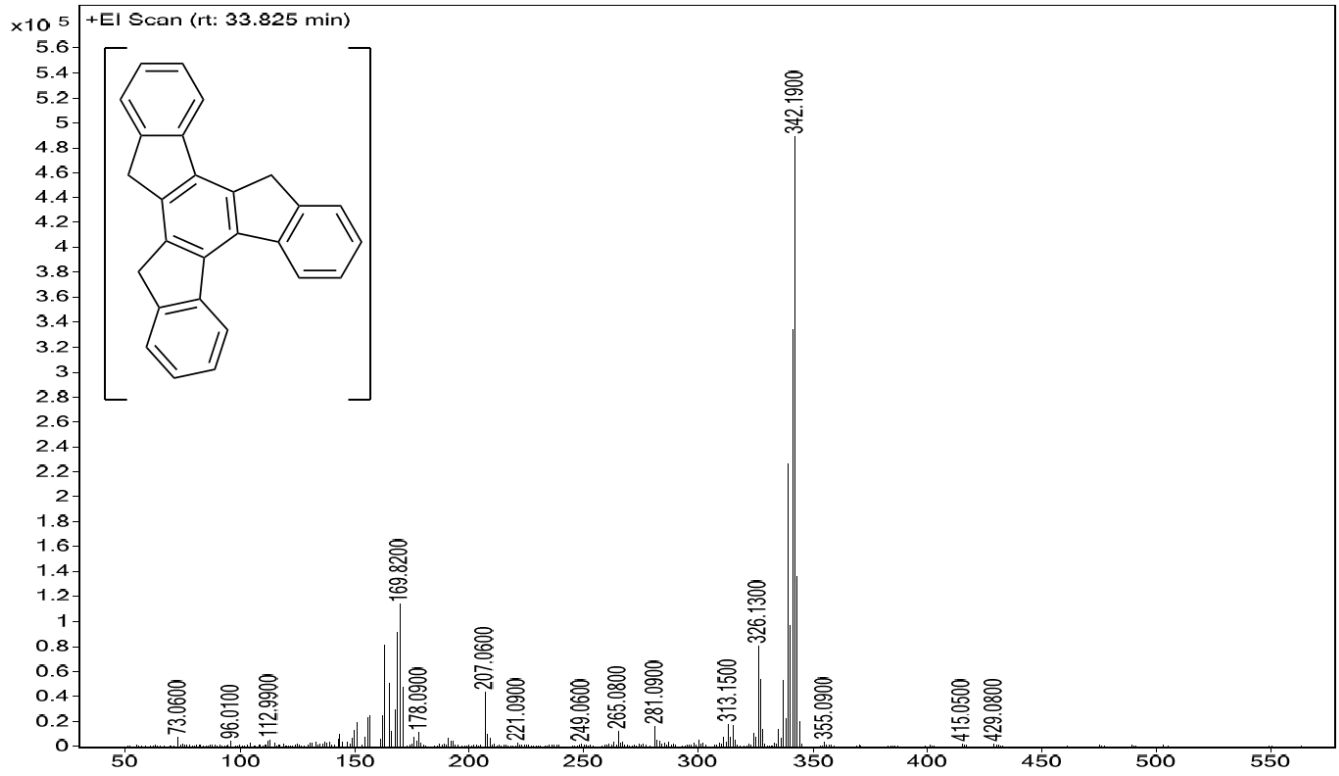

Figure S54. Mass spectrum (EI) of the GC peak of the filtered reaction mixture of **1** with 1 equivalent of 9-fluorenone in THF-d_8 at ambient temperature for 3 d at 33.825 min, suggested compound (mainlib) 3H,3'H,3''H-trisindeno[1,2-a:2',1'-c:1'',2''-e]benzene.

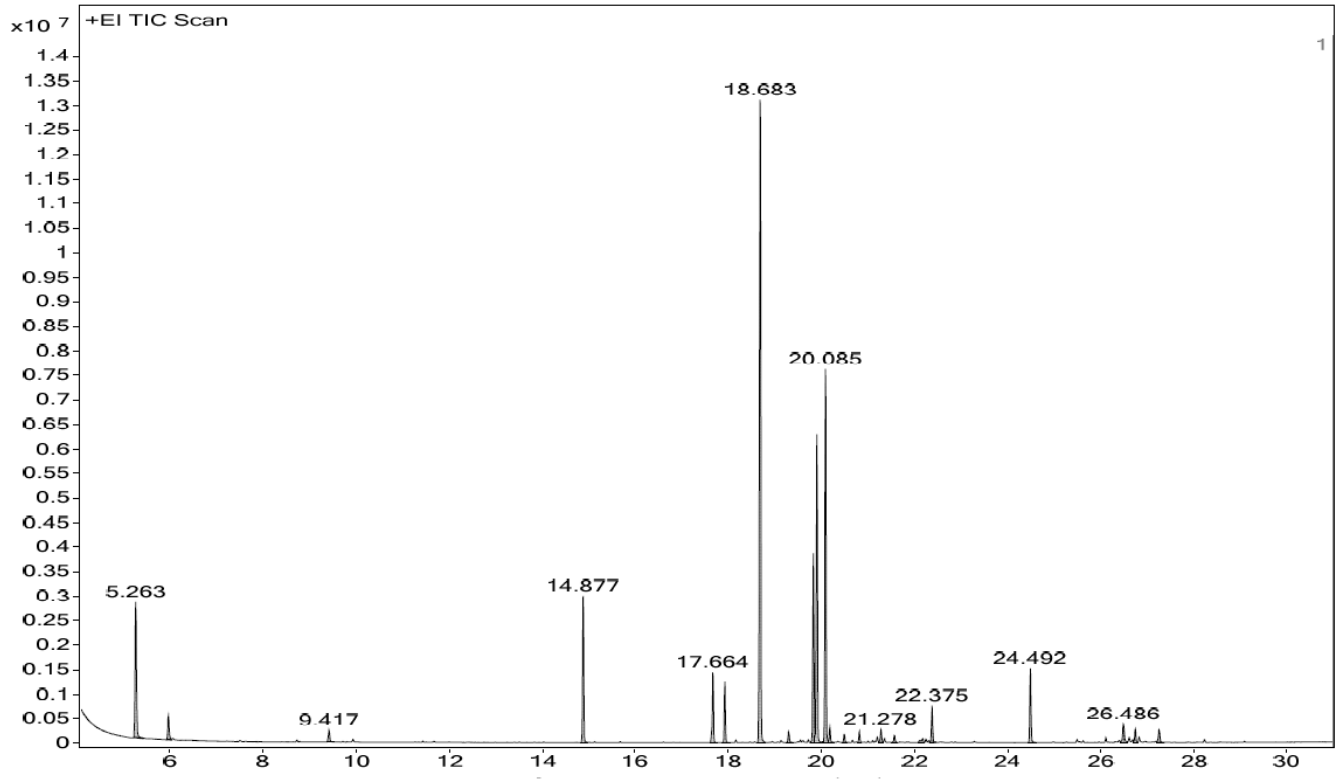

Figure S55. Gas chromatogram of the reaction of **1** with 1 equivalent of cyclohexanone in THF-d_8 at ambient temperature for 3 d.

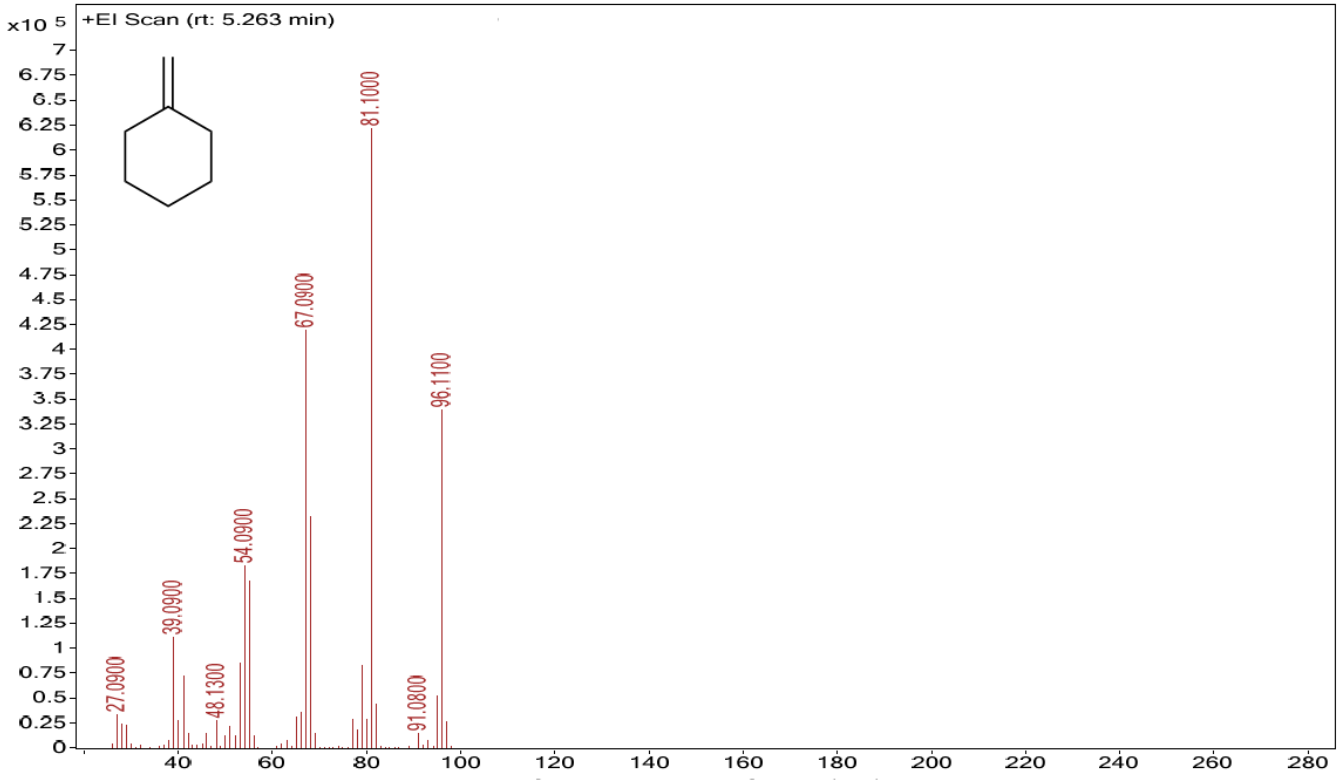

Figure S56. Mass spectrum (EI) of the GC peak of the reaction of **1** with 1 equivalent of cyclohexanone in THF-d_8 at ambient temperature for 3 d at 5.263 min, suggested compound (mainlib) methylene-cyclohexane.

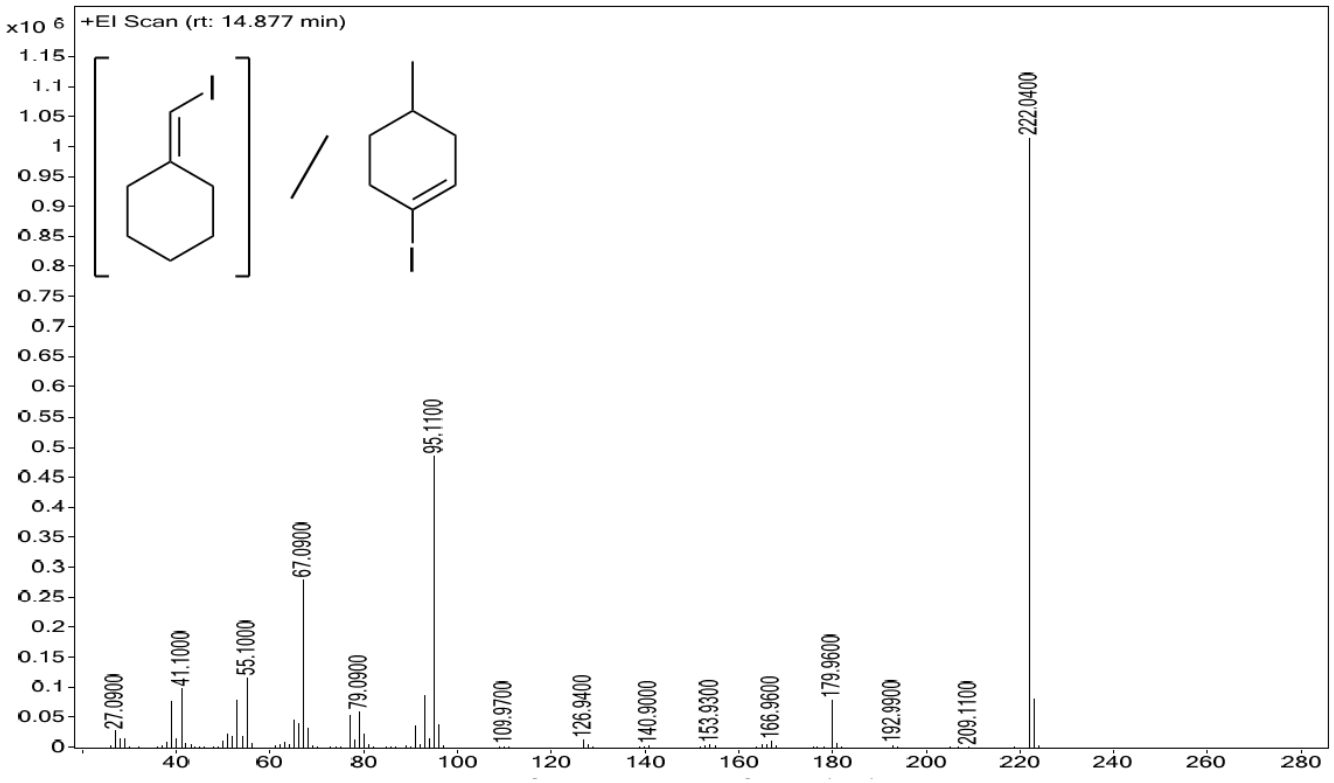

Figure S57. Mass spectrum (EI) of the GC peak of teh reaction of **1** with 1 equivalent of cyclohexanone in THF-d_8 at ambient temperature for 3 d at 14.877 min, suggested compound Iodomethylene-cyclohexane / (mainlib) 1-iodo-4-methyl-cyclohex-1-ene.

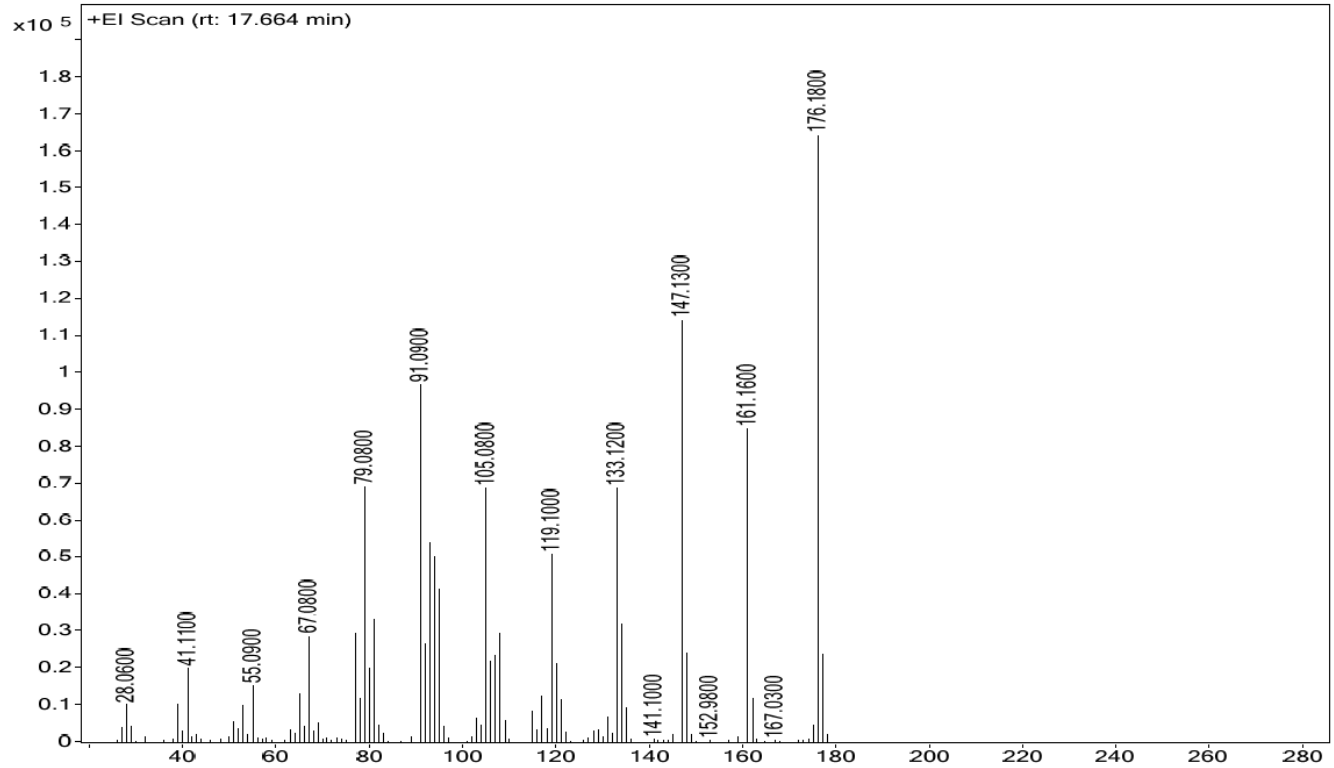

Figure S58. Mass spectrum (EI) of the GC peak of the reaction of **1** with 1 equivalent of cyclohexanone in THF-d_8 at ambient temperature for 3 d at 17.664 min.

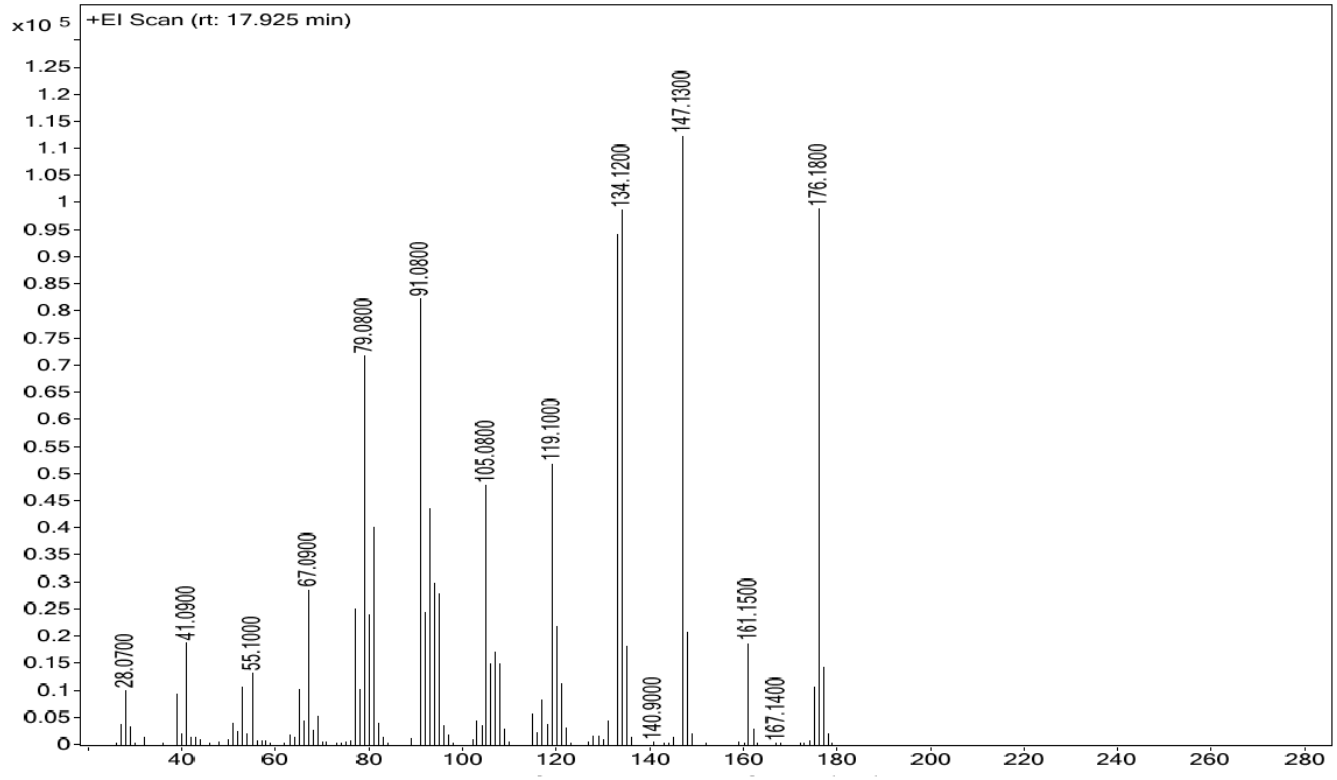

Figure S59. Mass spectrum (EI) of the GC peak of the reaction of **1** with 1 equivalent of cyclohexanone in THF-d_8 at ambient temperature for 3 d at 17.925 min.

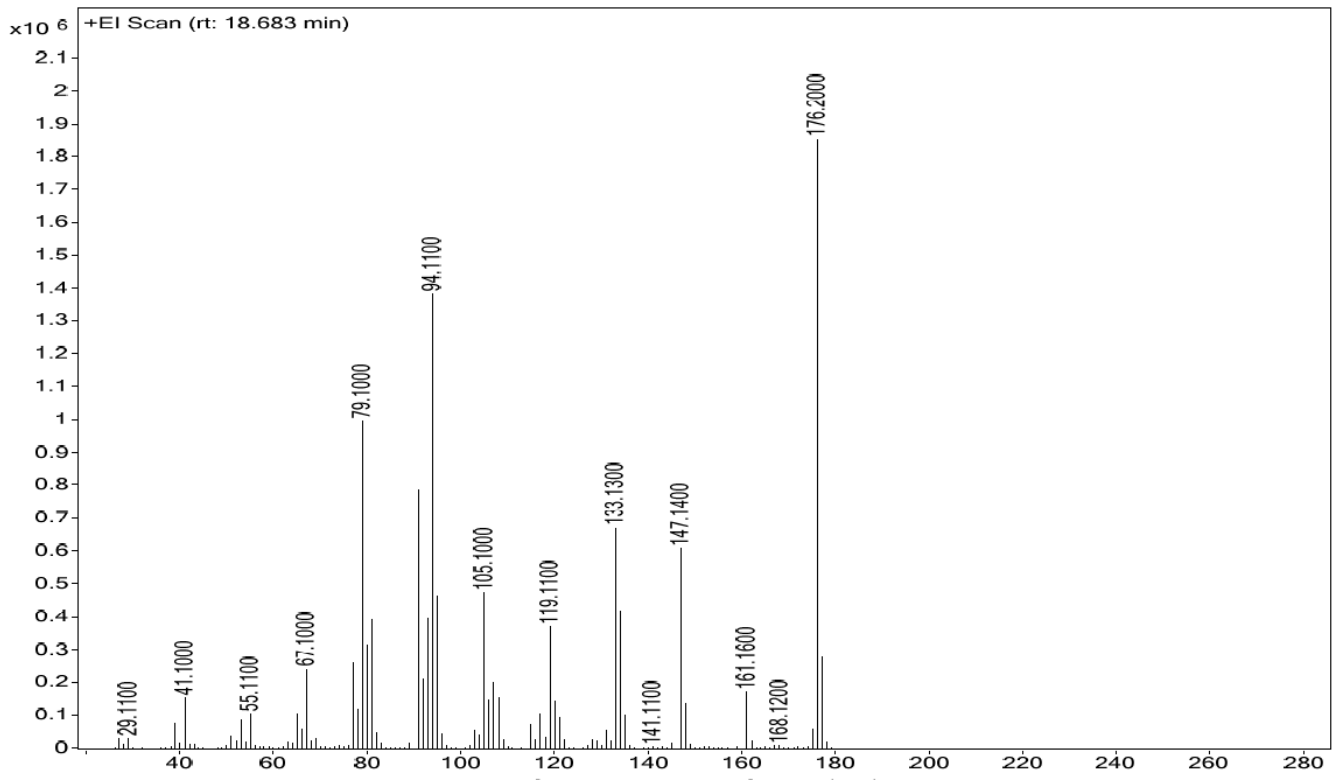

Figure S60. Mass spectrum (EI) of the GC peak of the reaction of **1** with 1 equivalent of cyclohexanone in THF-d_8 at ambient temperature for 3 d at 18.683 min.

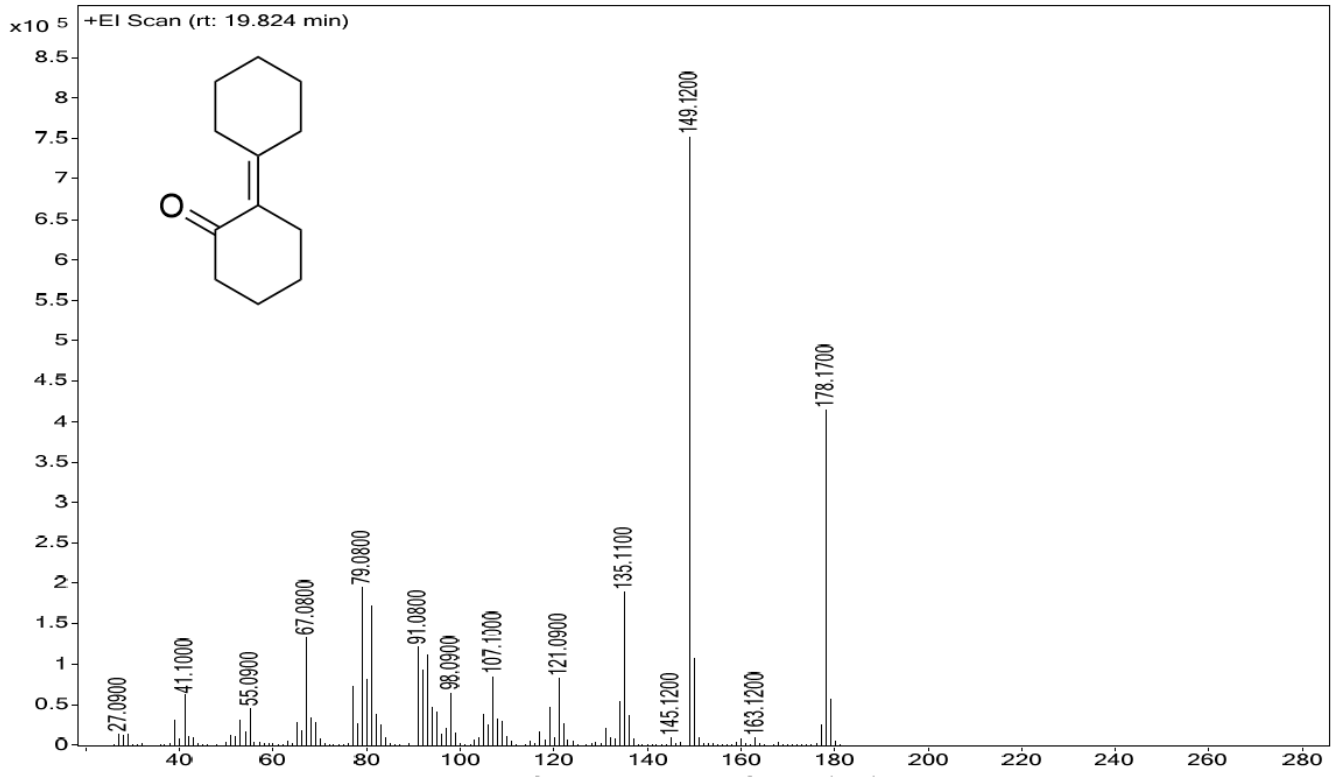

Figure S61. Mass spectrum (EI) of the GC peak of the reaction of **1** with 1 equivalent of cyclohexanone in THF-d_8 at ambient temperature for 3 d at 19.824 min, suggested compound (mainlib) 2-cyclohexylidene-cyclohexanone.

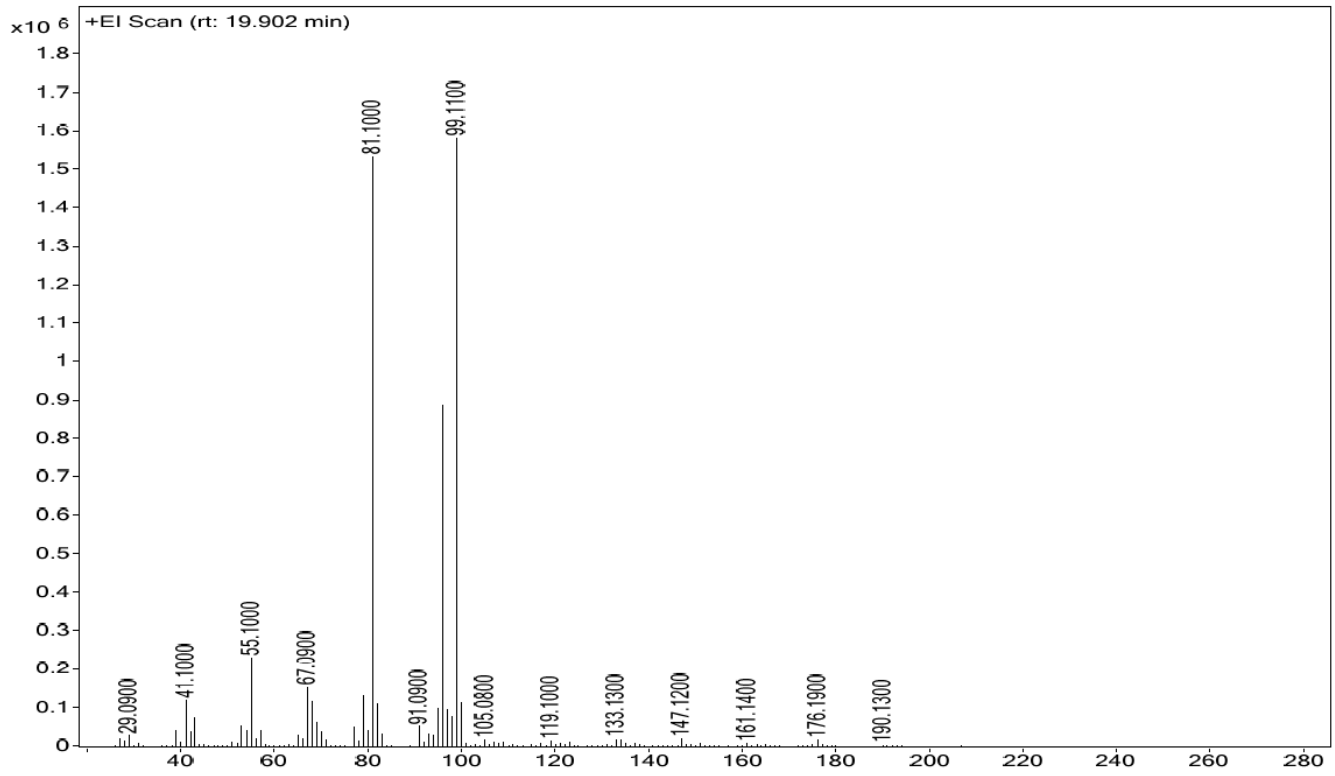

Figure S62. Mass spectrum (EI) of the GC peak of the reaction of **1** with 1 equivalent of cyclohexanone in THF-d_8 at ambient temperature for 3 d at 19.902 min.

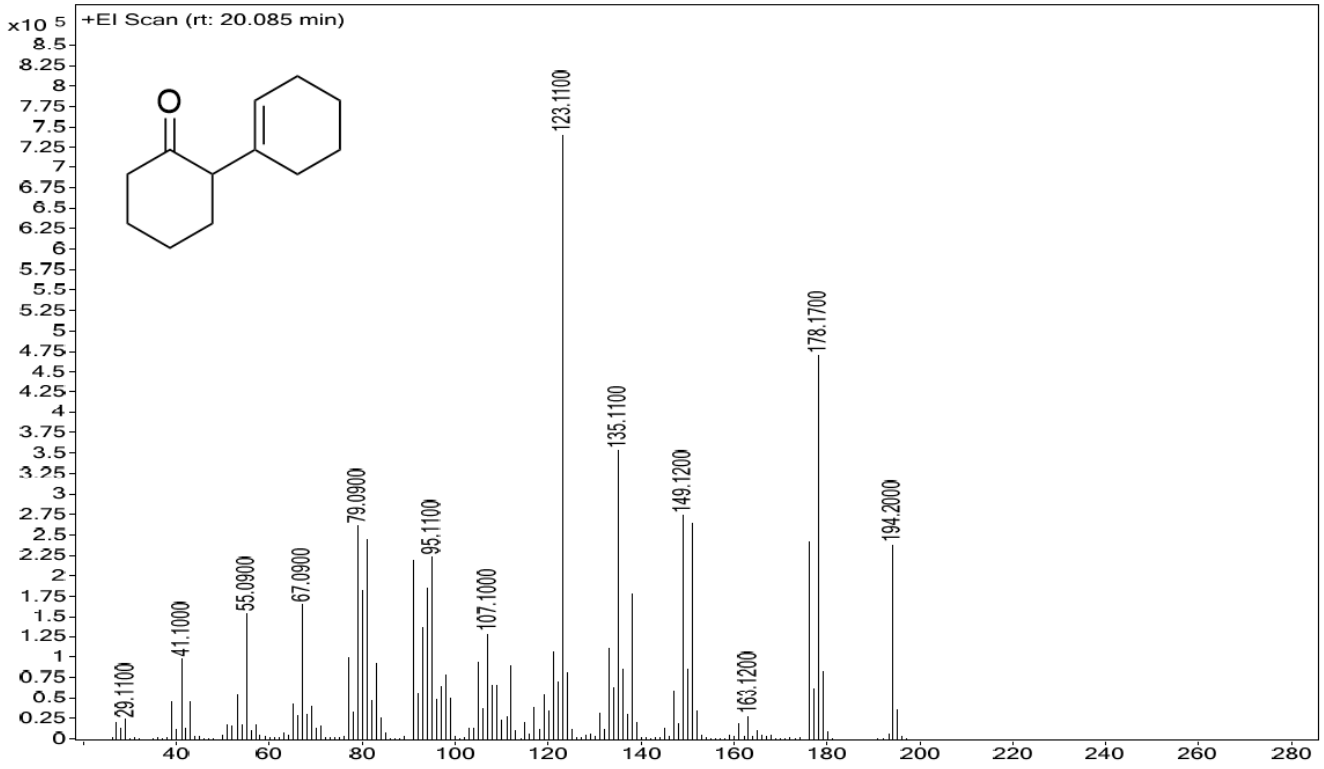

Figure S63. Mass spectrum (EI) of the GC peak of the reaction of **1** with 1 equivalent of cyclohexanone in THF-d_8 at ambient temperature for 3 d at 20.085 min, suggested compound (mainlib) 2-(1-cyclohexen-1-yl)-cyclohexanone.

Figure S64. Mass spectrum (EI) of the GC peak of the reaction of **1** with 1 equivalent of cyclohexanone in THF-d_8 at ambient temperature for 3 d Peak at 24.492 min.

References

[1] R. A. Heintz, R. L. Ostrander, A. L. Rheingold, K. H. Theopold, *J. Am. Chem. Soc.* **1994**, *116*, 11387-11396.

[2] G. R. Fulmer, A. J. M. Miller, N. H. Sherden, H. E. Gottlieb, A. Nudelman, B. M. Stoltz, J. E. Bercaw, K. I. Goldberg, *Organometallics* **2010**, *29*, 2176–2179.

[3] a) D. F. Evans *J. Chem. Soc.*, **1959**, 2003-2005; b) E. M. Schubert *J. Chem. Educ.*, **1992**, *69*, 62.

[4] Agilent MassHunter WorkStation - Qualitative Analysis for GC/MS (RRID:SCR_016657).

[5] P. Linstrom, *NIST Chemistry WebBook, NIST Standard Reference Database 69*, National Institute of Standards and Technology, **1997**.

[6] COSMO, v. 1.61; Bruker AXS Inc., Madison, WI, 2012.

[7] APEX 3, v. 2016.5-0; Bruker AXS Inc., Madison, WI, 2012.

[8] SAINT, v. 8.34A; Bruker AXS Inc., Madison, WI, 2010.

[9] L. Krause, R. Herbst-Irmer, G. M. Sheldrick, D. Stalke*, J. Appl. Cryst.* **2015**, *48*, 3-10.

[10] G. M. Sheldrick, *(2009), TWINABS,* University of Göttingen, Germany.

[11] G. M. Sheldrick, *Acta Crystallogr.*, Sect. A **2015**, *71*, 3-8.

[12] C. B. Hübschle, G. M. Sheldrick, B. J. Dittrich, *J. Appl. Cryst.* **2011**, *44*, 1281-1284.

[13] D. Kratzert, J. J. Holstein, I. Krossing, DSR: enhanced modelling and refinement of disordered structures with SHELXL. *J. Appl. Cryst.* **2015**, *48*, 933-938.

[14] C. F. Macrae, I. J. Bruno, J. A. Chisholm, P. R. Edgington, P. McCabe, E. Pidcock, L. RodriguezMonge, R. Taylor, J. van de Streek, P. A. Wood, *J. Appl. Cryst.* **2008**, *41*, 466-470.

[15] G. A. Bain, J. F. Berry, *J. Chem. Educ.* **2008**, *85*, 532-536.

Paper II

Chromous siloxides of variable nuclearity and magnetism

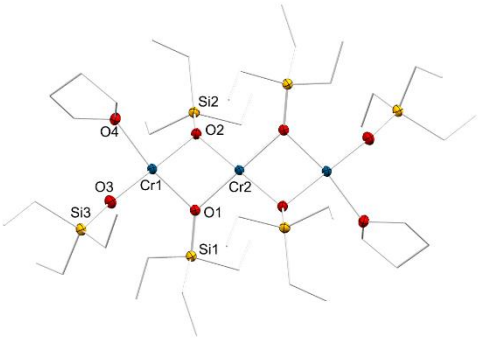

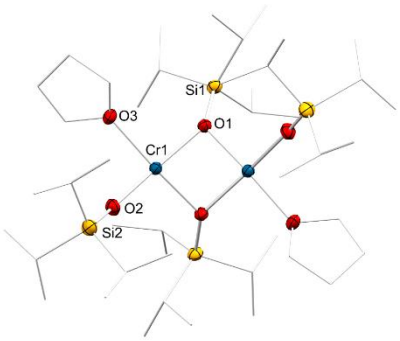

Dalton Transactions

ROYAL SOCIETY OF CHEMISTRY

PAPER

View Article Online
View Journal | View Issue

Cite this: *Dalton Trans.*, 2022, **51**, 5072

Chromous siloxides of variable nuclearity and magnetism†

Simon P. O. Trzmiel,[a] Jan Langmann,[b] Cäcilia Maichle-Mössmer[a] and Reiner Anwander *[a]

Received 4th February 2022,
Accepted 25th February 2022

DOI: 10.1039/d2dt00354f

rsc.li/dalton

Treatment of $Cr[N(SiMe_3)_2]_2(thf)_2$ with $HOSiR_3$ (R = Et, *i*Pr) in THF afforded the bridged Cr^{II} siloxide complexes $Cr_3(OSiEt_3)_2(\mu\text{-}OSiEt_3)_4(thf)_2$ and $Cr_2(OSi{i}Pr_3)_2(\mu\text{-}OSi{i}Pr_3)_2(thf)_2$ in high yield. Exposure of these compounds to vacuum in aliphatic solvents led to the loss of coordinated THF and to the formation of the homoleptic chromous siloxides $Cr_4(\mu\text{-}OSiEt_3)_8$ and $Cr_3(OSiiPr_3)_2(\mu\text{-}OSi{i}Pr_3)_4$, respectively, in moderate to high yield. Use of TMEDA as a potentially bidentate donor molecule gave the monomeric *cis*-coordinated siloxide $Cr(OSiiPr_3)_2(tmeda)$ (tmeda = *N*,*N*,*N*′,*N*′-tetramethylethane-1,2-diamine). Oxidation of $Cr_2(OSi{i}Pr_3)_2(\mu\text{-}OSi{i}Pr_3)_2(thf)_2$ with CHI_3 and C_2Cl_6 produced the trigonal bipyramidal chromic compound $Cr^{III}(OSi{i}Pr)_3(thf)_2$ and asymmetrically coordinated $Cr_2Cl_3(OSi{i}Pr_3)_3(thf)_3$, respectively. Magnetic measurements (Evans and SQUID) hinted at (a) antiferromagnetic interactions between the Cr^{II} centres, (b) revealed higher effective magnetic moments (μ_{eff}) for *cis*-coordinated monomeric heteroleptic complexes compared to *trans*-coordinated ones, and (c) pointed out the highest (μ_{eff}) for the tetranuclear complex $Cr_4(\mu\text{-}OSiEt_3)_8$ (6.26μ_B, SQUID, 300 K; Cr···$Cr_{adjacent}$ avg. 2.535 A).

Introduction

Siloxy ligands are thermally robust, electron withdrawing, and redox-innocent, and as such provide a stabilizing environment for chromium in distinct oxidation states (Cr^{II}, Cr^{III}, Cr^{IV}, Cr^{V}, Cr^{VI}).[1] Early studies on transition metal-based heterosiloxanes, displaying M–O–Si linkages, have been surveyed by Schindler and Schmidbaur in 1967.[2] Initial reports on discrete chromosiloxanes featuring monoanionic siloxy ligands include silyl chromates $CrO_2(OSiR_3)_2$ (R = Me, Ph)[3,4] and tetravalent $Cr(OSiEt_3)_4$.[5] Sterically demanding siloxy ligands like $[OSi(O{t}Bu)_3]$ and $[OSi{t}Bu_3]$ were shown to afford discrete, low-valent chromo(II)siloxanes, obtained as homoleptic [LCr(μ-L)CrL] dimers and $[CrL_2(Do)_n]$ monomers in the presence of donor molecules Do.[6–11] Structurally authenticated homoleptic Cr^{II} siloxides comprise $[Cr(OSi{t}Bu_3)(\mu\text{-}OSi{t}Bu_3)]_2$ (ref. 6) and $[Cr\{OSi(O{t}Bu)_3\}_2]_2$ (Fig. 1).[7] Heteroleptic Cr^{II} siloxide complexes include $Cr[OSi(O{t}Bu)_3]_2(NHEt_2)_2$,[8] $Cr_2(OSiPh_3)_2(\mu\text{-}OSiPh_3)_2(thf)_2$,[9] $Cr[OSi(O{t}Bu)_3]_2(tmeda)$[10] and $[Cr\{N(Ar)SiMe_2N(Ar)SiMe_2O\}(thf)]_2$ (Ar = $C_6H_2Me_3$-2,4,6).[11]

Homoleptic Cr^{III} and Cr^{IV} siloxides feature trigonal planar $Cr[OSi{t}Bu_3]_3$,[12] square-pyramidal $Cr[OSi(O{t}Bu)_3]_3$,[13] and tetrahedral $Cr(OSiMe{t}Bu_2)_4$,[14] as well as $Cr[OSi(O{t}Bu)_3]_4$,[13] respectively (Fig. 1). Heteroleptic complexes of the more elusive oxidation states Cr(IV) and Cr(V) exhibit commonly employed ligands $[OSiMe_3]$ or $[OSiPh_3]$ and are further represented by mixed alkoxy/siloxy complex $Cr(OCMe{t}Bu_2)_3(OSiMe_3)$,[15] imide

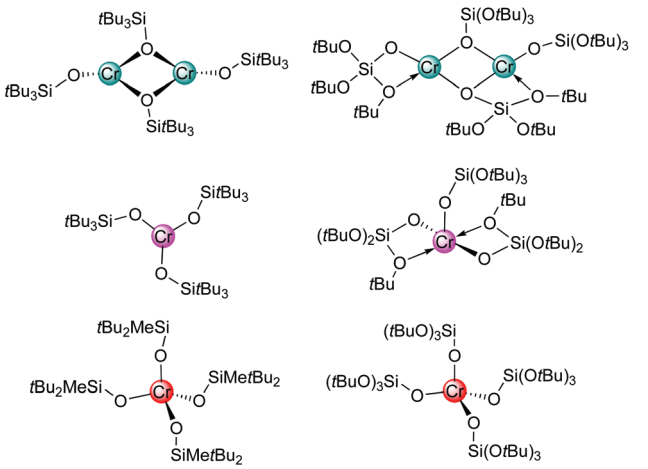

Fig. 1 Homoleptic chromium siloxides (Cr^{II}, blue; Cr^{III}, purple; Cr^{IV}, red).

[a]*Institute of Inorganic Chemistry, Eberhard Karls Universität Tübingen, Auf der Morgenstelle 18, D-72076 Tübingen, Germany.*
E-mail: reiner.anwander@uni-tuebingen.de
[b]*Institut für Physik, Universität Augsburg, Universitätsstr. 1, 86159 Augsburg, Germany*

† Electronic supplementary information (ESI) available. CCDC 2149139–2149146. For ESI and crystallographic data in CIF or other electronic format see DOI: 10.1039/d2dt00354f

[CrO(NSiMe$_3$)(py)(μ-OSiMe$_3$)]$_2$ (ref. 16), amide [CrO[N*t*Bu(C$_5$H$_3$F$_2$-2,5)]$_2$(OSiPh$_3$)]$_2$,[17] and CrO[OSi(O*t*Bu)$_3$]$_3$.[13]

Early studies on chromium siloxide complexes were mainly driven by the generation of new inorganic polymers, inspired by naturally abundant metallosilicates.[2] In the meantime a great deal of investigations has been concerned with a better understanding of the chromium-based heterogeneous Phillips catalyst, applied in industrial polyethylene fabrication.[18] Materials chemistry and modelling of the Phillips catalyst mainly involved [Cr{OSi(O*t*Bu)$_3$}] moieties.[7–9,13,19] On the other hand, low-valent chromium siloxide complexes have been successfully employed in redox-transformations giving access to high-valent chromium imide complexes[6] or promoting dioxygen activation.[20] Our interest in chromium siloxide complexes was sparked by their potential role as mimics/models of silica-grafted chromium surface species[21] as well as the feasibility of halogenido/siloxy exchange in otherwise difficult to handle chromium reagents (*e.g.*, Takai olefination reagent).[10]

Protonolysis reactions like (silyl)amine elimination and alcoholysis emerged as useful protocols for the synthesis of chromium siloxide complexes.[8,9,13,22] As importantly, careful selection of the siloxy ligand might change complex geometry through steric pressure and the presence of donor molecules affect the bridging capabilities and hence complex nuclearity.[12] These features, as well as their stabilizing properties, make siloxy ligands an interesting target for the synthesis of otherwise elusive compounds.[5,10,14] Since the aggregation of the complexes is also known to bear on their magnetic properties we aimed at increasing the scope of readily available Cr^{II} siloxides by introducing the ligands [OSiEt$_3$] and [OSi*i*Pr$_3$].

Results and discussion

Synthesis and structural characterization of chromium(II) complexes bearing the [OSi*i*Pr$_3$] ligand

The general synthesis approach according to the protonolysis of Cr[N(SiMe$_3$)$_2$]$_2$(thf)$_2$ (ref. 22) with the respective silanol proligand was selected because of the ready availability of the Cr^{II} silylamide compound through salt metathesis and the exceptionally easily removed side product HN(SiMe$_3$)$_2$ (pK_a [HN(SiMe$_3$)$_2$]$_{THF}$ = 25.8).[23] Accordingly, the dimeric compound Cr$_2$(OSi*i*Pr$_3$)$_2$(μ-OSi*i*Pr$_3$)$_2$(thf)$_2$ (**1**) was obtained *via* protonolysis of Cr[N(SiMe$_3$)$_2$]$_2$(thf)$_2$ with two equivalents of HOSi*i*Pr$_3$ in THF at ambient temperature (Scheme 1). Reactions conducted in *n*-hexane solution consistently yielded mixtures of products preventing direct isolation of **1** without further THF addition. The red purple reaction solution was dried under reduced pressure to give **1** as a red-purple sticky solid. Dissolution of this solid in *n*-pentane or *n*-hexane led to a colour change to blue. Crystallization from this blue *n*-pentane solution generated two different kinds of crystals that persistently co-crystallized. The hand-picked red-purple blocks were identified by X-ray diffraction (XRD) as Cr$_2$(OSi*i*Pr$_3$)$_2$(μ-OSi*i*Pr$_3$)$_2$(thf)$_2$ (**1**) (Fig. 2), while the remaining clear blue platelets were not suitable for an XRD analysis due to bad crystal quality. Compound **1** exhibits a

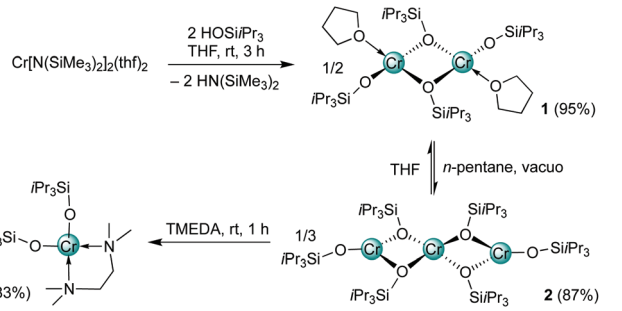

Scheme 1 Synthesis of Cr$_2$(OSi*i*Pr$_3$)$_2$(μ-OSi*i*Pr$_3$)$_2$(thf)$_2$ (**1**), conversion to Cr$_3$(OSi*i*Pr$_3$)$_2$(μ-OSi*i*Pr$_3$)$_4$ (**2**) and subsequent deoligomerization to Cr(OSi*i*Pr$_3$)$_2$(tmeda) (**3**) (tmeda = *N*,*N*,*N*′,*N*′-tetramethylethane-1,2-diamine).

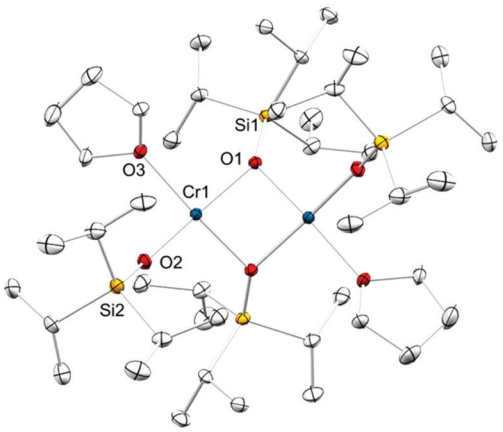

Fig. 2 Crystal structure of **1** (ellipsoids set to 50% probability). All hydrogen atoms are omitted for clarity. Selected interatomic distances (Å) and angles (°): Cr1···Cr1′ 2.7960(6), Cr1–O1 2.0134(12), Cr1–O2 1.9185(13), Cr1–O3 2.0914(13), Si1–O1 1.6515(13), Si2–O2 1.6034(14); O2–Cr1–O1 98.40(5), O2–Cr1–O3 88.59(6), O1–Cr1–O3 169.60(6), Cr(1)–O(1)–Si(1) 126.38(7), Cr(1)–O(2)–Si(2) 150.15(9).

dimeric structure, with the chromium centres adopting a distorted square planar coordination geometry with high resemblance to Cr$_2$(OSiPh$_3$)$_2$(μ-OSiPh$_3$)$_2$(thf)$_2$.[9] Each Cr^{II} is bound to each one terminal and two bridging triisopropylsiloxy ligands and coordinatively saturated by one molecule of THF. The terminal Cr1–O2/Cr1′–O2′ distances are 1.9185(13) Å, while the bridging ones (Cr1–O1/Cr1′–O1′) are significantly elongated at 2.0134(12) Å. The Cr···Cr distance of 2.7960(6) Å is in the expected range of Cr^{II} siloxides, which were reported between 2.6365(15) Å for Cr$_2$(OSi*t*Bu$_3$)$_2$(μ-OSi*t*Bu$_3$)$_2$ (ref. 6) and 2.880(1) Å for Cr$_2$(OSiPh$_3$)$_2$(μ-OSiPh$_3$)$_2$(thf)$_2$.[9] The dihedral angle between the two planes spanned by O2–Cr1–O3 and O1–Cr1–O1′ was calculated as 12.83°.

When *n*-pentane solutions of Cr$_2$(OSi*i*Pr$_3$)$_2$(μ-OSi*i*Pr$_3$)$_2$(thf)$_2$ were solidified under vacuum a blue to violet residue was obtained. Addition of a few drops of THF to a highly concentrated solution of this residue in *n*-pentane led to the precipitation of large quantities of a red-purple solid. This observation suggested an equilibrium consisting of **1** and putative

$[Cr(OSi\textit{i}Pr_3)_2]_x$ as the two species present in the solution. As Cr^{II} (d^4) exhibits strong paramagnetic properties, the ^1H NMR spectra recorded in THF-d_8 could not prove this hypothesis since all proton signals were strongly/extremely broadened. To gain conclusive insights into the composition of this mixture, the thf adduct **1** was repeatedly dissolved in *n*-pentane or *n*-hexane with subsequent solvent evaporation *in vacuo*. After three to six reruns of this procedure, a light blue solution was obtained. Similar thf-desolvation behaviour was reported for siloxy-bridged $[Cr\{N(Ar)SiMe_2N(Ar)SiMe_2O\}(thf)]_2$, effecting a colour change from violet to dark green.[11]

Crystallization from a highly concentrated *n*-hexane solution gave clear, slightly blue platelets, which were identified as donor-free trinuclear $Cr_3(OSi\textit{i}Pr_3)_2(\mu\text{-}OSi\textit{i}Pr_3)_4$ (**2**) by XRD analysis (Fig. 3). Clearly, the isolation of compound **2** proved that the donor solvent in compound **1** is only weakly bound to the metal centres. At ambient temperature, longer exposures of **1** to vacuum (10^{-2} Torr) led only to partial loss of coordinated THF as indicated by the microanalysis of the blue residue. A striking feature of the solid-state structure of compound **2** is the distinct coordination of the chromium centres. The two peripheral Cr^{II} adopt a trigonal planar geometry similar to the one detected in $Cr_2(OSi\textit{t}Bu_3)_2(\mu\text{-}OSi\textit{t}Bu_3)_2$.[6] The central Cr^{II} is coordinatively saturated by four siloxy ligands in a distorted square planar geometry. The terminal Cr–O distances amount to 1.850(2) Å (Cr1–O1) and 1.858(3) Å (Cr3–O6) and range from 1.925(2) to 2.034(2) Å for those bridging to the central metal. The angles Cr1–O1–Si1/Cr3–O6–Si1 involving the terminal siloxy groups (168.21(15)° and 172.2(2)°) are slightly less bent in comparison to the respective ones in $[Cr(OSi\textit{t}Bu_3)_2]_2$ which average 166.3(28)°. The Cr···Cr distances in **2** deviate considerably (Cr1···Cr2, 2.9611(6) Å and Cr2···Cr3, 2.8965(16) Å) and are markedly elongated compared to 2.6365(15) Å in $Cr_2(OSi\textit{t}Bu_3)_2(\mu\text{-}OSi\textit{t}Bu_3)_2$.[6] The overall constrained geometry likely contributes to instability of **2** in solvents even at −35 °C. After a few days, a solution in *n*-pentane turned green and it was not possible to recover any product. In crystalline or dried form, however, compound **2** could be stored indefinitely. When compound **2** was dissolved in *n*-pentane and fresh donor THF was admitted, the colour instantly changed to red-violet due to the regeneration of compound **1**.

Given the donor solvent dependent aggregation observed for dimeric **1** and trimeric **2**, we wondered about the effect of potentially chelating donor ligands. When TMEDA (TMEDA = *N*,*N*,*N*′,*N*′-tetramethylethane-1,2-diamine) instead of THF was added, the colour changed to bright violet. Crystallization from the concentrated reaction solution gave bright violet square platelets of monomeric compound $Cr(OSi\textit{i}Pr_3)_2$(tmeda) (**3**) as revealed by an XRD analysis (Fig. 3). Complex **3** displays a highly distorted *cis*-square planar geometry due to the steric constraint exerted by the bidentate tmeda ligand. The dihedral distortion between the planes O1–Cr1–O2 and N1–Cr1–N2 was determined as 26.15° in stark contrast to 8.03° (calculated with MERCURY)[24] for $Cr[OSi(O\textit{t}Bu)_3]_2$(tmeda).[10] These differences likely originate from the distinct sterics of *i*Pr *versus* O*t*Bu. The Cr–O distances in **3** are 1.9360(10) and 1.9345(10) Å matching those in $Cr[OSi(O\textit{t}Bu)_3]_2$(tmeda) with 1.9307(12) and

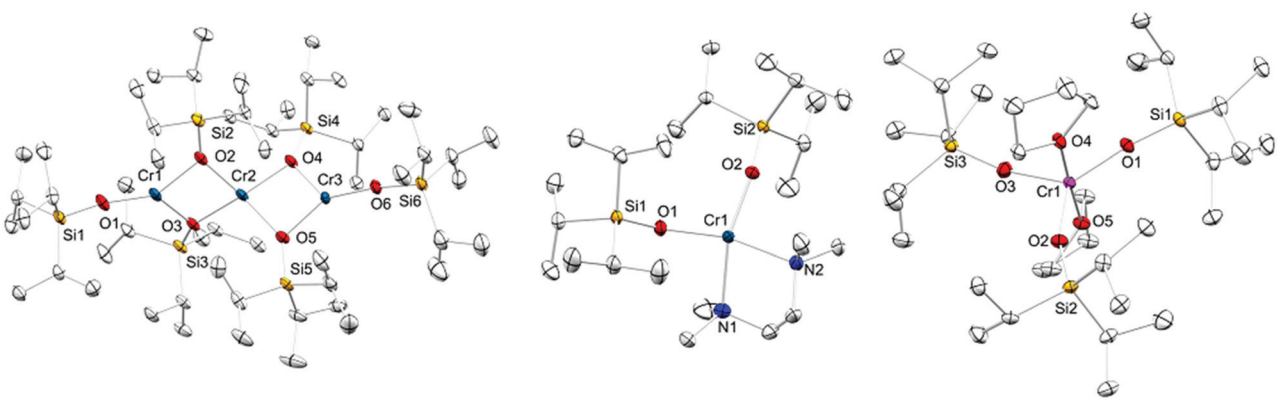

Fig. 3 Crystal structures of complexes **2** (left), **3** (middle) and **4** (right), with ellipsoids set at the 50% level. Hydrogen atoms are omitted for clarity. Two additional molecules of **3** and additional molecule of **4** in the unit cell are omitted for clarity. Selected interatomic distances (Å) and angles (°): **2** Cr1···Cr2 2.9611(6), Cr2···Cr3 2.8965(16), Cr1–O1 1.850(2), Cr1–O3 1.978(2), Cr1–O2 1.9862(17), Cr2–O2 2.034(2), Cr2–O4 2.0195(17), Cr2–O3 2.0204(17), Cr2–O5 2.0314(19), Cr3–O4 1.925(2), Cr3–O5 1.979(2), Cr3–O6 1.858(3), Si1–O1 1.624(2), Si2–O2 1.654(2), Si3–O3 1.6631(19), Si4–O4 1.6638(18), Si5–O5 1.6619(19), Si6–O6 1.620(3); O1–Cr1–O3 132.78(8), O1–Cr1–O2 142.44(9), O3–Cr1–O2 84.79 (7), O1–Cr1–Cr2 170.71(7), O4–Cr2–O3 154.84(7), O4–Cr2–O5 82.23(7), O3–Cr2–O5 106.06(7), O4–Cr2–O2 105.66(7), O3–Cr2–O2 82.49(7), O5–Cr2–O2 142.41(7) Si1–O1–Cr1 168.21(15) Si6–O6–Cr3 172.2(2); **3** Cr1–O1 1.9360(10), Cr1–O2 1.9345(10), Cr1–N1 2.1882(13), Cr1–N2 2.1772(13), O1–Si1 1.6097(10), Si2–O2 1.6056 (10); O2–Cr1–O1 103.26(5), O2–Cr1–N2 89.61(5), O1–Cr1–N2 158.06(5), O2–Cr1–N1 158.59(5), O1–Cr1–N1 91.73(5), N2–Cr1–N1 81.36(5) Cr(1)–O(1)–Si(1) 139.40(6), Cr(1)–O(2)–Si(2) 143.02(6); **4** Cr1–O1 1.868(3), Cr1–O2 1.870(2), Cr1–O3 1.868(3), Cr1–O4 2.048(2), Cr1–O5 2.053(2), Si1–O1 1.631(3), Si2–O2 1.615(2), Si3–O3 1.609(3); O1–Cr1–O3 127.66(10), O1–Cr1–O2 131.69(13), O3–Cr1–O2 100.64(13), O1–Cr1–O4 88.69(10), O3–Cr1–O4 92.62(11), O2–Cr1–O4 90.19(8), O1–Cr1–O5 89.54(10), O3–Cr1–O5 88.64(11), O2–Cr1–O5 90.82(8), O4–Cr1–O5 178.21(12), Si1–O1–Cr1 171.43(15), Si2–O2–Cr1 159.36(19), Si3–O3–Cr1 167.02(17) Cr(1)–O(1)–Si(1) 171.43(15), Cr(1)–O(2)–Si(2) 159.36(19), Cr(1)–O(3)–Si(3) 167.02(17).

1.9380(12) Å.[10] Monomeric chromous siloxides are rare and additionally feature *trans*-square-planar Cr[OSi(O*t*Bu)$_3$]$_2$(NHEt$_2$)$_2$,[8] and Cr(OSi*t*Bu$_3$)$_2$(OCPh$_2$)$_2$.[6]

Oxidation of $Cr_2(OSi\mathit{i}Pr_3)_2(\mu\text{-}OSi\mathit{i}Pr_3)_2(thf)_2$

In an attempt to further extend the scope of Takai-type olefination reagents (Takai: $Cr_2Cl_4(CHI)(thf)_4$),[25] three equivalents of **1** were treated with CHI_3 in THF at ambient temperature. Unlike previously found for the reaction of $[Cr\{OSi(O\mathit{t}Bu)_3\}_2]_2$, which afforded isolable trivalent $Cr_2Cl_2\{OSi(O\mathit{t}Bu)_3\}_2(CHI)(thf)_4$ and mixed-valent $Cr_2I_2\{OSi(O\mathit{t}Bu)_3\}_2(CHI_2)$,[10] the reaction of **1** led only to the serendipitous isolation of trivalent $Cr(OSi\mathit{i}Pr_3)_3(thf)_2$ (**4**) (Fig. 3). Chromic compound **4** was only detected in low quantities as a side product, forming green blocks when crystallization was successful from toluene. The reaction mixture also contained $CrCl_2(thf)_2$ as well as $CrI_2(thf)_2$ as identified by XRD measurements. Unfortunately, it was not possible to identify any other product of this reaction. Compound **4** exhibits a trigonal bipyramidal coordination geometry. The Cr^{III} atom is coordinated by three equatorial [OSi*i*Pr$_3$] ligands and two apical molecules of THF. The Cr–O distances range from 1.868(3) to 1.870(2) Å, which are elongated compared to the 3-coordinate complex $Cr(OSi\mathit{t}Bu_3)_3$ [12] (avg 1.778(6) Å) but match those in the similar trigonal bipyramidal complexes Cr[OSi(O*t*Bu)$_3$]$_3$(NHEt$_2$)$_2$ (avg. 1.890 Å)[8] and Cr[OSi(O*t*Bu)$_3$]$_3$(thf)$_2$ (avg. 1.869 Å).[26] The O4–Cr1–O5 angle involving the two THF molecules is nearly linear with 178.21(12)° (*cf.*, Cr[OSi(O*t*Bu)$_3$]$_3$(thf)$_2$: 175.71(8)°). The O–Cr–O angles involving the triisopropylsiloxy ligands are 100.64(13) 127.66(10) and 131.69(13)°, attributable to the slightly lower steric demand and higher flexibility of *i*Pr compared to *t*Bu substituents in Cr(OSi*t*Bu$_3$)$_3$ (O–Cr–O: 119.20(7), 119.22(7) and 121.57(7)°). Therefore, the shape of the trigonal core in complex **4** could more precisely be described as "Y" shaped. The unusual coordination number for Cr^{III} leads to high instability, since compound **4** is, in crystallized form, highly temperature and moisture sensitive and "decomposed" (likely *via* THF dissociation) within seconds when handled at temperatures above −35 °C. Attempts to synthesize compound **4** by oxidation of compound **1** with 0.5 equivalents of C_2Cl_6 in THF failed. Instead, the latter reaction generated a dimeric chromic complex **5** of composition $Cr_2Cl_3(OSi\mathit{i}Pr_3)_3(thf)_3$ (Fig. 4). Asymmetric **5** could be crystallized in small amounts from *n*-hexane as violet blocks. The generation of this compound could either be the result of ligand rearrangement, to the thermodynamically most stable coordination number of six for octahedral coordinated Cr^{III}, or the decomposition of **4** and subsequent reaction with left over C_2Cl_6.

Complex **5** features one chromium atom (Cr1) bound to two terminal siloxy ligands and one THF molecule, which is connected to the second chromium atom (Cr2) *via* three bridging chloridos. The 6-fold coordination of Cr2 is completed by a terminal siloxy ligand and two THF molecules. The asymmetry of the molecule is also nicely pictured in the Cr–Cl distances (Cr1–Cl avg 2.474 Å, Cr2–Cl avg 2.364 Å). Both Cr centres adopt a slightly distorted octahedral coordination geometry. The distortion around Cr1 was measured to 3.63° (angle between planes O1–Cr1–O2 and Cl1–Cr1–Cl3) and to 9.59° around Cr2 (planes O5–Cr2–O6 and Cl1–Cr2–Cl3). The Cr1···Cr2 distance amounts to 3.131 Å. **5** could only be obtained in low yield (23%), as its crystallization proved rather difficult, probably due to other soluble co-products. When compound **5** was exposed to vacuum (10^{-2} Torr) for extended periods of time at ambient temperature, a viscous green compound was generated, putatively a donor ligand free variant of **5**. It was not possible to clearly identify the latter compound or any other product by crystallization or other analytical means.

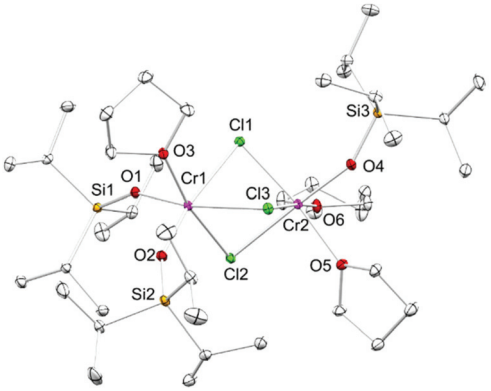

Fig. 4 Crystal structure of complex **5**, with ellipsoids set at the 50% level. Hydrogen atoms are omitted for clarity. Selected interatomic distances (Å) and angles (°): Cr1···Cr2 3.131, Cr1–O1 1.8446(9), Cr1–O2 1.8507(9), Cr1–O3 2.0414(9), Cr2–O4 1.8406(9), Cr2–O5 2.0506(9), Cr2–O6 2.0434(9), Cr2–Cl1 2.3386(4), Cr1–Cl1 2.5555(4), Cr1–Cl2 2.3719(4), Cr2–Cl2 2.4100(4), Cr2–Cl3 2.3422(4), Cr1–Cl3 2.4953(4); Cr2–Cl1–Cr1 79.400(13), Cr1–Cl2–Cr2 81.789(13), Cr2–Cl3–Cr1 80.589(12) Cr(1)–O(1)–Si(1) 151.61(6), Cr(1)–O(2)–Si(2) 153.71(6), Cr(2)–O(4)–Si(3) 154.05(6).

Synthesis and structural characterization of chromium(II) complexes bearing the $[OSiEt_3]$ ligand

The protonolysis of $Cr[N(SiMe_3)_2]_2(thf)_2$ with two equivalents of the sterically less demanding triethylsilanol afforded trinuclear $Cr_3(OSiEt_3)_2(\mu\text{-}OSiEt_3)_4(thf)_2$ (**6**) (Scheme 2). Upon addition of the silanol, the bright purple silylamide solution immediately changed colour to red violet. Crystallization of **6** (Fig. 5) as red plates was performed from a concentrated *n*-hexane

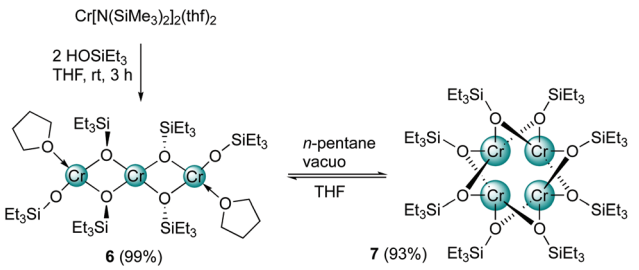

Scheme 2 Synthesis of $Cr_3(OSiEt_3)_2(\mu\text{-}OSiEt_3)_4(thf)_2$ (**6**) and conversion to $Cr_4(\mu\text{-}OSiEt_3)_8$ (**7**).

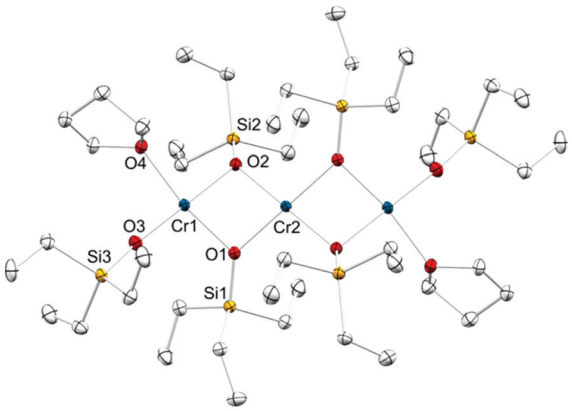

Fig. 5 Crystal structure of **6** (ellipsoids set to 30% probability). All hydrogen atoms are omitted for clarity. Selected interatomic distances (Å) and angles (°): Cr1···Cr2 2.9096(2), Cr1–O1 1.9948(10), Cr2–O1 1.9964(9), Cr1–O2 2.0350(10), Cr2–O2 2.0165(9), Cr1–O3 1.9076(10), Cr1–O4 2.0921(10), Si1–O1 1.6435(10), Si2–O2 1.6418(10), Si3–O3 1.5986(11); Cr1–O1–Cr2 93.60(4), Cr2–O2–Cr1 91.80(4), O3–Cr1–O1 99.24(4), O3–Cr1–O2 179.07(5), O1–Cr1–O2 81.07(4), O3–Cr1–O4 88.70(4), O1–Cr1–O4 170.05(4), O2–Cr1–O4 91.09(4), O3–Cr1–Cr2 136.81(3), Cr(1)–O(1)–Si(1) 128.17(6), Cr(2)–O(1)–Si(1) 134.89(6), Cr(2)–O(2)–Si(2) 128.04(6), Cr(1)–O(2)–Si(2) 124.25(6), Cr(1)–O(3)–Si(3) 167.94(7).

solution. Compound **6** shows a structural motif similar to that of **2** (Fig. 3).

The central Cr2 is surrounded by four bridging siloxy ligands in square planar coordination, while the coordination of the two peripheral ones (Cr1/Cr1′) is completed by a terminal siloxy and a "terminating" THF molecule. The latter coordination environment shows high similarity to $Cr_2(OSiPh_3)_2(\mu\text{-}OSiPh_3)_2(thf)_2$,[9] and $Cr_2(OSi\textit{i}Pr_3)_2(\mu\text{-}OSi\textit{i}Pr_3)_2(thf)_2$ (**1**). The Cr–O distance of the terminal siloxy ligand of 1.9076(10) Å in **6** is slightly shorter in comparison to **1** (1.9185(13) Å) and significantly shorter than in $Cr_2(OSiPh_3)_2(\mu\text{-}OSiPh_3)_2(thf)_2$ (1.928(2) Å).[9] The bridging Cr–O distances in **6** range from 1.9948(10) to 2.0350(10) Å. Dissolving compound **6** in *n*-pentane did not lead to an immediate colour change. Only upon exposure to vacuum, the colour gradually changed to a darker tone of red, nearly brown. Repetition of this process and crystallization from *n*-pentane finally yielded crystals of un-solvated homoleptic complex $Cr_4(\mu\text{-}OSiEt_3)_8$ (**7**) (Scheme 2). The ^{1}H NMR spectrum of **7** shows a broadened peak at δ = 1.24 ppm ($\nu 1/2 \approx 120$ Hz, C_6D_6). The tetranuclear complex **7** features a "homo-bridged" variant of the previously reported chromous "box" $[Cr(\mu\text{-}Cl)(\mu\text{-}OSi\textit{t}Bu_3)]_4$,[12] with the chromium centres residing in a pseudo square planar environment of either four triethylsiloxy ligands (Fig. 6) or each two *trans*-positioned chlorido and siloxy ligands, respectively.

This structural motif was first mentioned for neosilyl complex $Cr_4[CH_2Si(CH_3)_3]_8$ in 1986,[27] which was crystallographically authenticated in 2002.[28] The four Cr^{II} centres in complex **7** form a nearly perfect rectangle with Cr–Cr–Cr angles ranging between 89.04(3) (Cr2–Cr1–Cr2′) and 90.83(2)°

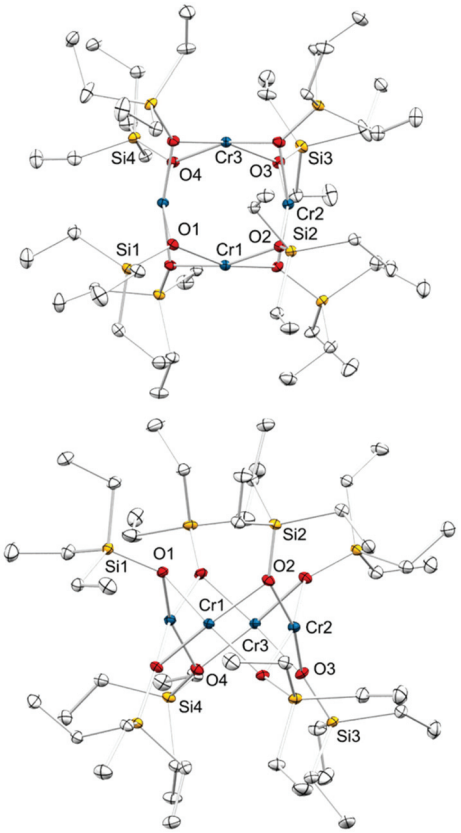

Fig. 6 Distinct molecular views of the crystal structure of **7** (ellipsoids set to 50% probability). All hydrogen atoms have been omitted for clarity. Selected interatomic distances (Å) and angles (°): Cr1···Cr2 2.5381 (6), Cr2···Cr3 2.5325(6), Cr1–O2 2.0046(17), Cr1–O1 2.0199(17), Cr2–O2 1.9907(17), Cr2–O3 1.9940(18), Cr3–O3 1.9939(17), Cr3–O4 2.0077(18), Si1–O1 1.6448(19), Si2–O2 1.6453(18), Si3–O3 1.6425(18), Si4–O4 1.6370(19); O2–Cr1–O1 98.30(7), O2–Cr1–Cr2 50.32(5), O1–Cr1–Cr2 114.93(5), Cr1–Cr2–Cr3 90.83(2), Cr(1)–O(1)–Si(1) 136.95(11), Cr(1)–O(2)–Si(2) 132.78(11), Cr(2)–O(2)–Si(2) 143.38(11), Cr(2)–O(3)–Si(3) 143.57(11), Cr(3)–O(3)–Si(3) 137.32(11), Cr(3)–O(4)–Si(4) 137.91(11).

(Cr1–Cr2–Cr3). The adjacent Cr···Cr distances average 2.5353 Å and are considerable shorter than in $(Cr_4(\mu\text{-}Cl)_4(\mu\text{-}OSi\textit{t}Bu_3)_4$: 2.679 Å).[12] The tips of the "double crown" in **7** point outwards at an angle of 54.36 (planes Cr1–Cr2–Cr3 and Cr1–O2–Cr2) and 55.16° (planes Cr1–Cr2–Cr3 and Cr2–O3–Cr3). The Cr–O distances in **7** range from 1.9907(17) to 2.0199(17) Å thus being comparable to the bridging ones in complex **6**. The use of highly purified $Cr[N(SiMe_3)_2]_2(thf)_2$ is crucial to the synthesis of **7**. $Cr[N(SiMe_3)_2]_2(thf)_2$ generated from $Na[N(SiMe_3)_2]$ and $CrCl_2$ in THF may contain small amounts of ate complex $Na(thf)Cr[N(SiMe_3)_2]_3$.[29] Traces of this impurity led to the generation of small amounts of heterobimetallic $Na_4Cr_2(OSiEt_3)_8$ **8** (Fig. S23 and S24†). Crystals of **8** suitable for XRD analysis were crystallized from *n*-pentane as brown blocks.

Magnetic measurements

The magnetic properties of the complexes in dissolved (solvent: benzene/deuterated benzene) and solid form were

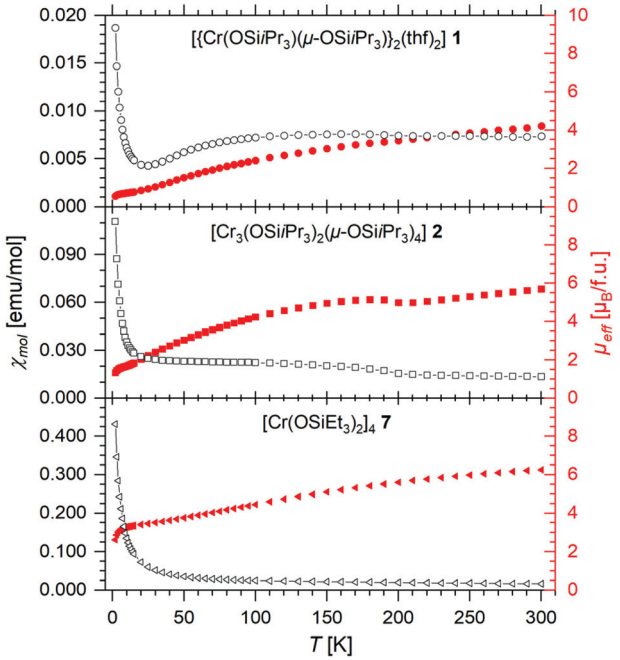

Fig. 7 Temperature-dependent molar magnetic susceptibility $\chi_{mol}(T)$ (black open symbols; left ordinate) and effective magnetic moment $\mu_{eff}(T)$ (red filled symbols; right ordinate) as obtained by SQUID magnetic measurements on crystalline powder of **1** (top), **2** (middle) and **7** (bottom) in an applied field H = 10 kOe. The $\chi_{mol}(T)$ data was corrected for diamagnetic contributions (**1**: -6.432×10^{-4} emu mol^{-1}; **2**: -8.438×10^{-4} emu mol^{-1}; **7**: -8.404×10^{-4} emu mol^{-1}; calculated from Pascal's constants),[31] and a spin-only g factor of 2.0 was assumed in the calculation of $\mu_{eff}(T)$.

investigated using the Evans Method[30] (reference: HMDSO = hexamethyldisiloxane) and SQUID magnetic measurements (Fig. 7), respectively. For complexes with isolated Cr^{II} centres in high-spin d^4 configurations (S = 2) effective magnetic moments μ_{eff} of 4.90μ_B (mononuclear), 6.93μ_B (dinuclear), 8.49μ_B (trinuclear) and 9.80μ_B (tetranuclear) are expected. Low-spin configurations (S = 1) lead to μ_{eff} values of 2.83μ_B (mononuclear), 4μ_B (dinuclear), 4.90μ_B (trinuclear) and 5.66μ_B (tetranuclear). The magnetic moments μ_{eff} referred to in the following discussion state values at temperatures close to ambient temperature, with minor variations between 295 and 333 K (*cf.*, Table 1).

The mononuclear complex $Cr(OSi\textit{i}Pr_3)_2(tmeda)$ (**3**) displays a magnetic moment μ_{eff} = 5.13μ_B (Evans) at ambient temperature, close to the high-spin case (4.90μ_B). However, it is noteworthy that the magnetic moments of *cis*-coordinated **3** and $Cr[OSi(O\textit{t}Bu)_3]_2(tmeda)$ are considerably higher compared to other monomeric trigonal and square planar complexes (Table 1). By contrast, effective magnetic moments significantly below the uncoupled high-spin limit, but still above the uncoupled low-spin limit were detected for all investigated multinuclear complexes (Table 1). Dinuclear $Cr_2(OSi\textit{i}Pr_3)_2(\mu\text{-}OSi\textit{i}Pr_3)_2(thf)_2$ (**1**) exhibits μ_{eff} values of 4.88μ_B (Evans) and 4.20μ_B (SQUID). For the ate complex $Na_4Cr_2(OSiEt_3)_8$ (**8**) a value of 4.66μ_B was measured by the Evans method. The magnetic moments of dinuclear chromous siloxide complexes span a wide range of 2.8–6.0μ_B, being markedly affected by the coordination geometry and coligands (Table 1). Dinuclear $Cr_2(OSi\textit{i}Pr_3)_2(\mu\text{-}OSi\textit{i}Pr_3)_2(thf)_2$ (**1**) may be compared to $Cr_2Li_2[PhSi(OPh_2O)_3](MeCN)_4$ (Cr···Cr distance of 3.2606(10) Å) exhibiting a drop of μ_{eff} from 6.1μ_B at ambient temperature to 0.8μ_B at 2 K.[20a]

Table 1 Compilation of coordination and magnetic data for selected chromous siloxides

Compound	CN/nuclearity	Geometry	Cr···Cr [Å]	μ_{eff} [μ_B] (T, method)[a]	Ref.
$Cr(OSi\textit{t}Bu_3)_3Na$(benzene)	3/monomer	Trigonal planar ("Y-shaped")	—	4.8 (295 K, Evans)	12
$[Cr(OSi\textit{t}Bu_3)_3][Na$(dibenzo-18-crown-6)]	3/monomer	Trigonal planar	—	4.7 (295 K, SQUID)	12
$Cr[OSi(O\textit{t}Bu)_3]_2(NHEt_2)_2$	4/monomer	*trans*-Square planar	—	4.7 (333 K, Evans)	8
$Cr(OSi\textit{t}Bu_3)_2(OCPh_2)$	4/monomer	*trans*-Square planar	—	4.8 (293 K, Evans)	6
$CrLi_2[O(SiPh_2O)_2]$	4/monomer	Square planar	—	4.78 (295 K, SQUID)	20*b*
$Cr[OSi(O\textit{t}Bu)_3]_2(tmeda)$	4/monomer	*cis*-Square planar	—	5.73 (295 K, Evans)	10
$Cr(OSi\textit{i}Pr_3)_2(tmeda)$ (**3**)	4/monomer	*cis*-Square planar	—	5.1 (295 K, Evans)	*b*
$Cr_2(OSi\textit{t}Bu_3)_2(\mu\text{-}OSi\textit{t}Bu_3)_2$	3/dimer	Pseudo-trigonal planar ("Y-shaped")	2.63/2.68[c]	2.8 (293 K, Evans) ~3.5 (300 K, SQUID)	6
$[Cr\{OSi(O\textit{t}Bu)_3\}_2]_2$	4/dimer	Dist. square planar	2.884(2)	5.99 (Evans)[d]	7
$Cr_2Li_2[PhSi(OPh_2O)_3](MeCN)_4$	4/dimer	Square planar	3.2606(10)	6.1 (293 K, SQUID)	20*a*
$[Cr\{N(Ar)SiMe_2N(Ar)SiMe_2O\}(thf)]_2$[e]	4/dimer	Square planar	3.019	2.88 (298 K)	11
$Cr_2(OSi\textit{i}Pr_3)_2(\mu\text{-}OSi\textit{i}Pr_3)_2(thf)_2$ (**1**)	4/dimer	Dist. square planar	2.7960(6)	4.88 (295 K, Evans) 4.2 (300 K, SQUID)	*b*
$Cr_3(OSi\textit{i}Pr_3)_2(\mu\text{-}OSi\textit{i}Pr_3)_4$ (**2**)	3,4/trimer	Trigonal ("Y-shaped")/square planar	2.9611(6), 2.8965(16)	5.22 (295 K, Evans) 5.68 (300 K, SQUID)	*b*
$Cr_3(OSiEt_3)_2(\mu\text{-}OSiEt_3)_4(thf)_2$ (**6**)	4/trimer	Dist. square planar	2.9096(2)	5.36 (295 K, Evans)	*b*
$[Cr(\mu\text{-}Cl)(\mu\text{-}OSi\textit{t}Bu_3)]_4$	4/tetramer	Dist. square planar	2.670(3)–2.688(3)[f]	1.7 (295 K, Evans) ~1.1 (295 K, SQUID)	12
$Cr_4(\mu\text{-}OSiEt_3)_8$ (**7**)	4/tetramer	Dist. square planar	2.5381(6), 2.5325(6)[f]	5.15 (295 K, Evans) 6.62 (300 K, SQUID)	*b*

[a] Evans' method performed in benzene/deutero-benzene. [b] This work. [c] Two independent isostructural dimers in the asymmetric unit. [d] T not indicated. [e] Ar = $C_6H_2Me_3$-2,4,6. [f] Adjacent chromium centres.

Unsolvated trinuclear $Cr_3(OSi\textit{i}Pr_3)_2(\mu\text{-}OSi\textit{i}Pr_3)_4$ (**2**) is characterized by effective magnetic moments of $5.22\mu_B$ (Evans) and $5.68\mu_B$ (SQUID) similar to trinuclear $Cr_3(OSiEt_3)_2(\mu\text{-}OSiEt_3)_4(thf)_2$ (**6**) with $\mu_{eff} = 5.36\mu_B$ (Evans). Finally, μ_{eff} values of $5.15\mu_B$ (Evans method) and $6.26\mu_B$ (SQUID) were determined for tetranuclear complex $Cr_4(\mu\text{-}OSiEt_3)_8$ (**7**). Temperature-dependent studies (SQUID) revealed further decreases of μ_{eff} upon cooling for **1** (rt: $4.20\mu_B$; 2 K: $0.55\mu_B$), **2** (rt: $5.68\mu_B$; 2 K: $1.33\mu_B$) and **7** (rt: $6.26\mu_B$; 2 K: $2.63\mu_B$) (Fig. 7). Notably, trinuclear unsolvated **2** revealed an intermediate re-increase of μ_{eff} below approx. 200 K warranting further investigation. Similar magnetic behaviour with an unexpectedly low effective magnetic moment at ambient temperature and a further decrease towards lower temperatures has already been reported for other multinuclear Cr^{II} complexes in the literature and interpreted in terms of antiferromagnetic interactions between Cr^{II} centres.[32] Complexes related to tetranuclear $Cr_4(\mu\text{-}OSiEt_3)_8$ (**7**) are the chlorido-bridged $[Cr^{II}(\mu\text{-}Cl)(\mu\text{-}OSi\textit{t}Bu_3)]_4$ (rt: $1.1\mu_B$; 60 K: $0.3\mu_B$)[12] and $Cr^{II}_4(CH_2Si(CH_3)_3)_8$ (rt: $1.61\mu_B$, 2 K: $0.3\mu_B$),[29] displaying markedly lower magnetic moments. The strongly increased magnetic moment of tetrameric homo-bridged **7** compared to hetero-bridged $[Cr^{II}(\mu\text{-}Cl)(\mu\text{-}OSi\textit{t}Bu_3)]_4$ is particularly striking because the Cr⋯Cr distances in **7** are even comparatively smaller (avg. 2.679 *versus* 2.535 Å). These Cr⋯Cr distances are quite short and fall into the range of Cr–Cr single bonds (2.65–2.97 Å).[33,34] For further comparison, the type of bridging ligand (amido *versus* siloxy) was found to have a marked impact on chromous Cr⋯Cr distances and concomitantly any antiferromagnetic coupling, suggesting siloxy ligands as poorer mediators of magnetic exchange.[11]

Conclusions

Silylamine elimination reactions of amido complex $Cr[N(SiMe_3)_2]_2(thf)_2$ with silanols $HOSiR_3$ (R = Et, *i*Pr) generate chromous siloxides of variable nuclearity. The homoleptic siloxy-bridged complexes $Cr_3(OSi\textit{i}Pr_3)_2(\mu\text{-}OSi\textit{i}Pr_3)_4$ and $Cr_4(\mu\text{-}OSiEt_3)_8$ can be easily obtained by THF displacement from $Cr_2(OSi\textit{i}Pr_3)_2(\mu\text{-}OSi\textit{i}Pr_3)_2(thf)_2$ and $Cr_3(OSiEt_3)_2(\mu\text{-}OSiEt_3)_4(thf)_2$, respectively. Monomeric *cis*-$Cr(OSi\textit{i}Pr_3)(tmeda)$ can be obtained from $Cr_2(OSi\textit{i}Pr_3)_2(\mu\text{-}OSi\textit{i}Pr_3)_2(thf)_2$ *via* THF/TMEDA donor exchange. Treatment of $Cr_2(OSi\textit{i}Pr_3)_2(\mu\text{-}OSi\textit{i}Pr_3)_2(thf)_2$ with the halogenating oxidants CHI_3 and C_2Cl_6 led to the isolation of the chromic species $Cr(OSi\textit{i}Pr_3)_3(thf)_2$ and $Cr_2Cl_3(OSi\textit{i}Pr_3)_3(thf)_3$. A Takai-like halomethylidene species could not be observed. The obtained compounds considerably increase the scope of available Cr^{II} siloxides. The shortest $Cr\cdots Cr_{adjacent}$ distances were detected in tetranuclear $Cr_4(\mu\text{-}OSiEt_3)_8$ (avg. 2.535 Å), the longest ones in trinuclear $Cr_3(OSi\textit{i}Pr_3)_2(\mu\text{-}OSi\textit{i}Pr_3)_4$ (2.9611(6) Å). Magnetic measurements (Evans and SQUID) hinted at significant antiferromagnetic interactions in the $\{Cr_n\}$ complexes (n = 2, 3, 4). In accordance with a previous study, siloxy ligands seem to only weakly mediate magnetic exchange between the Cr^{II} centres.

Experimental section

General considerations

All manipulations were performed using a glovebox (MBraun UNIlab^{pro}ECO; <0.1 ppm O_2, <0.1 ppm H_2O), or Schlenk line techniques under an atmosphere of purified argon in oven dried glassware. Solvents (THF, *n*-hexane, *n*-pentane and toluene) were purified by Grubbs-type columns (MBraun SPS, solvent purification system), and stored in a glovebox. THF was further stored over 3 Å molecular sieves. Chromium(II) chloride was purchased from Abcr (99.99% pure, trace metal basis), and used as received. Iodoform was purchased from Sigma-Aldrich and sublimed before use. Hexamethyldisiloxane, hexamethyldisilazane, triethylsilanol and triisopropylsilanol were purchased from Sigma-Aldrich and used as received. $Cr[N(SiMe_3)_2]_2(thf)_2$ was synthesized according to a literature procedure.[22] The NMR spectra of air and moisture sensitive compounds were performed in pre-dried (over NaK alloy) benzene-d_6 or THF-d_8, with J. Young-valved NMR tubes. NMR spectra were recorded on a Bruker AVII+400 instrument (^{1}H: 400.13 MHz, ^{13}C: 100.16 MHz) at 26 °C. ^{1}H NMR measurements were performed with a scan range of 200 ppm (−100–100 ppm). ^{1}H shifts are referenced to a solvent resonance and reported in parts per million (ppm) relative to tetramethylsilane (TMS). Analyses of the NMR spectra were performed with Bruker TOPSPIN (version 3.6.1). IR spectra were recorded on a Thermo Fisher Scientific NICOLET 6700 FTIR ($\tilde{\nu}$ = 4000–400 cm^{-1}), using a DRIFT chamber with dry KBr/sample mixtures and KBr windows, and prepared in a glovebox. UV-Vis measurements were performed on a PG Instruments T60 UV-Vis spectrophotometer in *n*-hexane. Magnetic measurements according to the Evans method[30] were performed with samples in benzene/deuterated benzene and with hexamethyldisiloxane as a reference. The concentrations of the complexes in benzene solution ranged from 8–16 mg mL^{-1}. Additional measurements of the DC magnetic moment in solid samples were performed using the SQUID magnetometer Quantum Design MPMS-XL. The temperature dependence of the magnetic moment was determined between 2 K and 300 K in an applied magnetic field of 10 kOe. Additional field-dependent data were collected between −50 kOe and 50 kOe at a temperature of 2 K. The samples were supplied in powdered crystalline form and held by gelatine capsules packed into surrounding plastic straws. All sample containers showed a minor magnetic moment in the range of 10^{-5} emu in the temperature range between 2 K and 300 K at an applied field of 10 kOe. Continuous inert conditions were ensured by sample preparation in a glovebox under argon atmosphere and subsequent transfer to the magnetometer in an air-tight transport vessel. Elemental analysis (C, H, N) was performed on an Elementar vario MICRO cube.

Synthesis of $Cr_2(OSi\textit{i}Pr_3)_2(\mu\text{-}OSi\textit{i}Pr_3)_2(thf)_2$ (1)

Silanol $HOSi\textit{i}Pr_3$ (52.5 mg, 301 μmol) was added to a stirred violet solution of $Cr[N(SiMe_3)_2]_2(thf)_2$ (77.5 mg, 150 μmol) in ~2 mL THF. The colour changed to blue over several seconds.

After 18 h, the solvent was removed *in vacuo* giving **1** as a pale violet solid. Yield: 67.2 mg (71.4 μmol, 95%). Red-violet crystals suitable for XRD analysis were isolated from a dilute THF solution. ^{1}H NMR (THF-d_8): inconclusive due to strong paramagnetic broadening. DRIFT (KBr, cm^{-1}): 2940 (vs), 2887 (vs), 2863 (vs), 1458 (m), 1388 (w), 1362 (w), 1245 (w), 962 (m), 882 (m), 850 (m), 669 (m), 554 (w), 516 (w). Elemental analysis (%) calculated for $C_{44}H_{100}Cr_2O_6Si_4$ (941.61 g mol^{-1}): C 56.13, H 10.71. Found: C 55.98, H 10.35. UV–vis (*n*-hexane solution, λ_{max}, nm): 590.

Synthesis of $Cr_3(OSi\textit{i}Pr_3)_2(\mu\text{-}OSi\textit{i}Pr_3)_4$ (2)

Silanol HOSi*i*Pr$_3$ (100 mg, 574 μmol, 2 eq.) was added to a stirred blue solution of $Cr[N(SiMe_3)_2]_2(thf)_2$ (150 mg, 290 μmol) in ~5 mL *n*-pentane. The colour changed slowly to a lighter blue. After 2 h, the solution was dried under reduced pressure. The violet residue was then dissolved again in *n*-pentane, giving a blue solution. This process was repeated until no additional violet solid was formed. The viscous blue residue was then crystallized from *n*-pentane to give **2** as blue platelets. Yield: 100.8 mg (84.3 μmol, 87%). Blue crystals suitable for XRD analysis were isolated from a diluted *n*-pentane solution. ^{1}H NMR (benzene-d_6): δ 2.17 (broad, s) ppm. DRIFT (KBr, cm^{-1}): 2959 (vs), 2939 (vs), 2887 (s), 2863 (vs), 1457 (m), 1387 (w), 1252 (w), 1010 (w), 988 (m), 961 (m), 915 (m), 883 (s), 852 (s), 694 (s), 676 (s), 653 (m), 587 (w), 516 (w). Elemental analysis (%) calculated for $C_{54}H_{126}Cr_3O_6Si_6$ (1196.09 g mol^{-1}): C 54.23, H 10.62; found: C 53.66, H 10.25. UV–vis (*n*-hexane solution, λ_{max}, nm): 727.

Synthesis of $Cr(OSi\textit{i}Pr_3)_2(tmeda)$ (3)

TMEDA (2 mg, 17.2 μmol) was added to a stirred blue solution of (9.8 mg, 8.2 μmol) $Cr_3(OSi\textit{i}Pr_3)_2(\mu\text{-}OSi\textit{i}Pr_3)_4$ (**2**) in ~2 mL *n*-pentane. A bright purple crystalline solid was formed over seconds. The supernatant was discarded and the solid dried under reduced pressure. Yield: 8.9 mg (17.3 μmol, 83%). Bright purple crystals suitable for XRD analysis were isolated from a diluted TMEDA/*n*-pentane mixture. ^{1}H NMR (THF-d_8): inconclusive due to very strong paramagnetic broadening. DRIFT (KBr, cm^{-1}): 2934 (vs), 2883 (s), 2855 (vs), 1464 (m), 1006 (s), 971 (m), 885 (w), 800 (w), 664 (m), 637 (w), 570 (w), 524 (w). Elemental analysis (%) calculated for $C_{24}H_{58}CrN_2O_2Si_2$ (514.91 g mol^{-1}): C 55.98, H 11.25, N 5.44; found: C 55.29, H 11.05, N 5.26. UV–vis (*n*-hexane solution, λ_{max}, nm): 508.

Synthesis of $Cr(OSi\textit{i}Pr_3)_3(thf)_2$ (4)

CHI_3 (8 mg, 20.3 μmol) dissolved in 1 mL THF was added to a stirred blue solution of $Cr_2(OSi\textit{i}Pr_3)_2(\mu\text{-}OSi\textit{i}Pr_3)_2(thf)_2$ (**1**) (56.7 mg, 60.2 μmol) in 1 mL THF. The colour of the solution changed to dark yellow immediately. The solution was dried under reduced pressure, the residue extracted with *n*-pentane and filtered. Crystallization from toluene at −35 °C gives green plates of $Cr(OSi\textit{i}Pr_3)_3(thf)_2$ (**4**). The yield could not be determined due to impurities.

Synthesis of $Cr_2Cl_3(OSi\textit{i}Pr_3)_3(thf)_3$ (5)

$Cr_2(OSi\textit{i}Pr_3)_2(\mu\text{-}OSi\textit{i}Pr_3)_2(thf)_2$ (**1**) (50 mg, 53.1 μmol) in ~2 mL THF was reacted with C_2Cl_6 (12 mg, 50.7 μmol) at −40 °C. The colour changed immediately from violet to red-violet. The solution was stirred for 30 min, warmed to ambient temperature and dried *in vacuo*. After removing the solvent, the red residue was extracted with *n*-pentane giving a red-violet solution. Crystallization from *n*-pentane with small amounts of THF yielded purple blocks of **5**. Yield: 24 mg (25.4 μmol 48%). ^{1}H NMR (THF-d_8): δ 2.45 (broad, s) ppm. Elemental analysis (%) calculated for $C_{24}H_{58}CrN_2O_2Si_2$ (514.91 g mol^{-1}): C 49.48, H 9.26; found: C 49.58, H 9.21.

Synthesis of $Cr_3(OSiEt_3)_2(\mu\text{-}OSiEt_3)_4(thf)_2$ (6)

Silanol $HOSiEt_3$ (42.5 mg, 321.3 μmol) was added to a stirred bright violet solution of $Cr[N(SiMe_3)_2]_2(thf)_2$ (81.5 mg, 157.6 μmol) in ~2 mL THF. The colour changed immediately to red violet. After 18 h, the solvent was removed *in vacuo* giving **6** as a pale red solid. The red violet residue was redissolved in THF and stored at −35 °C for crystallization, yielding red violet crystals suitable for XRD analysis. Yield: 56.7 mg (52.1 μmol, 99%). ^{1}H NMR (benzene-d_6): inconclusive due to strong paramagnetic broadening. DRIFT (KBr, cm^{-1}): 2949 (vs), 2906 (vs), 2875 (vs), 1458 (m), 1415 (w), 1378 (vw), 1236 (m), 1009 (vs), 964 (s), 870 (vs), 740 (vs), 729 (vs), 667 (m), 506 (m). Elemental analysis (%) calculated for $C_{44}H_{106}Cr_3O_8Si_6$ (1087.82 g mol^{-1}): C 48.58, H 9.82; found: C 47.87, H 9.54. UV–vis (*n*-hexane solution, λ_{max}, nm): 360 (sh): 380 (sh), 410 (sh), 528, 664.

Synthesis of $Cr_4(\mu\text{-}OSiEt_3)_8$ (7)

$Cr_3(OSiEt_3)_2(\mu\text{-}OSiEt_3)_4(thf)_2$ (**6**) (81.7 mg 75.1 μmol) was dissolved in 2 mL of *n*-pentane. The solution changed colour to a dark orange red. After stirring for 30 minutes at ambient temperature, the solvent was removed under reduced pressure and the orange red solid redissolved in *n*-pentane. After three to six repetitions of this process, **7** was crystallized from *n*-pentane at −35 °C as red-brown crystals suitable for XRD analysis. Yield: 65.9 mg (56.3 μmol, 93%). DRIFT (KBr, cm^{-1}): 2953 (vs), 2909 (s), 2876 (vs), 1457 (m), 1417 (w), 1237 (m), 1015 (s), 894 (s), 869 (s), 738 (vs), 667 (m), 484 (m). Elemental analysis (%) calculated for $C_{48}H_{120}Cr_4O_8Si_8$ (1258.14 g mol^{-1}): C 45.82, H 9.61; found: C 46.07, H 9.80. ^{1}H NMR (benzene-d_6): δ 1.25 (broad, s), 0.87 (s), 0.07 (s) ppm. UV–vis (*n*-hexane solution, λ_{max}, nm): 340, 361, 380, 400 (sh), 425 (sh), 450 (sh), 520, 580, 600.

Synthesis of $Na_4Cr_2(OSiEt_3)_8$ (8)

Note: Bimetallic complex $Na_4Cr_2(OSiEt_3)_8$ (**8**) was originally obtained as an adventitious impurity in reactions of $Cr[N(SiMe_3)_2]_2(thf)_2$ with $HOSiEt_3$ in THF. As a likely explanation for the formation of **8** we assumed contamination of the chromous silylamide with small amounts of ate complex $Na(thf)Cr[N(SiMe_3)_2]_3$. To target a higher yield of **8** the following one-pot experimental approach was pursued.

To a suspension of $CrCl_2$ (10.5 mg, 85.4 μmol) in 2 mL THF a solution of $NaN(SiMe_3)_2$ (31.5 mg, 171.8 μmol) in 2 mL THF was added. The suspension changed colour from grey to turbid violet. After stirring for 1 h at ambient temperature, $HOSiEt_3$ (22.6 mg, 170.9 mmol) was added. The clear red-violet

solution was stirred for 1 h and afterwards the solvent removed *in vacuo*. Repeated dissolution of the red-brown residue in *n*-pentane and removal of the solvent gave a brown residue. Crystallization from *n*-pentane at −35° yielded **8** (9.5 mg, 7.6 μmol, 18%) as red-brown rhombic crystals suitable for XRD analysis. ^{1}H NMR (benzene-d_6): inconclusive due to strong paramagnetic broadening. DRIFT (KBr, cm^{-1}): 2954 (vs), 2908 (vs), 2876 (vs), 2729 (vw), 1458 (m), 1414(w), 1378 (vw), 1237 (m), 1072 (vw), 1014 (m), 917 (s), 714 (s), 659 (w), 480 (m), 443 (w) cm^{-1}. Elemental analysis (%) calculated for $C_{48}H_{120}Cr_2Na_4O_8Si_8$ (1246.11 g mol^{-1}): C 46.27, H 9.71; found: C 46.51, H 9.68. UV–vis (*n*-hexane solution, λ_{max}, nm): 340, 360, 380, 400 (sh), 425 (sh), 450 (sh), 510, 580, 600.

X-ray crystallography and crystal structure determinations

Crystals for XRD analysis were grown using saturated solutions of toluene, THF, TMEDA, *n*-hexane or *n*-pentane. Crystals suitable for XRD analysis were selected inside a glovebox and coated with Parabar 10312 (previously known as Paratone N, Hampton Research) and fixed on a microloop. X-ray data were collected on a Bruker APEX II DUO instrument equipped with an IμS microfocus sealed tube and QUAZAR optics for MoK$_\alpha$ (λ = 0.71073 Å) radiation. The data collection strategy was determined using COSMO[35] employing ω-scans. Raw data were processed using APEX[36] and SAINT,[37] corrections for absorption effects were applied using SADABS.[38] The structures were solved by direct methods and refined against all data by full-matrix least-squares methods on F^2 using SHELXTL[39] and SHELXLE.[40] All graphics were produced employing CSD Mercury 4.1.0.[25] Disorder models are calculated using DSR,[41] a program included in SHELXLE, for refining disorder models. Further details regarding the refinement and crystallographic data are listed in Table S1† and in the CIF files. CCDC depositions and contain all the supplementary crystallographic data for this paper.

Conflicts of interest

There are no conflicts to declare.

Acknowledgements

We gratefully acknowledge support from the German Science Foundation (Grant: AN 238/15-2).

Notes and references

1 C. Krempner, *Eur. J. Inorg. Chem.*, 2011, 1689–1698.
2 F. Schindler and H. Schmidbaur, *Angew. Chem., Int. Ed. Engl.*, 1967, **6**, 683–694.
3 M. Schmidt and H. Schmidbaur, *Angew. Chem.*, 1958, **70**, 704.
4 B. Stensland and P. Kierkegaard, *Acta Chim. Scand.*, 1970, **24**, 211–220.
5 E. C. Alyea, J. S. Basi, D. C. Bradley and M. H. Chisholm, *J. Chem. Soc. A*, 1971, 772–776.
6 O. L. Sydora, D. S. Kuiper, P. T. Wolczanski, E. B. Lobkovsky, A. Dinescu and T. R. Cundari, *Inorg. Chem.*, 2006, **45**, 2008–2021.
7 M. P. Conley, M. F. Delley, G. Siddiqi, G. Lapadula, S. Norsic, V. Monteil, O. V. Safonova and C. Copéret, *Angew. Chem., Int. Ed.*, 2014, **53**, 1872–1876.
8 K. W. Terry, P. K. Gantzel and T. D. Tilley, *Inorg. Chem.*, 1993, **32**, 5402–5404.
9 P. Qiu, R. Cheng, B. Liu, B. Tumanskii, R. J. Batrice, M. Botoshansky and M. S. Eisen, *Organometallics*, 2011, **30**, 2144–2148.
10 D. Werner and R. Anwander, *J. Am. Chem. Soc.*, 2018, **140**, 14334–14341.
11 F. Haftbaradaran, G. Mund, R. J. Batchelor, J. F. Britten and D. B. Leznoff, *Dalton Trans.*, 2005, 2343–2345.
12 O. L. Sydora, P. T. Wolczanski, E. B. Lobkovsky, C. Buda and T. R. Cundari, *Inorg. Chem.*, 2005, **44**, 2606–2618.
13 D. Trummer, K. Searles, A. Algasov, S. A. Guda, A. V. Soldatov, H. Ramanantoanina, O. V. Safonova, A. A. Guda and C. Copéret, *J. Am. Chem. Soc.*, 2021, **143**, 7326–7341.
14 M. P. Marshak and D. G. Nocera, *Inorg. Chem.*, 2013, **52**, 1173–1175.
15 S. Groysman, D. Villagrán and D. G. Nocera, *Inorg. Chem.*, 2010, **49**, 10759–10761.
16 H. Lam, G. Wilkinson, B. Hussain-Bates and M. B. Hursthouse, *J. Chem. Soc., Dalton Trans.*, 1993, 1477–1482.
17 A. L. Odom, D. J. Mindiola and C. C. Cummins, *Inorg. Chem.*, 1999, **38**, 3290–3295.
18 M. P. McDaniel, *Adv. Catal.*, 2010, **53**, 123–606; E. Groppo, C. Lamberti, S. Bordiga, G. Spoto and A. Zecchina, *Chem. Rev.*, 2005, **105**, 115–184.
19 (*a*) M. J. Lamb, D. C. Apperley, M. J. Watson and P. W. Dyer, *Top. Catal.*, 2018, **61**, 213–224; (*b*) P. Qiu, R. Cheng, Z. Liu, B. Liu, B. Tumanskii and M. S. Eisen, *J. Organomet. Chem.*, 2012, **699**, 48–55; (*c*) J. Zhang, P. Qiu, Z. Liu, B. Liu, R. J. Batrice, M. Botoshansky and M. S. Eisen, *ACS Catal.*, 2015, **5**, 3562–3574.
20 (*a*) F. Schax, E. Bill, C. Herwig and C. Limberg, *Angew. Chem., Int. Ed.*, 2014, **53**, 12741–12745; (*b*) F. Schax, S. Suhr, E. Bill, B. Braun, C. Herwig and C. Limberg, *Angew. Chem., Int. Ed.*, 2015, **54**, 1352–1356; (*c*) M.-L. Wind, S. Hoof, B. Braun-Cula, C. Herwig and C. Limberg, *J. Am. Chem. Soc.*, 2019, **141**, 14068–14072.
21 (*a*) S. N. König, C. Maichle-Mössmer, K. W. Törnroos and R. Anwander, *Z. Naturforsch., B: J. Chem. Sci.*, 2014, **69**, 1375–1383; (*b*) S. N. König, PhD thesis, Eberhard Karls Universität Tübingen, 2014.
22 D. C. Bradley, M. B. Hursthouse, C. W. Newing and A. J. Welch, *J. Chem. Soc., Chem. Commun.*, 1972, 567–568.
23 R. R. Fraser, T. S. Mansour and S. Savard, *J. Org. Chem.*, 1985, **50**, 3232–3234.

24 C. F. Macrae, I. Sovago, S. J. Cottrell, P. T. A. Galek, P. McCabe, E. Pidcock, M. Platings, G. P. Shields, J. S. Stevens, M. Towler and P. A. Wood, *J. Appl. Crystallogr.*, 2020, **53**, 226–235.
25 (*a*) M. Murai, R. Taniguchi, N. Hosokawa, Y. Nishida, H. Mimachi, T. Oshiki and K. Takai, *J. Am. Chem. Soc.*, 2017, **139**, 13184–13192; (*b*) M. Murai, R. Taniguchi, T. Kurogi, M. Shunsuke and K. Takai, *Chem. Commun.*, 2020, **56**, 9711–9714; (*c*) T. Kurogi, K. Irifune, T. Enoki and K. Takai, *Chem. Commun.*, 2021, **57**, 5199–5202.
26 A. Ciborska, J. Chojnacki and W. Wojnowski, *Acta Crystallogr., Sect. E: Struct. Rep. Online*, 2007, **63**, m1103–m1104.
27 (*a*) P. D. Smith and E. T. Hsieh, *U.S. Patent* 4587227, 1986; (*b*) P. D. Smith and M. P. McDaniel, *J. Polym. Sci., Part A: Polym. Chem.*, 1990, **28**, 3587–3601.
28 C. Schulzke, D. Enright, H. Sugiyama, G. LeBlanc, S. Gambarotta, G. P. A. Yap, L. K. Thompson, D. R. Wilson and R. Duchateau, *Organometallics*, 2002, **21**, 3810–3816.
29 S. N. König, D. Schneider, C. Maichle-Mössmer, B. M. Day, R. A. Layfield and R. Anwander, *Eur. J. Inorg. Chem.*, 2014, **2014**, 4302–4309.
30 D. F. Evans, *J. Chem. Soc.*, 1959, 2003–2005.
31 G. A. Bain and J. F. Berry, *J. Chem. Educ.*, 2008, **85**, 532–536.
32 M. M. Levitsky, A. N. Bilyachenko, E. S. Shubina, J. Long, Y. Guari and J. Larionova, *Coord. Chem. Rev.*, 2019, **398**, 213015.
33 D. S. Richeson, S. W. Hsu, N. H. Fredd, G. van Duyne and K. H. Theopold, *J. Am. Chem. Soc.*, 1986, **108**, 8273–8274.
34 J. J. H. Edema and S. Gambarotta, *Comments Inorg. Chem.*, 1991, **4**, 195–214.
35 *COSMOv. 1.61*, Bruker AXS Inc., Madison, WI, 2012.
36 (*a*) *APEX2 V. 2012.10_0*, Bruker AXS Inc., Madison, WI, 2012; (*b*) *APEX3, V. 2016.5–0*, Bruker AXS Inc., Madison, WI, 2016.
37 *SAINT v. 8.34A*, Bruker AXS Inc., Madison, WI, 2013.
38 L. Krause, R. Herbst-Irmer, G. M. Sheldrick and D. Stalke, SADABS, *J. Appl. Crystallogr.*, 2015, 3–10.
39 G. M. Sheldrik, *Acta Crystallogr., Sect. C: Struct. Chem.*, 2015, 3–8.
40 C. B. Hübschle, G. M. Sheldrick and B. Dittrich, SHELXLE, ShelXle: a Qt graphical user interface for SHELXL, *J. Appl. Crystallogr.*, 2011, 1281–1284.
41 D. Kratzert, J. J. Holstein and I. Krossing, DSR: enhanced modelling and refinement of disordered structures with SHELXL, *J. Appl. Crystallogr.*, 2015, 933–938.

Supporting Information

Chromous siloxides of variable nuclearity and magnetism

Simon P. O. Trzmiel,[a] Jan Langmann,[b] Cäcilia Maichle-Mössmer,[a] and Reiner Anwander[a,*]

a) Institut für Anorganische Chemie, Eberhard Karls Universität Tübingen, Auf der Morgenstelle 18, 72076 Tübingen, Germany

b) Institut für Physik, Universität Augsburg, Universitätsstr. 1, 86159 Augsburg, Germany

*E-mail for R. A.: reiner.anwander@uni-tuebingen.de

Table of Contents

Magnetic Measurements

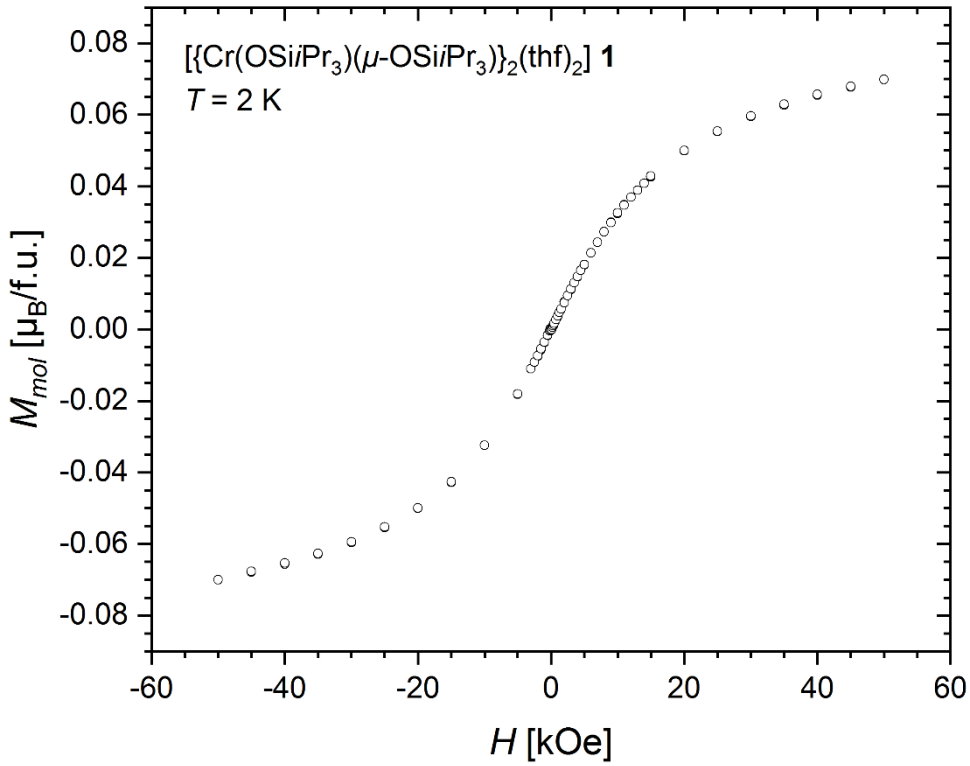

Figure S1. Field-dependent molar magnetization $M_{mol}(H)$ (black open circles) as obtained by SQUID magnetic measurements on crystalline powder of **1** at a temperature T = 2 K.

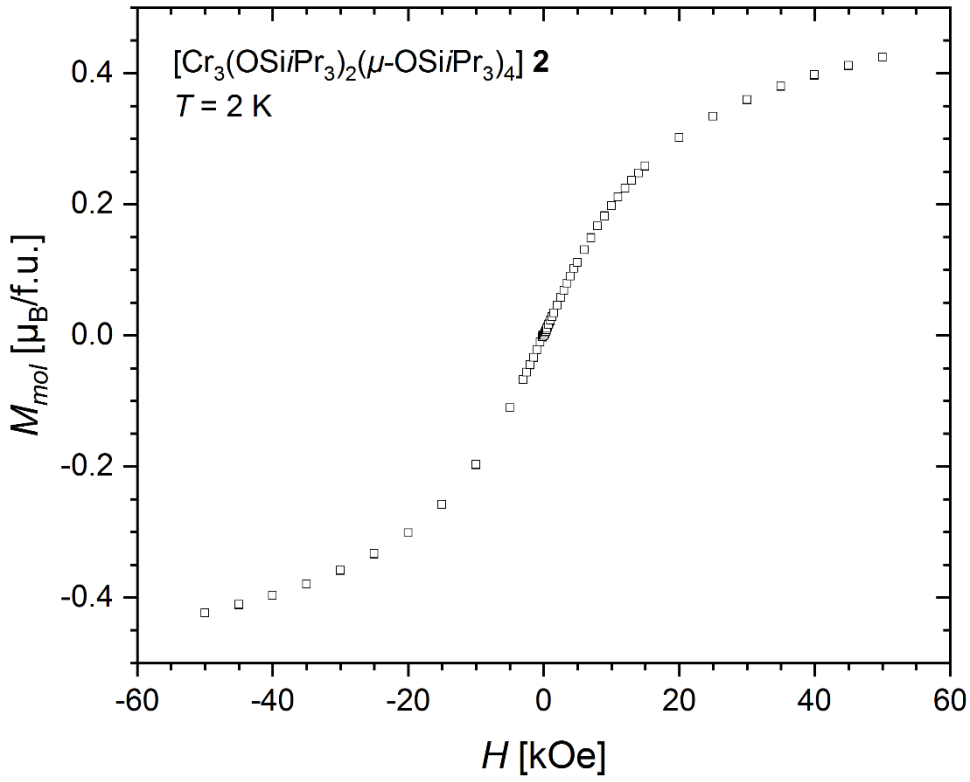

Figure S2. Field-dependent molar magnetization $M_{mol}(H)$ (black open circles) as obtained by SQUID magnetic measurements on crystalline powder of **2** at a temperature T = 2 K.

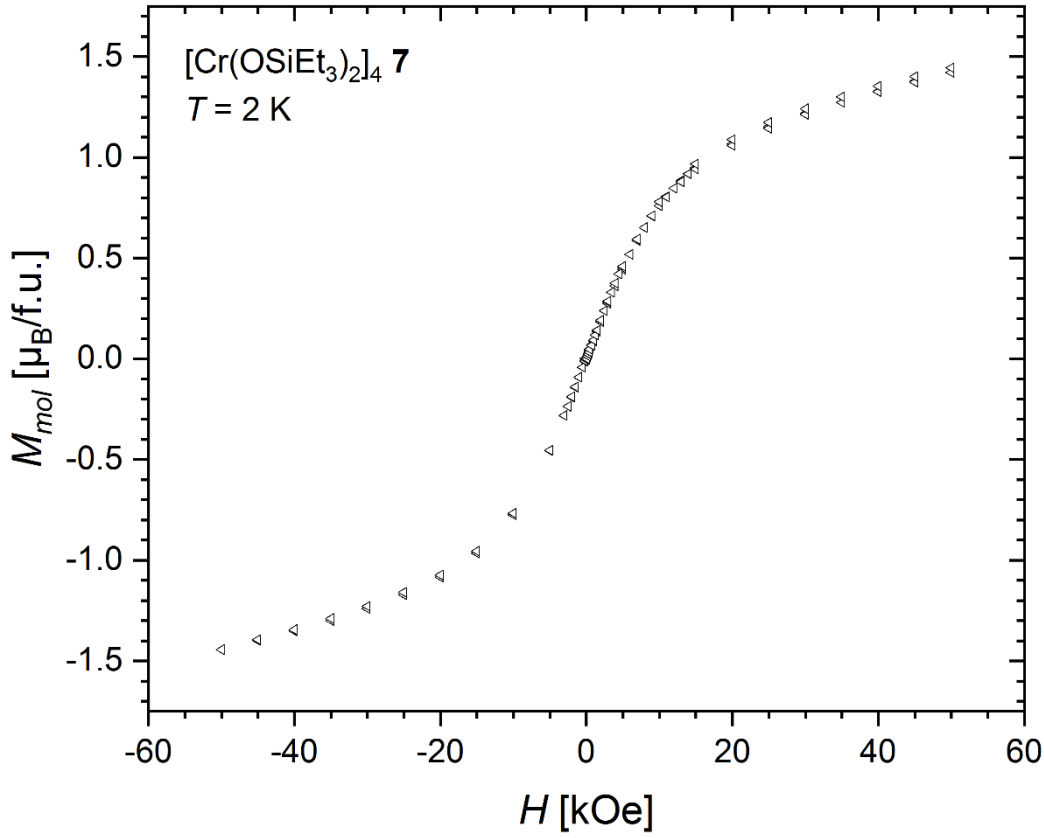

Figure S3. Field-dependent molar magnetization $M_{mol}(H)$ (black open circles) as obtained by SQUID magnetic measurements on crystalline powder of **7** at a temperature T = 2 K.

NMR Spectra

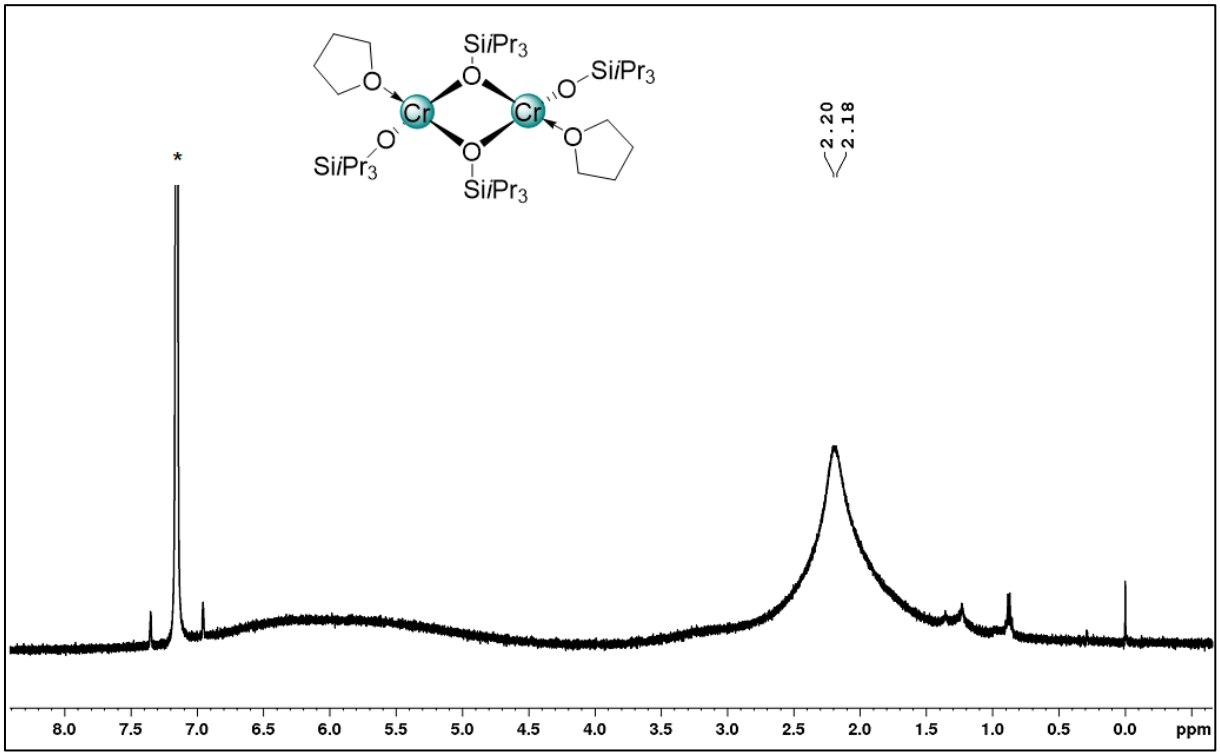

Figure S4. ^{1}H NMR spectrum (26 °C, 400.13 MHz, benzene-d_6) of $Cr_2(OSi{i}Pr_3)_2(\mu\text{-}OSi{i}Pr_3)_2(thf)_2$ (**1**).

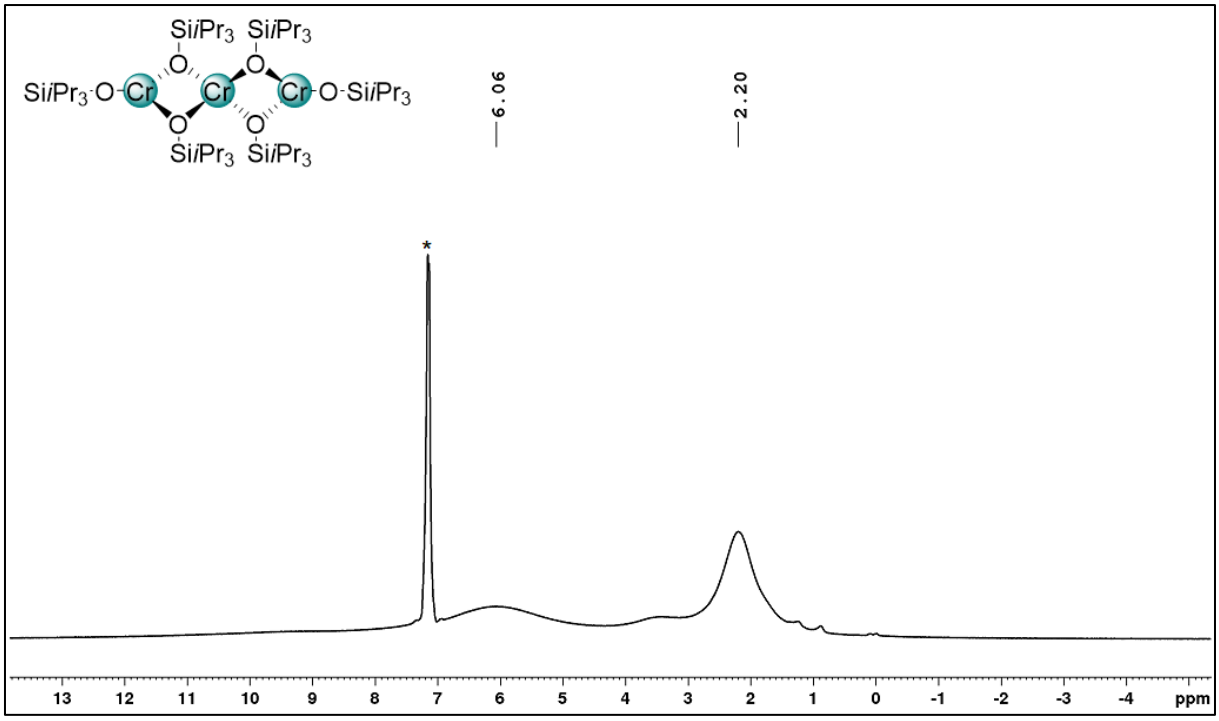

Figure S5. ^{1}H NMR spectrum (26 °C, 400.13 MHz, benzene-d_6) of $Cr_3(OSi{i}Pr_3)_2(\mu\text{-}OSi{i}Pr_3)_4$ (**2**).

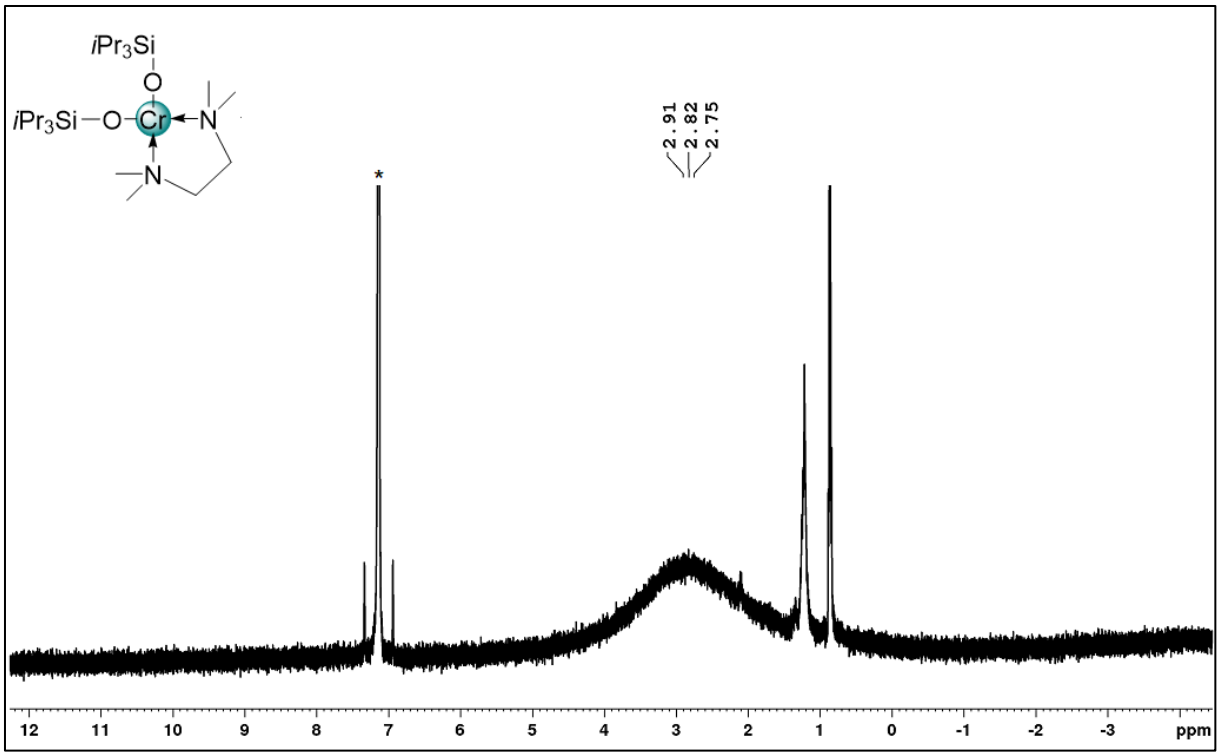

Figure S6. ^{1}H NMR spectrum (26 °C, 400.13 MHz, benzene-d_6) of Cr(OSi*i*Pr$_3$)$_2$(tmeda) (**3**).

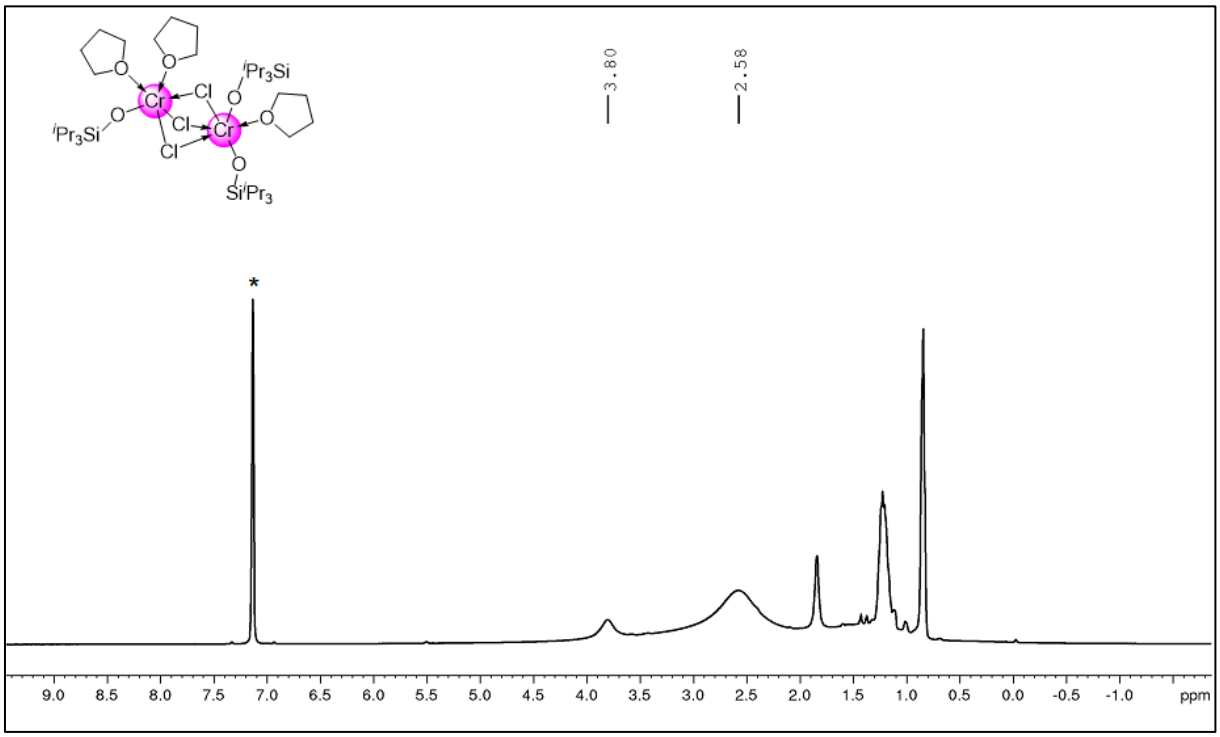

Figure S7. ^{1}H NMR spectrum (26 °C, 400.13 MHz, benzene-d_6) of $Cr_2Cl_3(OSiiPr_3)_3(thf)_3$ (**5**).

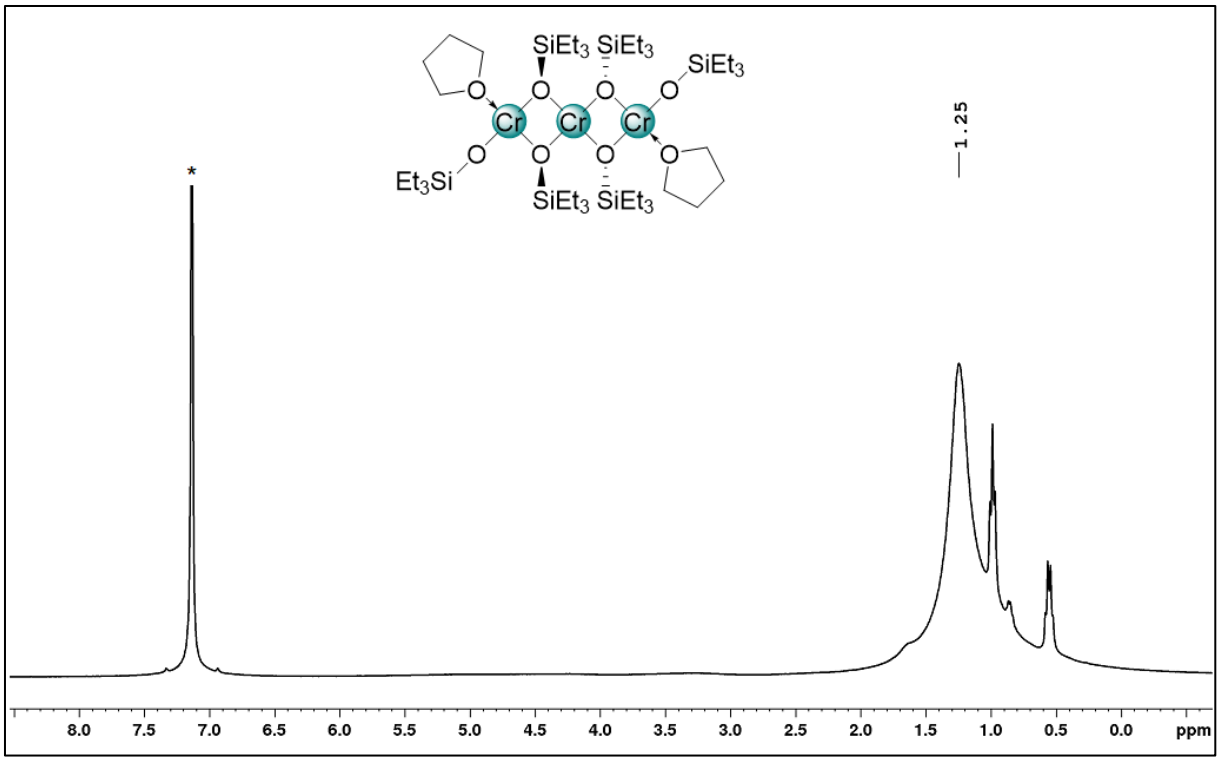

Figure S8. ^{1}H NMR spectrum (26 °C, 400.13 MHz, benzene-d_6) of $Cr_3(OSiEt_3)_2(\mu\text{-}OSi\textit{Et}_3)_4(thf)_2$ (**6**).

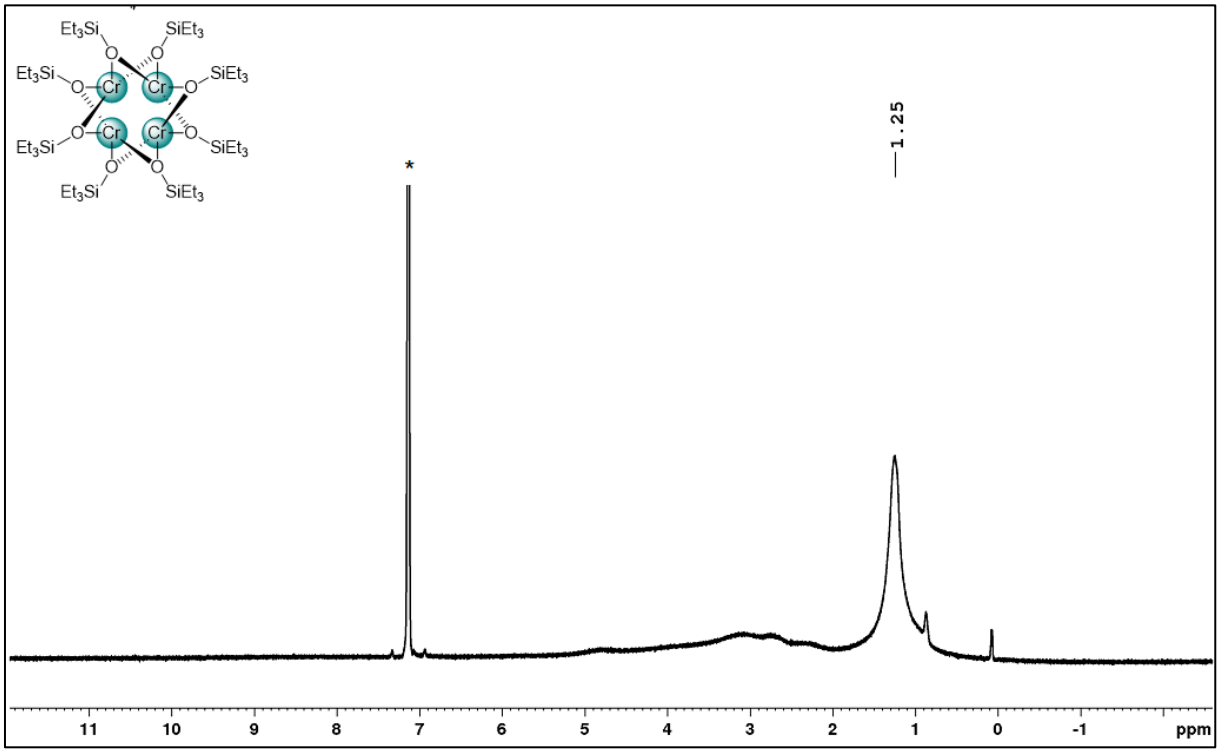

Figure S9. ^{1}H NMR spectrum (26 °C, 400.13 MHz, benzene-d_6) of $Cr_4(OSiEt_3)_8$ (**7**).

IR Spectra

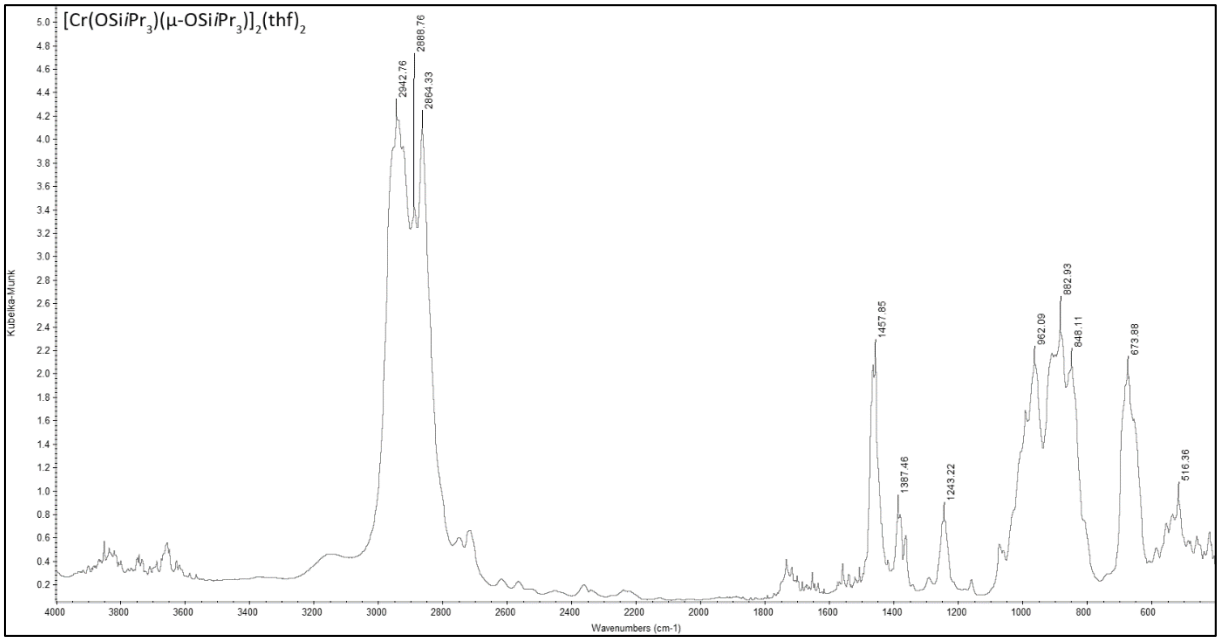

Figure S10. DRIFT spectrum of compound **1** measured on KBr.

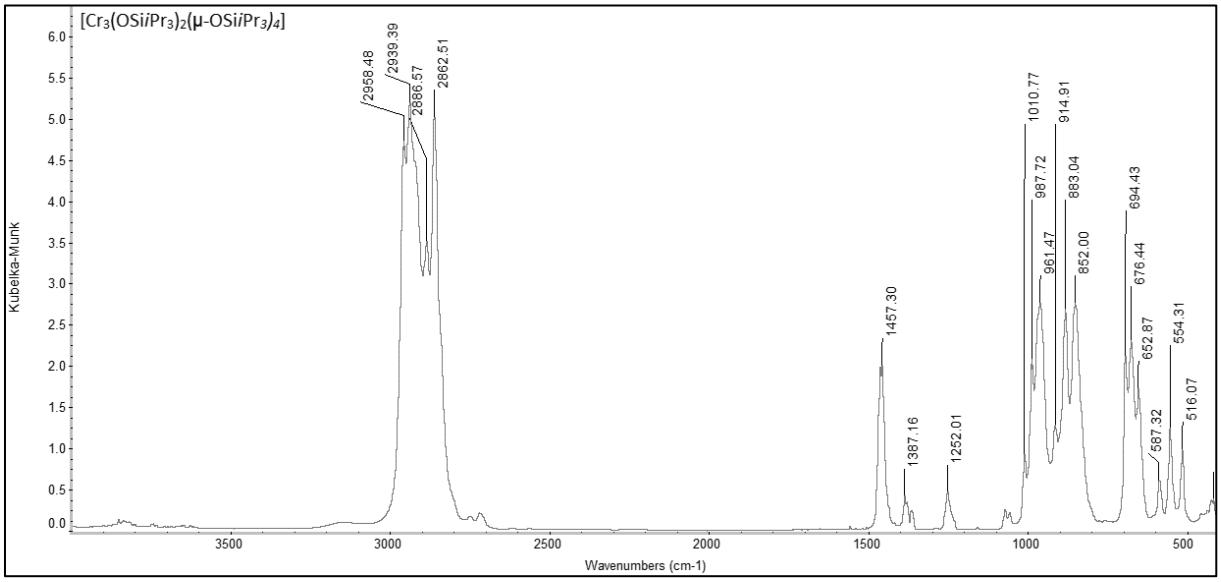

Figure S11. DRIFT spectrum of compound **2** measured on KBr.

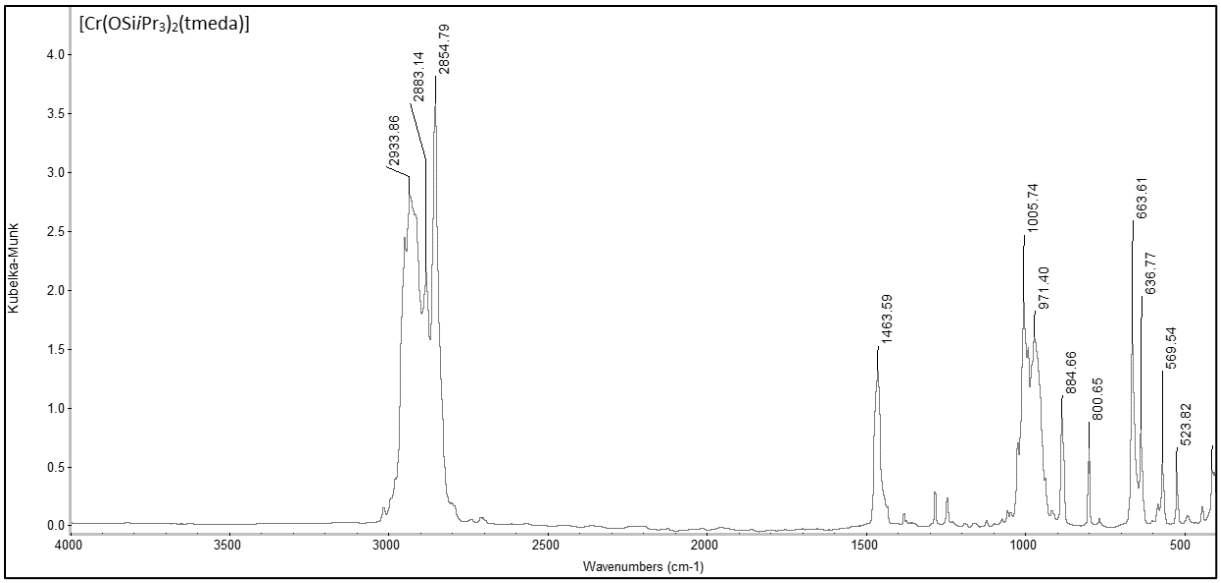

Figure S12. DRIFT spectrum of compound **3** measured on KBr.

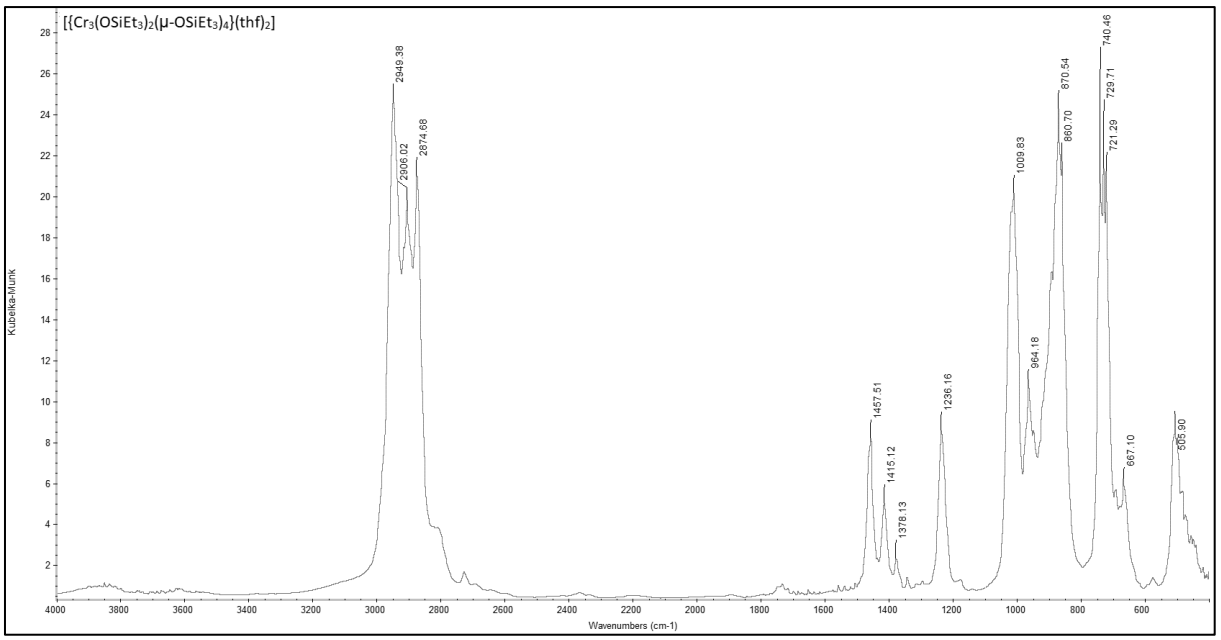

Figure S13. DRIFT spectrum of compound **6** measured on KBr.

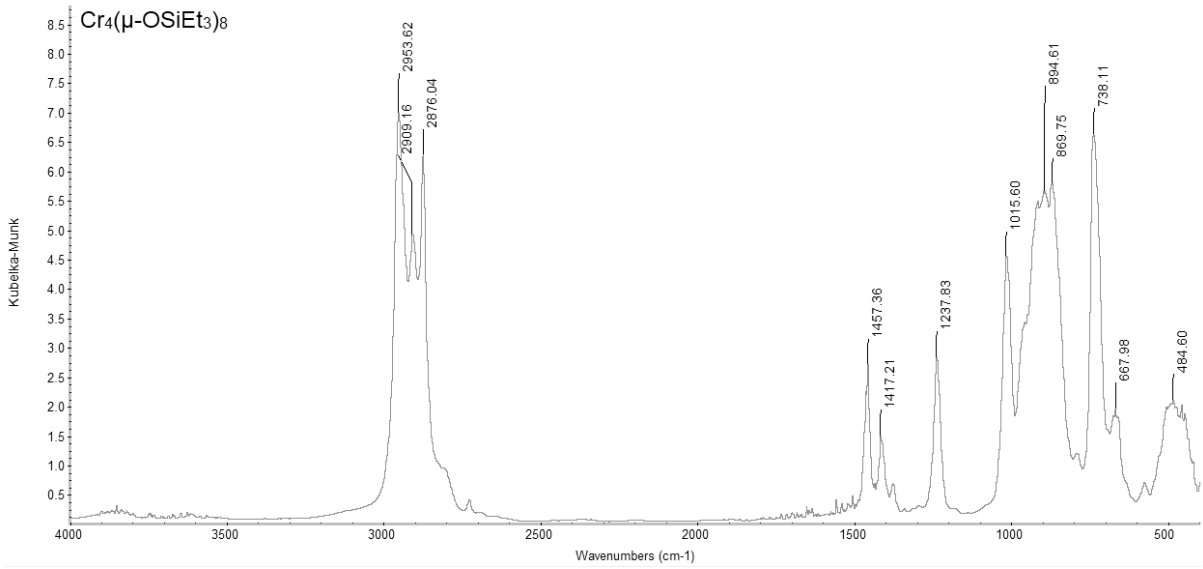

Figure S14. DRIFT spectrum of compound **7** measured on KBr.

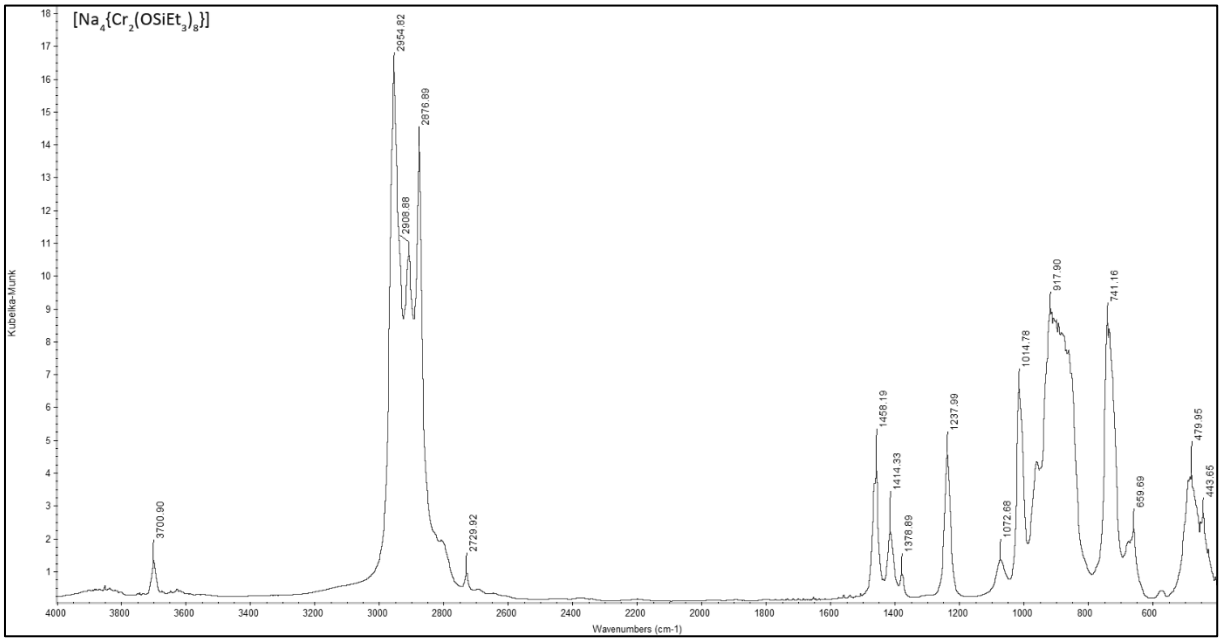

Figure S15. DRIFT spectrum of compound **8** measured on KBr.

UV-vis Spectra

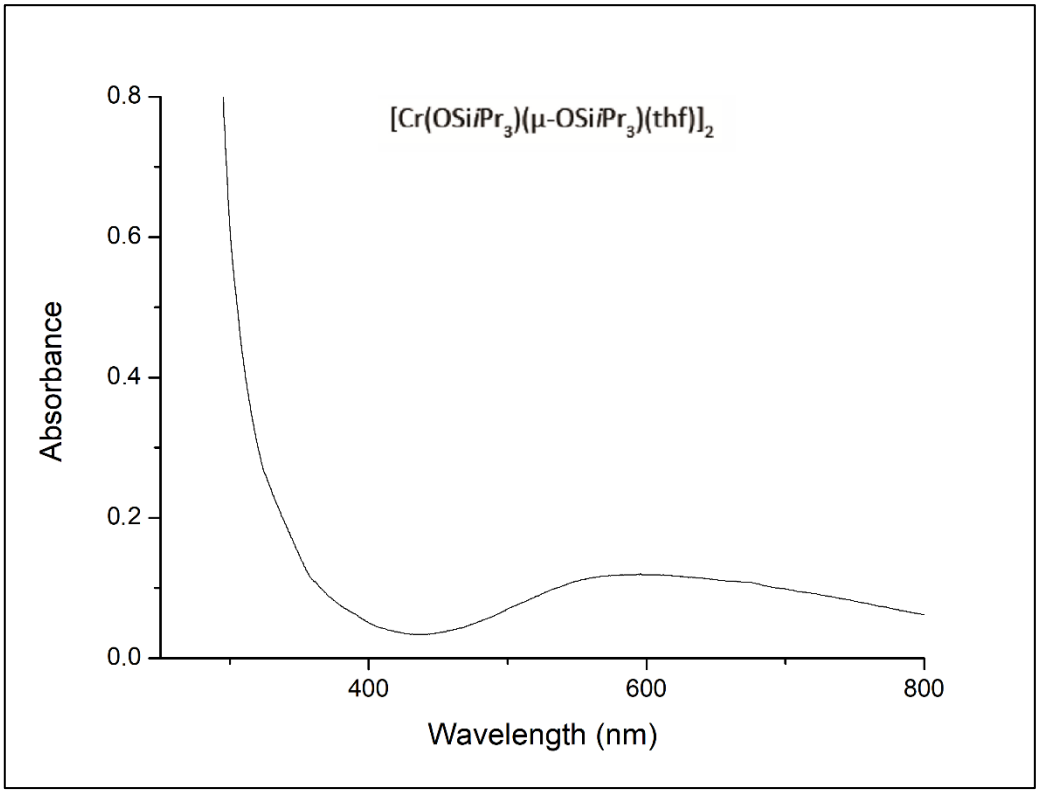

Figure S16. UV-vis spectrum of compound **1** in dilute *n*-hexane solution (concentration c = $4.9*10^{-6}$ [mol*L^{-1}], ε_{590}= $2.4*10^4$ L*mol^{-1}*cm^{-1}).

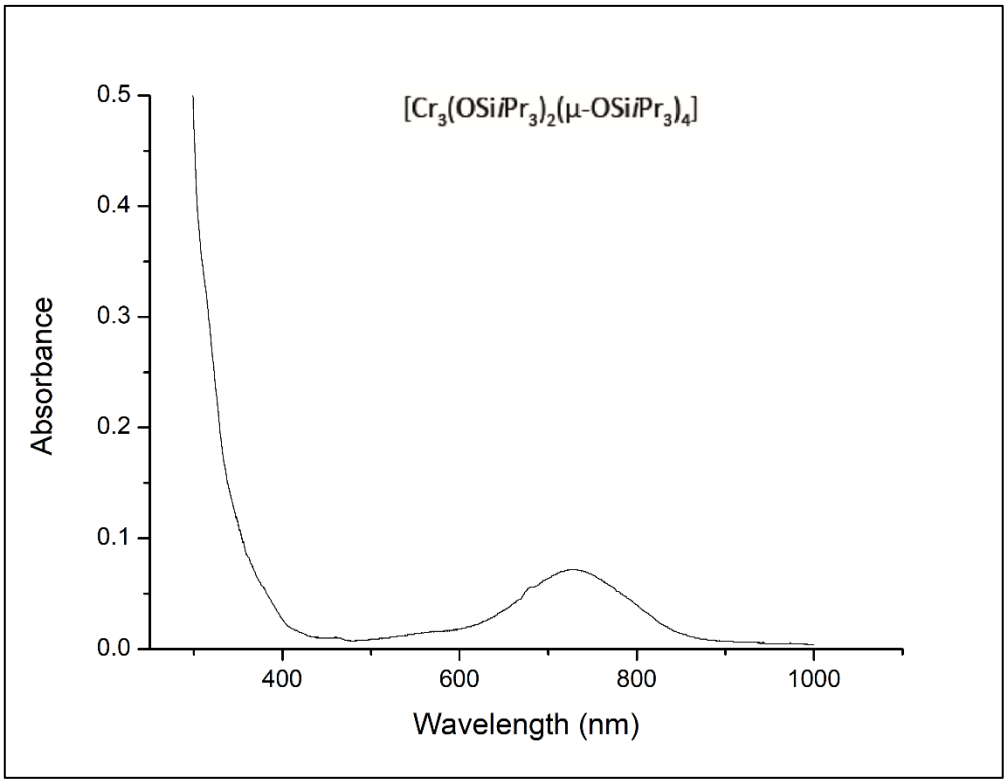

Figure S17. UV-vis spectrum of compound **2** in dilute *n*-hexane solution (c = $3.9*10^{-6}$ [mol*L^{-1}], ε_{727}= $1.8*10^4$ L*mol^{-1}*cm^{-1}).

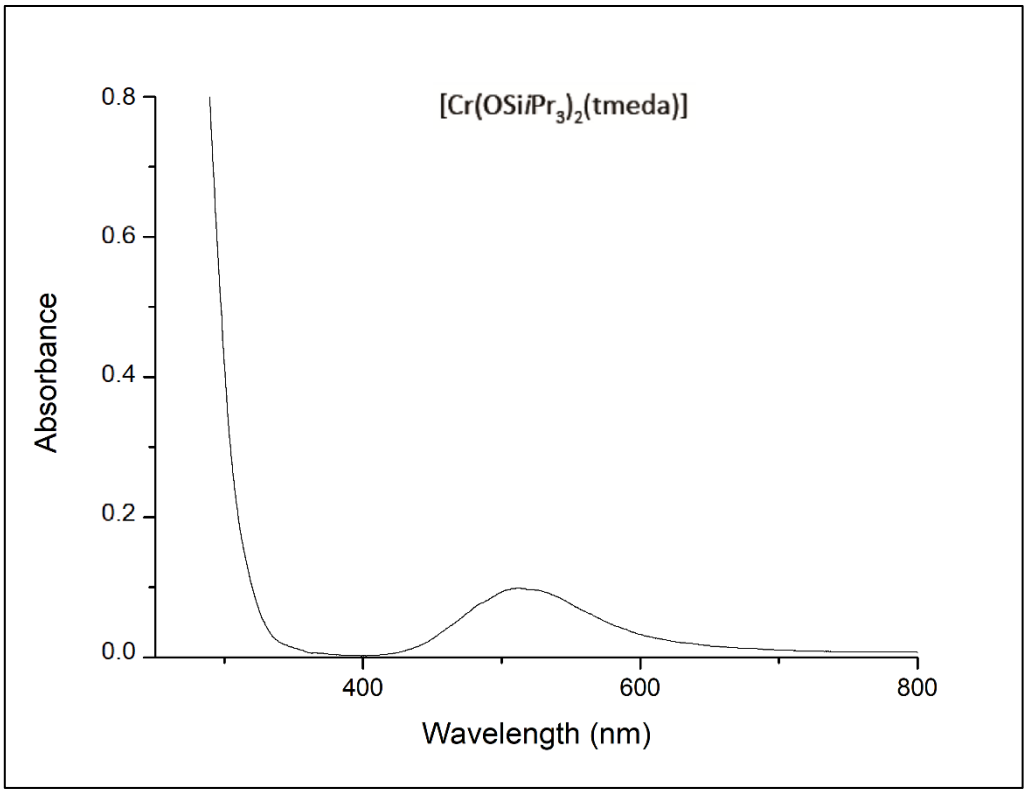

Figure S18. UV-vis spectrum of compound **3** in dilute *n*-hexane solution (concentration c = $2.2*10^{-5}$ [mol*L^{-1}], ε_{508}= $4.3*10^{4}$ L*mol^{-1}*cm^{-1}).

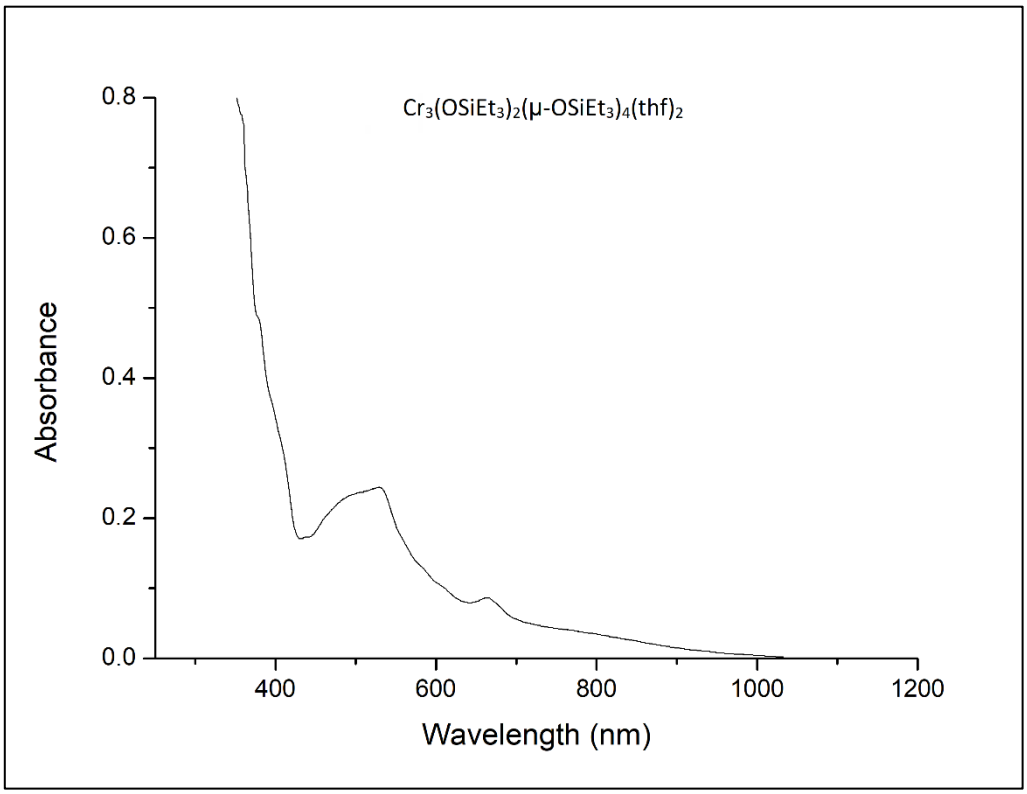

Figure S19. UV-vis spectrum of compound **6** in dilute *n*-hexane solution (concentration c = $1.1*10^{-5}$ [mol*L^{-1}], ε_{528}= $2.2*10^{4}$ L*mol^{-1}*cm^{-1}).

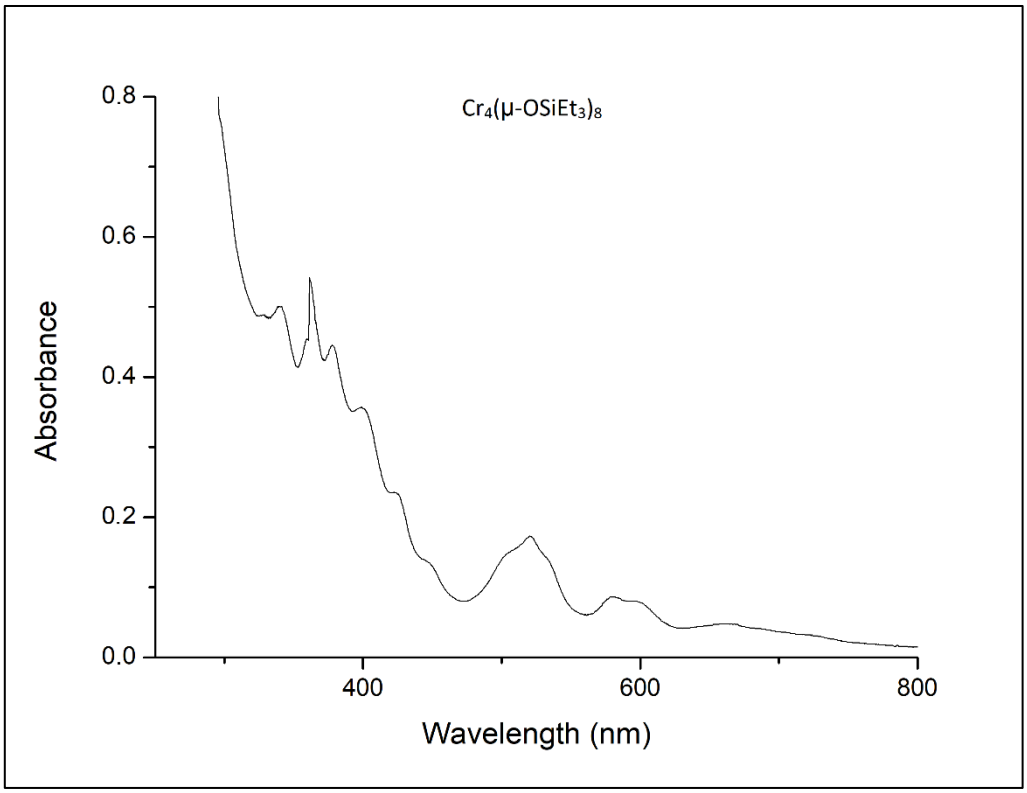

Figure S20. UV-vis spectrum of compound **7** in dilute *n*-hexane solution (concentration c = $6.2*10^{-6}$ [mol*L^{-1}], ε_{520}= $2.7*10^{4}$ ε_{361}= $8.7*10^{4}$ L*mol^{-1}*cm^{-1}).

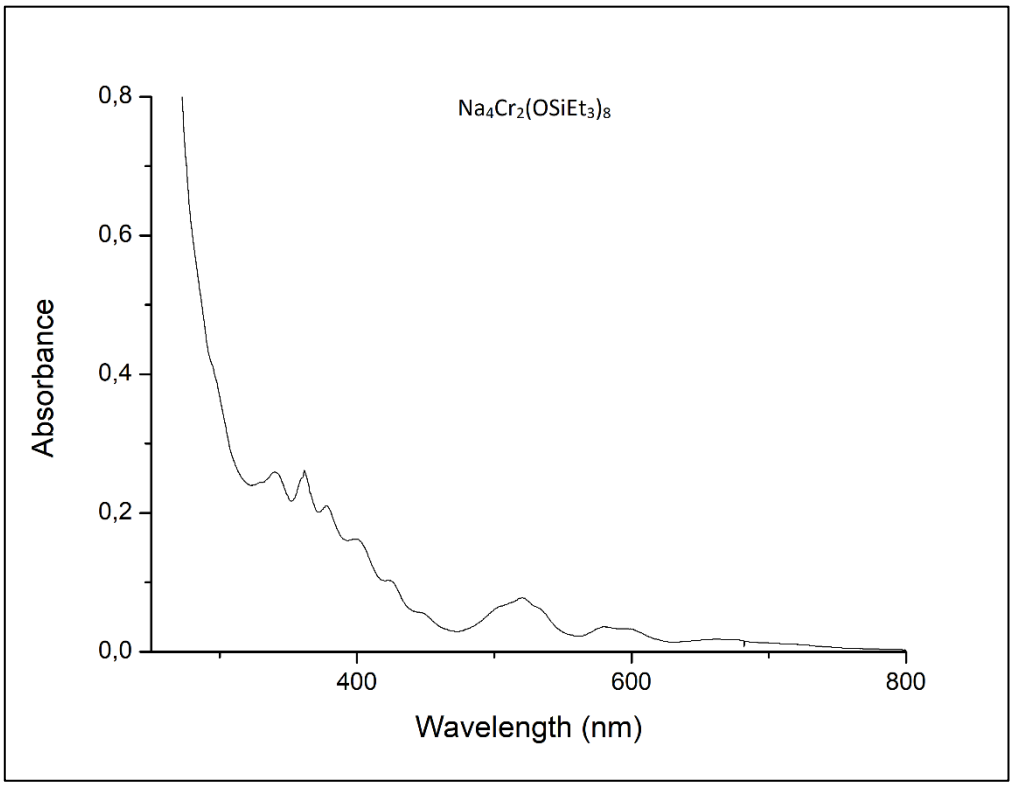

Figure S21. UV-vis spectrum of compound **8** in dilute *n*-hexane solution.

Crystallographic Information

Table S1. Crystallographic data for compound **1**, **2**, **3, 4** and, **5**

	[Cr(OSi*i*Pr$_3$)(μ-OSi*i*Pr$_3$)(thf)]$_2$ (**1**)	[Cr$_3$(OSi*i*Pr$_3$)$_2$(μ-OSi*i*Pr$_3$)$_4$] (**2**)	[Cr(OSi*i*Pr$_3$)$_2$(tmeda)] (**3**)	[Cr(OSi*i*Pr$_3$)$_3$(thf)$_2$] (**4**)	[Cr$_2$Cl$_3$(OSi*i*Pr$_3$)$_3$(thf)$_3$] (**5**)
Formula	$C_{44}H_{100}Cr_2O_6Si_4$	$C_{54}H_{126}Cr_3O_6Si_6$	$C_{24}H_{58}CrN_2O_2Si_2$	$C_{35}H_{79}CrO_5Si_3$	$C_{39}H_{87}Cl_3Cr_2O_6Si_3$
CCDC	2149139	2149143	2149140	2149142	2149145
M_r [g mol^{-1}]	941.59	1196.08	514.90	716.25	946.70
color	violet/blocks			violet/block	violet plates
crystal system	Monoclinic	Triclinic	Monoclinic	Orthorhombic	Monoclinic
space group	C 2/c	$P\bar{1}$	P2$_1$/c	P n a 21	P2$_1$/c
a [Å]	26.0872(13)	13.8340(8)	20.997(4)	45.286(4)	12.7399(15)
b [Å]	11.7092(6)	14.4338(9)	29.553(5)	13.8630(12)	20.409(2)
c [Å]	21.6971(11)	18.5308(11)	15.170(3)	13.4511(11)	20.149(2)
α [°]	90	104.537(2)	90	90	90
β [°]	123.1860(10)	100.026(2)	102.489(2)	90	104.579(2)
γ [°]	90	95.480(2)	90	90	90
V [Å^3]	5546.6(5)	3489.2(4)	9191(3)	8444.6(12)	5070.1(10)
Z	4	2	12	8	4
T [K]	100(2)	173(2)	173(2)	100(2)	100(2)
ρ_{calcd} [g cm^{-3}]	1.128	1.138	1.116	1.127	1.240
μ [mm^{-1}]	0.517	0.602	0.472	0.391	0.696
F (000)	2064	1308	3408	3160	2040
total reflns	40844	113301	167843	61112	101344
observed reflns (I>2σ)	5008	10791	16855	17260	11698
R_1/wR_2 (I > 2σ)[a]	0.0377/ 0.0882	0.0453/ 0.1093	0.0463/ 0.1224	0.0421/ 0.0994	0.0271/ 0.0690
R_1/wR_2 (all data)[a]	0.0557/ 0.0989	0.0594/0.1228	0.0817/ 0.1479	0.0540/ 0.1064	0.0321/ 0.0726
GOF	1.035	1.035	1.015	1.030	1.026

[a] $R1 = \Sigma(||F_0|-|F_c||)/\Sigma|F_0|, F_0 > 4s(F_0)$. $\omega R2 = \{\Sigma[\boldsymbol{\omega}\,(F_0^2-F_c^2)^2/\Sigma[\omega\,(F_0^2)^2]\}^{1/2}$.

Table S2. Crystallographic data for compounds **6**, **7** and **8**

	$[Cr_3(OSiEt_3)_2(\mu\text{-}OSiEt_3)_4(thf)_2]$ (**6**)	$[Cr(OSiEt_3)_2]_4$ (**7**)	$[Na_4Cr_2(OSiEt_3)_8]$ (**8**)
Formula	$C_{44}H_{106}Cr_3O_8Si_6$	$C_{48}H_{120}Cr_4O_8Si_8$	$C_{48}H_{120}Cr_{2.20}Na_{3.80}O_8Si_8$
CCDC	2149144	2149141	2149146
M_r [g mol^{-1}]	1087.82	1258.15	1252.01
color	red/blocks	brown/ blocks	brown/ blocks
crystal system	Triclinic	Monoclinic	Trigonal
space group	$P\bar{1}$	C2/c	R3c
a [Å]	11.4293(5)	25.353(3)	14.251(3)
b [Å]	12.4998(6)	12.0914(15)	14.251(3)
c [Å]	12.9835(6)	24.967(3)	59.481(12)
α [°]	62.2170(10)	90	90.00(3)
β [°]	67.7320(10)	116.114(2)	90.00(3)
γ [°]	89.9490(10)	90	120.00(3)
V [Å^3]	1483.26(12)	6872.5(15)	10462(5)
Z	1	4	6
T [K]	100(2)	100(2)	99(2)
ρ_{calcd} [g cm^{-3}]	1.218	1.216	1.192
μ [mm^{-1}]	0.703	0.797	0.544
F (000)	590	2720	4072
total reflns	54868	48774	60582
observed reflns (I>2σ)	6198	5628	6074
R_1/wR_2 (I > 2σ)[a]	0.0297/0.0756	0.0432/ 0.0948	0.0382/ 0.0994
R_1/wR_2 (all data)[a]	0.0357/0.0797	0.0685/ 0.1076	0.0463/ 0.1085
GOF	1.084	1.028	1.036

[a] $R1 = \Sigma(||F_0|-|F_c||)/\Sigma|F_0|, F_0 > 4s(F_0)$. $\omega R2 = \{\Sigma[\boldsymbol{\omega}\ (F_0^2-F_c^2)^2/\Sigma[\boldsymbol{\omega}\ (F_0^2)^2]\}^{1/2}$.

Molecular Drawings

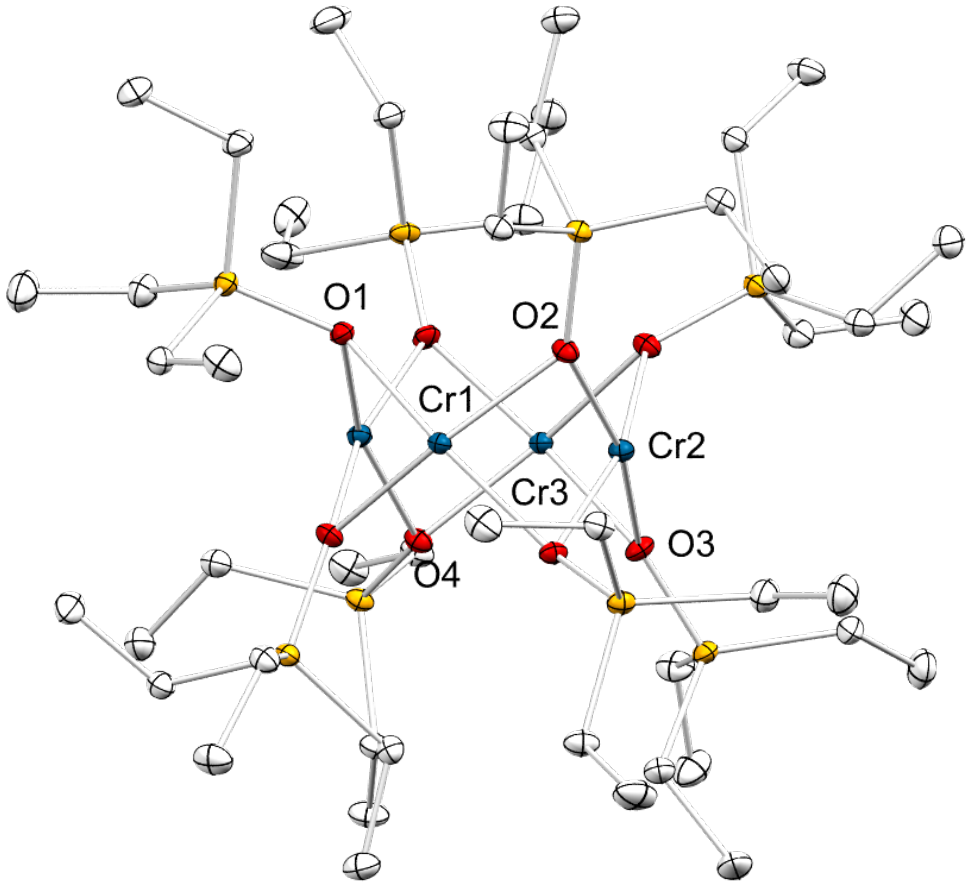

Figure S22. MERCURY representation (30% probability ellipsoids) of $Cr_4(OSiEt_3)_2]_8$ (**7**). Hydrogen atoms are omitted for clarity. Selected interatomic distances (Å) and angles (°): Cr1···Cr2 2.5381(6), Cr2···Cr3 2.5325(6), Cr1–O2 2.0046(17), Cr1–O1 2.0199(17), Cr2–O2 1.9907(17), Cr2–O3 1.9940(18), Cr3–O3 1.9939(17), Cr3–O4 2.0077(18), Si1–O1 1.6448(19), Si2–O2 1.6453(18), Si3–O3 1.6425(18), Si4–O4 1.6370(19); O2–Cr1–O1 98.30(7), O2–Cr1–Cr2 50.32(5), O1–Cr1–Cr2 114.93(5), Cr1–Cr2–Cr3 90.83(2), Cr(1)–O(1)–Si(1) 136.95(11), Cr(1)–O(2)–Si(2) 132.78(11), Cr(2)–O(2)–Si(2) 143.38(11), Cr(2)–O(3)–Si(3) 143.57(11), Cr(3)–O(3)–Si(3) 137.32(11), Cr(3)–O(4)–Si(4) 137.91(11).

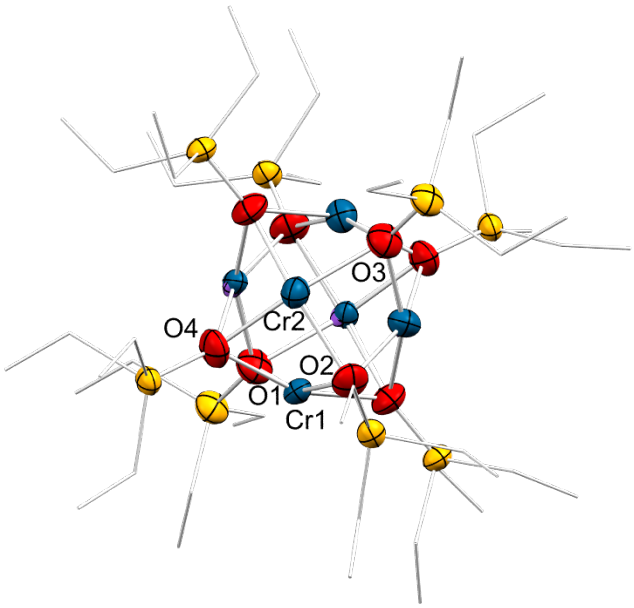

Figure S23. MERCURY representation (30% probability ellipsoids) of $Na_4Cr_2(OSiEt_3)_8$ (**8**). Hydrogen atoms are omitted for clarity Na1 and Na2 are completely covered by the ellipsoids of Cr1 and Cr2 and therefore not visible.

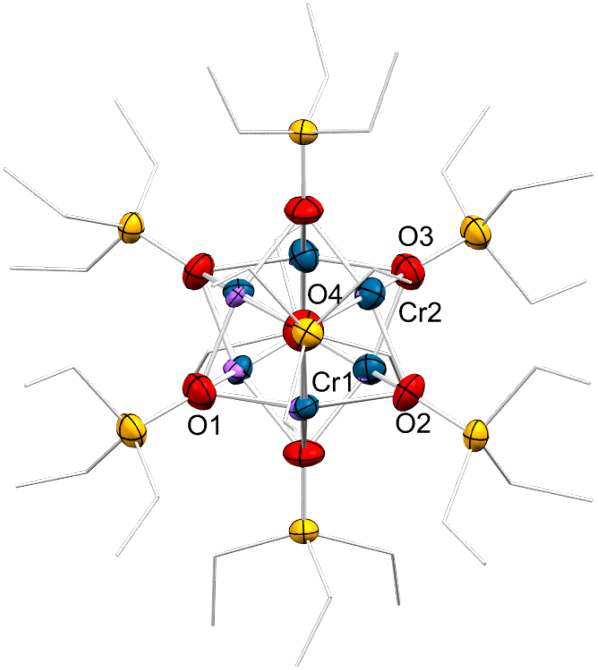

Figure S24. MERCURY representation (30% probability ellipsoids) of $Na_4Cr_2(OSiEt_3)_8$ (**8**). Hydrogen atoms are omitted for clarity.

The octahedron is built by Na and Cr. All six positions are partially occupied by Na and Cr. The disorder model should reveal a Na:Cr ratio of 2:1, to become at least a Na_4Cr_2 core. The refinement for the two positions in the asymmetric unit shows exact that ratio for one position, but for the second one we have a divergence (0.588:0.422). This result may be caused by the difficulties in structure solution and the overall disorder in the molecule. In the crystal, the "ball-like" cluster is orientated in distinct directions. Therefore, the averaged contents of the unit cell are obtained by averaging over the space, which leads to substitutional disorder. The divergence for the second position regarding the Na/Cr disorder might be also affect by partial hydrolysis as indicated by a significant OH stretching vibration in the IR spectrum (Figure S15).

F

Appendix

Appendix

Analytical data of compounds not included in the main results or manuscript

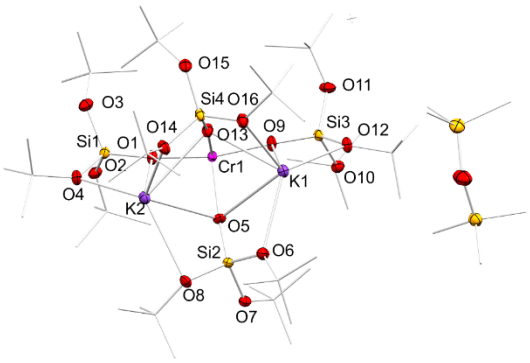

$CrCl_2$ + $KOSi(OtBu)_3$ → (THF, rt, 1 h) → $[K_2Cr\{OSi(OtBu)_3\}_2]$

$[K_2Cr\{OSi(OtBu)_3\}_2]$ ST040
"Serendipitous finding"
R1[I>sigma(I)] = 5.49%, wR_2 = 15.10%
a = 28.350(4) Å, α = 90°
b = 16.719(2) Å, β = 123.156(2)°
c = 20.253(3) Å, γ = 90°
Additional analyses: ^{1}H NMR (C_6D_6)

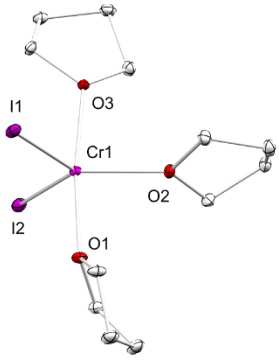

6 $Cr(OMe)_2$ + CHI_3 → (THF, 50 °C, 3 h) → $CrI_2(thf)_2$

$[CrI_2(thf)_3]$ ST050
R1 [I>sigma(I)]= 2.58%, wR_2 = 5.86%
a = 10.7362(13) Å, α = 90°.
b = 11.3928(13) Å, β = 90°.
c = 13.9571(16) Å, γ = 90°.

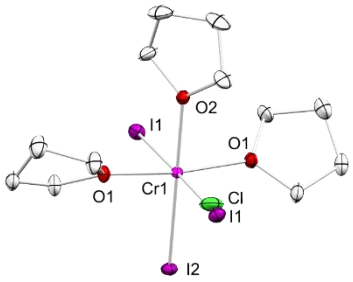

6 $CrCl_2$ + CHI_3 → (MeCN/Et_2O 2:1, rt, 1 h) → $CrI_3(thf)_3$

$[CrI_3(thf)_3]$ ST065
R1[I>sigma(I)] = 3.15%, wR_2 = 6.23%
a = 8.8675(5) Å, α = 90°.
b = 14.1182(8) Å, β = 90°.
c = 14.1785(8) Å, γ = 90°.
Additional analyses: EA
Different unit cell to: CCDC 1875599
Citation: R. Fischer, H. Görls, R. Suxdorf, and M.Westerhausen, *Organometallics* **2019**, 38, *2*, 498–511.

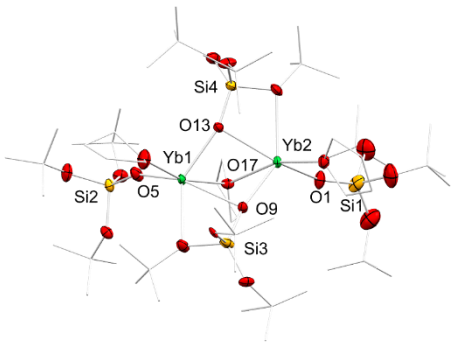

$Yb[N(SiMe_3)_2]_2(thf)_2$ + $HOSi(OtBu)_3$ → (THF, –35 °C, 1h) → $Yb[OSi(OtBu)_3]_4$

$[Yb_2\{OSi(OtBu)_3\}_4]$ ST083
R1 [I>sigma(I)]= 6.53%, wR_2 = 17.79%
a = 20.0628(19) Å, α = 90°
b = 17.3360(16) Å, β = 90.421(2)°
c = 23.602(2) Å, γ = 90°
Additional analyses: ^{1}H NMR, EA

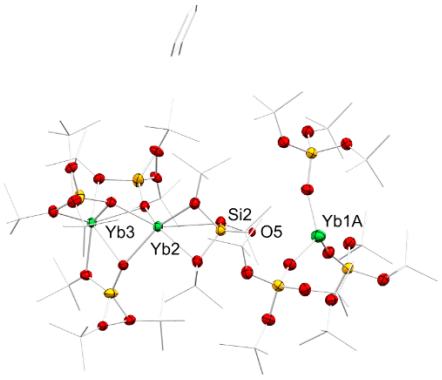

See ST083
$[Yb_3\{OSi(OtBu)_3\}_7]$ ST083b(yellow)
Serendipitous finding
R1 [I>sigma(I)]= 4.36%, wR_2 = 12.43%
a = 22.0085(7) Å, α= 90°.
b = 22.0085(7) Å, β= 90°.
c = 47.6279(15) Å, γ = 120°.
Additional analyses: EA

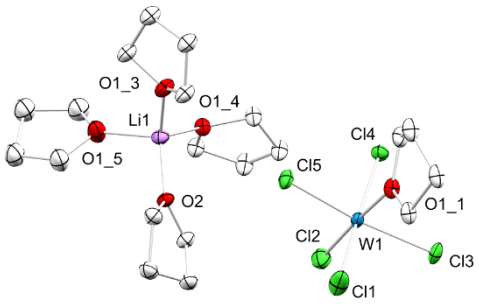

$WOCl_4$ + 2 MeLi —THF, –40 °C, 1 h→ $[Li(thf)_4]WCl_5(thf)$

$[Li(thf)_4]WCl_5(thf)$ ST234
R1 [I>sigma(I)]= 5.79%, wR_2 = 13.11%
a = 11.1658(12) Å, α= 90°
b = 14.7668(15) Å, β= 96.132(2)°
c = 17.2395(18) Å, γ = 90°
Additional analyses: ^{1}H NMR (THF-d_8)

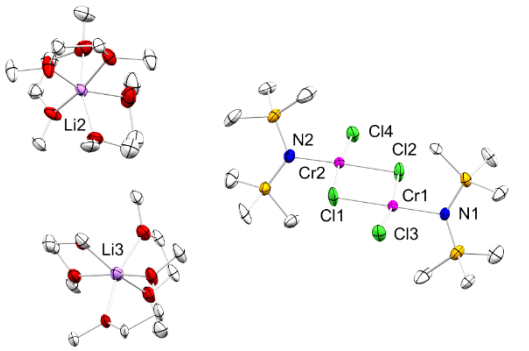

$CrCl_2$ + $Li[N(SiMe_3)_2]$ —THF, rt,1 h→ $[Li_2(DME)_6]Cr_2Cl_4\{N(SiMe_3)_2\}_2$

$[Li_2(DME)_6]Cr_2Cl_4\{N(SiMe_3)_2\}_2$ ST087
Crystallized from THF + DME
R1 [I>sigma(I)]= 7.84%, wR_2 = 24.53%
a = 24.563(5) Å, α= 90°
b = 13.793(3) Å, β= 105.837(3)°
c = 19.244(4) Å, γ = 90°
Additional analyses: EA

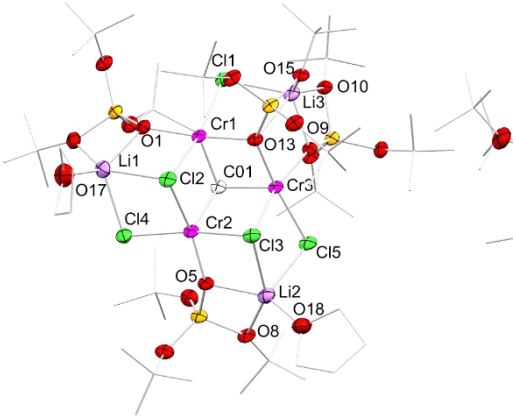

$Cr_3Cl_6(\mu_3\text{-}CH)(thf)_6$ + 3 $LiOSi(OtBu)_3$ —THF, –40 °C, 1 h→ $[Li_3Cr_3Cl_5(\mu_3\text{-}CH)\{OSi(OtBu)_3\}_4(thf)]$

$[Li_3Cr_3Cl_5(\mu_3\text{-}CH)\{OSi(OtBu)_3\}_4(thf)]$
ST247_5
R1 [I>sigma(I)]= 6.27%, wR_2 = 18.48%
a = 13.7478(15) Å, α= 97.881(4)°.
b = 24.264(3) Å, β= 94.720(4)°.
c = 26.739(3) Å, γ = 99.524(4)°.

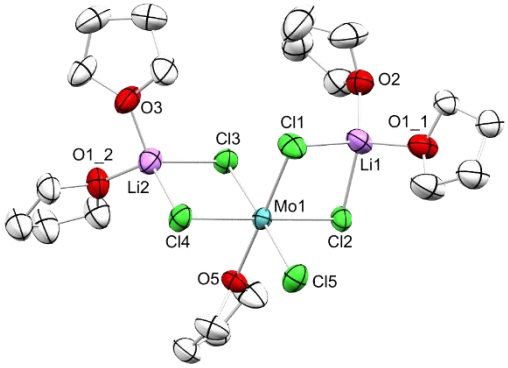

$MoOCl_3(thf)_2$ + 2 $Li[N(SiMe_3)_2]$ → (THF, –40 °C, 1 h) $[Li_2(thf)_4]MoCl_5(thf)$

$[Li_2(thf)_4]MoCl_5(thf)$ ST251
R1 [I>sigma(I)]= 8.07%, wR_2 = 23.54%
a = 10.547(3) Å, α= 90°.
b = 19.696(6) Å, β= 101.821(5)°.
c = 14.743(4) Å, γ = 90°.
Additional analyses: ^{1}H NMR (THF-d_8)

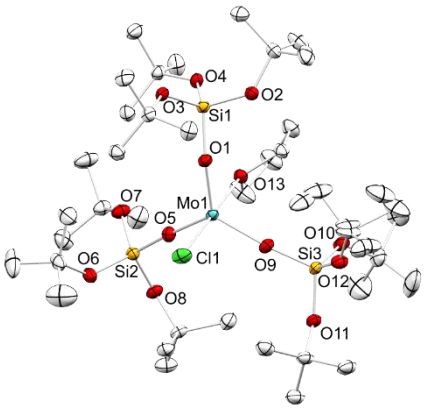

$MoOCl_3(thf)_2$ + $KOSi(OtBu)_3$ → (Tol, rt, 1 h) $[MoCl\{OSi(OtBu)_3\}(thf)]$

$[MoCl\{OSi(OtBu)_3\}(thf)]$ ST296
R1 [I>sigma(I)]= 3.48%, wR_2 = 8.60%
a = 14.3546(7) Å, α= 90°
b = 21.5724(11) Å, β= 107.3260(10)°
c = 18.4979(10) Å, γ = 90°

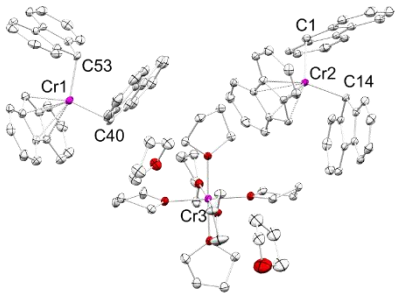

$Cr_3Cl_6(\mu_3\text{-}CH)(thf)_6$ + $3Na(C_{13}H_9)$ → (THF, –40 °C, 3 h) $[Cr(thf)_6][Cr(C_{13}H_9)_3]_2$*2THF

$[Cr(thf)_6][Cr(C_{13}H_9)_3]_2$*2THF NS13
R1 [I>sigma(I)]= 5.64%, wR_2 = 15.37%
a = 21.4487(14) Åα= 90°.
b = 19.1022(11) Åβ= 90°.
c = 21.7089(13) Åγ = 90°.
Additional analyses: ^{1}H NMR (THF-d_8)

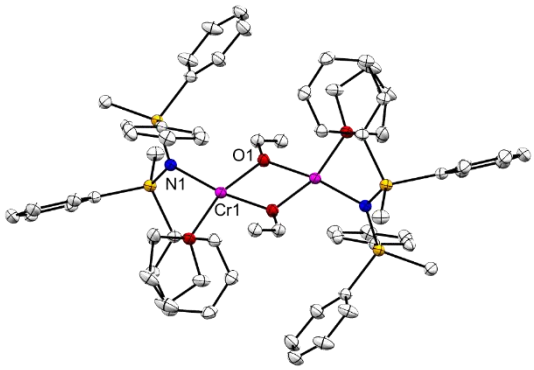

$CrCl_2$ + $L(thf)_2N(SiPh_3)_2$ → (THF, rt, 5 h) $[Cr\{N(SiPh_3)_2\}(\mu\text{-}OEt)]_2$

$[Cr\{N(SiPh_3)_2\}(\mu\text{-}OEt)]_2$ JR18
R1 [I>sigma(I)]= 3.48%, wR_2 = 8.60%
a = 25.227(6) Å, α= 90°
b = 10.808(3) Å, β= 113.162(5)°
c = 23.753(6) Å, γ = 90°
Additional analyses: ^{1}H NMR (THF-d_8)